

**THE MEIOTIC RECOMBINATION INITIATION LANDSCAPE IN YEAST:
EVOLUTIONARY DYNAMICS AND FACTORS THAT SHAPE ITS DISTRIBUTION**

by

Isabel Lam

A Dissertation

Presented to the Faculty of the Louis V. Gerstner Jr.

Graduate School of Biomedical Sciences,

Memorial Sloan Kettering Cancer Center

In Partial Fulfillment of the Requirements for the Degree of

Doctor of Philosophy

New York, NY

March 2016

Scott N. Keeney, PhD
Dissertation Mentor

Date

Copyright © Isabel Lam 2016

DEDICATION

This thesis is dedicated to those who dreamed of furthering their education and of pursuing a career, but could not because of life circumstances. I feel very fortunate to have had the option and my family's unconditional support to walk in this path.

ABSTRACT

Recombination is required for the accurate segregation of homologous chromosomes in meiosis, and generates new allele combinations. Meiotic recombination is initiated by developmentally programmed DNA double-strand breaks (DSBs). Sites of meiotic recombination are nonrandomly distributed along the genome, and this can be partly attributed to factors operating at different size scales that influence DSB formation. Theoretical studies have proposed that individual hotspots—favored sites of recombination initiation—either evolve rapidly toward extinction or may be conserved, especially if they are located in chromosomal features under selective constraint, such as gene promoters. Here, I empirically tested these competing theories by comparing genome-wide maps of meiotic recombination initiation from widely divergent species in the *Saccharomyces* clade (up to 15 My and 30% sequence divergence). My analyses of the DSB distributions in *S. cerevisiae*, *S. paradoxus*, *S. mikatae*, and *S. kudriavzevii* indicate that hotspots frequently overlap with promoters in all species tested and, consequently, hotspot positions are well conserved. Remarkably, the relative strength of individual hotspots is also highly conserved, as are larger-scale features of the distribution of recombination initiation. This stability, not predicted by prior models, suggests that the particular shape of the yeast recombination landscape is adaptive, and helps in understanding evolutionary dynamics of recombination in other species.

Conservation of meiotic DSB distribution and frequency in *Saccharomyces* species implies conservation of the molecular mechanisms shaping the DSB landscape. The DSB landscape is shaped by multiple factors that can be conceptually categorized as intrinsic (chromosomal features governing accessibility or activity of the DSB machinery), or extrinsic (feedback and other regulatory networks). One of the intrinsic factors influencing DSB formation and its distribution is higher-order chromatin structure.

Meiotic chromosomes are organized into distinct loop-axis structures, with chromatin loops emanating from a protein-rich axis. Proteins localizing to chromosome axes include Red1, Hop1, and Mek1. To gain a better understanding of the role of chromosome structure proteins in shaping the DSB landscape, I generated genome-wide meiotic recombination initiation maps in *S. cerevisiae red1*, *hop1*, and *mek1* mutants. Analyses of these maps suggest that Red1 and Hop1 have both intrinsic and extrinsic roles in shaping the DSB landscape—they are required for normal DSB levels genome-wide, and promote more DSBs on short chromosomes (“intrinsic”), and also appear to contribute to homolog engagement feedback inhibition (“extrinsic”). Mek1 influences DSB numbers through regulatory circuits (“extrinsic”), and appears to have little or no intrinsic role in DSB formation. Analysis of the DSB distribution in the absence of chromosome structure proteins further supports the prevailing model of the DSB landscape being shaped by a hierarchical combination of factors.

BIOGRAPHICAL SKETCH

Isabel Lam was born on May 10, 1985 in Cumaná, Venezuela, and grew up in Brooklyn, New York. She obtained her Bachelor of Arts degree in Biology with minors in Computer Science and Fine Arts from New York University (NYU). Isabel conducted her undergraduate honors thesis research in the lab of Dr. Hannah Klein in the Department of Biochemistry at NYU Medical School, where she was first exposed to yeast genetics and DNA repair mechanisms. After graduating from NYU, she worked as Research Technician in the laboratory of Dr. James Salzer in the Neuroscience Department at NYU Medical School. Isabel started the doctoral program at Louis V. Gerstner Jr. Sloan Kettering Graduate School in 2008. She joined the laboratory of Dr. Scott Keeney in the Molecular Biology Program at Memorial Sloan Kettering Cancer Center in 2009, where she conducted her doctoral dissertation on meiotic recombination initiation in yeast.

ACKNOWLEDGEMENTS

First and foremost, I would like to thank Scott Keeney for this amazing journey. In German, the word for PhD advisor is *Doktorvater*, which literally translates to “doctoral father.” When I first learned this a few years ago, I knew this was the exact description for the influence that Scott has had in my scientific training. More than just an advisor, he has been a true mentor and scientific parent: he has been there at every step of the way, from the faltering baby steps to the last steps I take as a PhD student.

I am immensely grateful to Scott for the opportunities to grow and develop as a scientist; for giving me the freedom to explore; for his dedication to mentoring and training; and most of all, for believing in me despite my shortcomings, and for not letting go during moments of uncertainty. Graduate school, and the nature of scientific research itself, is an exercise in failing and finding the strength to get up again and keep pushing forward. Scott has always been there to provide assistance and perspective when it was needed, and his uncanny sixth sense has helped me push through obstacles. Perhaps this is what allowed me to gradually have the courage to take on new and bigger challenges—the knowledge that he would be there to steer me in the right direction if I got lost. I hoped that over the years, some of his brilliance would rub off on me, but sadly that did not happen. Nevertheless, I have been very fortunate to learn from him, and to have been exposed to his approach to science, his clarity of vision, and his wisdom and integrity both as a scientist and as a human being. Under his tutelage I have learned that despite it not being easy to embrace the unknown, within this infinite realm lies possibilities even greater than what you would have imagined. I will carry and treasure all the lessons I have learned from him as I embark on the next chapter.

I am extremely grateful to the Keeney lab members for making the lab a collegial, fun and friendly environment, and a great place to grow up as a scientist, as a

professional, and as a person. They have become a family, and the lab has become a home: the place I look forward to when coming back from a trip. Moments of frustration and uncertainty are inherent to learning and conducting research, but the encouragement and support from my labmates over the years have been a tremendous source of comfort. I would like to thank Drew Thacker for being my rotation mentor and for his countless sage advice throughout the years (and for continuing to provide advice all the way from the west coast). Sam Globus and Drew were my first baymates, and I am thankful to them for showing me the ways of the lab. They were at times, (in their words) “the annoying older brothers I never had and never wanted,” but the perk of having them as older brothers was that they always had my back. I thank Mariko Sasaki, my lab older sister, for being a role model. To the young graduate student I was back then, Mariko made me feel like one day I could be successful like her in the Keeney lab. Ryan Kniewel and Jim Dowdle, the other lab older brothers, patiently answered any questions and provided advice when I was just learning the ropes; Xuan Zhu and Sam Tischfield, my more or less contemporaneous siblings, were always there to commiserate with and bounce off data analysis ideas. Some experiences are very specific to the graduate student experience, and it was nice to have others going through the same thing. Erman Karasu and Xiaojing Mu became my lab little siblings; I hope I have been as encouraging and supportive with them as the previous generation of graduate students were with me.

I am also grateful to all the postdocs I overlapped with in the Keeney lab for their support, encouragement, advice, and friendship: Liisa Kauppi, Ignasi Roig, Esther de Boer, Francesca Cole, Hajime Murakami, Julian Lange, Neeman Mohibullah, Viji Subramanian, Megan van Overbeek, Monika Mehta, Eleni Mimitou, Corentin Claeys-Bouaert, Devanshi Jain, Seoyoung (Sarah) Kim, Shintaro Yamada, Laurent Acquaviva, David Ontoso Picón, and Michiel Boekhout. Sometimes getting that high-five from your

labmates after a lab meeting presentation—though a small gesture—makes all the difference. Everyone in the Keeney lab has helped shape (even in small ways) the person I have become over the years. I would like to especially thank Elena for her friendship—I never would have imagined back then (10 years ago, perhaps?) when I first met her at the Frick that we would end up working in the same lab; Neeman for setting the example of lab citizenship and for making everything seem easy; Hajime and Seoyoung for all the lovely conversations; Jodi-Ann Sampson for being my cheerleader since day one in the Keeney lab. Her unconditional support through the ups and downs of the PhD has been invaluable. Jodi extended an arm whenever I fell into holes, and celebrated all my successes no matter how small. I also cannot imagine my PhD experience without the other half of “Lamge.” Julian has provided encouragement, advice, friendship, and has been a true partner in crime in all sorts of lab adventures and creative projects. Our years as lab detectives were some of the finest. Puns, Shakespeare’s sonnets, haikus, and video compilations with music set to the beat will never be the same to me. Intelligence does not rub off, but OCD does, apparently! Or as he prefers to phrase it, I was always detail-oriented, but with his influence, this feature was honed and brought out.

There have been many moments of generosity that have had a lasting impact on the colleague and mentor I strive to be, and I am grateful to those individuals who have made such an impression on me. Francesca Cole took the time and generously provided candid advice in my early days as graduate student; Megan invited me to her apartment one evening after putting her daughter to bed to provide critical feedback on my fellowship proposal. Her kind gesture was instrumental in shaping my ideal of a lab mentor to young graduate students, and encourages me to pay it forward. In addition, Megan’s optimism, positive encouragement, and belief in my abilities have helped me develop a vision for my future self that I would not have imagined before. Hajime

generously gave his time and did a Southern blot for me so he could demonstrate his method step-by-step, even though I was only expecting to receive some verbal advice upon facing technical problems. Neeman taught me Spo11-oligo purification in her characteristic approach of making everything (even a complex protocol) seem easy; without her help, I probably would have sat on the protocol for half a year. Julian kindly taught me Spo11 oligo library preparation, and patiently helped design my first quality control experiments.

I am indebted to Hannah Klein for putting me in this path. Hannah was the first to encourage me to apply for a PhD program back when I had little idea what it meant to be a research scientist. Without her guidance and encouragement, I never would have embarked on this amazing experience. She has been a mentor in the nearly 11 years since we first met, and is undoubtedly one of my most steadfast supporters. Hannah has provided valuable and honest advice at every step of my career. I would also like to thank Jim Salzer for his kindness and encouragement. Working in Jim's lab affirmed my decision to pursue a PhD, because working with his postdocs and graduate students made me want to become one of them. My attempt to tackle an independent project in his lab also made me want to obtain solid training in how to think like a scientist. I am grateful to members of the Salzer lab for giving me a glimpse of what it is like to be a scientist. I am glad to know that I am always welcome with open arms whenever I drop by the NYU Medical School.

I would like to thank my family for their unconditional support in this journey, even if they did not quite understand all that it entails. I thank my parents for instilling in me the values of education and hard work, and my sisters for always helping me pursue my dreams. I thank my friends who helped me sail through graduate school: Kathy Chan, Malgorzata Wysocka, Enric Domènech-Estévez, Hasna Baloui, Julie Young, Lisa Hang, Prabha Sarangi, Koyi Choi, Lei Wei, Jenny Jiang, Tejas Yadav, Hyejin Choi, Kate Gao,

Elizabeth Wasmuth, Shefali Krishna, and the countless other people that should be on this list but I am blanking on right now. I also thank the people who helped lay the foundations in my first year of graduate school, and who provided valuable advice in the early days: Francesca, Nicolas Siaud, Jan LaRocque, Nicole Christ, Deniz Simsek, Maria Barbera, Patricia Sung, Vladimir Yong-Gonzalez, Catherine Cremona, David Liu, Xiaolan Zhao, Maria Jasin, and my first-year mentor Jackie Bromberg. I would like to thank the Gerstner Sloan Kettering graduate school administration and staff for their hard work to ensure that everything runs smoothly, and for their personal attention throughout the years: Maria Torres, Iwona Abramek, Ivan Gerena, Carlene Grant, Ady Gupta, Katherine Gentile, Gita Bosch, Linda Burnley, and Ken Marians. It has been a terrific graduate school experience.

I am grateful to Michael Lichten for his blessing on the hotspot evolution project, and to everyone who helped me become acquainted with *Saccharomyces* species by providing strains and/or advice on how to work with them: Gianni Liti, Ed Louis, Carolin Müller, Jeremy Roop, Duncan Greig, Marita Cohn, and Chris Hittinger. I would also like to thank Leslie Higuaita-Montoya for generating the first *rec104* RxxS/T site mutants during her summer undergraduate research stint in the summer of 2011; Hajime for providing fruitful discussion and suggestions on the *red1*, *hop1*, and *mek1* project; Julian for generously passing on some of his reagents when I first picked up that project; Xuan, Sam T. and Julian for helpful discussion during the early days of learning R; Agnès Viale and members of the MSKCC Integrated Genomics Operation for sequencing, and Nicholas Socci for mapping Spo11 oligo and MNase-seq reads.

I would like to express my gratitude to my Advisory Committee members, Maria Jasin and Iestyn Whitehouse, for their helpful comments from the beginning, even as the projects shifted from Rec104 phosphorylation to yeast hotspot evolution and the DSB landscape; William Holloman for agreeing to be my External Examiner, and John Petrini

for agreeing to be Chairperson of the Dissertation Committee. I would like to thank Scott for critical reading of the thesis draft; Hajime, Seoyoung, and Laurent for feedback and discussion on selected thesis chapters; and Keeney lab members and friends for emotional support during the thesis writing. My apologies for dragging them into my “vortex of unproductivity” during times of intense writer’s block, procrastination, and frustration.

TABLE OF CONTENTS

LIST OF FIGURES	XV
LIST OF TABLES	XVIII
ABBREVIATIONS	XIX
CHAPTER 1: INTRODUCTION	1
Meiotic recombination	2
The cast of players involved in meiotic DSB formation in <i>S. cerevisiae</i>	4
Conservation of DSB proteins in other organisms	7
The meiotic DSB landscape in yeast.....	17
Approaches for mapping the DSB landscape	18
Intrinsic factors that shape the DSB landscape	20
Extrinsic factors that shape the DSB landscape	25
The meiotic recombination initiation landscape in other organisms	31
Fission yeast.....	31
Mouse and Human	33
Other species.....	36
Chromosome structure proteins and their roles in shaping the DSB landscape	37
Domain structure of Red1, Hop1, and Mek1 proteins.....	37
The multiple roles of Red1, Hop1, and Mek1 in meiotic recombination.....	39
How might Red1, Hop1, and Mek1 influence meiotic DSB formation?.....	44
Evolutionary dynamics of the meiotic recombination landscape	45
Models predicting divergence vs. conservation of the recombination landscape	46
Comparison of recombination landscapes across and within species.....	54
Aims of the thesis	59
CHAPTER 2: EVOLUTIONARY DYNAMICS OF THE MEIOTIC DSB LANDSCAPE IN SACCHAROMYCETES	60
Summary	60
Results	62
The <i>Saccharomyces sensu stricto</i> clade	62
Conservation of Spo11 oligos	62
Targeting of DSBs to promoters is conserved	68
Conservation of DSB frequency in hotspots	69
Conservation of the DSB landscape over larger size scales	71
Chromosome length directly affects DSB density.....	73
Discussion	77
Conservation of the yeast DSB landscape reflects conservation of the factors that determine it	77
Model for conservation or divergence of the recombination landscape.....	78
CHAPTER 3: INFLUENCE OF CHROMOSOME STRUCTURE PROTEINS ON THE MEIOTIC DSB LANDSCAPE	93
Summary	93
Results	94
Global meiotic DSBs are reduced in the absence of Red1, Hop1, or Mek1	94
Generating high-resolution DSB maps in <i>red1</i> , <i>hop1</i> , and <i>mek1</i> mutants.....	97

DSB patterns within hotspots are unchanged in the absence of Red1, Hop1, or Mek1	97
Within chromosomes, regions exhibit different degrees of DSB reduction	98
DSB suppression near centromeres, telomeres, and rDNA are maintained	99
DSBs on short chromosomes are most affected in the absence of Red1 and Hop1	100
DSB reduction within subchromosomal domains in <i>red1</i> and <i>hop1</i> is weakly correlated with enrichment of Red1	112
Discussion	115
The role of Red1 and Hop1 in DSB formation	115
The extrinsic role of Mek1 in regulating DSB numbers	117
Why are some loci more depleted for DSBs in <i>red1</i> or <i>hop1</i> ?	119
Dual layer of control promotes DSBs on short chromosomes	124
Axial element proteins and homolog engagement feedback inhibition of DSBs....	126
Sites of preferred DSB formation are robust to changes in meiotic chromosome organization	127
CHAPTER 4: CONCLUDING DISCUSSION	129
Main conclusions	129
Potential implications and perspectives	130
The shape of the yeast DSB landscape may be under selection	132
Implications of recombination evolutionary dynamics on genome organization	136
Future directions.....	138
DSB landscape conservation in yeast	138
Role of chromosome structure proteins in shaping the DSB landscape.....	140
CHAPTER 5: MATERIALS AND METHODS	142
APPENDIX: INVESTIGATING THE ROLE OF REC104 PHOSPHORYLATION	161
Summary	161
Introduction.....	161
DSB proteins in <i>S. cerevisiae</i>	161
Characteristics of Rec104.....	162
Possible regulatory function of Rec104 phosphorylation in meiotic recombination	163
Results	166
The <i>rec104-4A[R]</i> allele causes defects in phosphorylation, subcellular localization, and DSB formation	166
The <i>myc-rec104-3A[C]</i> allele causes delayed DSB formation.....	168
Conclusions	173
Materials and Methods	174
REFERENCES	180

LIST OF FIGURES

Figure 1.1.	Reductional and equational divisions in meiosis.....	9
Figure 1.2.	The meiotic recombination pathway.....	10
Figure 1.3.	Interaction maps of DSB proteins in <i>S. cerevisiae</i> and <i>S. pombe</i>	12
Figure 1.4.	A combination of factors operating at different size scales influences the distribution of breaks in the DSB landscape.....	19
Figure 1.5.	Meiotic chromosome organization.....	29
Figure 1.6.	Temporal and spatial coordination of DSB formation in <i>S. cerevisiae</i>	30
Figure 1.7.	Protein domain structure of Red1, Hop1, and Mek1.....	47
Figure 1.8.	Model for pathway of chromosomal recruitment of Red1 and Hop1, and Mek1 kinase activation.....	49
Figure 2.1.	Schematic of <i>Saccharomyces</i> phylogeny.....	64
Figure 2.2.	Characteristics of sporulation and Spo11-oligo complexes in different <i>Saccharomyces</i> strains and species.....	65
Figure 2.3.	Reproducibility of Spo11-oligo maps in <i>Saccharomyces</i> species.....	66
Figure 2.4.	Conserved targeting of DSBs to promoters.....	79
Figure 2.5.	Conservation of hotspot locations.....	81
Figure 2.6.	Conservation of hotspot strength.....	82
Figure 2.7.	Large-scale features of the DSB landscape are conserved.....	84
Figure 2.8.	The kinetochore suppresses centromere-proximal DSBs in every chromosome.....	85
Figure 2.9.	The kinetochore protects the centromere-proximal domain from DSBs.....	86
Figure 2.10.	Large-scale hot and cold interstitial domains are conserved.....	87

Figure 2.11.	The anticorrelation between chromosome length and DSB density is conserved in <i>Saccharomyces</i> species.....	89
Figure 2.12.	DSB density is influenced by chromosome length.....	90
Figure 2.13.	An accidental experiment testing the Kaback Effect: the serendipitous YPS128 T(III;XIII) translocation.....	91
Figure 3.1.	Spo11 tagged with Flag or PrA has little or no defect in DSB levels in <i>red1</i> , <i>hop1</i> , or <i>mek1</i> mutant backgrounds.....	101
Figure 3.2.	Fewer DSBs form in <i>red1</i> , <i>hop1</i> , and <i>mek1</i> mutants.....	102
Figure 3.3.	Reproducibility of biological replicate Spo11-oligo maps in <i>red1</i> , <i>hop1</i> , and <i>mek1</i> mutants.....	104
Figure 3.4.	Fine-scale DSB patterns are minimally affected in the absence of Red1, Hop1, or Mek1.....	105
Figure 3.5.	Regional variation along chromosomes in response to <i>red1</i> , <i>hop1</i> , or <i>mek1</i> mutation.....	106
Figure 3.6	DSB suppression in sub-chromosomal regions are maintained in <i>red1</i> , <i>hop1</i> , and <i>mek1</i> mutants.....	108
Figure 3.7.	Short chromosomes behave differently in terms of DSB density in <i>red1</i> and <i>hop1</i> , but not in <i>mek1</i>	109
Figure 3.8.	Genomic regions that exhibit the greatest fold decrease in DSBs in <i>red1</i> and <i>hop1</i> mutants exhibit a weak tendency to have been most enriched for Red1 in the wild type.....	119
Figure 3.9.	Domains of correlated behavior are altered in <i>red1</i> and <i>hop1</i> , but not in <i>mek1</i>	121
Figure 3.10.	Model for the effects of Red1, Hop1, and Mek1 on DSB numbers.....	122
Figure 4.1.	<i>CEN-MAT</i> linkage increases the formation of spores with opposite mating types under limited nutrient availability.....	135

Figure A.1.	Rec104 amino acid sequence alignment in <i>Saccharomyces</i> species.....	165
Figure A.2.	Spore viability, phosphorylation, and nuclear localization phenotypes of the <i>rec104</i> RxxS/T mutant alleles.....	167
Figure A.3.	The <i>rec104-4A</i> [R] alleles exhibit reduced levels of DSBs.....	170
Figure A.4.	Spore viability, phosphorylation, and subcellular localization phenotypes of the <i>rec104</i> Cdc7 consensus site mutation alleles.....	171
Figure A.5.	The <i>myc-rec104-3A</i> [C] allele causes a delay in DSB formation.....	172

LIST OF TABLES

Table 1.1.	List of proteins required for meiotic DSB formation in different organisms.....	11
Table 1.2.	Summary of DSB phenotypes in <i>red1</i> , <i>hop1</i> , and <i>mek1</i> mutants.....	48
Table 2.1.	Mapping statistics for yeast species Spo11 oligo sequences.....	67
Table 3.1.	Mapping statistics for <i>red1</i> , <i>hop1</i> , and <i>mek1</i> Spo11 oligo sequences...	103
Table 5.1.	Yeast strains (<i>Saccharomyces</i> species).....	154
Table 5.2.	Yeast strains (<i>red1</i> , <i>hop1</i> , <i>mek1</i>).....	155
Table A.1.	Yeast strains (<i>rec104</i> mutant alleles).....	179

ABBREVIATIONS

CDK-S	S-phase cyclin dependent kinase (Cdc28-Clb5/Clb6)
ChIP	chromatin immunoprecipitation
CO	crossover
DDK	Dbf4-dependent kinase (Cdc7)
dHJ	double Holliday junction
DSB	double-strand break
DSBC	DSB catalytic core (<i>S. pombe</i> Rec6, Rec12, Rec14)
H3K4me	H3K4 methylation
H3K4me3	H3K4 trimethylation
IGR	intergenic region
IH	interhomolog
IP	immunoprecipitation
IS	intersister
LiNE	linear element
MRX	Mre11, Rad50, Xrs2
NCO	non-crossover
NDR	nucleosome-depleted region
rDNA	ribosomal DNA
SC	synaptonemal complex
SCD	S/T-Q cluster domain
SDSA	synthesis-dependent strand annealing
SFT	Seven, Fifteen, Twenty-four (<i>S. pombe</i> Rec7, Rec15, Rec24)
ssDNA	single-stranded DNA
TLAC	tethered loop-axis complex

CHAPTER 1: INTRODUCTION¹

In most organisms, meiotic recombination is critical for accurate segregation of homologous chromosomes and the production of viable gametes/spores. Recombination also results in the shuffling of alleles and generates genetic diversity. Thus, it is not surprising that cells take great measures to regulate where meiotic recombination occurs along chromosomes, and one layer of this regulation is controlling where meiotic recombination initiates. Meiotic recombination is initiated by developmentally programmed DNA double-strand breaks (DSB). Understanding how the meiotic recombination initiation landscape is determined, and how this mechanism affects landscape conservation/divergence over evolutionary time-scales are the overarching goals of this thesis.

This introductory chapter begins with a general outline of meiotic recombination, the proteins required to start the recombination process, and the factors that make a particular genomic region more prone to undergo meiotic recombination than others. The focus is mainly on *S. cerevisiae*, but where appropriate, sections on other organisms are included to illustrate conserved and diverged aspects. Next, a detailed review of chromosome structure proteins and their influence on the meiotic DSB distribution will be provided, which will be directly relevant to the topic of **Chapter 3**. The last part covers a comprehensive review on the evolutionary fate of meiotic recombination sites that is of direct relevance to **Chapter 2**.

¹ Portions of this chapter were reprinted from Lam I, Keeney S. (2014) Mechanism and regulation of meiotic recombination initiation. *Cold Spring Harb Perspect Biol.* **7**, a016634.

Meiotic recombination

Meiosis is a specialized cell division that involves ploidy reduction and generates spores in yeast, or gametes in multicellular organisms. Halving the genetic complement occurs through one round of replication followed by two consecutive rounds of chromosome segregation (**Fig. 1.1**). Homologous chromosomes are segregated in the first division (meiosis I), and sister centromeres are separated in the second division (meiosis II).

Prophase of meiosis I is typically subdivided into five stages based on cytological observations: leptotema, zygotema, pachynema, diplonema, and diakinesis (Kleckner 1996; Page and Hawley 2003; Zickler and Kleckner 2015). During the leptotene stage, replicated chromosomes are visible as thin threads and have a tangled appearance, but start to condense. At the zygotene stage, homologous chromosomes begin to synapse and a proteinaceous, tripartite structure called the synaptonemal complex (SC) starts to form between the homologs. By pachynema, homologs are fully synapsed, with the SC extending along their entire lengths. During diplonema, the SC disappears and homologs desynapse, coming apart except at sites where they are physically connected (chiasmata). At diakinesis, spindle fibers form and homologs further condense in preparation for alignment on the metaphase I spindle. Most of the processes described in the following sections pertain to the early stages of meiotic recombination (DSB formation), which begin during leptotema.

Meiotic recombination is a prominent feature of prophase I, and it comprises the formation and repair of programmed DNA DSBs. Meiotic DSBs are generated by the conserved Spo11 protein (**Fig. 1.2**) (Szostak et al. 1983; Sun et al. 1989; Cao et al. 1990; Bergerat et al. 1997; Keeney et al. 1997). Spo11 remains covalently linked to the 5' terminus of each broken DNA strand, but is eventually released by nearby endonucleolytic cleavage, likely by Mre11 endonuclease and/or Sae2, followed by 3' to

5' resection towards the DSB by Mre11 exonuclease activity (de Massy 1995; Keeney and Kleckner 1995; Liu et al. 1995; Neale et al. 2005; Garcia et al. 2011). DNA ends are then resected 5' to 3' by Exo1 exonuclease to expose 3' single-stranded tails (Sun et al. 1991; Zakharyevich et al. 2010). Members of the RecA family of strand exchange proteins (Dmc1, Rad51) bind these tails, forming nucleoprotein filaments that catalyze strand invasion into homologous duplex DNA (Chen et al. 2008b; San Filippo et al. 2008). In meiosis, recombination occurs most often between homologs, but some DSBs are repaired via the sister chromatid (Schwacha and Kleckner 1994; Goldfarb and Lichten 2010).

Recombination can yield reciprocal exchange of chromosome arms flanking the DSB site (crossovers, CO), or no exchange (non-crossovers, NCO) (Hunter 2007; Serrentino and Borde 2012). Most COs are thought to arise through a double Holliday junction (dHJ) intermediate, whereas most NCOs are formed primarily by synthesis-dependent strand annealing (SDSA) (Allers and Lichten 2001; Cromie and Smith 2007b; McMahon et al. 2007) (**Fig. 1.2**). In the dHJ pathway, initial strand invasion is followed by capture of the second DSB end, forming a dHJ that is resolved to generate primarily COs. In SDSA, the invading strand is extended by DNA synthesis, but is then displaced and anneals to the other DSB end.

In many species, the homology search accompanying recombination promotes recognition and pairing of homologs (Burgess 2002; Bhalla and Dernburg 2008). Unlike sister chromatids, which are held together by cohesins as they are synthesized, homologous chromosomes are not usually physically associated with one another. Recombination events that become COs provide physical linkages between homologs, which, combined with sister chromatid cohesion, ensure correct homolog orientation on the meiotic spindle and proper segregation in meiosis I. Depending on the species, absence of recombination or COs results in randomized chromosome segregation,

gamete aneuploidy, meiotic arrest, and/or apoptosis (Székvölgyi and Nicolas 2010). A byproduct of recombination is the reshuffling of maternal and paternal alleles, thereby increasing genetic diversity in progeny (Handel and Schimenti 2010; Székvölgyi and Nicolas 2010).

The cast of players involved in meiotic DSB formation in *S. cerevisiae*

Spo11 generates DSBs to initiate meiotic recombination, but it is not sufficient for DSB formation *in vivo*, as essential partners (referred to as DSB proteins) have been identified in many organisms (**Table 1.1**). In *S. cerevisiae*, this cast includes nine proteins that interact directly or indirectly with Spo11 (Keeney 2001; Hunter 2007; Keeney 2007; de Massy 2013). Null mutants in any of these fail to form DSBs and show reduced sporulation and severely reduced spore viability from chromosome missegregation. The precise molecular function of DSB proteins has been a longstanding question, but recent findings are providing a clearer understanding.

Meiotic DSB formation by Spo11. DSB formation by Spo11 orthologs appears to be a nearly universal feature of meiotic recombination initiation in fungi, invertebrates, mammals, and plants (Keeney 2001; Keeney 2007). A single gene encodes Spo11 in most organisms, but many plants have multiple SPO11 homologs, of which at least one functions in meiotic recombination (Edlinger and Schlögelhofer 2011).

Spo11 is homologous with TopVIA, the catalytic subunit of archaeal topoisomerase VI, a type II DNA topoisomerase (Bergerat et al. 1997; Keeney et al. 1997). Topoisomerase VI is composed of two A and two B subunits that form a heterotetramer (Corbett et al. 2007; Graille et al. 2008). Recently, proteins homologous with the B subunit of topoisomerase VI have been identified as partners of SPO11 in plants (MTOPVIB) and mice (TOPOVIBL) (Robert et al. 2016; Vrielynck et al. 2016). Archaeal TopVIB contains an ATP binding and hydrolysis domain (Corbett et al. 2007;

Graille et al. 2008), but it is not clear whether this is conserved in the meiotic homologs (Robert et al. 2016; Vrielynck et al. 2016).

Structure-function analyses in *S. cerevisiae*, *S. pombe* (Rec12), and *A. thaliana* (SPO11-1) motivated by the crystal structure of Top6A from *M. jannaschii* strongly support the hypothesis that Spo11 catalyzes meiotic DSB formation via a topoisomerase II-like mechanism (Nichols et al. 1999; Diaz et al. 2002; Kan et al. 2010; Shingu et al. 2010). Thus, Spo11 likely dimerizes and cleaves DNA in a transesterification reaction, resulting in phosphodiester links between the active site tyrosines of the Spo11 protomers with the 5' DSB ends. DNA cleavage yields a two-nucleotide 5' overhang (Liu et al. 1995).

Other proteins required for DSB formation. The ten proteins required for DSB formation in *S. cerevisiae* behave functionally as three interacting subgroups or subcomplexes (Spo11-Ski8-Rec102-Rec104, Rec114-Mei4-Mer2, and Mre11-Rad50-Xrs2 [MRX]) (**Fig. 1.3A**) (Keeney 2007; Maleki et al. 2007). Besides the catalytic role of Spo11 and the post-DSB role of the MRX complex in DNA resection and repair, the roles of DSB proteins are not clear. Why does absence of any one of them prevent Spo11 from forming DSBs? Proposed functions include recruiting Spo11 to specific sites, activating Spo11 catalytic activity, and coordinating DSB formation with chromatin and higher-order chromosome structure (Keeney 2007). Recent findings support the latter, and point towards temporal and spatial regulation of Spo11 cleavage by coordinating DSB formation with replication.

Ski8 is involved in RNA metabolism in vegetative cells, but during meiosis it relocates to the nucleus, where it stabilizes the nuclear localization and chromatin association of Spo11, and to a lesser extent, of Rec102-Rec104 (Arora et al. 2004; Kee et al. 2004; Prieler et al. 2005). The WD propeller motif in Ski8 is speculated to function as a scaffold for DSB protein complex assembly, but it is not known whether Ski8

contributes in other ways to DSB formation (Keeney 2007). Rec102 and Rec104 interact with Spo11 and Ski8, and also with Mei4 and Rec114, so one possible role for Rec102 and Rec104 is to bridge the Rec114-Mei4-Mer2 subcomplex with Spo11 and Ski8 (Arora et al. 2004; Maleki et al. 2007). Rec102 and Rec104 behave as a functional unit, and are required for Spo11 nuclear localization, chromatin association, and binding to hotspots (Kee et al. 2004; Prieler et al. 2005; Sasanuma et al. 2007). Rec104 is phosphorylated, but the function of this modification is unknown (Kee et al. 2004) (see **Appendix**). Consistent with the close interaction with Spo11, Rec102 has recently been reported to share structural similarity with archaeal TopVIB (Robert et al. 2016).

Rec114, Mei4, and Mer2 behave as a subcomplex based on two-hybrid, coimmunoprecipitation, and cytological studies (Arora et al. 2004; Henderson et al. 2006; Li et al. 2006). Mer2 is phosphorylated by the S-phase cyclin-dependent kinase (Cdc28-Clb5/Clb6, also referred to as CDK-S) and the Dbf4-dependent kinase Cdc7 (DDK) (Henderson et al. 2006; Murakami and Keeney 2008; Sasanuma et al. 2008; Wan et al. 2008), and these events promote temporal coordination of DSB formation with premeiotic replication (Murakami and Keeney 2008; Murakami and Keeney 2014). Mer2 is also involved in the spatial coordination between DSBs and higher-order chromosome structure (Acquaviva et al. 2012; Sommermeyer et al. 2013). The role of Mer2 in these two regulatory aspects will be discussed further in the next section. Rec114 is phosphorylated in response to DSBs by the DNA-damage signal transduction kinases Tel1 and/or Mec1 (Sasanuma et al. 2008; Carballo et al. 2013). The role of Rec114 phosphorylation is not altogether clear, but it has been proposed to mediate a negative feedback loop to inhibit DSB formation (Carballo et al. 2013).

Mre11 requires all the other DSB proteins (except Rad50) for association with DSB sites, suggesting the MRX complex is recruited last, once Spo11 is poised to make DSBs (Borde et al. 2004). Recruitment of MRX might occur through Xrs2 interaction with

Mer2, dependent on Mer2 phosphorylation by CDK-S (Arora et al. 2004; Henderson et al. 2006). It is speculated that requiring MRX for DSB formation facilitates rapid coordination with repair, ensuring that all breaks are efficiently processed (Borde et al. 2004).

Conservation of DSB proteins in other organisms

Spo11 in other organisms also requires other proteins for break formation (**Table 1.1**) (Cole et al. 2010; Edlinger and Schlögelhofer 2011; de Massy 2013). Some of the *S. cerevisiae* DSB proteins discussed in the preceding section are conserved across phyla, whereas others are unique to species within a narrowly defined clade, or their sequences have diverged to the point of concealing obvious homology. Most meiotic proteins undergo rapid evolutionary divergence (Richard et al. 2005; Keeney 2007), which hinders homology detection. In other instances, homologs of *S. cerevisiae* DSB proteins in other species are not functionally conserved (e.g., MRX, Ski8). Thus, although Spo11 is highly conserved, the other proteins involved and/or the molecular processes that lead to break formation may be more diverged.

DSB proteins in S. pombe. There are six known Rec12 partners (Rec6, Rec7, Rec14, Rec15, Rec24, Mde2), and a chromosome structure component (Rec10) essential for DSB formation (**Fig. 1.3B**) (Cromie and Smith 2007a; Keeney 2007). *S. pombe* does not form SCs, but instead forms structures called linear elements (LinEs) similar to the axial element precursors of the SC in *S. cerevisiae* (Loidl 2006). The LinE protein Rec10 is homologous to *S. cerevisiae* Red1, but is absolutely required for DSB formation in *S. pombe* (Ellermeier and Smith 2005; Lorenz et al. 2006; Bonfils et al. 2011). DSB proteins in *S. pombe* may play a role in recruiting Rec12 to chromatin and/or activating Rec12. Other chromosome structure proteins (Rec25, Rec27, Mug20) are not essential for DSB formation, but determine DSB hotspot location, and likely stabilize or

activate Rec12 already bound to chromatin (Fowler et al. 2013). MRX orthologs (Rad32-Rad50-Nbs1) are required for repair of meiotic DSBs but not their formation (Young et al. 2004).

Rec7, Rec15, and Rec24 are orthologs of *S. cerevisiae* Rec114, Mer2, and Mei4, respectively, and form the SFT subcomplex (Seven, Fifteen, Twenty-four) (Malone et al. 1997; Molnar et al. 2001; Kumar et al. 2010; Miyoshi et al. 2012). As in budding yeast and mouse, Rec7 (Rec114) and Rec24 (Mei4) physically interact, and co-localize with LinEs independently of DSBs through Rec10-Rec15 (Mer2) interaction (Lorenz et al. 2006; Steiner et al. 2010; Bonfils et al. 2011; Miyoshi et al. 2012). Rec7 is phosphorylated independently of DSB formation, but the kinase responsible and the role for the modification are unknown (Miyoshi et al. 2012).

Rec6 and Rec14, along with Rec12, form the DSBC subcomplex (DSB Catalytic core) (Miyoshi et al. 2012). Rec6 is the ortholog of *S. cerevisiae* Rec102, mouse TOPOVIBL, plant MTOPVIB, and fly MEI-P22 (Robert et al. 2016), whereas Rec14 is the ortholog of *S. cerevisiae* Ski8 (Evans et al. 1997). Mde2 interacts with components in both SFT and DSBC complexes, and is thought to bridge the two subcomplexes (Miyoshi et al. 2012). No orthologs of Mde2 have been identified (Gregan et al. 2005).

DSB proteins in mouse. Several mouse proteins are known or hypothesized to be required along with SPO11 to generate DSBs (MEI1, MEI4, REC114, TOPOVIBL, IHO1). It is not known whether mouse MRX orthologs (MRE11, RAD50, NBS1) are required for meiotic DSB formation because they are essential for viability (Xiao and Weaver 1997; Luo et al. 1999; Zhu et al. 2001), but their role in repair of meiotic DSBs appears to be conserved (Borde 2007; Cherry et al. 2007; Kumar and de Massy 2010). WDR61 is the Ski8/Rec14 homolog, but whether its meiotic function is conserved is not known (Kumar and de Massy 2010).

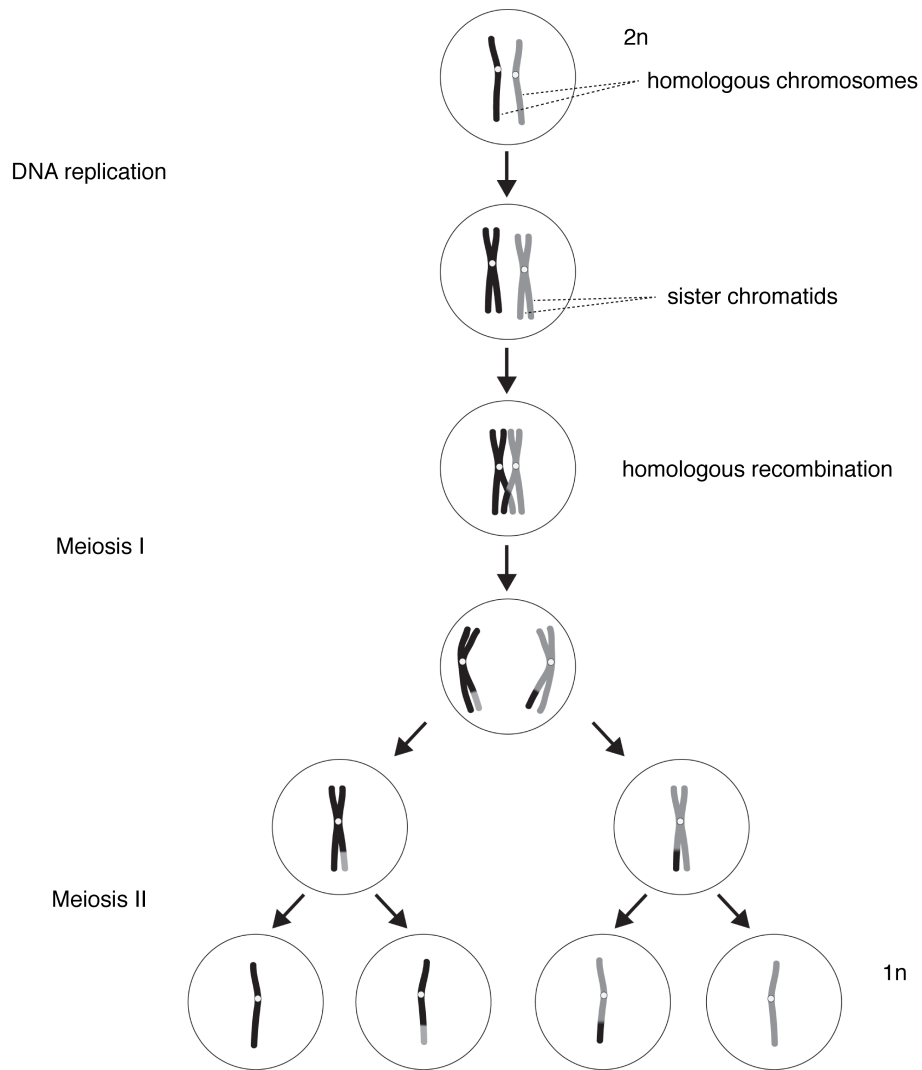


Figure 1.1. Reductional and equational divisions in meiosis. In meiosis, the genome content of the parental cell ($2n$) is reduced in half by undergoing two consecutive rounds of division following one round of DNA replication (premeiotic S phase). After replication, each homologous chromosome consists of a pair of sister chromatids. Meiosis I is a reductional division in which homologous chromosomes are segregated. Homologous recombination is required at this stage to bring together each paternal and maternal homolog pair and physically connect them, thereby allowing their correct segregation onto daughter cells. Meiosis II is an equational division in which sister chromatids are segregated. Note that besides the difference in ploidy, the genome contents of the products of meiosis (spores in fungi, gametes in multicellular organisms) are not entirely identical to that of the progenitor cell due to reassortment of alleles between the paternal and maternal homolog that occurred during recombination.

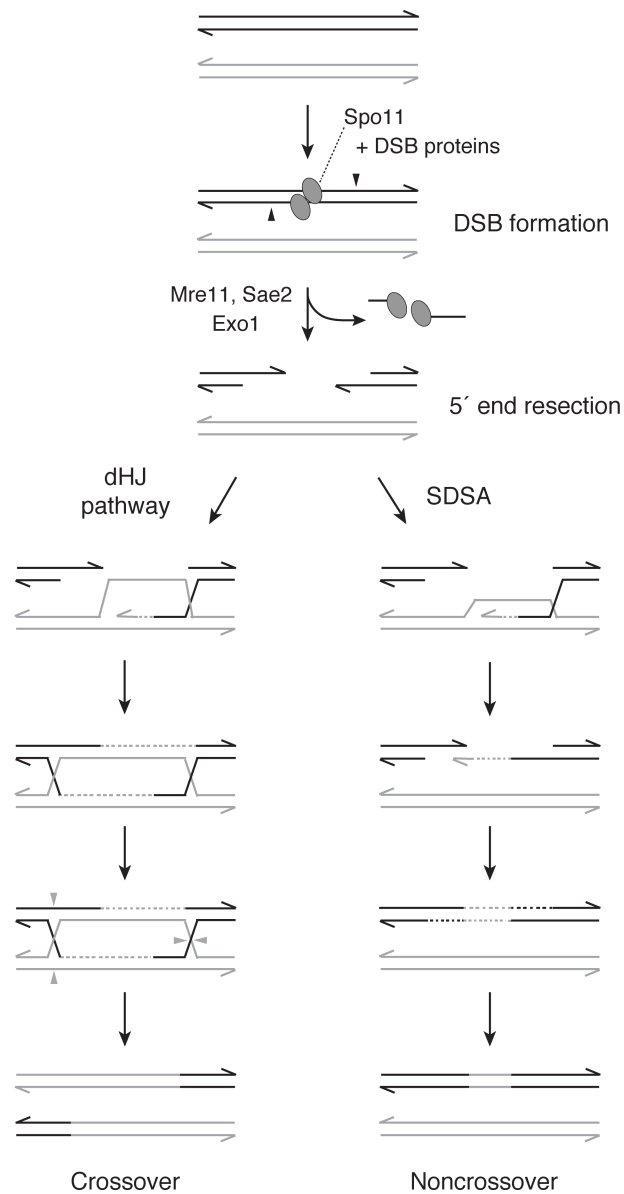


Figure 1.2. The meiotic recombination pathway. A segment of one sister chromatid from each homolog (black, gray) is shown. Spo11 (ovals) generate DNA DSBs, in association with partner proteins. Endonucleolytic cleavage on either side of the DSB (black arrowheads) releases Spo11 covalently attached to a short oligonucleotide. The DNA ends undergo 5' to 3' resection. A 3' ssDNA tail invades a homologous duplex DNA and initiates repair synthesis. Repair can proceed by either a double Holliday Junction (dHJ) pathway, or synthesis-dependent strand annealing (SDSA). Only one cleavage pattern for dHJ resolution is shown (gray arrowheads). Note that the allele receiving the DSB (black) copies information from the uncut allele (gray) during its repair, a process referred to as biased gene conversion. Adapted from (Lam and Keeney 2014).

Table 1.1. List of proteins required for meiotic DSB formation in different organisms

<i>S. cerevisiae</i>	<i>S. pombe</i>	<i>M. musculus</i>	<i>C. elegans</i>	<i>D. melanogaster</i>	<i>A. thaliana</i>
Spo11	Rec12	SPO11	SPO11	MEI-W68	SPO11-1 SPO11-2 SPO11-3*
Ski8	Rec14	WDR61 [#]			SKI8/VIP3*
Rec102	Rec6	TOPOVIBL		MEI-P22	MTOPVIB
Rec104					
Rec114	Rec7	REC114			PHS1*
Mei4	Rec24	MEI4			PRD2
Mer2	Rec15	IHO1/CCDC36			
Mre11	Rad32*	MRE11 [#]	MRE-11		MRE11*
Rad50	Rad50*	RAD50 [#]	RAD-50 [§]		RAD50*
Xrs2	Nbs1*	NBS1 [#]			NBS1*
	Mde2				
		MEI1			PRD1
			DSB-1		
			DSB-2 [§]		
			HIM-5 [§]		
			HIM-17		
			REC-1 [§]		
				Trem	
				Vilya	
					PRD3
					SWI1
					DFO
Red1 [§]	Rec10	SYCP3 ^{*a}			ASY3
Hop1 [§]	Hop1 [§]	HORMAD1 [§] HORMAD2 [§]	HIM-3*		ASY1*
			HTP-1 [§] HTP-2* HTP-3 [§]		

[§] Partial contribution to meiotic DSB formation

* No detectable contribution to meiotic DSB formation

[#] Role in DSB formation is not known

^a Weak sequence similarity also reported with SYCP2 (see text)

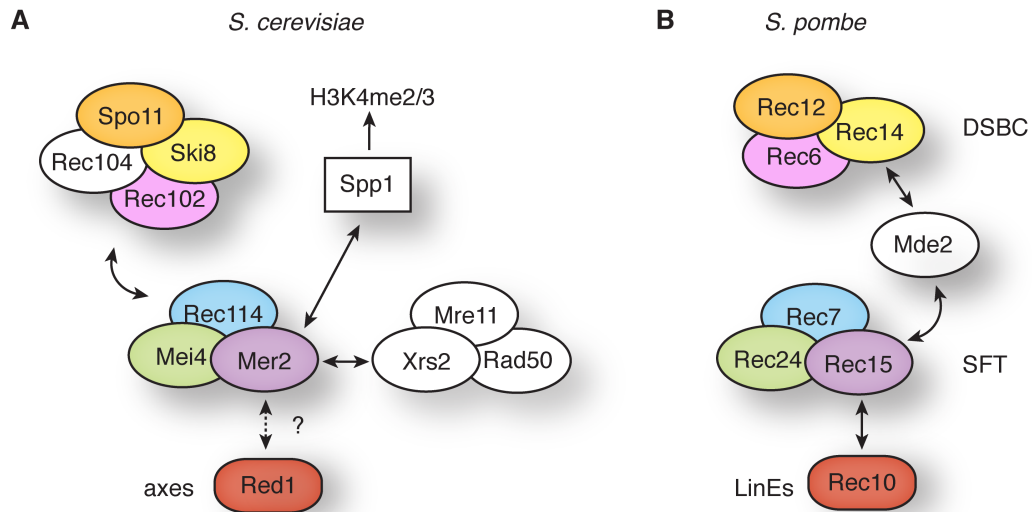


Figure 1.3. Interaction maps of DSB proteins in *S. cerevisiae* and *S. pombe*. (A) In *S. cerevisiae*, the 10 proteins required for DSB formation form three interacting subcomplexes. Mer2 also interacts with Spp1, which recognizes and binds H3K4me2/me3 marks on chromatin loops. Mer2 and other DSB proteins localize to the chromosome axes, but it is not known whether this is via interaction with the axial element protein Red1 (dashed arrows and question mark), analogous to the interaction of their homologous proteins in *S. pombe*. (B) In *S. pombe*, the 7 proteins required for DSB formation form two subcomplexes (DSBC and SFT) that interact via Mde2. Rec15 in the SFT interacts with Rec10, a component of linear elements (LinEs) similar to axial elements in *S. cerevisiae*. Homologous proteins are shown in the same color for the two species; proteins with no known homologs (or the homolog is not involved in DSB formation) in the other species are shown in white (except for Spp1, whose homolog in *S. pombe* is not shown). Since *S. cerevisiae* Rec104 and *S. pombe* Mde2 are the only DSB proteins without an identified homolog in the other species, it is plausible that Rec104 and Mde2 are distantly related. Adapted from (Lam and Keeney 2014).

MEI1 is required for DSB formation, as *Mei1*^{-/-} mutant spermatocytes exhibit many phenotypes similar to *Spo11*^{-/-} mutants (Baudat et al. 2000; Romanienko and Camerini-Otero 2000; Di Giacomo et al. 2005): reduced staining for γH2AX (a phosphorylated form of histone H2AX that is a marker of DSBs), absence of RAD51 foci, defective chromosome synapsis and prophase I arrest (Libby et al. 2002; Libby et al. 2003; Reinholdt and Schimenti 2005). The biochemical function of MEI1 is unknown. No orthologs have been found in invertebrates (Libby et al. 2003), but MEI1 shares modest homology with plant PRD1. It is unknown whether MEI1 physically interacts with SPO11, as for PRD1 (De Muyt et al. 2007).

MEI4 localizes to discrete foci on chromosome axes independent of SPO11 but dependent on MEI1, the meiosis-specific cohesin subunits RAD21L and REC8, and the axial element component HORMAD1 (Kumar et al. 2010; Kumar et al. 2015). *Mei4*^{-/-} spermatocytes exhibit greatly reduced γH2AX; lack of RAD51, DMC1, and RPA foci; synapsis defects; and meiotic prophase arrest, which are diagnostic of failure to make DSBs (Kumar et al. 2010). MEI4 interacts with REC114 via conserved motifs in the N-terminal region (Kumar et al. 2010), as also seen in *S. cerevisiae* and *S. pombe* orthologs (Maleki et al. 2007; Steiner et al. 2010).

TOPOVIBL was identified in mouse through weak homology with plant MTOPVIB (discussed below) (Robert et al. 2016). TOPOVIBL interacts with SPO11 (specifically the SPO11β splice variant responsible for the majority of DSBs in mice (Kauppi et al. 2011)), and these two proteins appear to assemble into a heterotetramer like archaeal topoisomerase VI (Robert et al. 2016). *Top6b*^{-/-} spermatocytes exhibit all the hallmark features manifested by lack of meiotic DSBs: reduced γH2AX levels, undetectable RPA foci, and persistence of MEI4 foci (Robert et al. 2016).

IHO1/CCDC36 is the functional equivalent of *S. cerevisiae* Mer2 and *S. pombe* Rec15; IHO1 exists as a chromatin-bound complex with REC114 and MEI4, and

contains coiled-coil domain like Mer2/Rec15 (Stanzione et al. submitted). IHO1 is required for DSB formation, as indicated by the absence of detectable RAD51, DMC1, and RPA foci, and SPO11-oligonucleotide complexes in *Iho1*^{-/-} spermatocytes (Stanzione et al. submitted). HORMAD1 physically interacts with and recruits IHO1 to chromosome axes, thus implicating break formation within the context of higher-order chromosome structure (Stanzione et al. submitted).

DSB proteins in *A. thaliana*. Several *A. thaliana* genes required for DSB formation have been identified through genetic screens (*PRD1*, *PRD2*, *PRD3*, *MTOPVIB*, *SWI1*, *DFO*) (Edlinger and Schlögelhofer 2011; Mercier et al. 2015; Vrielynck et al. 2016). Some are homologs of DSB proteins in yeasts or mammals (*PRD1*, *PRD2*, *MTOPVIB*), whereas the rest have no clear homologs outside the plant kingdom. Besides *PRD1* and *MTOPVIB*, it is not known whether these DSB proteins interact with *SPO11*, or amongst themselves in an interaction network similar to those in yeasts. *MRX* and *Ski8* homologs in plants are dispensable for DSB formation (Bleuyard et al. 2004; Pawlowski et al. 2004; Puizina et al. 2004; Jolivet et al. 2006).

PRD1, *PRD2*, *PRD3*, and *MTOPVIB* are the orthologs of *MEI1*, *Mei4/Rec24*, rice *PAIR1*, and *Rec102/Rec6/TOPOVIBL/MEI-P22*, respectively (Nonomura et al. 2004; De Muyt et al. 2007; De Muyt et al. 2009; Kumar et al. 2010; Vrielynck et al. 2016). Mutants in any of these four genes exhibit a range of phenotypes consistent with failure to make DSBs (De Muyt et al. 2007; De Muyt et al. 2009; Vrielynck et al. 2016). *PRD1* interacts with itself and *SPO11-1* (De Muyt et al. 2007). *PRD2* and *PRD3* were initially identified as proteins with coiled-coil motifs with no homologs outside of the plant kingdom (De Muyt et al. 2009). However, sequence motifs in *PRD2* were subsequently found to exhibit homology with short signature sequence motifs in fungal *Mei4/Rec24* (Kumar et al. 2010). *MTOPVIB* forms a complex with *SPO11-1* and *SPO11-2* and is required for *SPO11-1/SPO11-2* heterodimer formation in *A. thaliana*; thus, it has been proposed that

SPO11-1, SPO11-2, and two MTOPVIB subunits form a heterotetramer similar to the topoisomerase VI complex comprising two A subunits and two B subunits (Vrielynck et al. 2016).

SWI1/DYAD is required for DSB formation, and is also involved in sister chromatid cohesion, axial element formation, homolog pairing and synapsis, recombination, and proper histone modification during prophase I (Mercier et al. 2001; Agashe et al. 2002; Mercier et al. 2003; Hamant et al. 2006; Boateng et al. 2008). DFO also exhibits impaired DSB formation, and is predicted to have structural motifs (coiled-coil, helix-turn-helix) that might mediate protein-protein interactions and DNA binding (Zhang et al. 2012).

DSB proteins in D. melanogaster. In *Drosophila*, three proteins are known to be required for DSB formation besides the Spo11 ortholog MEI-W68: MEI-P22 (Liu et al. 2002; Mehrotra and McKim 2006), Trem (Page et al. 2007; Lake et al. 2011), and Vilya (Lake et al. 2015). MEI-P22 is the homolog of fungal Rec102/Rec6, mouse TOPOVIBL, and plant MTOPVIB (Robert et al. 2016). MEI-P22 forms discrete foci on meiotic chromosomes, independently of DSBs, but dependent on Trem (Mehrotra and McKim 2006; Lake et al. 2011). Trem (Trade embargo) is a C2H2 zinc finger protein, and may have a separate role in fertility (Page et al. 2007; Lake et al. 2011). Hawley and colleagues hypothesize that the failure to form DSBs in *trem* mutants is due to the failure in MEI-P22 foci formation (Lake et al. 2011). Vilya physically interacts with MEI-P22 and localizes to DSB sites as discrete foci (Lake et al. 2015). Vilya shares homology with Zip3-like proteins (N-terminus RING domain, coiled-coil domain in the middle of the protein, serine-rich C-terminus) and is a component of recombination nodules, which mark the sites of CO formation (Lake et al. 2015). Vilya has been proposed to link DSB formation with recombination outcome, and its requirement for DSB formation may be through its interaction with MEI-P22 (Lake et al. 2015).

DSB proteins in *C. elegans*. Several *C. elegans* proteins besides SPO-11 are involved in meiotic recombination initiation (MRE-11, RAD-50, DSB-1, DSB-2, HIM-17, HIM-5, REC-1, HTP-3), but it is not yet clear whether their roles are direct or indirect.

DSB-1 is essential for DSB formation (Stamper et al. 2013). On the other hand, its paralog DSB-2 is not essential but is required for efficient DSB formation (Rosu et al. 2013). DSB-1 and DSB-2 show a similar localization pattern, associating with chromatin independently of DSBs from early meiotic prophase to mid-pachytene, which corresponds to the stage of DSB formation (Rosu et al. 2013; Stamper et al. 2013). Chromatin association of DSB-1 and DSB-2 are thought to indicate a DSB-permissive state, and formation of CO recombination intermediates triggers the removal of DSB-1 and DSB-2 from chromatin, which presumably inactivates DSB formation, thus invoking an obligate CO checkpoint or a negative feedback mechanism (Rosu et al. 2013; Stamper et al. 2013). No homologs of DSB-1 or DSB-2 have been found outside the genus *Caenorhabditis*. Both DSB-1 and DSB-2 have potential target sites for ATM/ATR family of protein kinases, but it is not known whether they are phosphorylated (Rosu et al. 2013; Stamper et al. 2013).

HIM-17 is required for meiotic DSB formation and proper accumulation of H3K9 methylation on prophase chromosomes (Reddy and Villeneuve 2004). HIM-17 has six C2CH repeat modules seen in zinc finger DNA binding motifs (Reddy and Villeneuve 2004). It is not known whether the H3K9 methylation is a prerequisite for SPO-11 to cleave DNA, or whether these are two separate roles of HIM-17. Thus, it is possible that the effect of HIM-17 on DSB formation is indirect, through histone modifications that alter chromosome structure and make it amenable for SPO-11 catalytic activity. HIM-5 promotes DSBs specifically on the X chromosome, but loss of function alters the crossover distribution in both the X chromosome and the autosomes (Broverman and Meneely 1994; Meneely et al. 2012). HIM-5 could be targeting SPO-11 activity to the X

chromosome, either directly as a partner protein, or indirectly by modifying the heterochromatin on the X and distal autosome regions (Meneely et al. 2012). REC-1 is a distant paralog of HIM-5 that is phosphorylated by CDK *in vitro* (Chung et al. 2015). DSB formation is moderately reduced in the *rec-1* mutant, but severely reduced in the *rec-1*; *him-5* double mutant (Chung et al. 2015).

HTP-3 is a paralog of the axis protein HIM-3 (homolog of *S. cerevisiae* Hop1) and forms complexes with both MRE-11/RAD-50 and HIM-3, which has been proposed to link DSB formation with homolog alignment and synapsis (Zetka et al. 1999; Chin and Villeneuve 2001; Alpi et al. 2003; Couteau et al. 2004; Goodyer et al. 2008). HTP-3 and HIM-3 complex formation (as well as other combinations of HTP-3, HIM-3, and HTP1-2) occur through interactions between the N-terminal HORMA domain of one molecule with the C-terminal closure motif of another molecule, giving rise to hierarchical complexes (Kim et al. 2014). HTP-3 is required for DSB formation, is a component of meiotic axes, and is required for HIM-3 localization to axes, homolog alignment, synapsis, and crossing over (Goodyer et al. 2008). Unlike yeast or mouse, meiotic recombination is not necessary for homolog recognition, presynaptic alignment, and synapsis in worms, therefore the role of HTP-3 in DSB formation and downstream recombination events likely reflect separate functions in recombination (Dernburg et al. 1998; McKim et al. 1998; Goodyer et al. 2008).

The meiotic DSB landscape in yeast

The location of DSBs and subsequent recombination is important for genome integrity. DSBs in repetitive DNA sequence (e.g., rDNA, transposable elements) are at risk of genome rearrangement if repaired using nonallelic homologous sequences as template (Sasaki et al. 2010). Crossovers near centromeres cause an elevated

frequency of precocious separation of sister chromatids at meiosis I, resulting in aneuploidy and spore inviability in yeast (Rockmill et al. 2006). Nonetheless, where Spo11 generates a DSB (or not) is not determined by a single factor, but rather by multiple factors operating collectively over different size scales (**Fig. 1.4**). Factors that shape the DSB landscape can be grouped conceptually into two categories: intrinsic and extrinsic (Keeney et al. 2014). Intrinsic factors are features of the chromosome (“substrate”) and the DSB-forming machinery (“enzyme”) that dictate preferences for where DSBs occur. These involve accessibility or activity of Spo11 towards specific locations along chromosomes. Extrinsic factors are features layered on top of the intrinsic features, and these tend to be more dynamic and regulatory (e.g., feedback circuits). Intrinsic factors are properties inherent to the enzyme-substrate relationship, whereas extrinsic factors tend to be properties that allow modification of the DSB-likelihood in a responsive manner as meiosis proceeds. This will be discussed in more detail for *S. cerevisiae*, where it is best understood, but emerging evidence suggest that multiple layers govern the spatial distribution of DSBs in other organisms as well.

Approaches for mapping the DSB landscape

Several methods have been developed over the years to map where Spo11 makes DSBs genome-wide. Gerton, Petes and colleagues generated the first genome-wide map of meiotic DSBs by harnessing microarray technology (Gerton et al. 2000). Covalent protein-DNA fragments in a *rad50S* mutant were purified and used as hybridization probes on DNA microarrays containing all *S. cerevisiae* open reading frames. In the *rad50S* mutant, Spo11 release from the break ends is blocked, so DSBs are not resected or repaired, resulting in enrichment of DSBs with covalent Spo11 association (Alani et al. 1990; Keeney et al. 1997).

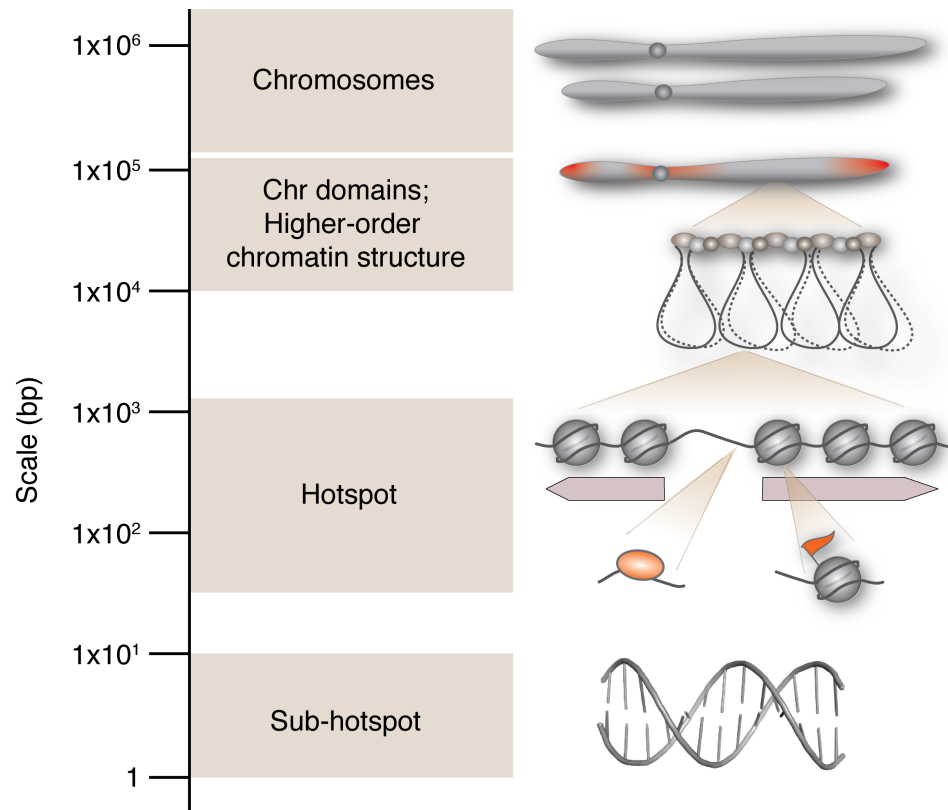


Figure 1.4. A combination of factors operating at different size scales influences the distribution of breaks in the DSB landscape. At the whole-chromosome scale, shorter chromosomes exhibit higher density of DSBs than longer chromosomes, attributed to homolog engagement feedback inhibition on DSBs. Chromosomal subdomains exhibit regions where DSBs are suppressed (near centromeres, telomeres, rDNA array) and regions where DSBs preferentially occur, such as chromatin loops within interstitial regions of chromosomes. DSBs at the hotspot scale are influenced by promoter nucleosome organization, histone modifications, and transcription factors. At the sub-hotspot scale, DSB formation is influenced by local base composition.

A subsequent approach to map meiotic DSBs was done in a *dmc1* mutant, since *rad50S* (and *rad50S*-like) mutants exhibit altered DSB distributions (reduced DSBs near centromeres, telomeres, and late-replicating regions) (Baudat and Nicolas 1997; Borde et al. 2000; Blat et al. 2002). In *dmc1* mutants, DSBs are resected but not repaired (Bishop et al. 1992). Two groups independently purified single-stranded DNA (ssDNA) in *dmc1* mutants by chromatography on benzoylated naphthoylated DEAE-cellulose and hybridized to whole-genome microarrays (Blitzblau et al. 2007; Buhler et al. 2007).

More recently, Pan, Sasaki, Keeney, and colleagues developed a method to map meiotic DSBs at near-nucleotide resolution in wild-type backgrounds (Pan et al. 2011). This method takes advantage of the release of Spo11 covalently linked to short oligos after break formation (Neale et al. 2005). Two major classes of Spo11-oligo complexes are detected when resolved by SDS-PAGE; one class consists of Spo11 covalently linked to oligos ~21–37 nt long, and the other class to oligos ≤12 nt (Neale et al. 2005). These Spo11-oligo complexes, particularly the nucleotide at the 5' end of oligos, represent the precise genomic locations where Spo11 cleaved DNA. Spo11-oligo complexes are immunoprecipitated, deproteinized to digest Spo11 protein, and the oligos deep sequenced. Genomic regions where the 5' ends of oligos map with high frequency represent DSB hotspots.

Intrinsic factors that shape the DSB landscape

In budding yeast, approximately 160 DSBs form in each cell undergoing meiosis (Buhler et al. 2007; Pan et al. 2011). Meiotic DSBs are not randomly distributed along chromosomes, but instead display multiple levels of spatial organization that interact hierarchically with one another (Lichten and Goldman 1995; Petes 2001; Kauppi et al. 2004; Lichten and de Massy 2011; Pan et al. 2011; Cooper et al. 2016). Locally, there are narrow regions (typically ~200 bp) where Spo11 cleaves preferentially, referred to as

DSB hotspots. Importantly, not one factor provides complete predictive power for whether a region will be cleaved by Spo11 (Pan et al. 2011; Cooper et al. 2016). For example, a promoter nucleosome-depleted region (NDR) might not be a favored site for DSB formation if it is located close to the chromosome axis (Ito et al. 2014).

Spo11 cleavage preferences. Spo11 has no target sequence specificity, but sequence biases are detectable. Spo11 cleavage is favored 3' of C, and cleavage 3' of G is disfavored (Murakami and Nicolas 2009; Pan et al. 2011). Spo11 binds preferentially to AT-rich sequence, as seen in sequence bias 10–12 bp surrounding the cleavage site, and it binds preferentially to GC-rich sequence 11–16 bp to the right and left of the cleavage site (Pan et al. 2011). The latter preference may reflect the preferential binding of a Spo11-interacting protein or a Spo11 domain not modeled by the archaeal Spo11 homolog Top6A.

H3K4 trimethylation. Post-translational histone modification, in the form of H3K4 methylation, influences DSB sites. H3K4 trimethylation (H3K4me3) is enriched at the 5' end of genes, and is a histone mark associated with active transcription (Pokholok et al. 2005; Dehé and Géli 2006). In *S. cerevisiae*, Set1 is the catalytic subunit of the COMPASS complex responsible for all H3K4me, and DSB levels are reduced in the *set1* mutant, with sites of high H3K4me3 affected the most, and some novel DSB hotspots arising (Sollier et al. 2004; Dehé and Géli 2006; Borde et al. 2009; Acquaviva et al. 2012; Sommermeyer et al. 2013; Zhu 2015). However, the spatial correlation between H3K4me3 and DSB levels is weak genome-wide, and H3K4me3 abundance is a poor predictor of DSB hotspot location or heat (Tischfield and Keeney 2012). H3K4me3 is involved in coordinating DSB formation with higher-order chromosome structure (discussed further below) (Acquaviva et al. 2012; Sommermeyer et al. 2013).

Nucleosome occupancy. Most hotspots in *S. cerevisiae* are influenced by chromatin accessibility, and 88% are within NDRs in gene promoters (Ohta et al. 1994;

Wu and Lichten 1994; Berchowitz et al. 2009; Pan et al. 2011). However, chromatin accessibility is not sufficient, that is, not all NDRs are DSB hotspots. For example, NDRs at the 3' end of genes are not favored sites for Spo11 cleavage (Pan et al. 2011).

Transcription factors. DSB hotspots in budding yeast tend to be located in promoter regions; thus a natural question that follows is whether transcription factors are involved in promoting break formation. Binding of transcription factors Rap1, Bas1, and Bas2 at the *HIS4* promoter, but not transcription, stimulates recombination at that hotspot, possibly by influencing chromatin structure or interacting with the DSB machinery (White et al. 1993; Petes 2001). Transcription factors could also hypothetically occlude Spo11 access to DNA, preventing DSB formation at their binding sites. Systematic comparison of transcription factor binding sites and Spo11-oligo frequency indicated that some transcription factors show evidence for DSB occlusion at their binding sites, but others do not (Pan et al. 2011). However, transcription factor binding is not predictive of DSB frequency at the hotspot (Pan et al. 2011). Global analysis of Bas1 and Ino4 transcription factor binding sites and DSB hotspots in the absence of these transcription factors revealed that the effect of transcription factors on hotspot activity is highly context dependent (Mieczkowski et al. 2006; Zhu and Keeney 2015). In the absence of the transcription factor, some hotspots with binding site(s) for the transcription factor became hotter, others were unaffected, and yet others became colder. Changes to hotspot heat did not correlate with chromatin accessibility, H3K4me3, or transcript levels (Zhu and Keeney 2015).

Subchromosomal domains. At the chromosome level, DSBs form preferentially on chromosome arms, and are less frequent within pericentric and subtelomeric zones (~5–10 kb around centromeres and ~20 kb from telomeres) (Gerton et al. 2000; Blitzblau et al. 2007; Buhler et al. 2007; Pan et al. 2011). DSBs and recombination are also suppressed in regions flanking and within the repetitive ribosomal DNA (rDNA) array—

consisting of ~140 copies of a 9.1 kb repeat on chromosome XII (Petes and Botstein 1977; Eickbush and Eickbush 2007; Pan et al. 2011).

Centromere-proximal crossovers are associated with increased risk of chromosome missegregation (Hassold and Hunt 2001; Rockmill et al. 2006; Nambiar and Smith 2016). Cells suppress pericentric recombination through two distinct layers mediated by the Ctf19 kinetochore complex, one operating at the level of DSB formation, and the other at the repair stage by suppressing CO and NCO recombination (Vincenten et al. 2015). The highly repetitive DNA in subtelomeres and the rDNA array are potentially prone to non-allelic homologous recombination (Louis 1995; Sasaki et al. 2010). DSB suppression at subtelomeric regions and the rDNA are mediated in part by Sir2 histone deacetylase, presumably through heterochromatin formation, and also possibly by excluding Hop1 from the rDNA (Gottlieb and Esposito 1989; Fan and Petes 1996; San-Segundo and Roeder 1999; Mieczkowski et al. 2007). DSB suppression at the outermost rDNA repeats is mediated by the meiotic ATPase Pch2, which is recruited to the nucleolus by the origin recognition complex subunit Orc1 (Vader et al. 2011).

Within interstitial regions of the chromosome there are DSB-rich and DSB-poor domains on the order of ~100 kb (Baudat and Nicolas 1997; Borde et al. 1999). Within these domains, DSBs preferentially form in GC-rich chromatin loop regions rather than AT-rich axis-associated DNA (Blat et al. 2002; Kleckner 2006).

Loop-axis organization and targeting of DSBs. DSB formation and recombination are tightly integrated with higher-order chromosome structure. Pairs of sister chromatids are organized into a series of loops (~10–20 kb in budding yeast) anchored at their bases along a structural axis called the axial element (**Fig. 1.5A**) (Kleckner 1996; Zickler and Kleckner 1999; Kleckner 2006). At the pachytene stage, homologous chromosomes are held together along their lengths by the SC (**Fig. 1.5B**). The SC comprises two lateral elements (formerly the axial element of each homolog)

held together by transverse filaments (Zickler and Kleckner 1999). Axial elements are enriched with several protein components, which in budding yeast include Red1, Hop1, cohesin proteins Smc3 and Rec8, and condensin (Smith and Roeder 1997; Klein et al. 1999; Yu and Koshland 2003; Panizza et al. 2011).

DSBs form preferentially in chromatin loops, not the DNA embedded in axes as defined by ChIP enrichment for Rec8 and other axis components (Blat et al. 2002; Glynn et al. 2004; Kugou et al. 2009; Pan et al. 2011; Panizza et al. 2011; Ito et al. 2014). However, cytologically detectable recombination complexes containing Rad51 and/or Dmc1 are associated with axial elements and the SC in various organisms examined, so recombination takes place in the context of chromosome axes (Ashley et al. 1995; Anderson et al. 1997; Barlow et al. 1997; Moens et al. 1998; Tarsounas et al. 1999; Blat et al. 2002; Panizza et al. 2011). This apparent paradox—DSBs are in loops but recombination occurs on axes—can be resolved by the “tethered loop-axis complex” (TLAC) model of Kleckner and colleagues, in which DSB sites in loop DNA are recruited to the proximity of the axes (Blat et al. 2002; Kleckner 2006; Panizza et al. 2011). In principle, tethering could occur before or after DSB formation, but the observation that many DSB proteins are themselves enriched at axes supports a pre-DSB tethering model (Kleckner 2006; Panizza et al. 2011). TLAC structures may help ensure that DSBs form in the context of chromosome axes, thereby promoting interhomolog (IH) repair and thus accurate segregation of homologous chromosomes (Kim et al. 2010; Panizza et al. 2011). As discussed below, most available data can be interpreted in light of this model, but it is important to note that there is as yet no direct demonstration of TLACs.

Recent findings provide a mechanism for loop tethering through physical interaction between Mer2 and Spp1 (Acquaviva et al. 2012; Sommermeyer et al. 2013). Spp1 is part of the COMPASS complex (Set1 is the catalytic subunit) and has a PHD

finger motif that binds H3K4me2/me3 marks (Dehé et al. 2006; Shi et al. 2007; Murton et al. 2010). Simultaneous interaction of Spp1 with H3K4me2/me3 and with Mer2 via its C-terminus is proposed to tether chromatin loops to DSB proteins localized on the chromosome axes, thereby activating DSB formation in the NDR near the tethered portion of the chromatin loop (**Fig. 1.6B**). In the absence of normal function of this tethering mechanism (e.g., in *set1* or H3K4R mutants where there is no H3K4me), novel DSB hotspots appear, mostly at promoters of genes transcriptionally induced in *set1* or in chromatin loop regions closest to the axes (Sollier et al. 2004; Borde et al. 2009; Acquaviva et al. 2012; Sommermeyer et al. 2013). Thus, the Mer2-Spp1-H3K4me2/3 interaction influences the location of DSBs.

Axis proteins are required for normal levels of meiotic DSBs (discussed further in a later section). Their requirement for normal levels of DSBs may reflect the close spatial relationship between DSB formation and axial elements.

Extrinsic factors that shape the DSB landscape

Besides the intrinsic factors described above that make chromosomal regions favorable for Spo11-mediated DSBs (i.e., that determine hotspot locations), the DSB landscape is also shaped by extrinsic factors. Extrinsic factors regulate the timing of DSB formation and DSB frequency. Several feedback networks regulate DSB homeostasis by limiting the number of potentially hazardous DSBs, while also promoting sufficient numbers to ensure chiasma formation.

Regulation of DSB timing. DSBs are tightly controlled so that they occur at the right time and place. Meiotic DSB formation appears to be universally restricted to a narrow window of time within prophase I (Padmore et al. 1991; Cervantes et al. 2000; Mahadevaiah et al. 2001; Colaiácovo et al. 2003; Jang et al. 2003; Mehrotra and McKim

2006). In yeast, DSBs occur ~1 to 1.5 hours after premeiotic DNA replication (Borde et al. 2000; Cervantes et al. 2000; Murakami et al. 2003).

One way cells control when DSBs start to form is through gene expression, e.g., regulated meiosis-specific transcription of *SPO11* and other genes required for meiotic DSBs, or by meiosis-specific splicing (Keeney 2001; Keeney 2007). Another level of control is through coordination with premeiotic replication. In *S. cerevisiae*, DSB formation follows premeiotic replication through the dual roles of CDK-S and DDK kinases in replication origin firing and DSB formation (Schild and Byers 1978; Sclafani 2000; Smith et al. 2001; Masai and Arai 2002; Benjamin et al. 2003). The coordinate timing between replication and DSB formation is speculated to arise from competition for kinase activities, whereby lower levels are sufficient for replication origin firing, but onset of DSB formation occurs only after increased levels of kinase activity are available (Murakami and Keeney 2008). Recent findings suggest that the replication-DSB link is also more directly coordinated through physical association of DDK with replisome components (Murakami and Keeney 2014). Chromatin-bound Mer2 is phosphorylated by DDK upon replication fork passage, and this post-translational modification then recruits Rec114 and other proteins required for DSB formation (**Fig. 1.6A**) (Henderson et al. 2006; Sasanuma et al. 2008; Panizza et al. 2011; Murakami and Keeney 2014). Interestingly, premeiotic replication is not an absolute prerequisite for DSB formation (Hochwagen et al. 2005; Blitzblau et al. 2012) but DSB formation on partially replicated chromosomes is prevented by a Mec1-dependent checkpoint (Blitzblau and Hochwagen 2013).

Cells also regulate the termination of DSB activity, but how this is controlled is less clear (Padmore et al. 1991; Keeney 2001; Henderson et al. 2006). In *S. cerevisiae*, Spo11 and other DSB proteins persist on chromosomes past the time of DSB formation, and this is also observed for mouse SPO11 (Romanienko and Camerini-Otero 2000;

Arora et al. 2004; Kee et al. 2004; Prieler et al. 2005; Henderson et al. 2006; Li et al. 2006; Maleki et al. 2007). This suggests DSB formation is not simply regulated by eliminating the participating proteins. Instead, restriction of DSB formation to a narrow window of time may be under more direct cell cycle control. *S. cerevisiae* mutants that arrest in pachytene (e.g., *ndt80*, *cdc28*, *cdc36*, and *cdc39*) exhibit increased recombination frequency and detectable DSBs at later meiotic time points (Shuster and Byers 1989; Xu et al. 1995; Allers and Lichten 2001), suggesting that DSBs continue to form in pachytene-arrested cells and further implying that progression past pachynema and/or prophase terminates the window of opportunity for break formation (Allers and Lichten 2001; Keeney 2001; Henderson et al. 2006). Recent studies confirm these earlier observations, providing evidence that more DSBs are made in the absence of Ndt80 (Argunhan et al. 2013; Carballo et al. 2013; Gray et al. 2013; Rockmill et al. 2013; Thacker et al. 2014), a meiosis-specific transcription factor that controls pachytene exit (Xu et al. 1995; Chu and Herskowitz 1998; Sourirajan and Lichten 2008).

Regulation of DSB numbers via feedback control. Mechanisms for regulating DSB numbers have been described in different species. In *S. cerevisiae*, a DSB on one chromosome decreases the frequency of DSB formation on its homolog at the same and nearby positions (Xu and Kleckner 1995; Rocco and Nicolas 1996; Fukuda et al. 2008). This phenomenon, known as *trans* inhibition, appears to be dependent on the DNA damage signal transduction kinases Tel1 and Mec1, and tends to constrain DSBs to one per pair of homologs (Zhang et al. 2011). Inhibition in *cis*, where insertion of a strong DSB hotspot suppresses DSB formation on the same chromatid, has also been reported (Wu and Lichten 1995; Xu and Kleckner 1995; Fan et al. 1997; Fukuda et al. 2008), and this form of inhibition appears to be independent of Tel1 (N. Mohibullah and S. Keeney, unpublished). Another form of DSB suppression manifested by less frequent double-cutting on the same chromatid (i.e., DSB interference between DSB sites on the same

DNA molecule) is mediated by Tel1, and operates over short (<10 kb) and medium-long (70–100 kb) ranges, most likely reflecting DSB inhibition within the same chromatin loop, and on adjacent loops (Garcia et al. 2015).

Mice and flies appear to have a negative feedback loop, whereby DSBs catalyzed by SPO11 activate the Tel1 homolog ATM, which inhibits further DSB formation (Joyce et al. 2011; Lange et al. 2011). It is not clear how DSB inhibition is mediated in mice and flies. In *S. cerevisiae*, the negative feedback loop may involve regulation of the DSB protein Rec114 by Tel1 and/or Mec1-dependent phosphorylation (Carballo et al. 2013). A positive feedback loop mediated by Mec1 has also been described in *S. cerevisiae*, which promotes DSB formation when Spo11 activity is compromised (e.g., in *spo11* hypomorph alleles) (Gray et al. 2013).

DSB numbers are also regulated through a feedback mechanism mediated by homolog engagement. In mouse, unsynapsed chromosome regions continue to form DSBs, suggesting existence of a mechanism by which DSB formation ceases once IH interactions have been achieved, or by which unsynapsed regions are actively targeted for *de novo* DSB formation (Kauppi et al. 2013). A similar conclusion is suggested by the occurrence of elevated DSB numbers in *S. cerevisiae* mutants defective for engagement of homologous chromosomes (Thacker et al. 2014). Finally, a similar mechanism has also been proposed in worms (Hayashi et al. 2010; Henzel et al. 2011), based on elevated levels and presence of RAD-51 foci at later stages in mutants with synapsis defects, or with chromosomal translocations that prevent homologous synapsis (Alpi et al. 2003; Nabeshima et al. 2004; Carlton et al. 2006; Hayashi et al. 2007). CO precursors have also been proposed in worms to regulate the DSB-permissive state via chromatin association of DSB-1 and DSB-2, potentially either as a negative feedback loop, or an obligate CO checkpoint (Rosu et al. 2013; Stamper et al. 2013).

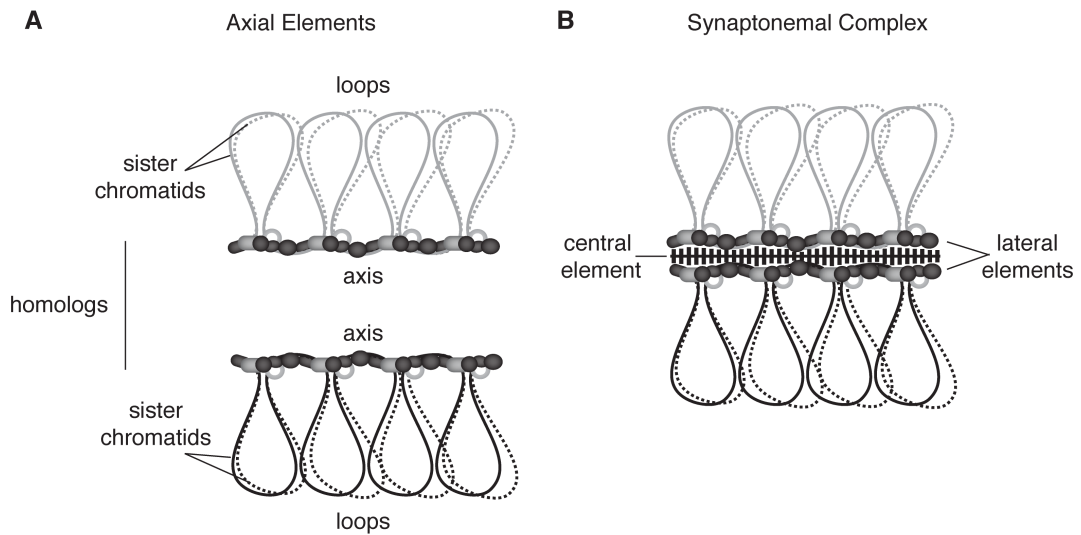


Figure 1.5. Meiotic chromosome organization. (A) Meiotic chromosomes are organized into a series of chromatin loops anchored at their bases by a proteinaceous axial core. (B) At the zygotene stage of prophase I, homologs start to synapse, with the homologous axial elements coming together to form the lateral elements of the synaptonemal complex (SC). The lateral elements are held together by transverse filaments, which together with central element proteins, make up the central region of the SC. SC formation is completed by the pachytene stage. Adapted from (Lam and Keeney 2014).

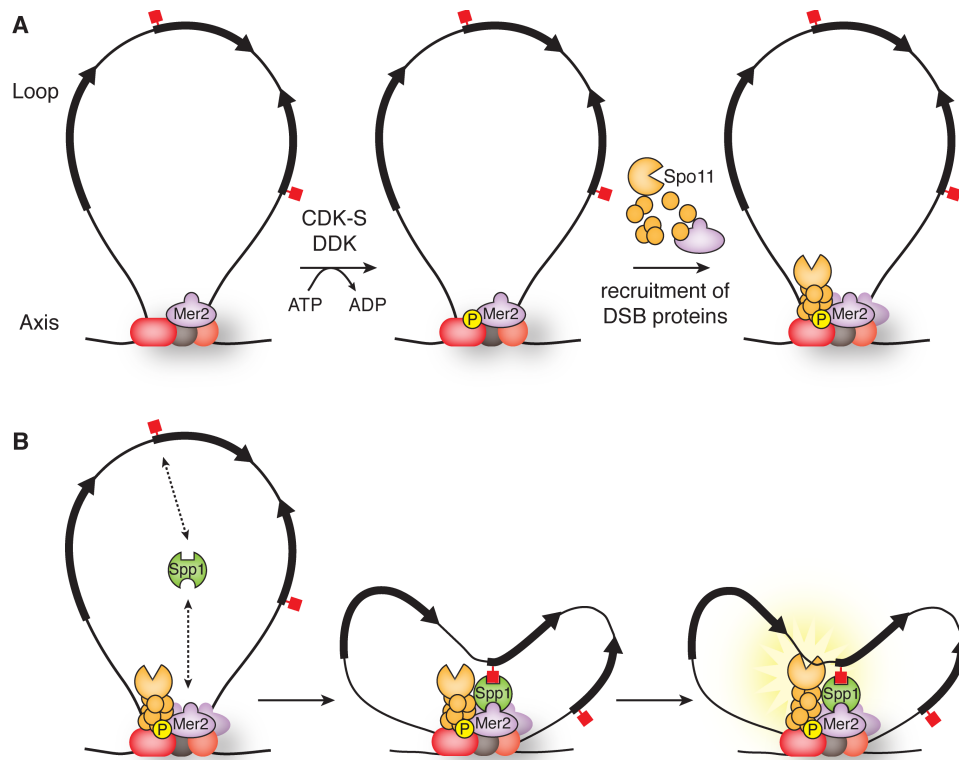


Figure 1.6. Temporal and spatial coordination of DSB formation in *S. cerevisiae*.

(A) Model for DSB regulation via Mer2 phosphorylation. Mer2 phosphorylation by the replication-associated kinases CDK-S and DDK leads to recruitment of DSB proteins that directly interact with Mer2 (Rec114, Mei4, Xrs2), and perhaps subsequently also other DSB proteins. Mer2 (purple) is localized at chromosome axes, along with axial element proteins Red1, Hop1, and cohesin Rec8 (red/gray ovals and circles), but is further enriched at axes upon phosphorylation by CDK-S. CDK-S primes Mer2 for further phosphorylation by DDK. Arrows on the chromatin loop represent gene open reading frames. Red squares represent H3K4me3 marks. Only one sister chromatid is shown for clarity. (B) Model integrating DSB formation with loop-axis chromosome structure. Axis-associated Mer2 interacts with Spp1, which binds H3K4me2/me3 marks and thereby tethers a chromatin loop to the axis. The nucleosome-depleted promoter near the tethered loop segment becomes accessible to Spo11, allowing DSB formation. The precise order of events (Mer2 phosphorylation, loop tethering to the axis) is not known. Spp1 interacts with Mer2 independent of Mer2 phosphorylation, so the potential interactions indicated in the left-most panel (H3K4me2/me3-Spp1-Mer2) could also occur in B, but are not shown. Adapted from (Lam and Keeney 2014).

The meiotic recombination initiation landscape in other organisms

Fission yeast

Prominent hotspots in *S. pombe* are usually widely separated (~50–100 kb apart) and tend to localize in large intergenic regions (IGR) (Cromie et al. 2007). Large IGRs often include clusters of closely spaced NDRs (de Castro et al. 2012), but NDRs are not as predictive of DSB hotspots in *S. pombe* as they are in *S. cerevisiae* (Fowler et al. 2014). Some hotspots are dependent on transcription factor binding (e.g., *ade6-M26* hotspot bound by Atf1-Pcr1 transcription factor), whereas others are independent of known transcription factors (e.g., *mbs1*) (Wahls and Smith 1994; Kon et al. 1997; Cromie et al. 2005; Hirota et al. 2007). Recent work implicates linear element components (Rec25, Rec27, Mug20) as hotspot determinants (Fowler et al. 2013).

Unlike *S. cerevisiae* or mouse, in *S. pombe* the distribution of DSB hotspots differs from the distribution of COs (Young et al. 2002; Cromie and Smith 2007a). Regions with few DSBs have CO frequencies similar to regions with prominent DSB hotspots, a phenomenon known as CO invariance (Hyppa and Smith 2010). At the heart of CO invariance is variation in the choice of preferred recombination partner; at DSB hotspots, DSB repair is biased toward the sister chromatid, whereas at DSB cold regions, DSB repair is biased toward the homolog. The mechanism behind this phenomenon is not currently understood.

Targeting DSBs in *S. pombe*. Ohta and colleagues have proposed a different mechanism for TLAC formation in *S. pombe* (Miyoshi et al. 2012; Miyoshi et al. 2013), through Mde2 tethering. Mde2 localizes preferentially to DSB hotspots and interacts with both SFT and DSBC (**Fig. 1.3B**) (Miyoshi et al. 2012). Through these physical interactions, Mde2 at potential DSB sites (proposed to be on loop sequence) could connect with LinEs and recruit DSBC, thereby tethering DSB sites to LinEs and bringing

DSB protein subcomplexes together. The model proposes that tethering of the loop to LinEs occurs prior to DSB formation. It is not known whether these proposed tethering interactions involve histone modifications analogous to *S. cerevisiae*, but *S. pombe* hotspots are enriched for H3K9 acetylation, and absence of this histone mark results in partially reduced DSB and Rec12 binding levels (Yamada et al. 2013). In contrast, hotspots are not associated with H3K4me3, although absence of Set1 results in more Rec12 binding, and reduced DSB and recombination activity at some hotspots (Yamada et al. 2013). It is possible that multiple chromatin-related factors influence DSB formation in *S. pombe*.

Smith and colleagues proposed an alternative scenario that does not invoke TLAC formation (Fowler et al. 2013; Martin-Castellanos et al. 2013). In this model, Rec12 binds both to hotspots and to DSB-cold regions, but only those binding events that occur in proximity to LiNE proteins Rec25, Rec27, and Mug20 result in DNA cleavage. Rec25, Rec27, and Mug20 are not absolutely required for DSBs, but they bind all hotspots with great specificity and are essential for DSBs at most hotspots (Martin-Castellanos et al. 2005; Davis et al. 2008; Fowler et al. 2013). Interestingly, Rec12 binding (as assessed by chromatin immunoprecipitation [ChIP] with a catalytically inactive mutant) is higher within transcription start sites, but DSB frequency is higher between genes, suggesting that Rec12 binding to DNA is not enough to initiate DSB formation, but rather its activation is controlled separately, most likely mediated by Rec25, Rec27, and Mug20 (Fowler et al. 2013). According to Smith and colleagues, the high correlation between DSB hotspots and binding sites for a subset of LinE proteins, in addition to the absence of any significant anti-correlation between Rec8 binding and DSB hotspots, argues against a TLAC-based model (Fowler et al. 2013). Further investigation will hopefully shed light on the mechanism for targeting DSBs in *S.*

pombe—whether it involves a TLAC mechanism, or is determined by a set of hotspot determinants, or a combination of both models.

Mouse and Human

Mouse and human recombination hotspots overlap both genic and intergenic regions, though human recombination rates are on average lower within transcribed regions of genes (McVean et al. 2004; Myers et al. 2005; Arnheim et al. 2007; Frazer et al. 2007; International HapMap et al. 2007; Coop et al. 2008; Kong et al. 2010; Smagulova et al. 2011; Lu et al. 2012). In both mouse and human, DSB hotspots overlap a subset of H3K4me3-enriched sites, but unlike budding yeast, this overlap does not generally include the strong H3K4me3-enriched regions around promoters (Baudat et al. 2009; Smagulova et al. 2011; Pratto et al. 2014). Instead, DSB hotspots in mouse and human are determined by the DNA binding specificity of PRDM9 methyltransferase (Baudat et al. 2010; Myers et al. 2010; Parvanov et al. 2010; Grey et al. 2011; Brick et al. 2012; Pratto et al. 2014).

PRDM9 has a PR/SET domain at the N-terminus with histone H3K4 methyltransferase activity, and multiple C2H2-type zinc finger DNA binding motifs at the C-terminus (Hayashi et al. 2005). The zinc-finger array evolves rapidly, such that numerous alleles with distinct DNA binding specificities are present in populations of humans, mice, and other mammalian species (Oliver et al. 2009; Thomas et al. 2009; Baudat et al. 2010; Berg et al. 2010; Parvanov et al. 2010). In humans, a degenerate 13-base pair motif was found to be associated with at least 40% of hotspots, and provided one route to the identification of PRDM9 as a hotspot-specifying factor (Myers et al. 2008; Baudat et al. 2010; Myers et al. 2010). This motif is specifically recognized by two PRDM9 variants frequently found in individuals of European descent, but variants common in other populations recognize different binding sites, and hence, are

associated with different hotspots (Baudat et al. 2010; Berg et al. 2010; Kong et al. 2010; Hinch et al. 2011; Pratto et al. 2014). Consistently, purified human PRDM9 zinc fingers from allelic variants exhibit different binding affinities to different hotspot consensus sequences *in vitro* (Narasimhan et al. 2016). Similarly, at least 73% of hotspots in mouse contain a consensus motif that matches the predicted binding site of PRDM9 (Smagulova et al. 2011), but this is likely an underestimate of PRDM9 binding sites *in vivo* because of current limitations on deducing PRDM9 binding from DNA sequence alone. Mouse strains with different *Prdm9* alleles exhibit widely different hotspot distribution with only 1% overlap in DSB hotspot locations (Brick et al. 2012; Smagulova et al. 2016). Analogously, humans with the same *PRDM9* alleles share 89% of DSB hotspots, but this number drops to 43% when only one of the alleles is the same (Pratto et al. 2014). These findings demonstrate that PRDM9 is responsible for defining most DSB hotspot locations in mouse and human.

Interestingly, PRDM9 is not required for DSB formation, but instead targets the DSB machinery: DSB hotspots occur in different locations in the *Prdm9*^{-/-} mouse, frequently but not exclusively located at H3K4me3-enriched sites associated with promoters, more reminiscent of the distribution in yeast, which has no PRDM9 ortholog (Brick et al. 2012). Based on this observation, it has been proposed that the *S. cerevisiae* system of hotspot positioning reflects the ancestral mode, and the adoption of a PRDM9 targeting system occurred later during mammalian evolution (Oliver et al. 2009; Cooper et al. 2016). However, it is not known how PRDM9 recruits SPO11 to generate breaks, for example, whether it directly recruits the DSB machinery through physical interaction, or indirectly through binding of the DSB machinery to H3K4me3 sites.

In addition to redistribution of the DSB landscape, *Prdm9*^{-/-} mice exhibit DSB repair defects, partial chromosome synapsis, and infertility, which suggest that there are

additional roles for PRDM9 besides H3K4me3 deposition, or that altered DSB landscapes can be deleterious (Brick et al. 2012; Davies et al. 2016). However, fertility defects may not be an inevitable consequence of lacking PRDM9 in mammals. It is important to note that *Prdm9* deficiency has only been examined in one inbred strain of mice (B6; (Brick et al. 2012)), and it is possible that infertility may not be generalizable, especially since dogs lack a functional PRDM9 (discussed further below) and are fertile. Moreover, loss of *PRDM9* function in human is compatible with fertility (Narasimhan et al. 2016). In a documented case of a woman with *PRDM9* loss of function, analysis of crossover sites transmitted from her gamete to her offspring indicate that few crossovers overlapped wild type *PRDM9* DSB hotspots, and unlike mouse *Prdm9*^{-/-}, few crossover intervals were associated with promoters or promoter-associated H3K4me3 (Narasimhan et al. 2016).

PRDM9 governs DSB hotspot distribution, but it does not influence properties of the DSB landscape at broader scales. In a study replacing the mouse zinc finger array of *Prdm9* with the corresponding human sequence, the hotspot landscape with the humanized *Prdm9* allele was completely altered compared to wild type mice, with only 2.6% overlap in hotspot location (Davies et al. 2016). Nevertheless, correlations between DSB maps strengthened over larger size scales, with a correlation of ~0.5 when analyzing DSB heat at the 1 Mb scale, and the correlation approximating 1 when analyzing the maps at the 10 Mb scale (Davies et al. 2016). Similar patterns were observed when comparing DSB landscapes in mice from different strain backgrounds with different *Prdm9* alleles, or when comparing wild type and *Prdm9*^{-/-} mice (Davies et al. 2016).

It is not yet clear whether DSB targeting in mammals involves coordination of local (hotspot-level) features with higher-order chromosome structure, but several lines of evidence suggest that it does. The *HORMAD1* structural component of axes (ortholog

of yeast Hop1) is required for normal DSB levels, reminiscent of Hop1 requirement for normal DSB levels in *S. cerevisiae* (Mao-Draayer et al. 1996; Woltering et al. 2000; Peciña et al. 2002; Niu et al. 2005; Carballo et al. 2008; Shin et al. 2010; Daniel et al. 2011). In addition, DSB proteins REC114, MEI4, and IHO1 localize to chromosome axes in mouse, and IHO1 physically interacts with HORMAD1, so break formation most likely occurs in the context of axial structures (Kumar et al. 2010; Kumar et al. 2015; Stanzione et al. submitted). Lastly, in mouse, DNA in the pseudoautosomal region (the only region of homology shared between the X and Y chromosomes) is organized on a longer axis with shorter chromatin loops compared to autosomes (Kauppi et al. 2011). DNA organized as short loops means more loops along the axis, thus more potential DSB sites; consistent with the TLAC model, the pseudoautosomal region exhibits higher DSB density (Kauppi et al. 2011).

Other species

The *A. thaliana* genome also contains discrete recombination hotspots, as evidenced by 80% of COs occurring within 26% of the sequence (Choi et al. 2013), comparable to that in *S. cerevisiae* (Chen et al. 2008a; Mancera et al. 2008) and humans (Myers et al. 2005). Recombination hotspots in *A. thaliana* tend to occur at gene promoters and terminators, and are associated with the active chromatin marks H2A.Z and H3K4me3, and low nucleosome density (Choi et al. 2013; Choi and Henderson 2015; Mercier et al. 2015). In canids and birds, recombination hotspots are located near CpG-rich regions and promoters (Auton et al. 2013; Singhal et al. 2015). Plants, canids, and birds lack a functional PRDM9 ortholog (Oliver et al. 2009; Zhang and Ma 2012) so it is notable that their recombination landscapes are more similar to that of *S. cerevisiae* (in terms of targeting to functional genomic elements) than to mammals with a PRDM9

system designating hotspot locations (e.g., mice, humans), thereby supporting the view that promoter targeting is a commonly observed, and possibly ancestral state.

Recombination hotspots are generally thought to be absent in *C. elegans* and *D. melanogaster* (Chan et al. 2012; Kaur and Rockman 2014; Smukowski Heil et al. 2015), and neither have a functional PRDM9 ortholog. The recombination landscapes in mice, primates, dogs, birds, and fruit flies will be discussed in the context of evolutionary dynamics in a later section.

Chromosome structure proteins and their roles in shaping the DSB landscape

This section will examine the meiotic roles of Red1, Hop1, and Mek1 in more detail. Red1, Hop1, and Mek1 are meiosis-specific components (along with Rec8) of the chromosome axis in yeast, and they function in multiple interconnected roles in DSB formation, SC formation, promoting IH recombination, and recombination checkpoint.

The *RED1* and *MEK1* genes were identified in a screen for sporulation-proficient, but meiotic lethal mutants (i.e., mutants that sporulate to yield largely inviable spores) (Rockmill and Roeder 1988; Rockmill and Roeder 1991). *MEK1* was also independently isolated when screening for mutants defective in meiotic, but not mitotic, recombination (Leem and Ogawa 1992). *HOP1* was identified in a screen for chromosome pairing mutants defective in IH exchange, but proficient in intrachromosomal recombination (Hollingsworth and Byers 1989).

Domain structure of Red1, Hop1, and Mek1 proteins

Red1 contains a coiled-coil structural motif (Smith and Roeder 1997; Woltering et al. 2000), and two SUMO-interacting motifs (SIM) in the C-terminus (Lin et al. 2010) (**Fig. 1.7A**). Red1 is phosphorylated, but whether the phosphorylation is dependent on

DSBs and/or Mek1, and whether its phosphorylation is important for meiosis is not clear, with different studies providing contrasting observations (Bailis and Roeder 1998; de los Santos and Hollingsworth 1999; Bailis and Roeder 2000; Wan et al. 2004; Lai et al. 2011). Red1 is also sumoylated, and this modification promotes normal timing of SC formation (Eichinger and Jentsch 2010). Red1 interacts with itself, with Hop1 (Hollingsworth and Ponte 1997; Woltering et al. 2000; Niu et al. 2005), Mek1 (Bailis and Roeder 1998), and with Mec3 and Ddc1 of the 9-1-1 checkpoint complex (Eichinger and Jentsch 2010). Orthologs of Red1 include Rec10 in *S. pombe* (Lorenz et al. 2004), SYCP3 in mammals (Dobson et al. 1994; Lammers et al. 1994; de los Santos and Hollingsworth 1999) (weak sequence similarity has also been reported with SYCP2 (Offenberg et al. 1998)), and ASY3 in plants (Ferdous et al. 2012) (**Table 1.1**).

Hop1 is a member of a conserved family of DNA-binding, HORMA domain containing proteins (Aravind and Koonin 1998; Muniyappa et al. 2014), with orthologs in *S. pombe* (Hop1; (Lorenz et al. 2004)), *C. elegans* (HIM-3 and its paralogs, HTP-1–3; (Zetka et al. 1999; Couteau and Zetka 2005; Goodyer et al. 2008)), mouse (HORMAD1 and HORMAD2 (Wojtasz et al. 2009; Fukuda et al. 2010; Shin et al. 2010)), human (HORMAD1 (Chen et al. 2005)), and *A. thaliana* (ASY1; (Caryl et al. 2000; Armstrong et al. 2002)) (**Table 1.1**). *S. cerevisiae* Hop1 contains a DNA-binding zinc finger domain (Anuradha and Muniyappa 2004), a HORMA domain involved in protein-protein interaction and oligomerization, and an S/T-Q cluster domain (SCD) with Tel1/Mec1 phosphorylation target sites (Carballo et al. 2008) (**Fig. 1.7B**). Structural studies of Hop1 orthologs in *C. elegans* revealed that these proteins form hierarchical complexes through intermolecular associations (i.e., the N-terminal HORMA domain of one molecule binds to the C-terminal closure motif of another molecule) (Kim et al. 2014). These HORMA domain-closure motif interactions appear conserved in mouse HORMAD1–2 (Kim et al. 2014). It is not clear whether *S. cerevisiae* Hop1 contains a C-terminal closure motif, but

previous studies do suggest formation of intermolecular interactions in the form of Red1 and Hop1 hetero- and homo-oligomers (Hollingsworth and Ponte 1997; Kironmai et al. 1998; de los Santos and Hollingsworth 1999; Woltering et al. 2000).

Mek1 is a meiosis-specific paralog of the Ser/Thr DNA-damage checkpoint kinase CHK2/Rad53 (Bailis and Roeder 1998; de los Santos and Hollingsworth 1999), contains a phospho-protein binding FHA domain (Durocher and Jackson 2002; Wan et al. 2004), and a dimerization domain in the C-terminus (Niu et al. 2007) (**Fig. 1.7C**). Mek1 kinase activity is activated by autophosphorylation in response to DSBs (Niu et al. 2007). Mek1 exists in a complex with Red1 and Hop1 (Smith and Roeder 1997; Bailis and Roeder 1998). No orthologs of Mek1 have been identified outside of budding and fission yeasts.

The multiple roles of Red1, Hop1, and Mek1 in meiotic recombination

DSB formation and recombination. Red1, Hop1, and Mek1 are required for normal levels of meiotic DSBs (**Table 1.2**). In *red1* mutants, both DSB formation and recombination are reduced to ~25% of wild type levels, though the level of reduction is variable depending on the locus (Rockmill and Roeder 1990; Mao-Draayer et al. 1996; Xu et al. 1997; Woltering et al. 2000; Hunter and Kleckner 2001; Blat et al. 2002; Peciña et al. 2002; Niu et al. 2005). Mutation in *hop1* leads to more severe reduction in DSBs, to approximately 5–10% of wild type (Mao-Draayer et al. 1996; Woltering et al. 2000; Peciña et al. 2002; Niu et al. 2005; Carballo et al. 2008), and recombination is reduced to ~10% of wild type (Hollingsworth and Byers 1989; Mao-Draayer et al. 1996). In *mek1* mutants, some reports observed similar reduction as *red1* mutants, with DSBs reduced to 10–20% of wild type (Leem and Ogawa 1992; Xu et al. 1997; Kim et al. 2010), and recombination reduced to ~1–15% of wild type, depending on the locus (Rockmill and Roeder 1991; Leem and Ogawa 1992). However, other studies reported wild-type levels

of break formation in the absence of Mek1 (Peciña et al. 2002; Niu et al. 2005). Decreased steady-state levels of DSBs in *mek1* reflect in part rapid repair through intersister (IS) recombination (Wan et al. 2004; Niu et al. 2005). Absence of Red1, Hop1, or Mek1 leads to reduced IH but not IS joint molecules (Schwacha and Kleckner 1994; Schwacha and Kleckner 1997; Hunter and Kleckner 2001; Kim et al. 2010). Consistently, all three mutants exhibit low spore viability due to chromosome nondisjunction in the first meiotic division (*red1* and *hop1*: ~1% spore viability (Rockmill and Roeder 1988; Hollingsworth and Byers 1989); *mek1*: 13% (Rockmill and Roeder 1991)). The DSB phenotypes in *red1*, *hop1*, and *mek1* suggest that the proteins somehow assist Spo11 in cleaving DNA, but are not absolutely required for break formation.

It is notable that HORMA domain containing proteins related to Hop1 promote DSB formation in almost all organisms examined (e.g., budding and fission yeasts Hop1, *C. elegans* HTP-1 and HTP-3, and mouse HORMAD1; but not *A. thaliana* ASY1) (Mao-Draayer et al. 1996; Couteau and Zetka 2005; Martinez-Perez and Villeneuve 2005; Sanchez-Moran et al. 2007; Goodyer et al. 2008; Latypov et al. 2010).

Red1 and Hop1 chromatin association. Based on genetic, biochemical, cytological, and molecular biology data, a model has emerged for Red1, Hop1, and Mek1 recruitment to chromosomes (**Fig. 1.8**). Red1 localizes to chromosomes in early prophase and recruits Hop1; both events occur independently of break formation (Smith and Roeder 1997). Rec8, the meiotic-specific kleisin subunit of cohesin, physically interacts with and modulates the localization of Red1 and Hop1 (Klein et al. 1999; Panizza et al. 2011; Sun et al. 2015). In the absence of Rec8, Red1 and Hop1 still associate with chromosomes, but their distribution along chromosomes is altered, indicating that some Red1 and Hop1 binding sites are more Rec8-dependent than others. By CHIP analysis, most Rec8 and Red1 peaks overlap, although there are sites of Rec8 enrichment that are not enriched for Red1 (Blat et al. 2002; Panizza et al. 2011).

By immunostaining analysis, Rec8- and Red1-enriched domains are observed to alternate along chromosomes (Kim et al. 2010). Therefore, some axis sites are probably enriched for Rec8, others for Red1/Hop1, and others for Rec8/Red1/Hop1 (Panizza et al. 2011). Hop1 also modulates Red1 deposition in a chromosome-dependent manner, resulting in less Red1 enrichment in medium and long chromosomes (Sun et al. 2015).

Recruitment of DSB proteins to chromosome axes. Red1 and Hop1 on chromosome axes recruit the DSB machinery. First, Mer2 is recruited, and phosphorylation of Mer2 at S30 by CDK-S then leads to the recruitment of other DSB proteins, such as Rec114 and Mei4 (Henderson et al. 2006; Panizza et al. 2011; Murakami and Keeney 2014). It is not known whether Mer2 recruitment to the axes involves direct protein interaction with Red1 and/or Hop1 analogous to the *S. pombe* Rec15-Rec10 interaction (orthologs of Mer2 and Red1) (Miyoshi et al. 2012). Other DSB proteins (e.g., Rec102, Rec104, Spo11) are also associated with chromosome axes, but are not as highly enriched as Rec114, Mer2, and Mei4 (Kee et al. 2004; Kugou et al. 2009; Panizza et al. 2011), suggesting that their distribution may be more dispersed.

Axial element and SC assembly/disassembly. The degree of SC formation is different in the three mutants, most likely reflecting their epistatic relationship with respect to axial element formation and SC assembly. Axial elements fail to form in *red1* (Rockmill and Roeder 1990), whereas fragments of axial elements are detectable in *hop1* (Hollingsworth and Byers 1989; Loidl et al. 1994), and axial elements form in *mek1* (though are less discrete than in wild type) (Rockmill and Roeder 1991). There is no SC assembly in *red1* and *hop1* mutants (Hollingsworth and Byers 1989; Rockmill and Roeder 1990), but nearly normal SC assembly occurs in *mek1* (stretches of SC are shorter than in wild type) (Rockmill and Roeder 1991). Therefore Red1, and to a lesser extent Hop1, are required for assembly of axial elements, and are also required for SC assembly, where they localize along the lateral elements (Roeder 1995). The ability of

red1 mutants to generate DSBs (albeit reduced) in the absence of axial elements suggests that Spo11 cleavage does not have to occur strictly in the context of axial elements.

Hop1 and Mek1 dissociate from chromosomes upon SC assembly, whereas Red1 seems to remain associated (Smith and Roeder 1997; Subramanian et al. 2016). Hop1 and Mek1 removal from synapsed chromosomes in both yeast and mice require the AAA+ ATPase Pch2/TRIP13 (Borner et al. 2008; Joshi et al. 2009; Wojtasz et al. 2009; Daniel et al. 2011; Chen et al. 2014; Subramanian et al. 2016). DSB proteins Rec114 and Mei4 (also Rec102, Rec104) dissociate from chromosomes with similar timing (Kee et al. 2004; Li et al. 2006; Maleki et al. 2007; Panizza et al. 2011; Carballo et al. 2013). The timing at which proteins involved in DSB formation are displaced, combined with increased DSB levels in SC mutants have led to the model whereby homolog engagement (synapsis and/or crossover formation) inhibits break formation, most likely mediated at the molecular level by chromosome dissociation of components necessary for Spo11 activity (e.g., Hop1, Rec114, Mei4) (Wojtasz et al. 2009; Keeney et al. 2014; Thacker et al. 2014).

Activation of Mek1 and IH bias in recombination partner choice. DNA DSBs repaired during mitosis principally use the sister chromatid as template to conserve sequence fidelity. However, a challenge presented during meiotic recombination is that the homologous chromosome must be used preferentially as template to yield productive crossovers that will allow correct homolog segregation in meiosis I. Red1, Hop1, and Mek1 are involved in recombination partner choice by promoting IH recombination (Humphryes and Hochwagen 2014).

Red1 and Hop1 recruit Mek1, possibly via binding of the Mek1 FHA domain to phosphorylated Red1 (Wan et al. 2004) and/or to phosphorylated Hop1 (Chuang et al. 2012). In response to break formation, Hop1 is phosphorylated by Mec1/Tel1 in the SCD

sites (Carballo et al. 2008). Hop1 phosphorylation leads to Mek1 dimerization, which probably facilitates kinase auto-activation by trans-phosphorylation at T327 (**Fig. 1.8**) (Niu et al. 2005; Niu et al. 2007). Mek1 interaction with phosphorylated Hop1 via its FHA domain appears to stabilize and protect the post-translational modification against protein phosphatase 4 (Chuang et al. 2012). Activated Mek1 then phosphorylates the Rad51 binding partner Rad54 at T132 (Niu et al. 2009), which along with meiosis-specific Hed1 suppression of Rad51 (Busygina et al. 2008), and likely other unknown factors (Niu et al. 2009), contributes to suppression of Rad51-mediated strand invasion of sister chromatids. In this model, Red1, Hop1, and Mek1 promote IH bias by creating a barrier to sister chromatid repair. Mek1 also phosphorylates histone H3 at T11, but the functional consequence of this modification is not well understood (Govin et al. 2010; Kniewel 2012). An alternative but not mutually exclusive view is that Mek1 positively promotes IH bias, either by enhancing IH strand invasion (Terentyev et al. 2010), or by counteracting a sister chromatid bias imposed by Rec8 (Kim et al. 2010). A recent study suggests that the role of Mek1 in partner choice might be to suppress the use of any proximal chromatid as template (Subramanian et al. 2016). The closer proximity of a DSB to its sister chromatid than to its homolog would thus allow Mek1 to suppress IS but not IH repair.

Recombination checkpoint roles. Red1, Hop1, and Mek1 are also implicated in the recombination checkpoint. The recombination checkpoint (also referred to as the pachytene checkpoint) ensures that progression through meiosis is prevented in the presence of unrepaired recombination intermediates (Bishop et al. 1992; Lydall et al. 1996; Xu et al. 1997; Roeder and Bailis 2000; Longhese et al. 2009; Subramanian and Hochwagen 2014). For example, accumulation of unrepaired resected DSBs in the *dmc1* mutant activates the recombination checkpoint and blocks exit from the pachytene stage of meiosis I (Bishop et al. 1992; Lydall et al. 1996). Absence of Red1, Hop1, Mek1, or

inhibition of Mek1 kinase activity allows the cell to overcome the block to meiotic progression imposed by *dmc1* (Schwacha and Kleckner 1997; Xu et al. 1997; Bishop et al. 1999; Wan et al. 2004; Niu et al. 2005; Carballo et al. 2008). In these scenarios, DSBs undergo Rad51-dependent repair by IS recombination, thereby alleviating the signal triggering the checkpoint but giving rise to inviable spores. By inference, in the wild type scenario Mek1 kinase activity suppresses IS repair to establish IH bias in recombination partner choice. However, cells can bypass the checkpoint in the absence of Red1 even when DSBs cannot be repaired (Xu et al. 1997), indicating that IS repair is not the only mechanism to allow meiotic progression. Instead, chromosome axis proteins are required to support checkpoint sensing or signaling, as discussed below (Xu et al. 1997).

The activation of Mek1 in a Tel1/Mec1-dependent manner is analogous to the Tel1/Mec1-dependent activation of Rad53/CHK2 in response to DSBs in the mitotic DNA damage response (Stracker et al. 2004; Finn et al. 2012). Thus, Red1, Hop1, and Mek1 are thought to transduce the DNA damage checkpoint signals in meiotic cells in response to programmed DSBs (Longhese et al. 2009; Subramanian and Hochwagen 2014). In this framework, axial element proteins Red1 and Hop1 may serve as adaptor proteins for the activation of meiotic checkpoint networks: Red1 interaction with Mec3 and Ddc1, members of the 9-1-1 complex, is required for proper signaling (Eichinger and Jentsch 2010), and Hop1 phosphorylation by two partially redundant pathways (Mec1/Rad17 and Tel1/Pch2/Xrs2) promotes Mek1 kinase activation (Ho and Burgess 2011).

How might Red1, Hop1, and Mek1 influence meiotic DSB formation?

As described in the preceding sections, Red1, Hop1, and Mek1 play multiple roles in meiotic recombination, most of which involve post-DSB events. Therefore, it is

puzzling why these proteins are needed to promote normal levels of DSB formation. One possibility is that axial element proteins foster Spo11 cleavage in the context of TLACs, either by promoting or stabilizing interactions between axis-bound DSB proteins and DNA within chromatin loops (Hunter 2007; Panizza et al. 2011). Consistent with this, overexpression of *REC104* has been reported to suppress the spore viability defect of a non-null *hop1* mutant allele (Hollingsworth and Johnson 1993; Friedman et al. 1994). This genetic interaction may reflect the association of both proteins to axial sites, but if this is the case, then overexpression of other DSB proteins closely associated with chromosome axes is expected to suppress the *hop1* allele as well. Nonetheless, the requirement for axial element proteins in normal DSB formation seems to ensure efficient coordination between break formation and processing towards IH repair within an environment equipped for handling checkpoint signaling in the event of persistent unrepaired DSBs. The role of Red1, Hop1, and Mek1 in shaping the DSB landscape will be further explored in **Chapter 3**.

Evolutionary dynamics of the meiotic recombination landscape

Besides promoting accurate homologous chromosome segregation, meiotic recombination also alters genetic linkage, thereby promoting genetic diversity and contributing to evolution (Kauppi et al. 2004; de Massy 2013). As mentioned in the preceding sections, meiotic DSBs and recombination are distributed nonrandomly across genomes, occurring often within hotspots (Kauppi et al. 2004). Early mechanistic studies on meiotic recombination led to the observation of biased gene conversion, whereby the allele receiving the DSB copies genetic information from the uncut allele (**Fig. 1.2**) (Gutz 1971; Nicolas et al. 1989). In a heterozygous scenario where hotspot alleles have different DSB activity, biased gene conversion results in overrepresentation

of the weaker hotspot allele among the offspring, to the detriment of the stronger allele. This type of meiotic drive is observed in many species including yeast (Nicolas et al. 1989), mice (Cole et al. 2014), and humans (Jeffreys and Neumann 2002). Biased gene conversion has spurred much debate on the fate of recombination hotspots over evolutionary time-scales. The following sections discuss contrasting models that predicted either rapid divergence or conservation of the recombination landscape. A summary of hotspot evolutionary dynamics observed in different species is also provided.

Models predicting divergence vs. conservation of the recombination landscape

Biased gene conversion predicts rapid changes to the recombination landscape. Theoretical work exploring evolutionary dynamics of recombination has led to a prevailing hypothesis, the “hotspot paradox”, which is based on biased gene conversion and predicts rapid hotspot extinction (Boulton et al. 1997; Coop and Myers 2007; Friberg and Rice 2008; Ubeda and Wilkins 2011). In studies simulating hotspots in a finite population, active hotspots became extinct by ~70 generations in the presence of biased gene conversion (Boulton et al. 1997; Pineda-Krch and Redfield 2005). When factoring the selective advantages of recombination on viability and fertility as a way to maintain hotspots (e.g., recombination generates favorable allele combinations with increased fitness, and prevents gamete aneuploidy), hotspot alleles persisted for more generations, but still became extinct. Thus, over evolutionary timescales, mutations that reduce or eliminate hotspot activity will be rapidly fixed in populations, while hotspot-activating mutations are rapidly extinguished (Boulton et al. 1997; Pineda-Krch and Redfield 2005; Coop and Myers 2007). The paradox is that hotspots exist at all despite the drive against them.

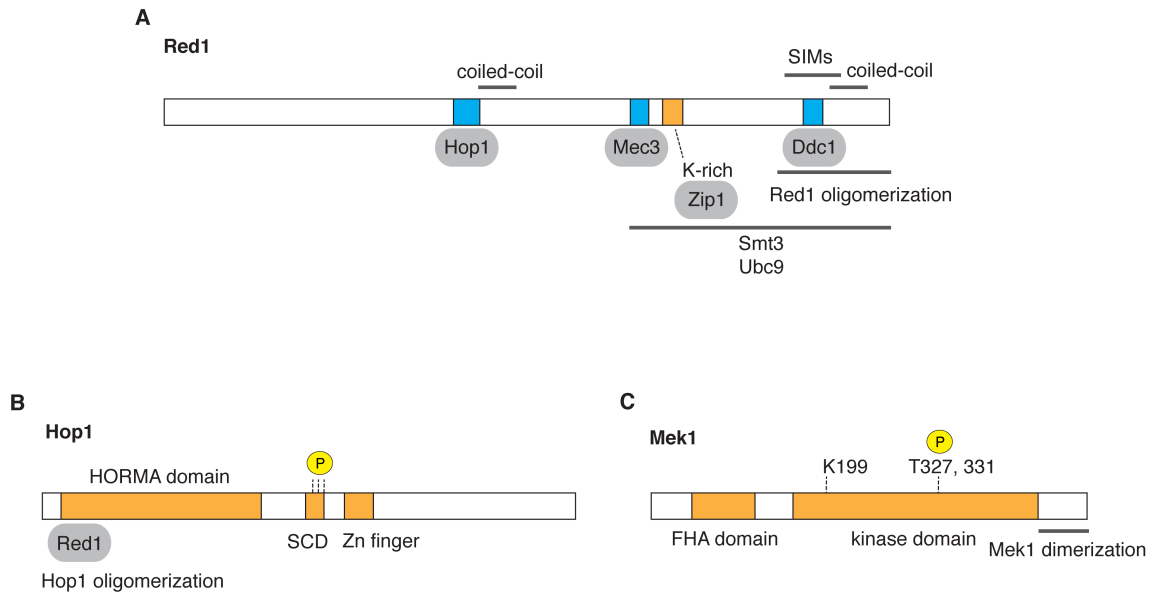
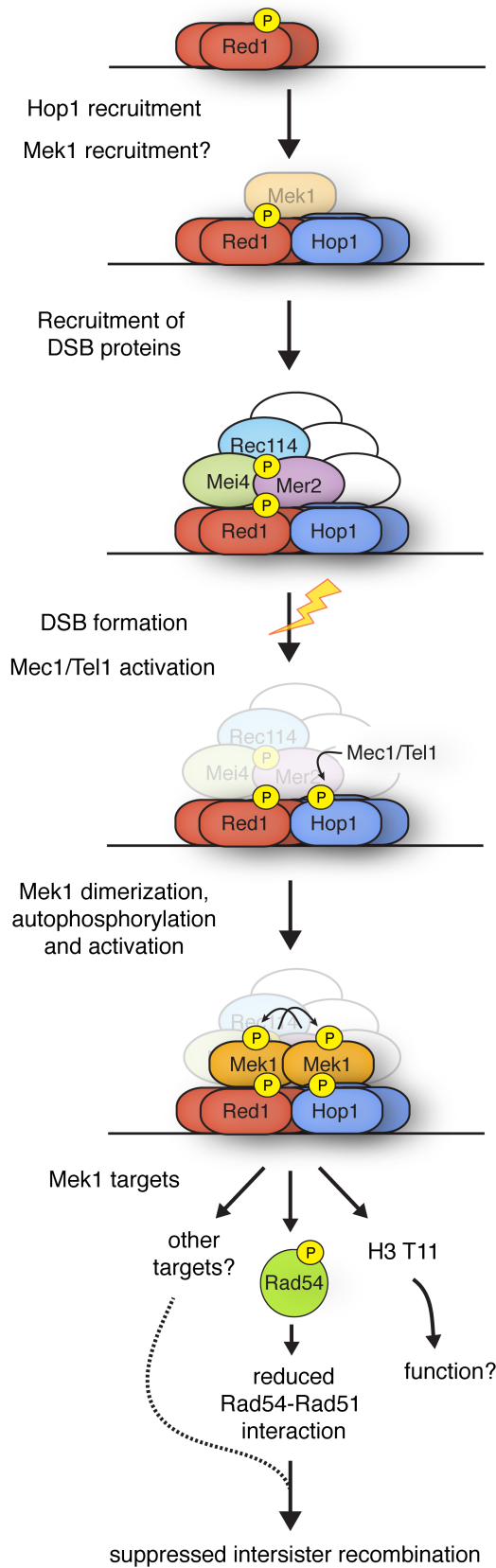


Figure 1.7. Protein domain structure of Red1, Hop1, and Mek1. (A) Red1 is an 827 amino acid protein with two coiled-coil domains, SUMO-interacting motifs (SIMs), regions that bind to Hop1, Mec3, Ddc1, Smt3 (SUMO) chains, and Ubc9. Red1 also has a lysine-rich (K-rich) region that interacts with Zip1 and is sumoylated. The C-terminus is required for Red1 oligomerization. (B) Hop1 is a 605 amino acid protein with a HORMA (Hop1, Rev7 and Mad2) domain, S/T-Q cluster domain (SCD) with target sites for Mec1/Tel1 phosphorylation, a zinc finger domain, and oligomerization and Red1 binding region in the N-terminus. T318 is one of the Mec1/Tel1 phosphorylation targets within the SCD (along with T298 and T311), and these residues are phosphorylated after Spo11-mediated DSB formation. (C) Mek1 is a 497 amino acid protein with an FHA domain in the N-terminus, which binds phosphorylated proteins, a kinase domain, and a dimerization domain in the C-terminus. K199 is required for kinase activity (K199R mutation results in kinase-dead Mek1), and auto-phosphorylation of T327 and T331 are required for activating kinase activity.

Table 1.2. Summary of DSB phenotypes in *red1*, *hop1*, *mek1* mutants

Genotype	DSB levels (% of WT)	Locus	Chr	Strain background	Reference
<i>red1</i>	25%	<i>HIS4-LEU2</i>	III	SK1	Schwacha and Kleckner 1997
<i>red1</i>	25%	<i>HIS4-LEU2</i>	III	SK1	Xu et al. 1997
<i>red1</i>	58%	<i>YCR048W</i>	III	SK1	Niu et al. 2005
<i>red1</i>	14%	<i>HIS4-LEU2</i>	III	SK1	Hunter and Kleckner 2001
<i>red1 rad50S</i>	5%	<i>HIS2</i>	VI	RM strain	Mao-Draayer et al. 1996
<i>red1 rad50S</i>	20%	<i>HIS4-LEU2</i>	III	SK1	Blat et al. 2002
<i>red1 rad50S</i>	25%	<i>YCR047C</i>	III	SK1	Blat et al. 2002
<i>red1 rad50S</i>	8%	<i>CYS3</i>	I	SK1	Blat et al. 2002
<i>red1 rad50S</i>	20%	<i>ARG4</i>	VIII	SK1	Blat et al. 2002
<i>red1 rad50S</i>	50%	<i>YCR048W</i>	III	SK1	Peciña et al. 2002
<i>red1 rad50S</i>	40%	<i>HIS4-LEU2</i>	III	SK1	Kim et al. 2010
<i>red1 rad50S</i>	40%	<i>YCR052W</i>	III	SK1	Lin et al. 2010
<i>red1 rad50S</i>	32%	Chr VII	VII	SK1	Lin et al. 2010
<i>red1 sae2</i>	46.8%	<i>THR4</i>	III	SK1	Woltering et al. 2000
<i>red1 sae2</i>	27%	<i>YCR048W</i>	III	SK1	Niu et al. 2005
<i>red1 dmc1</i>	25%	<i>HIS4-LEU2</i>	III	SK1	Schwacha and Kleckner 1997
<i>red1 dmc1</i>	barely detectable	<i>HIS4-LEU2</i>	III	SK1	Xu et al. 1997
<i>red1 rad51</i>	25%	<i>HIS4LEU2</i>	III	SK1	Schwacha and Kleckner 1997
<i>red1 rad51</i>	barely detectable	<i>HIS4-LEU2</i>	III	SK1	Xu et al. 1997
<i>red1 dmc1 rad51</i>	25%	<i>HIS4LEU2</i>	III	SK1	Schwacha and Kleckner 1997
<i>red1 rad51 dmc1</i>	20%	<i>HIS4-LEU2</i>	III	SK1	Blat et al. 2002
<i>red1 rad51 dmc1</i>	50%	<i>YCR047C</i>	III	SK1	Blat et al. 2002
<i>red1 rad51 dmc1</i>	50%	<i>CYS3</i>	I	SK1	Blat et al. 2002
<i>red1 rad51 dmc1</i>	10%	<i>ARG4</i>	VIII	SK1	Blat et al. 2002
<i>hop1</i>	4%	<i>YCR048W</i>	III	SK1	Niu et al. 2005
<i>hop1 rad50S</i>	5%	<i>HIS2</i>	VI	RM strain	Mao-Draayer et al. 1996
<i>hop1 rad50S</i>	5%	<i>YCR048W</i>	III	SK1	Peciña et al. 2002
<i>hop1 rad50S</i>	background levels	Chr III	III	SK1	Carballo et al. 2008
<i>hop1 sae2</i>	11.9%	<i>THR4</i>	III	SK1	Woltering et al. 2000
<i>hop1 sae2</i>	5%	<i>YCR048W</i>	III	SK1	Niu et al. 2005
<i>hop1 dmc1</i>	background levels	Chr III	III	SK1	Carballo et al. 2008
<i>hop1 dmc1 rad51</i>	background levels	Chr III	III	SK1	Carballo et al. 2008
<i>mek1</i>	10%	<i>HIS4-LEU2</i>	III	SK1	Leem and Ogawa 1992
<i>mek1</i>	10%	<i>ARG4</i>	VIII	SK1	Leem and Ogawa 1992
<i>mek1</i>	15%	<i>HIS4-LEU2</i>	III	SK1	Xu et al. 1997
<i>Mek1-as1 + inh</i>	"reduced"	<i>YCR048W</i>	III	SK1	Wan et al. 2004
<i>mek1 rad50S</i>	like WT	<i>YCR048W</i>	III	SK1	Peciña et al. 2002
<i>Mek1-as1(+IN) rad50S</i>	40%	<i>HIS4LEU2</i>	III	SK1	Kim et al. 2010
<i>mek1 dmc1</i>	15% of WT	<i>HIS4-LEU2</i>	III	SK1	Xu et al. 1997
<i>mek1 dmc1</i>	like WT	<i>YCR048W</i>	III	SK1	Niu et al. 2005
<i>mek1 dmc1</i>	fewer than <i>dmc1</i>	<i>YCR048W</i>	III	SK1	Callender and Hollingsworth 2010



- Axial element formation
- DSB formation
- Synaptonemal complex assembly
- Recombination partner choice
- Recombination checkpoint

Figure 1.8. Model for pathway of chromosomal recruitment of Red1 and Hop1, and Mek1 kinase activation. Red1, Hop1, and Mek1 are involved in many aspects of meiotic recombination (gray box). Red1 recruits Hop1 to chromosome axial sites before DSB formation, and Rec8 modulates their binding. Red1 (and to a lesser extent Hop1) is required for axial element formation, but both Red1 and Hop1 are required for synaptonemal complex assembly. The timing of Mek1 recruitment to chromosomes is not clear, but it is possible that Mek1 is also recruited to chromosomes prior to DSB formation (represented as faded Mek1). Red1 exists as a phosphoprotein independently of break formation. Red1 and Hop1 recruit Mer2, and Mer2 phosphorylation by CDK recruits Rec114 and Mei4, and presumably other DSB proteins. Upon DSB formation, Mec1/Tel1 kinases are activated and phosphorylate Hop1 (DSB proteins are shown faded for simplicity). Hop1 phosphorylation promotes Mek1 dimerization, which leads to autophosphorylation in trans, and kinase activation. Activated Mek1 phosphorylates Rad54 and most likely other targets, leading to suppression of intersister recombination and interhomolog bias in recombination partner choice. Mek1 also phosphorylates histone H3-T11, but the biological function of this modification is not known.

One answer to this paradox comes from PRDM9, a histone methyltransferase with zinc finger modules that rapidly evolve new DNA binding specificity, and which dictates hotspot positions in mice and humans (Hochwagen and Marais 2010; Baudat et al. 2013). PRDM9 targets SPO11 activity near its binding sites, thus dictating hotspot positions. PRDM9 recognition motifs, which have no known intrinsic function, are lost quickly from genomes of humans and mice because of meiotic drive from biased gene conversion (Myers et al. 2010; Cole et al. 2014; Baker et al. 2015), but appearance of new *PRDM9* alleles with different sequence specificity creates new hotspots and redraws the recombination landscape (Baudat et al. 2013). The rapid change in DNA binding specificity of PRDM9 is probably facilitated by the fact that the nucleotide sequence has a minisatellite-like structure that is prone to insertions and deletions (Ponting 2011). This hotspot-targeting mechanism confirms the rapid extinction predicted by the hotspot paradox and explains how hotspots can nonetheless exist.

Several lines of investigations in mice and humans provide evidence for hotspot erosion as a consequence of biased gene conversion. In other words, motifs with high binding affinity for PRDM9 have a greater tendency to disappear from the genome because they are DSB hotspots. First, the 13 bp consensus motif recognized by a human *PRDM9* allele is lost at a faster rate from the human genome compared to the chimpanzee genome, where the motif does not designate recombination hotspots (Myers et al. 2010; Lesecque et al. 2014). Second, new combinations of *Prdm9* alleles and genetic backgrounds in knock-in mice show increased hotspot number and activity, presumably because that particular PRDM9 did not co-evolve with that genome, so its target sequences have not been subject to erosion (Baker et al. 2015). Third, hybrid mice with subspecies-specific *Prdm9* alleles exhibit asymmetric PRDM9 binding and hotspot activity, where DSB hotspots associated with a *Prdm9* allele occur largely on the chromosome it did not co-evolve with (“non-self”) (Davies et al. 2016; Smagulova et al.

2016). Along the same lines, a humanized mouse *Prdm9* allele with the zinc finger array replaced with the corresponding human *PRDM9* sequence promotes hotspots on both PWD and B6 strain genomes in a hybrid, since the human PRDM9 binding sites have not experienced motif erosion in the mouse genomes (Davies et al. 2016). Also consistent with biased gene conversion causing hotspot erosion, novel hotspots identified in hybrid mice are 4-fold more likely to arise from PRDM9 binding site losses in the “self” genome than by hotspot-activating mutations in the “non-self” genome (Smagulova et al. 2016).

Biased gene conversion predicts that hotspots are short-lived. Based on comparisons of recombination hotspots in modern and archaic human lineages, Lesecque, Duret and colleagues predict that the 13 bp consensus motif determining a subset of human hotspots will be lost in ~3 My as a result of biased gene conversion (Lesecque et al. 2014). A shorter hotspot lifespan of 8,000–150,000 years has been predicted by Jeffreys and Neumann, based on simulations with the parameters observed in an actual human hotspot (e.g., population frequency and transmission distortion ratio into crossover progeny of the hotspot allele) (Jeffreys and Neumann 2009). In mouse, Cole, Jasin, Keeney, de Massy and colleagues demonstrated that the gene conversion tract can be offset from the DSB hotspot center, thereby preserving the PRDM9 binding site, and providing a mechanism to prolong hotspot lifespan (Cole et al. 2014). In fact, 80% of the gene conversion events at the mouse *A3* hotspot did not lead to loss of the PRDM9 binding site (Cole et al. 2014). Using the transmission frequency detected for *A3*, the speed of hotspot loss was modeled and hotspot extinction was estimated to take 4,176 generations, instead of 1,160 generations if every recombination event were to result in loss of the hotspot allele (Cole et al. 2014).

It is important to distinguish the two kinds of rapid changes to the DSB landscape described above. One is hotspot erosion, or the loss of DSB hotspot alleles, due to

biased gene conversion, particularly if the sites of preferred break formation are not under selective constraint (discussed in the next section). Hotspot erosion is relatively hotspot autonomous (loss of one hotspot is independent of other hotspots) and brings about gradual change to the DSB landscape, since not all gene conversion events result in loss of the DSB hotspot allele. However, hotspot erosion can be rapid over evolutionary time scales that are sufficiently long. The second kind of rapid change to the DSB landscape is via changes to the PRDM9 binding specificity. Changes to PRDM9 binding specificity result in global and abrupt changes to the DSB landscape, giving rise to many novel hotspots at once (and conversely, resulting in loss of hotspots due to reduced affinity to consensus motifs that designated hotspots under a different PRDM9 allele), and can occur from one generation to the next.

Targeting of recombination to genomic features under selective constraint suggests a means to conserve the recombination landscape. Nearly three decades ago, upon identification of a recombination hotspot in the *ARG4* promoter of budding yeast, Nicolas, Szostak and colleagues predicted that coupling hotspots with cellular processes under strong selective pressure would lead to conservation of recombination hotspot locations (Nicolas et al. 1989). That is, the selective pressure to maintain functional promoters would be enough to counteract the biased gene conversion drive to eliminate hotspots.

Based on our current understanding of the meiotic DSB distribution in yeast, combinations of direct and indirect selective pressures probably constrain the recombination landscape. Direct constraints include the selective advantage of recombination for proper homolog segregation and gamete viability (Coop and Przeworski 2007), and the selective advantage of certain genetic linkages. For example, the *CEN-MAT* linkage is believed to maintain heterozygosity in populations with high frequency of intratetrad mating, such as budding yeast (Taxis et al. 2005; Knop 2006;

Keller and Knop 2009). Indirect constraints on the DSB landscape are features that are under evolutionary constraint due to roles unrelated to meiosis, but which consequently contribute to DSB landscape conservation. Many of the factors that determine the DSB landscape in yeast have crucial roles in other biological processes: e.g., nucleosome occupancy, histone modifications, transcription factors, replication, sister chromatid cohesion, and their roles in gene expression, chromosome segregation, and compaction (Pan et al. 2011; Cooper et al. 2016). Nevertheless, modeling studies on hotspot lifespan have concluded that selective pressures to maintain recombination are not strong enough to counteract the effect of biased gene conversion on hotspots (Boulton et al. 1997; Pineda-Krch and Redfield 2005).

Comparison of recombination landscapes across and within species

Whether hotspots rapidly diverge or are conserved over evolutionary time-scales varies in different organisms. The following section summarizes empirical observations on evolutionary dynamics of recombination hotspots and the recombination landscape in different taxa. Most notably, it is increasingly becoming clear that it is possible for hotspots to be conserved, despite theoretical studies that considered it implausible for direct or indirect selective constraints to be sufficient to offset the effects of biased gene conversion. The evolutionary dynamics of hotspots appear to be linked to the underlying molecular mechanism of hotspot designation (i.e., Spo11 localizing to sites with or without the guidance of PRDM9).

Mouse. Hotspot locations vary in mouse strains carrying different *Prdm9* alleles (Baudat et al. 2010; Brick et al. 2012; Smagulova et al. 2016). For example, two congenic mouse strains with different *Prdm9* alleles share only ~1% of DSB hotspots, whereas two mouse strains with the same *Prdm9* allele share up to 98% of DSB hotspots (Brick et al. 2012; Smagulova et al. 2016). Different site usage between

congenic mouse strains with different *Prdm9* alleles (where the *Prdm9* allele has been replaced with one from another strain) is also detected when mapping PRDM9-dependent H3K4me3 peaks as a proxy for recombination hotspots (Baker et al. 2015).

Humans and chimpanzees. Chimpanzee recombination rates tend to be higher around CpG islands and near transcription start sites, but are reduced within genes (Auton et al. 2012). PRDM9 appears to help localize recombination hotspots in chimpanzees and other great apes (Stevison et al. 2015). The locations of recombination hotspots are not conserved between chimpanzees, bonobos, and gorillas (Stevison et al. 2015), and neither are they conserved between chimpanzees and humans (Ptak et al. 2005; Winckler et al. 2005; Myers et al. 2010; Auton et al. 2012). For example, only 8% of hotspots inferred from chimpanzee patterns of linkage disequilibrium overlapped a hotspot in humans (Ptak et al. 2005). However, broad-scale patterns (Mb) of recombination rates appear more conserved, with recombination rates elevated at subtelomeric regions in both species (Auton et al. 2012).

Recombination hotspots are also variable among humans, with hotspots being population-specific (Coop et al. 2008; Kong et al. 2010; Hinch et al. 2011; Pratto et al. 2014). In addition, recombination hotspots do not appear to have been shared between modern humans and the Denisovan archaic human lineage (Leseque et al. 2014). The lack of hotspot conservation between human populations, and between humans and their closest extant relative can be attributed to different *PRDM9* alleles that recognize different sequence motifs (Baudat et al. 2010; Berg et al. 2010; Myers et al. 2010; Berg et al. 2011; Hinch et al. 2011).

Yeast. There is no PRDM9 ortholog in yeast. In budding yeast, a recombination map of *S. paradoxus* chromosome III was estimated from linkage disequilibrium analysis of SNPs, and the locations of elevated recombination were compared with *S. cerevisiae* DSB hotspots (Tsai et al. 2010). The results suggest that large-scale recombination

distribution is conserved between the two species. However, this study was limited by the low resolution of the recombination map (kb), which precludes identification of individual hotspots (~0.2 kb), and instead detects clusters of hotspots. Secondly, chromosome III is an atypical chromosome, and therefore may not be representative. The recombination landscape of chromosome III is unique due to the *CEN-MAT* linkage, whereby the ~100 kb zone between these two loci is sparse in DSBs, correlating with low level of recombination events between the two markers (Mortimer et al. 1992; Baudat and Nicolas 1997). Since chromosome III is only ~316 kb long, DSBs (and ensuing crossovers) are restricted to the flanking regions in the remaining two-thirds of the chromosome. Chromosome III in yeasts may therefore tend to exhibit greater conservation of the large-scale recombination landscape, since limitations on where crossovers can occur are imposed. Finally, DSB hotspots were not directly examined. Thus, whether hotspots are conserved in other chromosomes, and whether the conclusions hold true at higher resolution were not addressed.

In fission yeast, meiotic DSB maps of *S. pombe* and *S. kambucha* (species with 0.5% sequence divergence) were generated by immunoprecipitating Rec12 in the *rad50S* mutant background, followed by hybridization of the covalently-linked DNA to a microarray (Cromie et al. 2007; Zanders et al. 2014). Comparison of these maps demonstrated that the DSB landscapes are conserved, both in terms of hotspot location and intensities (Zanders et al. 2014).

Canids. Over broad scales, the recombination landscape in dogs—from linkage disequilibrium-based estimates of recombination—appears similar to other mammals, with highest recombination rates in telomeric regions, and lowest in centromeric regions (Auton et al. 2013). At finer scales, recombination hotspots in dogs are located near CpG-rich regions, including gene promoters (Auton et al. 2013; Berglund et al. 2015). These features are markedly different from mice and humans, and are instead

reminiscent of the DSB pattern in *Prdm9*^{-/-} mice or in wild type budding yeast (Myers et al. 2005; International HapMap et al. 2007; Pan et al. 2011; Smagulova et al. 2011; Brick et al. 2012; Lu et al. 2012; Pratto et al. 2014).

The *PRDM9* ortholog is predicted to be nonfunctional in dogs and other canid species due to a premature stop codon and frameshift mutations (Oliver et al. 2009; Muñoz-Fuentes et al. 2011; Axelsson et al. 2012). Accordingly, recombination hotspots have been reported to be stable in dogs, inferred from patterns of GC-biased substitution at dog hotspot GC peaks compared with panda and cat GC peaks (Axelsson et al. 2012), supporting the hypothesis that recombination hotspots are stable in the absence of functional PRDM9. However, Auton, Boyko and colleagues concluded that recombination hotspots are not necessarily stable in the canid lineage, based on the lack of a detectable AT to GC skew in fox lineage polymorphisms around dog recombination hotspots (Auton et al. 2013).

A caveat to the studies in canids is that the available recombination maps have low spatial resolution, so the recombination hotspots reflect broad regions with elevated recombination rates rather than hotspots *per se*. Axelsson and colleagues generated dog recombination maps based on patterns of linkage disequilibrium inferred from 170,000 SNP markers, and identified recombination hotspots with an average width of 33 kb (Axelsson et al. 2012). Subsequently, Auton and colleagues generated linkage disequilibrium-based recombination maps from next-generation genome sequencing data with 3.5 million SNPs, and identified recombination hotspots with an average width of 22 kb (Auton et al. 2013; Berglund et al. 2015). In contrast, recombination hotspot widths have been mapped to ~1–2 kb in mouse and human using direct and indirect approaches to map recombination hotspots (Jeffreys et al. 2001; Kauppi et al. 2004; Coop and Przeworski 2007; Smagulova et al. 2011; Khil et al. 2012; Pratto et al. 2014). The low resolution of the recombination maps and the lack of direct molecular evidence

for where DSB hotspots are located in dogs make it difficult to discern patterns of hotspot activity with high confidence.

Birds. Recombination hotspots in finches are located near transcription start sites, transcription stop sites, and CpG islands, based on high-resolution recombination maps (identified hotspots were 2–5 kb wide) inferred from population genetic data (Singhal et al. 2015). Birds lack a functional PRDM9 ortholog (Oliver et al. 2009), and recombination hotspots are conserved between zebra finches and long-tailed finches (Singhal et al. 2015). Indirect methods to infer hotspots (through elevated GC content, which is evidence for GC-biased gene conversion and expected to be higher in hotspots) also suggested conserved hotspot locations between zebra finch and the collared flycatcher, species ~19 My diverged (Singhal et al. 2015).

Drosophila. *Drosophila* is different from most other organisms in that males do not undergo meiotic recombination (Morgan 1912), and homologous chromosome pairing and synapsis are not dependent on recombination (Hawley et al. 1992; Page and Hawley 2004). In *Drosophila*, there are no recombination hotspots, as defined by (1) short (<2kb), discrete genomic regions with elevated recombination frequency compared to the background rate, and (2) the majority of recombination events occurring within these regions (Singh et al. 2009; Chan et al. 2012; Manzano-Winkler et al. 2013; Smukowski Heil et al. 2015). Instead, recombination is more widely distributed across the genome. Only approximately 20 “hotspots” fit the criteria of being 500–5000 bp wide and having a recombination rate >10-fold higher than the background recombination rate (Chan et al. 2012; Smukowski Heil et al. 2015), whereas humans have >30,000 recombination hotspots (Consortium 2005; International HapMap et al. 2007). Recombination rates are reduced around transcription start sites and at the 5' end of genes (Smukowski Heil et al. 2015); therefore recombination is not preferentially located near promoters. This genus lacks a PRDM9-like system (Oliver et al. 2009; Heil and

Noor 2012). A comparison of two *Drosophila* species >3 My diverged—*D. pseudoobscura* and *D. miranda*—showed that recombination rate is conserved at broad scales (~500 kb), but fine-scale patterns (50 kb) appear to evolve rapidly (Smukowski Heil et al. 2015).

Aims of the thesis

Meiotic DSB formation and recombination are evolutionarily conserved across different phyla, but some mechanistic aspects, such as accessory factors and hotspot designation, have diverged. The overarching goal of this thesis is to further our understanding of the mechanisms that dictate and regulate the meiotic recombination initiation landscape. In **Chapter 2**, I approach this question through the angle of DSB landscape evolution in yeasts. Comparison of meiotic DSB hotspots and the DSB landscapes in different Saccharomycetes provides a framework for thinking about how the underlying mechanism of DSB formation affects its evolutionary dynamics. In **Chapter 3**, I examine the contribution of chromosome structure proteins to the meiotic DSB landscape. The DSB maps in *red1*, *hop1*, and *mek1* mutants uncover both intrinsic and extrinsic roles of chromosome structure proteins in shaping the DSB landscape. An overarching discussion of both stories is presented in **Chapter 4**, along with perspectives, implications, and future directions. Lastly, in the **Appendix**, I investigate the role of Rec104 phosphorylation in yeast meiotic recombination.

CHAPTER 2: EVOLUTIONARY DYNAMICS OF THE MEIOTIC DSB LANDSCAPE IN SACCHAROMYCETES²

Summary

The nonrandom distribution of meiotic recombination shapes heredity and genetic diversification. In theory, individual hotspots either evolve rapidly toward extinction or may be conserved. The prediction that hotspots evolve rapidly toward extinction derives from biased gene conversion, which is inherent to recombination (Boulton et al. 1997). There are many examples of rapidly diverging hotspots: recombination hotspots are not conserved between humans and chimpanzees (Ptak et al. 2005; Winckler et al. 2005; Myers et al. 2010; Auton et al. 2012), between mouse strains (Baudat et al. 2010; Brick et al. 2012; Smagulova et al. 2016), or between human individuals (Coop et al. 2008; Kong et al. 2010; Hinch et al. 2011; Pratto et al. 2014). These can be attributed to interplay between hotspot loss from biased gene conversion (Myers et al. 2010; Cole et al. 2014; Baker et al. 2015; Davies et al. 2016; Smagulova et al. 2016) and the rise of novel hotspots from the rapidly evolving DNA binding specificity of PRDM9, which determines recombination hotspot location in these organisms (Baudat et al. 2013). However, most taxa (including yeast and some mammals) lack such a system, so it has remained unclear how generalizable this solution is.

An alternative model is that hotspot positions can be evolutionarily stable if Spo11 targets genomic features that are under selective constraint for functions unrelated to their roles as hotspots (Nicolas et al. 1989; Pan et al. 2011). This hypothesis derives from correspondence of most hotspots in *S. cerevisiae* with promoter-containing IGRs (Pan et al. 2011). Gene promoters are under selective

² Adapted from Lam I, Keeney S. (2015) Nonparadoxical evolutionary stability of the recombination initiation landscape in yeast. *Science* **350**, 932-7. Reprinted with permission from AAAS. This chapter also includes portions reprinted from Vincenten N, Kuhl LM, Lam I, Oke A, Kerr AR, Hochwagen A, Fung J, Keeney S, Vader G, Marston AL. (2015) The kinetochore prevents centromere-proximal crossover recombination during meiosis. *Elife* **4**, e10850.

constraint due to their role in proper gene expression and cell survival. Yeasts have no *Prdm9* ortholog, and NDRs at gene promoters are conserved (Tsankov et al. 2010; Tsui et al. 2011). Therefore, conservation of most hotspots is predicted in *Saccharomyces* species. Recombination hotspots have been reported to be stable in canids, which lack *PRDM9* and have recombination hotspots near gene promoter regions (Muñoz-Fuentes et al. 2011; Axelsson et al. 2012; Auton et al. 2013). Concurrent with our investigation, Przeworski and colleagues detected conservation of recombination hotspots in finches, which lack *PRDM9* and have hotspots designated near functional genomic elements (Singhal et al. 2015).

Nevertheless, theoretical studies have considered selective constraint of genomic elements implausible as a mechanism to preserve hotspots (Boulton et al. 1997; Pineda-Krch and Redfield 2005). Instead, many studies start from the assumption that hotspot lifespan must always be short and that the fine-scale recombination initiation landscape will always be highly dynamic over evolutionary scales (Calabrese 2007; Friberg and Rice 2008; Smukowski and Noor 2011; Ubeda and Wilkins 2011). This assumption is appropriate for primates and mice because they use *PRDM9*, but has not been evaluated for other taxa. I empirically tested these theories by comparing genome-wide maps of meiotic recombination initiation from widely divergent species in the *Saccharomyces* clade (up to 15 My and 30% sequence diverged), and asked whether the DSB landscape is conserved. I find that hotspots frequently overlap with promoters in the species tested and, consequently, hotspot positions are well conserved. Remarkably, the relative strength of individual hotspots is also highly conserved, as are larger-scale features of the distribution of recombination initiation. This stability, not predicted by prior models, suggests that the particular shape of the yeast recombination landscape is adaptive, and helps in understanding evolutionary dynamics of recombination in other species.

Results

The *Saccharomyces sensu stricto* clade

S. cerevisiae belongs to the *Saccharomyces sensu stricto* clade, which last shared a common ancestor ~20 million years ago (Replansky et al. 2008; Liti et al. 2013) (**Fig. 2.1**). To address the question of DSB landscape plasticity in yeast species, I generated genome-wide meiotic DSB maps in the following *Saccharomyces* species: *S. paradoxus*, *S. mikatae*, and *S. kudriavzevii*. *S. paradoxus*, the most closely related species to *S. cerevisiae*, has coding sequence divergence from *S. cerevisiae* comparable to that between humans and mice (~100 million years divergence), and the most diverged species in my analysis, *S. kudriavzevii*, is roughly as distant as mammals from birds (~300 million years divergence) (Dujon 2006).

I also compared wild-derived *S. cerevisiae* strains from different lineages, YPS128 (North America) and UWOPS03-461.4 (Malaysia), with the lab strain SK1 commonly used in meiosis research (Liti et al. 2009) to evaluate intraspecies variation. The *S. cerevisiae* strains chosen display 0.5–0.7% sequence divergence, comparable to the polymorphism density between humans and chimpanzees. Most differences are simple sequence polymorphisms (SNPs and small indels), with few large-scale structural differences aside from one discussed below (Kellis et al. 2003; Liti et al. 2009).

Conservation of Spo11 oligos

All yeasts examined underwent synchronous and efficient meiosis when sporulated under standard lab conditions (**Fig. 2.2A**); hence the strain SK1 is not anomalous in this regard. I examined whether Spo11-oligo complexes form in these species as in *S. cerevisiae*. Spo11-oligo complexes are a byproduct of DSB formation, and represent Spo11 covalently linked to the 5' ends where the DNA was broken (Neale et al. 2005). Spo11-oligo complexes are detected by immunoprecipitating Spo11, end-

labeling the associated oligos, and resolving by SDS-PAGE (Neale et al. 2005; Neale and Keeney 2009). As in *S. cerevisiae*, two major size classes of Spo11-oligo complexes were detected in the other *Saccharomyces* species (**Fig. 2.2B, C**). In all species examined, Spo11-oligo complexes are not detectable immediately after transfer to sporulation media (t = 0 h), corresponding with meiosis-specific expression of Spo11, but levels increase, then decrease with meiotic progression (**Fig. 2.2B**), indicating that the mechanism and regulation of Spo11 endonucleolytic release from DSB ends is conserved in *Saccharomyces* species. *S. pombe* is diverged in this aspect, in that it exhibits only one size class of oligo complexes with its Spo11 homolog Rec12 (Milman et al. 2009).

Spo11 oligos can be isolated by deproteinizing Spo11-oligo complexes (Pan et al. 2011). Purified Spo11 oligos in *Saccharomyces* species were resolved by denaturing polyacrylamide gel electrophoresis to assess their size distribution. The resulting Spo11 oligos show similar length distribution in the different species (**Fig. 2.2D**).

Previously, population genetic data were used to deduce a recombination map in *S. paradoxus* and compare it to *S. cerevisiae* (Tsai et al. 2010). Partial conservation was inferred, but the data had insufficient resolution to detect individual hotspots (Pan et al. 2011). I overcame these limitations by comparing high-resolution, whole-genome DSB maps between widely diverged *Saccharomyces* species and between *S. cerevisiae* strains. DSB maps were generated by deep sequencing of Spo11 oligos, since each oligo is a tag recording where Spo11 generated a DSB (Pan et al. 2011). Spo11-oligo maps agree spatially and quantitatively with direct detection of DSBs by Southern blot (Pan et al. 2011). Biological replicate maps were highly reproducible (**Fig. 2.3**) and most sequenced reads (>97%) were mapped uniquely (**Table 2.1**).

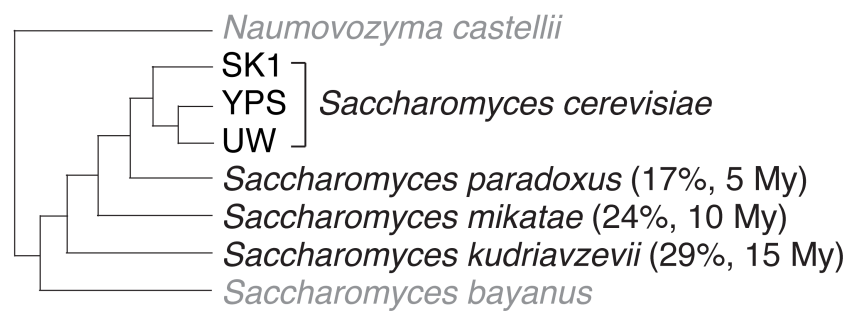


Figure 2.1. Schematic of *Saccharomyces* phylogeny. Based on (Replansky et al. 2008; Liti et al. 2009). Black, species/strains in this study. Genic sequence divergence from *S. cerevisiae* (Liti et al. 2013) and estimated time since last common ancestor (Replansky et al. 2008) are shown in parenthesis. YPS, YPS128; UW, UWOPS03-461.4. From (Lam and Keeney 2015). Reprinted with permission from AAAS.

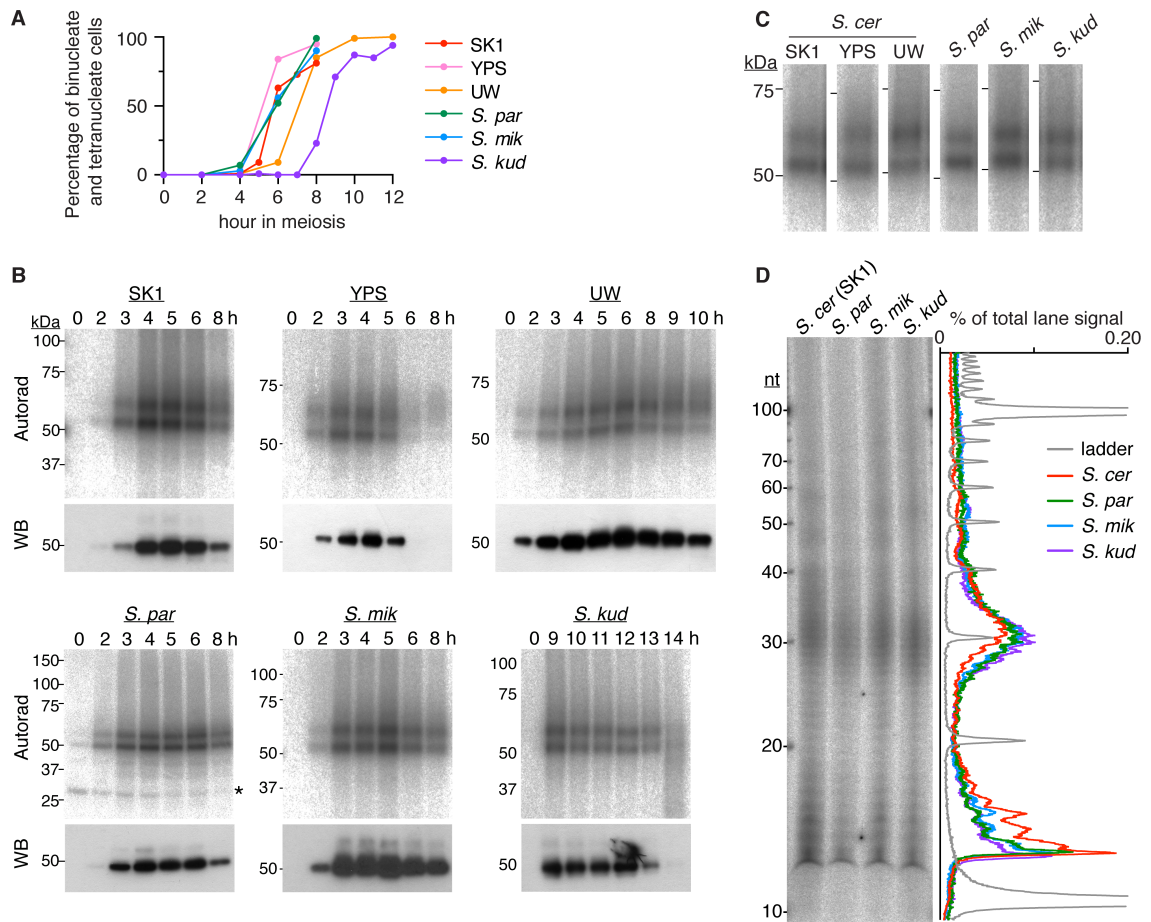


Figure 2.2. Characteristics of sporulation and Spo11-oligo complexes in different *Saccharomyces* strains and species. (A) Meiotic progression showing percentage of cells completing the first division (total bi- and tetranucleate cells). ≥ 100 cells were counted at each time point for each sample. (B) Spo11-oligo complex time courses. Epitope-tagged Spo11 was immunoprecipitated with anti-Flag antibody from denaturing extracts of meiotic cultures at the indicated times, then radioactively labeled with terminal deoxynucleotidyl transferase and $[\alpha\text{-}^{32}\text{P}]\text{dCTP}$. Labeling reactions were electrophoresed on SDS-PAGE gels. Radiolabeled Spo11-oligo complexes were detected by autoradiography (top) and total Spo11 was detected by anti-Flag western blot (WB). Note that nearly all of the western blot signal is from free Spo11, i.e., protein that has not made a DSB (Neale et al. 2005). Asterisk indicates labeling of a nonspecific species in *S. paradoxus* that also appears when carrying out mock immunoprecipitation on an untagged Spo11 strain, but that is not visible when performing two sequential rounds of immunoprecipitation for Spo11-oligo mapping. (C) Conserved sizes of Spo11-oligo complexes. A single, representative time-point for each species or strain is shown side-by-side. (D) Conserved sizes of Spo11 oligos. Immunoprecipitated, radiolabelled Spo11-oligo complexes were digested with proteinase K and resolved on a denaturing polyacrylamide gel. Autoradiographs (with lane traces in D) are shown in B–D. From (Lam and Keeney 2015). Reprinted with permission from AAAS.

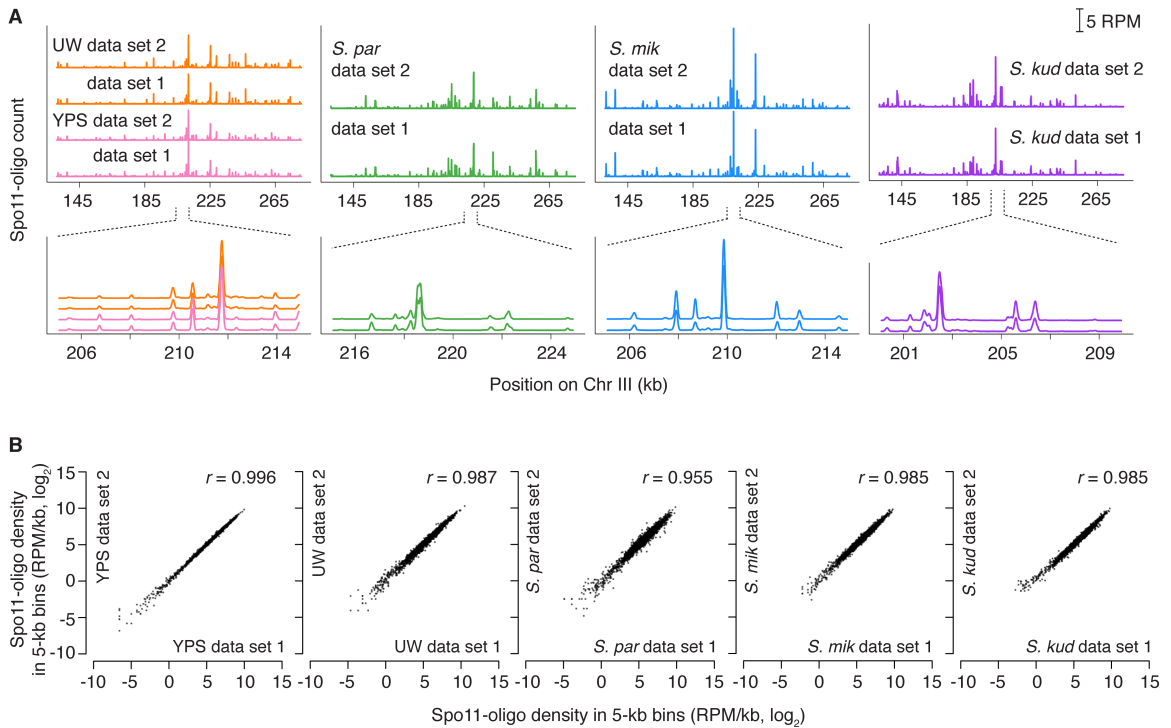


Figure 2.3. Reproducibility of Spo11-oligo maps in *Saccharomyces* species. (A) Qualitative analysis showing reproducibility of the biological replicate maps in an ~8 kb region of chromosome III. RPM, reads per million mapped; profiles were smoothed with 201-bp Hann window. (B) Quantitative analysis. Uniquely mapped Spo11 oligos were summed in non-overlapping 5-kb bins and expressed as RPM per kb (plotted on a log₂ scale). Pairwise correlation coefficients are shown (Pearson's r). Panel A from (Lam and Keeney 2015). Reprinted with permission from AAAS.

Table 2.1. Mapping statistics for yeast species Spo11 oligo sequences

Dataset	Strain	No. of total reads	Genome mapped to	No. mapped	No. mapped uniquely
YPS128-1	<i>S. cerevisiae</i> YPS128 T(III;XIII) SKY4632	6,093,081	<i>S. cerevisiae</i> S288C	5,550,288	5,472,547 (98.6%)
YPS128-2	<i>S. cerevisiae</i> YPS128 T(III; XIII) SKY4632	4,247,586	<i>S. cerevisiae</i> S288C	3,891,037	3,776,593 (97.1%)
YPS128-3	<i>S. cerevisiae</i> YPS128 SKY4633	20,987,066	<i>S. cerevisiae</i> S288C	19,316,922	19,085,392 (98.8%)
YPS128-4	<i>S. cerevisiae</i> YPS128 SKY4633	24,963,684	<i>S. cerevisiae</i> S288C	22,743,707	22,471,981 (98.8%)
UWOPS-1	<i>S. cerevisiae</i> UWOPS03- 461.4 SKY4664	5,871,998	<i>S. cerevisiae</i> S288C	5,087,159	4,996,549 (98.2%)
UWOPS-2	<i>S. cerevisiae</i> UWOPS03- 461.4 SKY4664	3,799,030	<i>S. cerevisiae</i> S288C	3,416,873	3,358,908 (98.3%)
Spar1	<i>S. paradoxus</i> YPS138 SKY4411	6,641,178	<i>S. paradoxus</i> YPS138	6,005,923	5,926,000 (98.7%)
Spar2	<i>S. paradoxus</i> YPS138 SKY4411	6,872,508	<i>S. paradoxus</i> YPS138	5,675,981	5,602,019 (98.7%)
Spar1_CBS432 ^a	<i>S. paradoxus</i> YPS138 SKY4411	6,641,178	<i>S. paradoxus</i> CBS432	4,625,865	4,534,439 (98.0%)
Spar2_CBS432 ^b	<i>S. paradoxus</i> YPS138 SKY4411	6,872,508	<i>S. paradoxus</i> CBS432	4,322,128	4,244,734 (98.2%)
Smik2	<i>S. mikatae</i> IFO1815 SKY4490	3,112,231	<i>S. mikatae</i> IFO1815	2,937,039	2,916,164 (99.3%)
Smik3	<i>S. mikatae</i> IFO1815 SKY4490	6,665,306	<i>S. mikatae</i> IFO1815	6,297,240	6,241,580 (99.1%)
Skud2	<i>S. kudriavzevii</i> ZP591 SKY4488	5,016,979	<i>S. kudriavzevii</i> ZP591	4,597,476	4,558,486 (99.2%)
Skud3	<i>S. kudriavzevii</i> ZP591 SKY4488	5,778,620	<i>S. kudriavzevii</i> ZP591	5,358,181	5,282,452 (98.6%)

^a Same sample as Spar1, but reads were mapped to *S. paradoxus* type strain CBS432

^b Same sample as Spar2, but reads were mapped to *S. paradoxus* type strain CBS432

Targeting of DSBs to promoters is conserved

I asked whether targeting of promoters is conserved among yeast. I mapped nucleosomes by sequencing micrococcal nuclease-resistant DNA (MNase-seq) from meiotic cultures. In *S. cerevisiae*, DSBs form preferentially in promoter-associated NDRs (Ohta et al. 1994; Wu and Lichten 1994; Fan and Petes 1996; Berchowitz et al. 2009; Pan et al. 2011), and promoter chromatin structure during mitotic growth is conserved among other *Saccharomyces* species (Tirosh et al. 2010; Tsankov et al. 2010; Tsui et al. 2011). Spo11 oligos were highly enriched in promoter NDRs in all species tested, whether examined at individual locations (**Figs. 2.4A**), or averaged across annotated genes (**Figs. 2.4B**). Many Spo11 oligos mapped to promoter-containing IGRs (i.e., IGRs flanked by divergent or tandemly oriented genes), whereas few mapped to convergent IGRs (i.e., lacking promoters) or within genes (**Figs. 2.4D**). I conclude that the Spo11 preference for promoters is a stable feature of the *Saccharomyces* DSB landscape.

Similar numbers of Spo11-oligo hotspots (~4000) were identified in all species (Table S3 in (Lam and Keeney 2015)). When ranked by Spo11-oligo count, hotspots formed a smooth continuum over a wide range, with nearly superimposable cumulative curves in all species (**Figs. 2.5A**). Hence, the distribution of DSBs among hotspots is the same. Hotspots had low average nucleosome occupancy (**Figs. 2.4C**) consistent with open chromatin structure providing a window of opportunity for Spo11 (Lichten 2008). The distribution of hotspot widths was also nearly identical (median hotspot width ~200 bp), with wider hotspots tending to have more Spo11 oligos (**Figs. 2.5B**). Conserved hotspot width agrees with conservation of NDR width observed previously (Tirosh et al. 2010; Tsankov et al. 2010; Tsui et al. 2011). Importantly, most hotspots overlapped the same promoter-containing IGRs in all species examined (**Figs. 2.5C, D**).

The low frequency of sex and outcrossing in yeasts could slow hotspot extinction compared to obligately outcrossed species (Tsai et al. 2010; Goodstadt and Ponting

2011), but the yeasts examined here have had ample sexual generations to allow biased gene conversion to erode hotspots. For example, there have been an estimated >200,000 outcrossed sexual generations since divergence of *S. cerevisiae* from *S. kudriavzevii*, comparable to the number of human sexual generations since divergence from chimpanzees (details in **Chapter 5**). Therefore, *Saccharomyces* species have undergone enough meioses for hotspots to evolve (and for biased gene conversion to exert its effect), and yet, hotspots are very well conserved. Thus, as predicted (Nicolas et al. 1989), DSB hotspot locations can be preserved when the targeted chromosome architecture is conserved.

Conservation of DSB frequency in hotspots

The hotspot paradox predicts that hotspot strength should vary widely even if their locations are conserved. Furthermore, the rate of hotspot extinction should scale with hotspot heat, because alleles that experience frequent DSBs provide more chances for loss (Boulton et al. 1997; Pineda-Krch and Redfield 2005; Calabrese 2007; Coop and Myers 2007; Cole et al. 2014). The selective constraint model is agnostic in this regard: if *cis*-acting sequence polymorphisms can quantitatively modulate DSB formation without ablating Spo11 targeting (which has been experimentally shown (e.g., White et al. 1993)), then hotspot heats will change rapidly. On the other hand, if DSB frequency (not just position) is tied to selectively constrained features, or if DSB frequency is itself constrained, then hotspot heats will tend to be conserved.

To address this question, I summed Spo11 oligos within 3426 promoter-containing IGRs that could be stringently and unambiguously matched between species on the basis of conservation of flanking coding sequences (**Fig. 2.6A**, Table S4 in (Lam and Keeney 2015)). To be considered a matched IGR, both genes flanking the IGR have to be conserved in the same order and in the same orientation, and reside on the same

chromosome in all four species. Convergent matched IGRs were excluded, as these do not encompass gene promoters. Since 88% of DSB hotspots overlap promoter regions in *S. cerevisiae* (Pan et al. 2011), these matched promoter IGRs serve as a proxy for comparing hotspot intensity in the absence of a common genomic coordinate for direct comparison of hotspots. This group of matched promoter IGRs contains 81% of divergent and tandem IGRs and accounts for 83% of promoter-proximal hotspots in *S. cerevisiae*, thus most of the relevant Spo11-targeted genomic space is included. An IGR-centric approach is preferable to relying on more arbitrary hotspot definitions because substantial sequence divergence within IGRs (where most hotspots lie) makes it difficult or impossible to match hotspot boundaries between species, whereas coding sequence of flanking genes are better conserved, allowing more precise definition of boundaries in genomic space between different species. Secondly, the arbitrary nature of hotspot definitions means that there is no biologically defined cutoff between what is and what is not a hotspot. Thirdly, comparing DSBs within promoter IGRs instead of DSB hotspots allows us to compare DSB-cold promoter regions as well.

Within-IGR Spo11-oligo counts were highly similar between *S. cerevisiae* strains: I observed correlation coefficients (0.89–0.92) (**Fig. 2.6B, C**) that were nearly as high as for comparisons between biological replicates (0.97–1.00). Thus, intra-species variation of DSB heat within these IGRs is low despite ~0.7–1% median sequence divergence.

Strong correlations were also found between species, with little change in correlation strength over large evolutionary distances (**Fig. 2.6B-C, E-F**). *S. cerevisiae* and *S. kudriavzevii*, which are species 15 My diverged, still show very strong positive correlation in local DSB heat (Pearson's $r = 0.64$ – 0.68 ; **Fig. 2.6B, C**). Moreover, the hottest 1% of promoter IGRs in *S. cerevisiae* SK1 were enriched among the hottest IGRs in other species, with a median percentile ranking within the top 5% even in *S. kudriavzevii* (**Fig. 2.6G, H**). This was only modestly greater than the extent of

conservation of the coldest IGRs (**Fig. 2.6G**). Theoretical modeling of biased gene conversion predicts that strong hotspots are less likely to be shared between species than weak ones (Coop and Myers 2007). I found specific examples where strong hotspots in one species were substantially weaker in other species (**Fig. 2.6I**), so there is no absolute barrier to evolutionary changes. But the behavior of most IGRs leads to the conclusion that the hottest hotspots present in the last common ancestor of *Saccharomyces* tended to retain high Spo11 target activity, and that it has been rare for ancestrally cold promoters to acquire strong hotspot activity.

This high degree of yeast hotspot conservation differs markedly from that in humans: DSB hotspot heat between men sharing the same or similar *PRDM9* alleles (Pratto et al. 2014) was less conserved than between *S. cerevisiae* strains despite much greater sequence identity (**Fig. 2.6D-F**). This difference is consistent with PRDM9 motif erosion contributing to variation in hotspot strength between individuals (Pratto et al. 2014).

Conservation of the DSB landscape over larger size scales

Hotspots are only one level of nonrandomness in the DSB landscape in that they reside within larger domains of greater or lesser DSB potential (Kauppi et al. 2004; Pan et al. 2011). In several taxa, conservation has been noted for the distribution of crossover recombination over broad genomic regions (Smukowski and Noor 2011), but conservation of DSB distributions has not been evaluated. We therefore investigated if large-scale features of the DSB landscape are also conserved in yeast. Spo11-oligo maps demonstrated that DSB suppression observed near telomeres and centromeres (Blitzblau et al. 2007; Buhler et al. 2007; Lichten 2008; Pan et al. 2011; Vincenten et al. 2015) is preserved (**Figs. 2.7**), suggesting the molecular mechanism for DSB suppression in these regions is also conserved. As in *S. cerevisiae* SK1, Spo11-oligo

counts averaged across the 32 chromosome arms are reduced below genome average in the region ~20 kb away from telomere ends in other *S. cerevisiae* strains and in *S. paradoxus* (**Fig. 2.7A, B**). Near centromeres, average Spo11-oligo counts are also reduced ~5 kb from centromeres in the other species (**Fig. 2.7C, D**). These results are not surprising, as recombination in these subchromosomal regions can interfere with genome integrity: subtelomeric regions are rife with repetitive DNA elements that can undergo nonallelic homologous recombination (Louis 1995), and crossing over that occurs close to centromeres can disrupt pericentric cohesion or interfere with kinetochore orientation to the spindle poles, thereby causing segregation errors (Rockmill et al. 2006; Nambiar and Smith 2016).

Centromeres are the sites where kinetochores bind, and these large protein complexes in turn facilitate attachment of chromosomes to microtubules (Przewloka and Glover 2009). Suppression of pericentric DSBs is mediated by the kinetochore, as demonstrated in collaboration with Vincenten, Marston, and colleagues (Vincenten et al. 2015). I generated Spo11-oligo maps in the absence of Mcm21, a component of the kinetochore Ctf19 sub-complex. The maps show elevated DSBs near at the centromere in chromosome I (*CEN1*) (**Fig. 2.8A**) and in all other chromosomes (**Figs. 2.8B, C**). The zone of DSB suppression mediated by Mcm21 and the Ctf19 complex is inferred to be ~6 kb away from centromeres (**Fig. 2.9A**), and strikingly, no residual DSB suppression is detected in the *mcm21* mutant (**Fig. 2.9B**). DSB elevation at *CEN1* was also detected in the absence of other Ctf19 complex components besides Mcm21 (Vincenten et al. 2015). Thus, in light of these findings, conservation of pericentric DSB suppression in other *Saccharomyces* species is not unexpected, since the kinetochore function in chromosome segregation is likely highly conserved.

Spo11-oligo counts were also well correlated between species when we compared ~20-kb segments in syntenic regions across interstitial (i.e., non-telomeric and

non-centromeric) portions of the chromosomes (**Fig. 2.10A-F**). This scale is comparable to the average length of the chromatin loops of meiotic chromosomes, and DNA segments of this size typically encompass multiple hotspots (Pan et al. 2011; de Massy 2013). These findings indicate that the larger-scale domain structure of the DSB landscape is also evolutionarily stable.

Spo11-oligo counts were correlated with G+C content of DNA in each species tested, with weaker correlation over short distances (~1 kb) and stronger correlations over large distances (**Fig. 2.10G**). This scale-dependent pattern is consistent with the hypothesis that large-scale DSB domains, like hotspots, reflect selective constraint on the underlying chromosomal architecture (Pan et al. 2011). Furthermore, large-scale domains presumably reflect factors—such as attachment of chromatin loops to chromosome axes—that work in *cis* but at a distance from DSB hotspots. Because such factors are too far to be frequently included in gene conversion tracts and are thus not subject to loss through biased gene conversion, they are not expected to evolve as rapidly as hotspots (Boulton et al. 1997; Coop and Myers 2007; Peters 2008; Smukowski and Noor 2011).

Chromosome length directly affects DSB density

In *S. cerevisiae*, DSB density is anti-correlated with chromosome size, i.e., smaller chromosomes on average incur more DSBs per kb than larger ones (Pan et al. 2011). This relationship is conserved in other Saccharomycetes (**Fig. 2.11**). Multiple chromosomal rearrangements have recently been reported for the Malaysian lineage strains, including UWOPS03-461.4 (Marie-Nelly et al. 2014), which most likely explains the lower than expected Spo11-oligo density on chromosome VIII (**Fig. 2.11**) (all *S. cerevisiae* Spo11-oligo reads were mapped to the type strain S288C, so the chromosome lengths do not necessarily reflect the actual lengths for the source strains).

The whole-chromosome control of DSB density is in large part a patterning effect of a negative feedback circuit in which homologous chromosomes that have successfully engaged one another stop making additional DSBs (Thacker et al. 2014). Perhaps smaller chromosomes tend to take more time to engage their homologs and thus enjoy a longer window of opportunity to make DSBs. It has been argued (Thacker et al. 2014) that this form of DSB regulation can account for the earlier finding that smaller chromosomes undergo more crossing over per kb than larger chromosomes (Kaback et al. 1989; Kaback et al. 1992; Mortimer et al. 1992). Chromosome bisection and fusion experiments have demonstrated that difference in chromosome length is the cause of variation in crossover density (Kaback et al. 1992). A similar effect has been observed in reduced recombination rates over human chromosome 2, which arose from a fusion event of the orthologous chimpanzee chromosomes 2a and 2b (Auton et al. 2012). However, the effect of chromosome length on DSB density has not been formally tested.

S. mikatae provides a natural experiment, as reciprocal translocations have placed parts of ancestral chromosome VI onto longer chromosomes in that species (Fischer et al. 2000), thereby allowing me to ask whether chromosome length directly affects DSB density. I compared Spo11-oligo density within syntenic segments that are on different chromosome length contexts in *S. cerevisiae* and *S. mikatae*—e.g., syntenic segment 6L is on a 270-kb chromosome in *S. cerevisiae* but on an 801-kb chromosome in *S. mikatae* (**Fig. 2.12A**). DNA segments syntenic with the left and right arms of ancestral chromosome VI had a Spo11-oligo density predicted by their chromosome length: density was higher when the segments resided on the short chromosome VI in *S. cerevisiae* but lower when on longer chromosomes in *S. mikatae* (**Fig. 2.12A**). Syntenic segments (4L, 11L) on similar-length chromosomes exhibited matched Spo11-oligo densities (**Fig. 2.12B**). These findings indicate that whole-chromosome variation in DSB density is a direct consequence of chromosome size *per se* and is thus in large part

extrinsic to the DNA sequence. These results also imply that homolog engagement feedback inhibition is conserved in *Saccharomyces* species, as this feedback control circuit regulates DSB density variations based on chromosome length (Thacker et al. 2014).

A spontaneous chromosomal translocation in YPS128. A spontaneous chromosomal translocation in *S. cerevisiae* YPS128 resulting in different chromosome lengths was detected by Southern blotting when comparing chromosome III meiotic DSBs in tagged and untagged *SPO11* strains. Chromosome III in YPS128 is 329 kb, but a longer version (>388 kb) was detected in the *SPO11-Flag* strain, suggesting that a translocation involving chromosome III occurred in that lineage (**Fig. 2.13A**). Since I had already generated Spo11-oligo maps for that *SPO11-Flag* strain, I made Spo11-oligo maps of another *SPO11-Flag* strain that had wild-type length chromosome III. Comparison of DSB density per chromosome demonstrated that chromosome III has lower DSB density in the translocation strain, as expected since it is a longer chromosome in that strain (**Fig. 2.13B**).

The next step was to determine which other chromosome(s) is involved in the translocation. I reasoned that I might be able to use the Spo11-oligo maps to deduce translocation partner(s) via detection of changes to the DSB pattern. I examined fold change in Spo11 oligos for each chromosome, in strains with and without the translocation. Spo11 oligos were noticeably reduced along most of chromosome III in the translocation strain, and a region ~30 kb around the centromere on chromosome XIII exhibited elevated Spo11 oligos, whereas no major change was detected on other chromosomes (e.g., chromosome VI) (**Fig. 2.13C**). Therefore, chromosome XIII was a candidate translocation partner.

I confirmed the reciprocal translocations between chromosomes III and XIII by Southern blot of pulsed-field gels with targeted probes. In the translocation strain, the left

arm of chromosome III (probed with *CHA1*) is in a longer chromosome context, whereas the right arm (probed with *GIT1*) is in a chromosome length context similar to, but slightly longer than wild type chromosome III (**Fig. 2.13D** lane 2 for heterozygous strain; lanes 3, 4 for homozygous strain with respect to the translocation). Both the left arm and centromere-proximal segment of chromosome XIII (probed with *ERO1* and *CCS1*, respectively) are on a shorter chromosome context in the translocation strain, whereas the right arm (probed with *ADE4*) is in a chromosome length similar to, but slightly shorter than wild type chromosome XIII (**Fig. 2.13D** lane 2 for heterozygous strain; lanes 3, 4 for homozygous strain with respect to the translocation). Taken together, a reciprocal translocation between chromosomes III and XIII occurred in the heterozygous *SPO11-Flag* strain of YPS128, which stitched most of chromosome III (except for the right-most part) onto the right arm of chromosome XIII (referred to as T(III;XIII)), and the left arm and centromere-proximal region of chromosome XIII onto the right-most part of chromosome III (referred to as T(XIII;III)) (**Fig. 2.13E**).

The short chromosome length of T(XIII;III) is consistent with the higher Spo11-oligo levels detected in the centromere-proximal region of chromosome XIII in the translocation strain (**Fig. 2.13C**). However, a puzzling observation remained: according to the Southern blot experiments, the left arm of chromosome XIII is also on the short chromosome T(XIII;III), yet Spo11-oligo levels are not elevated in the left arm. It turns out that the left arm of chromosome XIII is less sensitive to homolog engagement-mediated feedback regulation: Spo11 oligos are elevated less than average in this region in the *zip3* mutant (**Fig. 2.13C**, blue box). Thus, moving the left arm of chromosome XIII onto a different chromosome length results in relatively unchanged Spo1-oligo levels.

This serendipitous translocated strain effectively demonstrates that chromosome size directly influences DSB density. Furthermore, chromosomal domains that are

relatively insensitive to homolog engagement-mediated feedback do not show altered DSB density when affixed onto a different chromosome length, confirming that homolog engagement feedback regulation controls DSB differences between chromosomes.

Discussion

My observations in *Saccharomyces* species up to 15 My diverged fit the hypothesis that hotspots tend to be stable if Spo11 targets functional genomic elements that are evolutionarily constrained (Nicolas et al. 1989), and suggest that these selective forces are strong enough to counteract the effects of biased gene conversion. Thus, not only is it untrue that recombination initiation landscapes inevitably evolve rapidly, but conservation is likely to be a common pattern for many sexual species (as discussed below).

Conservation of the yeast DSB landscape reflects conservation of the factors that determine it

Strong conservation in *Saccharomycetes* of DSB frequencies within hotspots, across subchromosomal domains, and even across whole chromosomes supports the hypothesis that this conservation traces back to the DSB landscape being shaped by selectively constrained chromosomal features that work combinatorially, hierarchically, and over multiple size scales (Pan et al. 2011). For example, transcription, telomere and centromere function, and sister chromatid cohesion rely on and shape chromosome structures over scales ranging from tens to millions of base pairs. Because these structures in turn mold the DSB landscape, selective pressure to maintain them for gene expression, cell division, and other processes imposes a tendency to conserve the DSB landscape. However, the remarkable strength of conservation across millions of years of evolution might indicate that the specific shape of the yeast DSB landscape may confer

fitness benefits. The recombination distribution is a heritable trait subject to selection (Coop and Przeworski 2007; Smukowski and Noor 2011), so I speculate that selective pressures may operate more directly on the DSB landscape genome wide, perhaps related to accurate meiotic chromosome segregation and/or beneficial effects of disrupting or maintaining linkage groups at various size scales (discussed further in **Chapter 4**) (Coop and Przeworski 2007; Keller and Knop 2009).

Model for conservation or divergence of the recombination landscape

The hotspot paradox concept does not incorporate the molecular mechanisms of Spo11-mediated DSB formation and regulation, which is conserved in some aspects, but also exhibits important differences among organisms (e.g., PRDM9 determines where Spo11 makes DSBs in some mammals). Therefore, recombination initiation landscapes are not inevitably short-lived as a consequence of biased gene conversion, but whether they are conserved or diverged largely depends on the underlying architects that target meiotic DSB formation. Furthermore, within the recombination landscape, the degree of divergence or conservation also depends on the size scale analyzed. Several studies noted conservation of broad-scale recombination patterns, despite diverged fine-scale recombination patterns between species (Ptak et al. 2005; Auton et al. 2012; Smukowski Heil et al. 2015), and also diverged broad-scale recombination patterns despite conserved hotspots (Singhal et al. 2015). These observations suggest that different selective forces act over different distances (Coop and Przeworski 2007). Broad-scale recombination patterns are probably governed by the requirement for at least one crossover to ensure proper homolog segregation, as well as large-scale structural features that influence the DSB landscape, whereas fine-scale recombination patterns are dominated by hotspots and biased gene conversion.

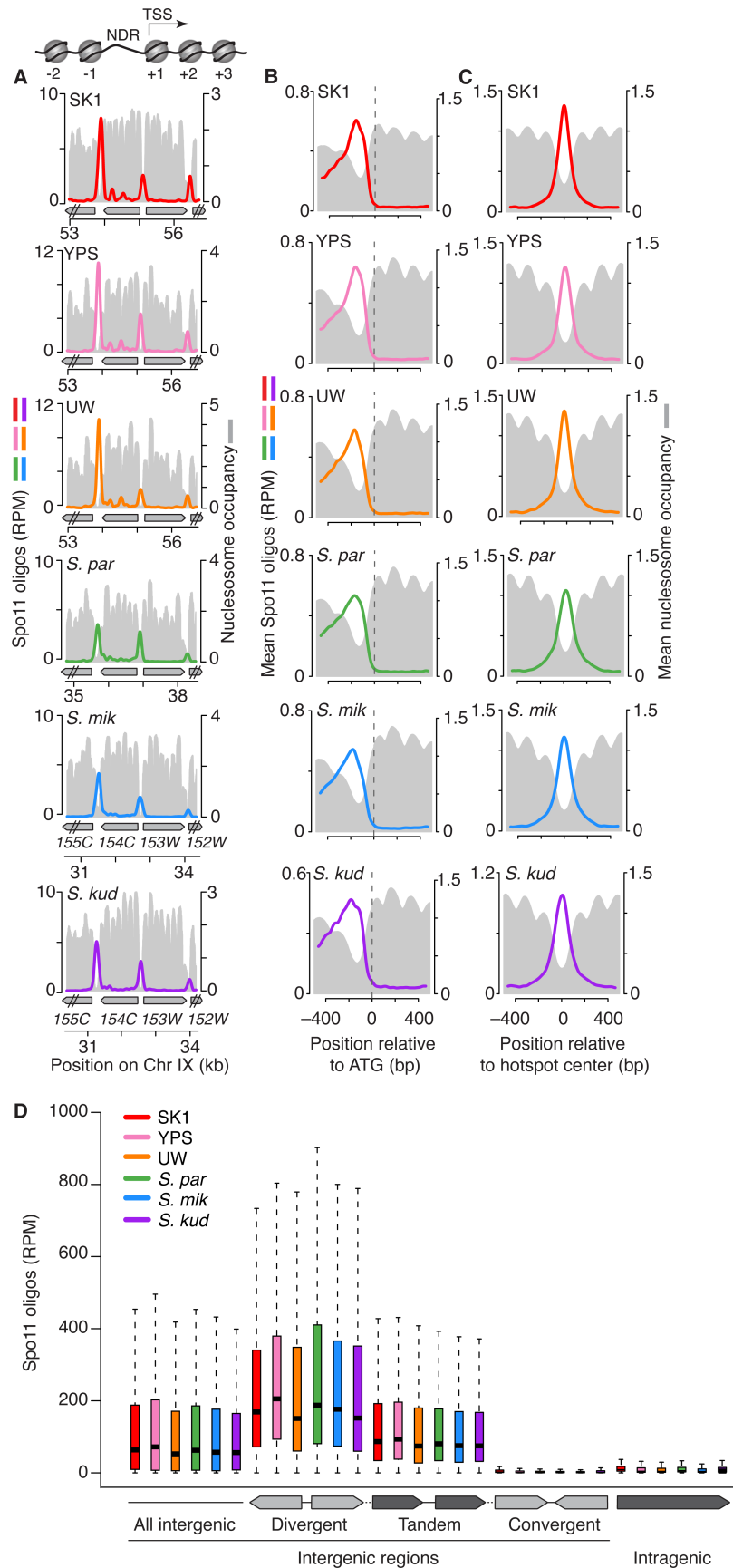


Figure 2.4. Conserved targeting of DSBs to promoters. (A) Overlap of DSB hotspots with promoter NDRs is evolutionarily conserved. The cartoon depicts the typical yeast promoter chromatin structure, with an NDR upstream of the transcription start site (TSS). The sample region (around *YIL154C*) compares Spo11 oligos with the nucleosome map (MNase-seq read depth relative to genome average). (B) Average Spo11 oligo and nucleosome profiles around start codons (*S. cer* strains, n=5766; *S. par*, n=5382 genes; *S. mik*, n=5684 genes; *S. kud*, n=5578). (C) Average Spo11 oligo and nucleosome profiles at hotspots (*S. cer* SK1, n=4099; *S. cer* YPS, n=4177; *S. cer* UW, n=3881; *S. par*, n=3833; *S. mik*, n=3829; *S. kud*, n=3976). Spo11-oligo profiles were smoothed with 201-bp (A) or 75-bp (B,C) Hann window. (D) In all species examined, Spo11 oligos map preferentially to IGRs that contain promoters. Genomes were divided into genic and intergenic compartments, and IGRs were further subdivided according to the orientation of adjacent transcription units. Thick horizontal lines indicate medians, box edges show the 25th and 75th percentiles, and whiskers indicate lowest and highest values within 1.5-fold of the interquartile range; outliers are not shown. The total number of IGRs and the breakdown by category in each species are as described in Chapter 5. The total number of genes ("intragenic") are as follows: *S. cer*, 5766; *S. par*, 5382; *S. mik*, 5841; *S. kud*, 5728. From (Lam and Keeney 2015). Reprinted with permission from AAAS.

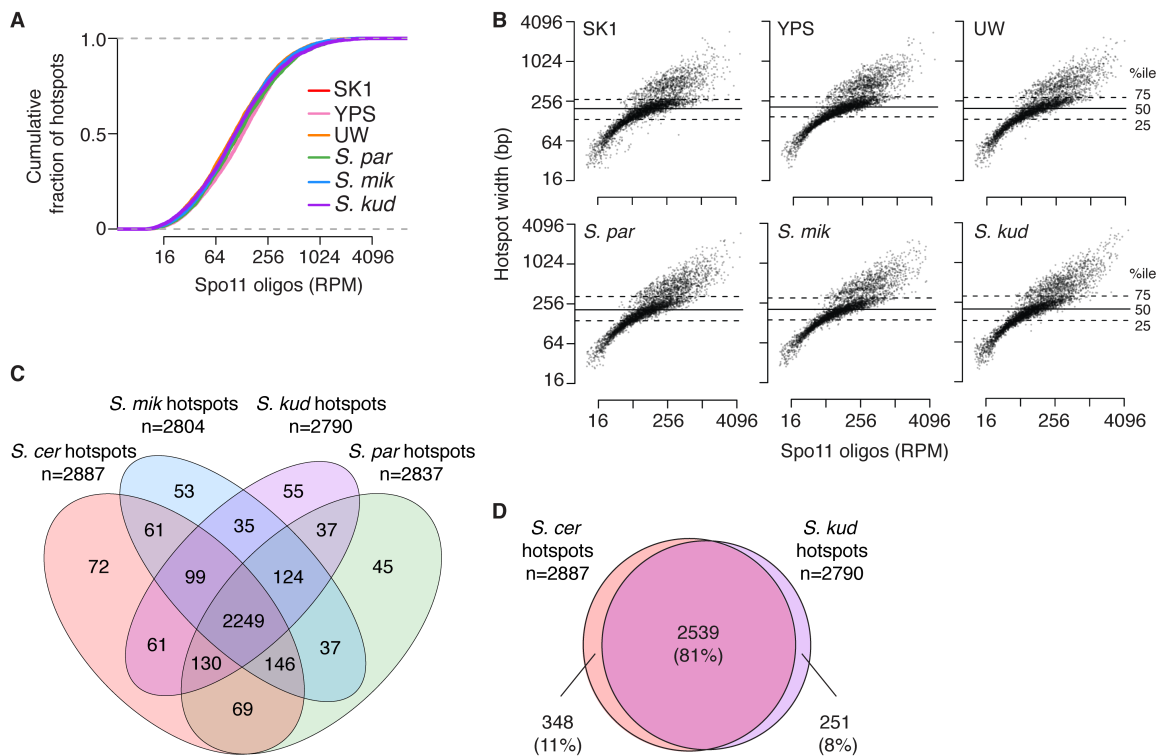


Figure 2.5. Conservation of hotspot locations. (A) Hotspot intensity varies over similar smooth continua in all species. (B) Similar distributions of widths vs. Spo11-oligo counts in hotspots. Data in A and B are plotted on a log₂ scale but labeled according to a linear scale. (C) Conservation of promoter-associated hotspots. Using a set of 3426 stringently matched promoter-containing IGRs that could be unambiguously defined in all four species (see Fig. 2.6A and Chapter 5), we first determined which hotspots called from each species' Spo11-oligo map overlapped such a promoter IGR. The four-way Venn diagram shows the number of hotspots overlapping the same promoter IGRs across all species examined. Most of these promoter-associated hotspots (2249) were shared between all four species, and another 499 were shared between three species. Promoter IGRs that were scored as hotspots in only one species were typically very weak, and one or more other species often yielded Spo11 oligos mapping to the same IGR but at levels below the arbitrary threshold set for the hotspot calling algorithm. (D) Venn diagram as in C, but only showing overlap of promoter-associated hotspots in *S. cerevisiae* and *S. kudriavzevii*. From (Lam and Keeney 2015). Reprinted with permission from AAAS.

Figure 2.6. Conservation of hotspot strength. (A) Promoter-containing IGRs were matched between species using conservation of flanking genes. (B) Comparison of Spo11-oligo counts (\log_2 scale) within 3426 IGRs that were matched in all four species. Correlation coefficients for the \log_2 -transformed data are shown (Pearson's r). (C) Comparison of Spo11-oligo counts (RPM, \log_2) within 3426 matched promoter IGRs among the different species/strains (expanded version of B). (D) Human data from (Pratto et al. 2014) for three men with identical or similar PRDM9 alleles (Baudat et al. 2010; Pratto et al. 2014). The scatter plots compare DSB hotspot strength between two men (designated AA₁ and AA₂) homozygous for the PRDM9 A allele common in populations of European descent, and one man (designated AB₁) heterozygous for the A allele and the closely related B allele ($n=37,345$ hotspots). DSB activities were measured by deep-sequencing of single-stranded DNA co-immunoprecipitated with the DMC1 strand exchange protein (Brick et al. 2012; Khil et al. 2012; Pratto et al. 2014). (E, F) Spo11-oligo counts in promoter IGRs remain highly correlated despite wide sequence divergence. Correlation coefficients (as in B–D) are plotted against the median sequence divergence within IGRs, which is substantially greater than the coding sequence divergence in Fig. 2.1 (Kellis et al. 2003). F is a zoomed view of the boxed region in E. Black lines highlight the yeast comparisons; they are not regression lines. Human data are from D; each had ~0.1% sequence difference from the reference genome (Pratto et al. 2014). (G) The hottest hotspots have stayed hot, and the coldest have stayed cold. Percentile rankings in other strains and species are shown for the matched promoter IGRs with the most (red) and least (cyan) Spo11 oligos in SK1 (top and bottom 1%). Box plots are as in Fig. 2.4. (H, I) Examples of a strong Spo11-oligo hotspot from SK1 whose heat is conserved (H, *YEL046C*) and one whose heat is not (I, *YPR124W*). From (Lam and Keeney 2015). Reprinted with permission from AAAS.

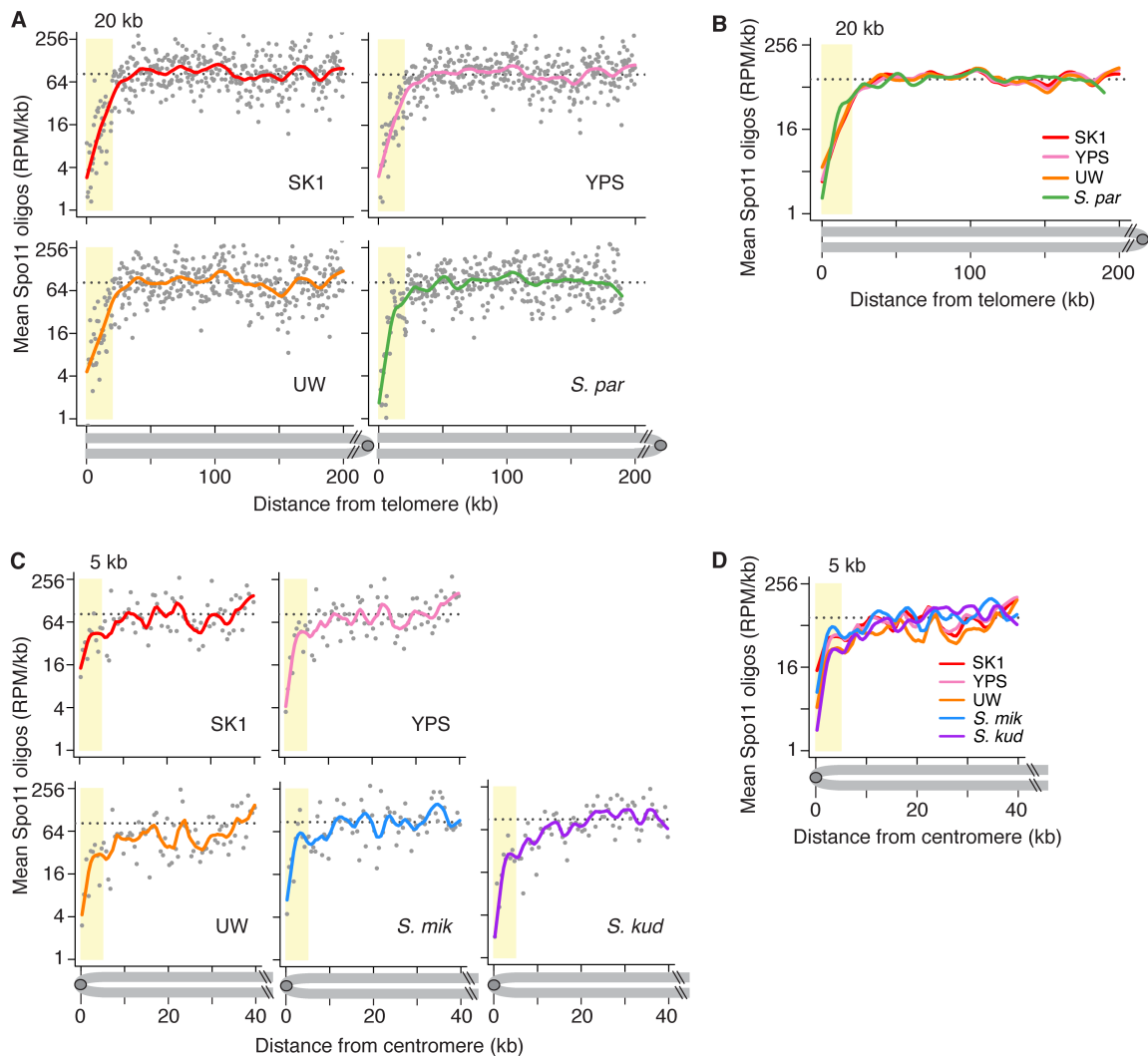


Figure 2.7. Large-scale features of the DSB landscape are conserved. (A) Telomere-proximal DSB suppression. Points are Spo11-oligo densities (plotted in log₂ scale) in 500-bp bins averaged across all 32 chromosome arms. Dashed line indicates genome average in SK1; colored lines indicate smoothed fit (Lowess); yellow shading, DSB suppression zones. (B) Lines are smoothed fit (Lowess) of Spo11-oligo densities from A. Genome assemblies are not complete enough to evaluate telomeres of *S. mikatae* or *S. kudriavzevii*. (C, D) Pericentric DSB suppression. Similar analysis as A and B. From (Lam and Keeney 2015). Reprinted with permission from AAAS.

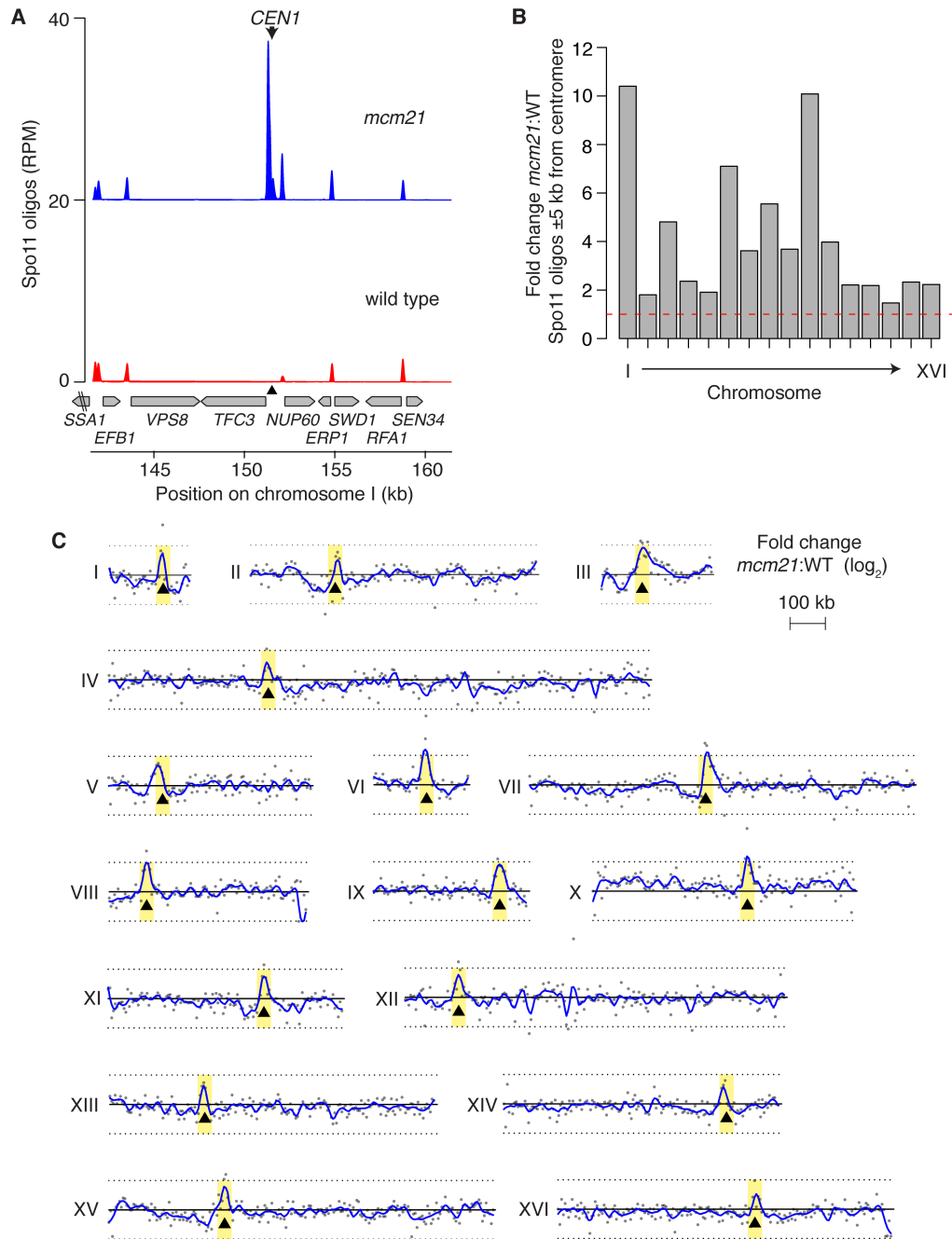


Figure 2.8. The kinetochores suppress centromere-proximal DSBs in every chromosome. (A) Appearance of a strong DSB hotspot proximal to *CEN1* in the *mcm21* mutant. Spo11 oligos are smoothed with a 201-bp Hann window. (B) Fold change (*mcm21* over wild type) in Spo11-oligo counts (RPM) within the 10 kb encompassing each centromere. Red dashed line, no change. (C) Whole-chromosome view of changes in the Spo11-oligo distribution in *mcm21*. Each point is the fold change (plotted on \log_2 scale) of *mcm21* over wild type Spo11 oligos (RPM) summed in 5-kb bins. Blue lines, smoothed fit (loess); black triangles, centromeres; yellow shading, centromere ± 20 kb; black solid line, 0 (\log_2 scale) indicating no change over wild type; black dotted lines, 2-fold change (\log_2 scale). Adapted from (Vincenten et al. 2015).

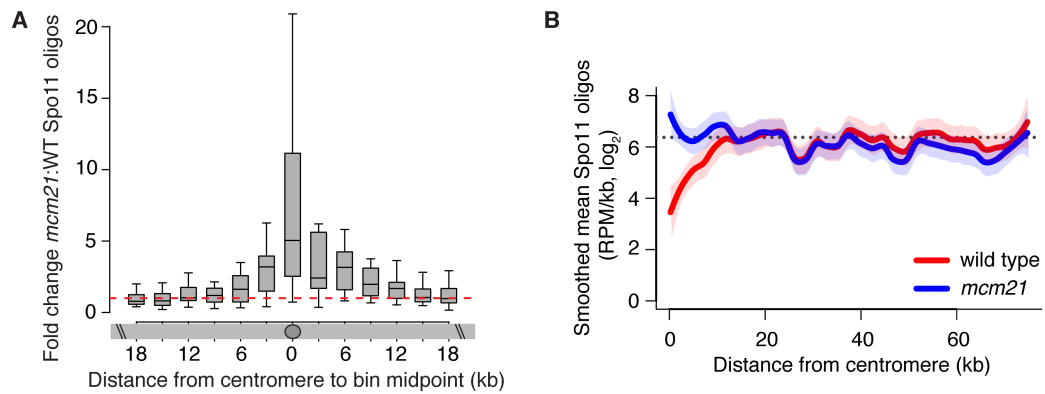


Figure 2.9. The kinetochore protects the centromere-proximal domain from DSBs. (A) Fold change (*mcm21* over wild type) in Spo11-oligo density within 3-kb segments centered at the centromere and moving 18-kb outwards into the left and right arms of the chromosome, averaged across all 16 chromosomes. (B) No residual pericentric DSB suppression in the absence of Mcm21. Spo11-oligo density within 500-bp bins starting from the centromere and moving up to 75-kb away were averaged across the 32 chromosome arms, then smoothed with loess. Red and blue shading indicates the 95% CI. Adapted from (Vincenten et al. 2015).

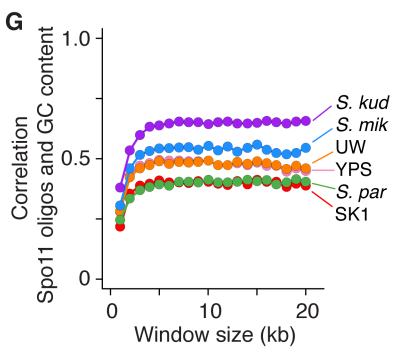
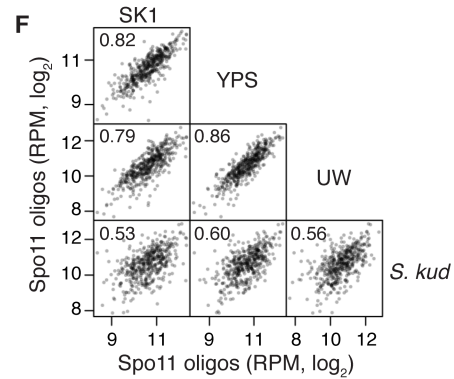
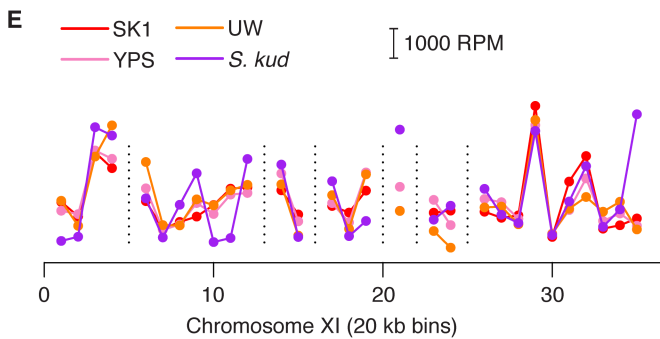
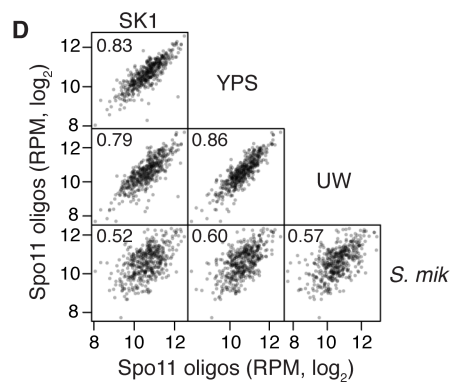
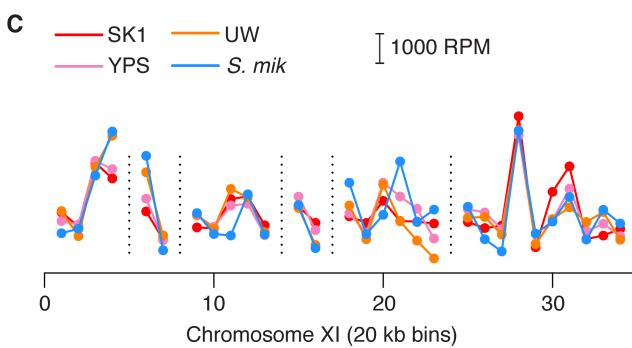
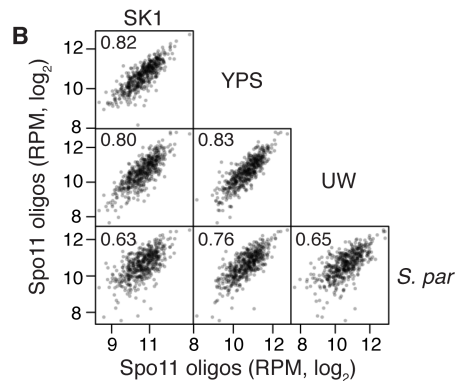
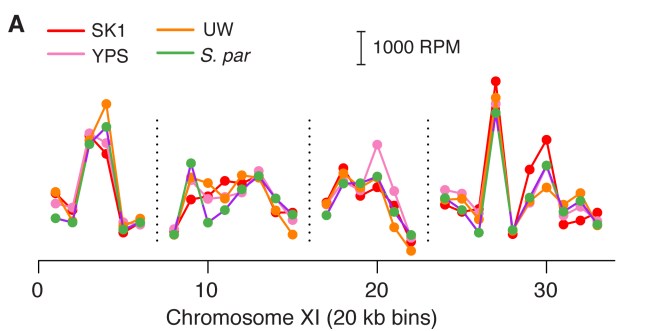


Figure 2.10. Large-scale hot and cold interstitial domains are conserved. Interstitial segments (excluding 20 kb from chromosome ends and 10 kb from centromeres based on *S. cerevisiae* annotation) were defined as syntenic if orthologous genes were in the same order in pairwise comparisons of *S. cerevisiae* with *S. paradoxus* (panels A, B), with *S. mikatae* (panels C,D) or with *S. kudriavzevii* (panels E, F). Spo11-oligo counts were then summed in these syntenic segments divided into 20-kb bins (Table S5 in (Lam and Keeney 2015)). Panels A, C, E show a representative genomic region. Vertical dashed lines denote breaks in synteny. Panels B, D, F show genome-wide scatter plots and correlation coefficients. Note that intra-species *S. cerevisiae* comparisons exhibit different correlation coefficients in the different figure panels because the correlations in a given panel are tested within syntenic interstitial segments that are defined in one pairwise species comparison. Species pairs do not all share precisely the same blocks of synteny, so there are small differences as to which portions of the genome are being compared in each panel. (G) Correlation (Pearson's r) between mean Spo11-oligo counts and GC content binned in windows of varying size. From (Lam and Keeney 2015). Reprinted with permission from AAAS.

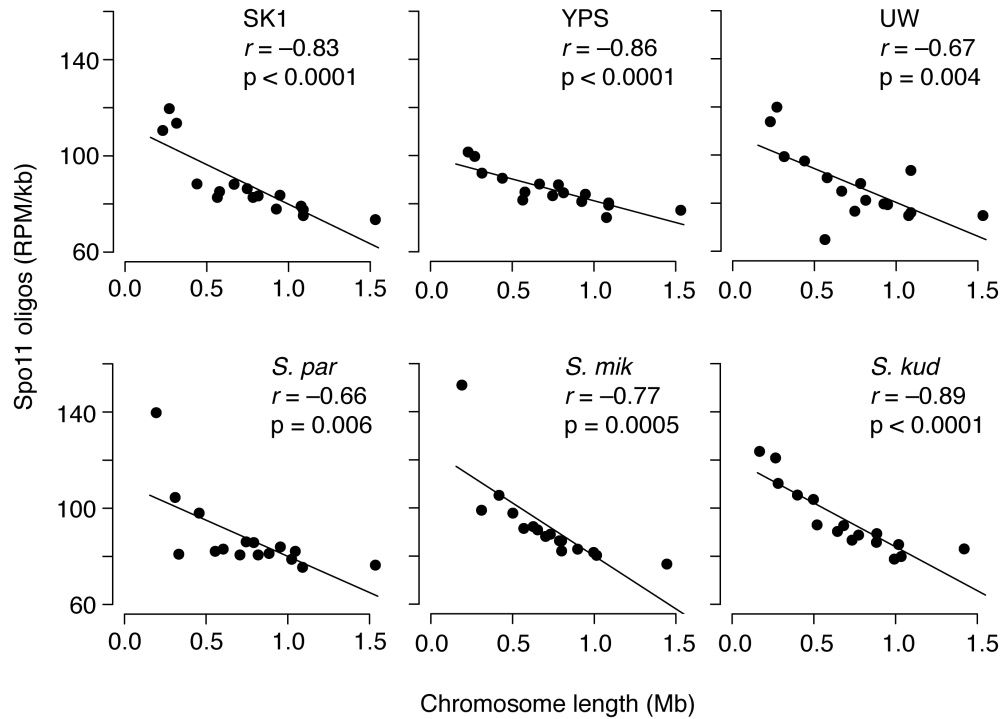


Figure 2.11. The anticorrelation between chromosome length and DSB density is conserved in *Saccharomyces* species. Each point is one chromosome. The point at ~60 RPM/kb in UW represents chromosome VIII (see text). From (Lam and Keeney 2015). Reprinted with permission from AAAS.

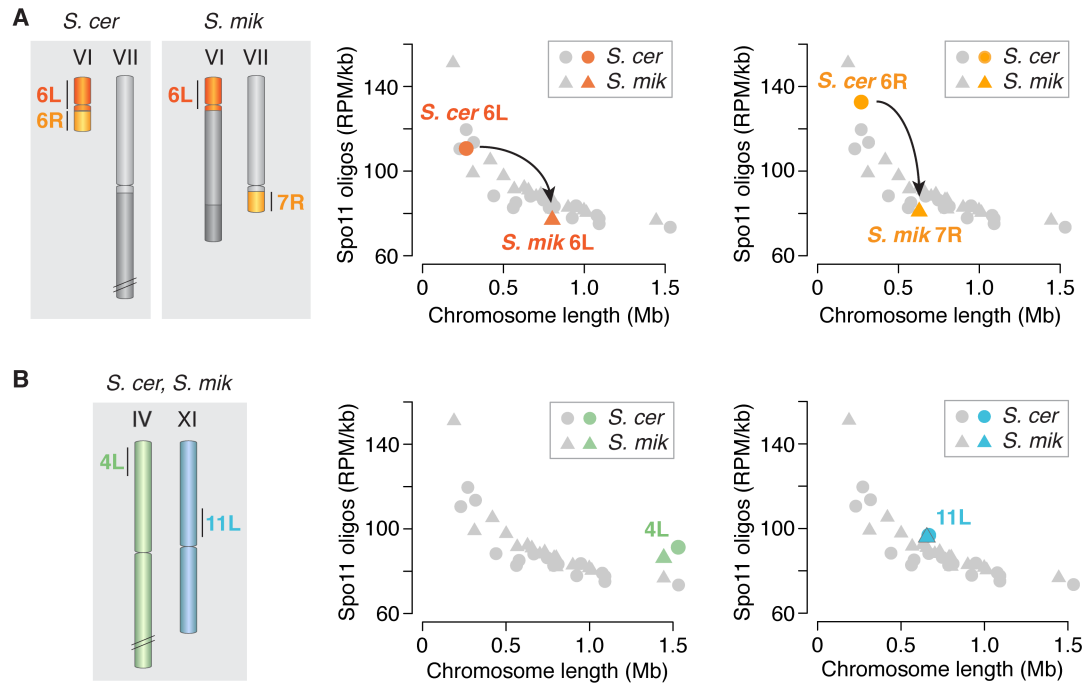


Figure 2.12. DSB density is influenced by chromosome length. (A) A natural experiment demonstrating chromosome length-dependent DSB control. The schematic illustrates syntenic segments on chromosomes of different size in *S. cerevisiae* and *S. mikatae*. The plots show that Spo11-oligo density is higher on these segments in *S. cerevisiae* (when on a short chromosome) than in *S. mikatae* (longer chromosomes). Gray symbols are whole-chromosome values from Fig. 2.11 for comparison. Note that the segments from ancestral chromosome VI display a Spo11-oligo density closely matched to the whole-chromosome value appropriate for the size of the chromosome on which they reside. (B) Control syntenic regions on similarly sized chromosomes have equivalent Spo11-oligo densities in both species. From (Lam and Keeney 2015). Reprinted with permission from AAAS.

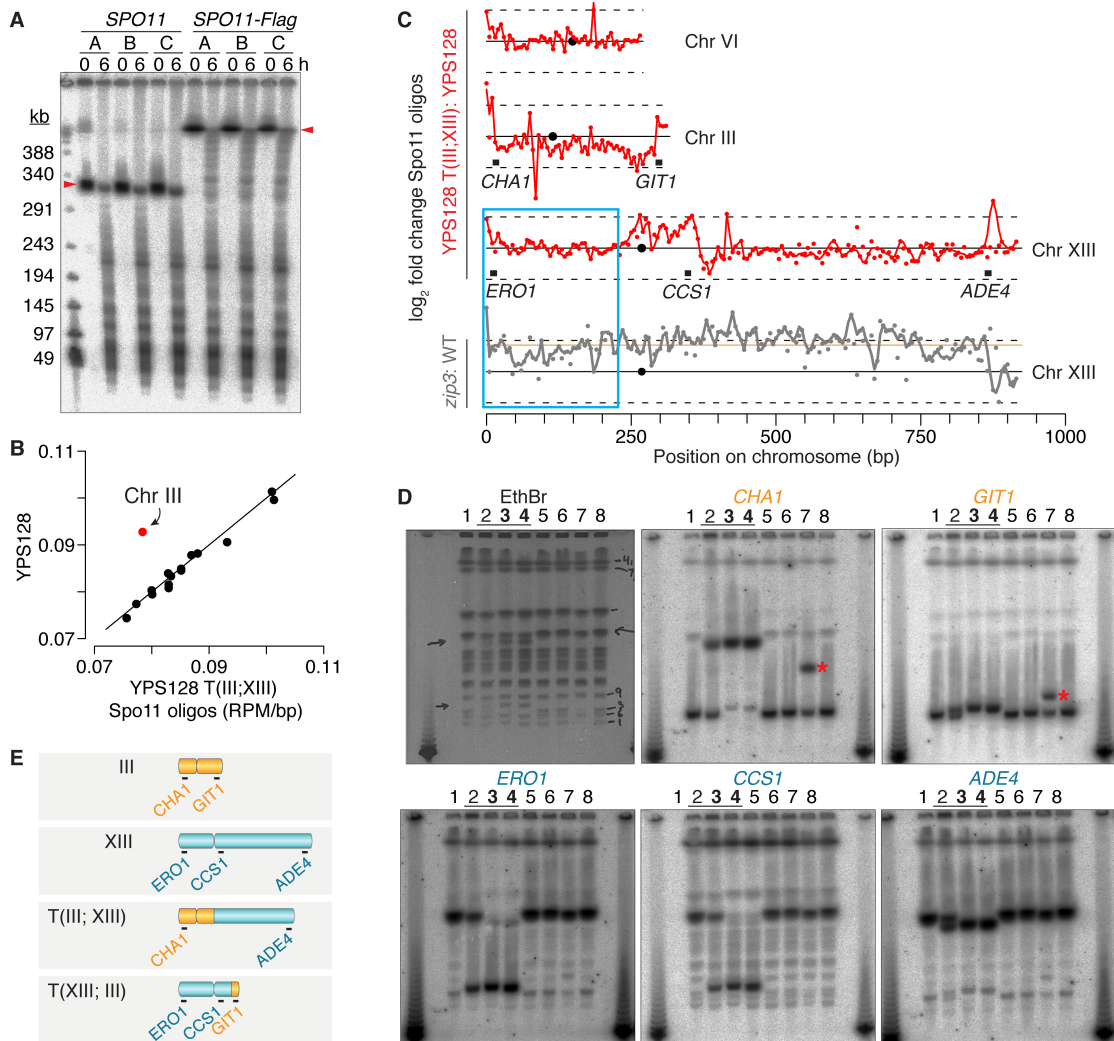


Figure 2.13. An accidental experiment testing the Kaback Effect: the serendipitous YPS128 T(III; XIII) translocation. (A) Southern blot to detect chromosome III DSBs (*CHA1* probe) in YPS128, *dmc1* background, from the indicated meiotic time points; A, B, C denote biological replicates. Arrowheads, full-length chromosome III. (B) Comparison of Spo11-oligo density within each chromosome between wild type and translocation strains. (C) Fold change in Spo11 oligos within 5-kb bins, plotted along chromosomes VI, III, and XIII and smoothed with loess. Solid black line, 0 (fold change of 1); dashed lines, 2-fold change (\log_2 of 2); orange line, average fold change in *zip3*; circles, centromere; squares, probes used in D; blue box, region in the left arm of chromosome XIII that is less sensitive to homolog engagement feedback. (D) Ethidium bromide staining of pulsed-field gel, and Southern blots to detect chromosomes involved in the translocation. Genomic DNA was extracted from mitotic cultures. Underlined lanes (2–4), strains with the translocation. Genotypes: 1, *SPO11*; 2, *SPO11-Flag/SPO11*; 3, *SPO11-Flag*; 4, *SPO11-Flag dmc1*; 5, *SPO11-Flag/SPO11*; 6, *SPO11-Flag*; 7, *SPO11-Flag/SPO11*, 8, *dmc1*. Strains in lanes 2, 5, 7 are sister spore clones; strains in lanes 3, 4 derive from strain in lane 2; likewise, strain in lane 6 derives from strain in lane 5. Asterisk, strain has two different lengths of chromosome III, aside from the translocation case investigated here. (E) Model for the reciprocal translocation in YPS128 T(III; XIII) based on D.

Based on the available evidence, I propose the following model for recombination landscape evolutionary dynamics. In organisms with a PRDM9-like system for hotspot designation, the recombination landscape undergoes rapid divergence due to the combined effects of rapidly evolving PRDM9 binding specificity, and biased gene conversion-mediated hotspot erosion, since SPO11 targets (PRDM9 binding sites) have no intrinsic function and are not under selective constraint. Examples include primates (Ptak et al. 2005; Winckler et al. 2005; Coop et al. 2008; Kong et al. 2010; Myers et al. 2010; Hinch et al. 2011; Auton et al. 2012; Pratto et al. 2014) and mice (Baudat et al. 2010; Brick et al. 2012; Smagulova et al. 2016). In organisms without PRDM9, recombination landscape conservation or divergence depends on whether recombination is targeted to functional genomic elements. If recombination is targeted to functional elements (e.g., promoters, CpG islands and/or other genomic elements that are under selective constraint to maintain non-meiotic functions), then the recombination landscape is conserved because these forces counteract biased gene conversion. Examples include *Saccharomyces* (this work), finches (Singhal et al. 2015), dogs (Axelsson et al. 2012) and plants (Choi et al. 2013; Choi and Henderson 2015). Conversely, evolutionary stability of DSB hotspots may indicate constrained function(s), even if that function is presently unknown. For example, DSB hotspots are well conserved between the *Schizosaccharomyces* species *S. pombe* and *S. kambucha* (Zanders et al. 2014), despite mapping to sites without known function (Fowler et al. 2014). Finally, if recombination is not targeted to functional elements, the recombination landscape tends to evolve rapidly due to biased gene conversion-mediated hotspot erosion. For example, in *Drosophila*, which lacks a PRDM9-like system but also does not preferentially target recombination to promoters or known functional elements (and recombination does not appear to be clustered in hotspots), the fine-scale distribution of recombination appears to evolve rapidly (Smukowski Heil et al. 2015).

CHAPTER 3: INFLUENCE OF CHROMOSOME STRUCTURE PROTEINS ON THE MEIOTIC DSB LANDSCAPE

Summary

Axial element proteins Red1 and Hop1 are the building blocks of higher-order meiotic chromosome structure and are implicated in multiple aspects of meiotic recombination, including formation of loop-axis structures, SC assembly, DSB formation, establishing IH bias in recombination partner choice, and recombination checkpoint signaling (Hunter 2007; Humphries and Hochwagen 2014; Subramanian and Hochwagen 2014). Mek1 is associated with Red1 and Hop1, and shares many of the functions listed above, but is not a core component of the chromosome axis. From the earliest experimental observations, Red1, Hop1, and Mek1 were noticed to be required for normal DSB levels (summarized in **Table 1.2**), although exactly how proteins located on the axial cores influence Spo11 activity remained unknown. More recent studies demonstrating that DSB proteins are enriched at axial sites in a Red1/Hop1-dependent manner (Panizza et al. 2011) provide a possible molecular link for the role of Red1 and Hop1 in DSB formation, especially when interpreted in the framework of DSBs occurring in the context of a TLAC (Blat et al. 2002; Kleckner 2006; Panizza et al. 2011). Since Red1 and Hop1 recruit DSB proteins to chromatin axes, one hypothesis is that absence of axial element proteins could result in a redistribution of the DSB landscape.

To determine the contribution of axial element proteins to the global DSB landscape, I mapped the sites of DSBs by Spo11-oligo sequencing in *red1* and *hop1* mutants. I also generated Spo11-oligo maps in the *mek1* mutant since it exhibits a DSB defect, and Mek1 interacts with Red1 and Hop1. Spo11-oligo complexes are reduced in all three mutants, although to different degrees (severity: *hop1* > *red1* > *mek1*). Analyses of the Spo11-oligo maps uncover roles of Red1 and Hop1 in both intrinsic and extrinsic

components of the DSB landscape. Red1 and Hop1 promote efficient DSB formation on all chromosomes, with an extra boost on short chromosomes (“intrinsic”) and also contribute to homolog engagement feedback inhibition of DSBs (“extrinsic”). The dependence of short chromosomes on Red1 and Hop1 for DSBs implies the existence of an extra layer of control to generate more DSBs on short chromosomes (separate from homolog engagement feedback inhibition), thereby increasing the chances of an obligate crossover needed to avoid missegregation at the first meiotic division. Within chromosomes, domains exhibit different degrees of DSB reduction, but the magnitude of DSB reduction in *red1* and *hop1* is only weakly correlated with wild type Red1 protein enrichment and DSB activity.

Mek1 shapes the DSB landscape through regulatory (“extrinsic”) circuits, and may have little or no intrinsic role in DSB formation. Mek1 appears to be involved in at least two extrinsic pathways controlling DSB numbers: homolog engagement feedback inhibition and Ndt80-dependent regulation of cell cycle progression. DSB patterns within hotspots (sub-kilobase) are minimally affected, and DSB suppression of sub-chromosomal domains (pericentromeres, subtelomeres, rDNA-proximal regions) is maintained in the absence of Red1, Hop1, or Mek1. These observations are consistent with the model of the DSB landscape being shaped by a combination of factors operating at different size scales.

Results

Global meiotic DSBs are reduced in the absence of Red1, Hop1, or Mek1

Previous studies describing the DSB defect in *red1*, *hop1*, and *mek1* (**Table 1.2**) relied on detection and quantification at single DSB hotspots or over an individual chromosome, which may not represent the genome-wide trend. Moreover, usage of

repair-deficient mutant backgrounds that do not accurately report wild type DSB levels (Borde et al. 2000) may present a distorted interpretation due to complex genetic interactions (Keeney et al. 2014). To assess the genome-wide DSB phenotype of *red1*, *hop1*, and *mek1* mutants in an otherwise wild-type background, I set out to examine Spo11-oligo complexes, the by-products of DSB formation that can be used to measure DSB numbers (Neale et al. 2005).

Spo11-oligo complex detection involves immunoprecipitation of Spo11, usually via an epitope tag. To rule out possible synergistic defects on DSB formation, I first determined whether tagged *SPO11* alleles exhibit any DSB defect when combined with null *red1*, *hop1*, or *mek1* alleles, measuring DSB levels on chromosome III by Southern blot. All strains were in the *rad50S* repair-deficient background to measure total DSB numbers (Alani et al. 1990; Keeney et al. 1997). DSB formation in *red1*, *hop1*, or *mek1* does not appear to be affected when combined with *SPO11-Flag* or *SPO11-PrA* alleles (**Fig. 3.1**) (Thacker et al. 2014). In agreement with previous studies (Blat et al. 2002; Peciña et al. 2002; Niu et al. 2005), I detected a ~6-fold reduction in DSBs in *red1* compared with wild type, ~15-fold reduction in *hop1*, and similar DSB levels as wild type in *mek1* (**Fig. 3.1B**). A slight difference in the DSB distribution was detected in the left arm of chromosome III in *red1 SPO11-FLAG*, with a more prominent band below 97 kb that appears to be specific for this allele combination (**Fig. 3.1A**, red asterisk). Overall, the Southern blots recapitulated published DSB phenotypes, and showed no major adverse effect of the *SPO11-Flag* allele. Therefore, I proceeded with the *SPO11-Flag* allele.

To measure Spo11-oligo complex levels, whole-cell extracts were prepared from *red1*, *hop1*, and *mek1* cultures at various times after transfer to sporulation medium. Spo11-oligo complexes were immunoprecipitated with anti-Flag antibody, end-labeled, resolved by SDS-PAGE, transferred to a membrane, and exposed by phosphorimager.

Spo11 protein levels were detected by anti-Flag immunodetection on the same membrane. In wild type, Spo11-oligo complexes began to be detected at ~2 h, reached a maximum at ~4 h, and then declined (**Fig. 3.2A**). The timing of Spo11-oligo complex appearance and disappearance is similar to that of DSBs (Neale et al 2005), but the mechanism of Spo11-oligo complex turnover is not currently well understood (discussed further below).

In the *red1* and *hop1* mutants, Spo11-oligo complex levels were reduced 3.9 and 7.5-fold, respectively (*red1* 25%, *hop1* 13% of wild type) when considering the entire time-course (area under the curve) (**Fig. 3.2B**). Spo11-oligo complex levels reached a maximum at 4 h in both *red1* and *hop1*, similar to wild type, but peak levels were 4-fold and 7.3-fold lower than wild type, respectively (**Fig. 3.2B**). In the *mek1* mutant, Spo11-oligo complex levels were reduced 1.9-fold over the span of the time-course (53% of wild type) (**Fig. 3.2B**). Spo11-oligo complex level peaked at 3 h in *mek1*, seemingly a bit earlier than in wild type, and peak level was 1.8-fold reduced compared with wild type.

Global DSB fold reductions in the three mutants are within the same range as the values reported in the literature at individual loci and in different repair-proficient and -deficient genotype backgrounds (*red1*: 2–6-fold reduction from wild type; *hop1*: 8–20-fold reduction; *mek1*: no reduction up to 10-fold reduction from wild type) (**Table 1.2** and references therein). The relative level of total DSBs in the mutants, based on quantification of Spo11-oligo complexes, provided a normalization factor to scale the *red1*, *hop1*, and *mek1* Spo11-oligo maps relative to the wild type map. In the analyses described below, the area under the curve measurements were used as normalization factors for scaling the mutant Spo11-oligo maps. Measuring Spo11-oligo complexes as area under the curve takes into account both their number and lifespan. In a previous publication from our lab, Spo11-oligo maps were scaled using the peak Spo11-oligo complex numbers (Thacker et al. 2014), a method that accounts for their rates of

formation and degradation. However, this relies on a single time point from each culture and assumes that the time point of maximal Spo11-oligo complex was captured. The area under the curve measurement does not rely on just a single time point, but assumes that Spo11-oligo complex lifespan is unaffected in the mutant. The numbers obtained as fold reduction in Spo11-oligo complexes in the mutants were very similar whether measuring area under the curve or peak levels (**Fig. 3.2B**).

Generating high-resolution DSB maps in *red1*, *hop1*, and *mek1* mutants

After confirming global reduction in Spo11-oligo complex levels, I next set out to determine whether the DSB distribution was altered in the *red1*, *hop1*, and *mek1* mutants. Spo11 oligos were purified from the 4 h time point of synchronous meiotic cultures in *red1*, *hop1*, and *mek1* strains. Since DSB levels are strongly reduced in *red1* and *hop1*, Spo11 oligos from 4–5 meiotic cultures were pooled at various stages of the purification process to obtain enough oligos for sequencing library preparation and mapping. DSBs are not as reduced in *mek1*, so Spo11 oligos were purified from single meiotic cultures. Spo11 oligos were deep sequenced, and sequencing reads were mapped to the *S. cerevisiae* S288C sacCer2 reference genome. Most reads mapped uniquely (**Table 3.1**). Two biological replicate Spo11-oligo maps were generated for each mutant, and each map was normalized to reads per million mapped (RPM). Biological replicate maps of the same genotype exhibit high reproducibility (Pearson's $r = 0.97$ – 0.98) (**Fig. 3.3**), so these were averaged into consensus maps.

DSB patterns within hotspots are unchanged in the absence of Red1, Hop1, or Mek1

Analysis of the Spo11-oligo maps revealed that in the absence of Red1, Hop1, or Mek1, Spo11 still preferentially targets NDRs upstream of ATG start sites (**Fig. 3.4A**).

Therefore, Spo11 does not depend on chromosome structure proteins to cleave in these genomic regions.

To discern whether the DSB pattern is altered at the sub-kilobase scale, I examined the Spo11-oligo distribution within hotspots in *red1*, *hop1*, and *mek1* mutants. The DSB pattern was very similar in all three mutants within the *ARE1* hotspot on chromosome III (**Fig. 3.4B**). DSBs were severely reduced in *red1* and *hop1* on chromosome I, so Spo11 oligos at the *CYS3* hotspot were barely detectable in these mutants in RPM-normalized maps (**Fig. 3.4C**). However, magnifying the y-axis scale indicated that even though the break frequency was reduced, the DSB distribution within the hotspot was largely maintained in all three mutants (**Fig. 3.4D**). Maintenance of fine-scale patterns within hotspots is consistent with axial element proteins operating at larger size scales (tens of kb) in the hierarchy of factors that collectively shape the DSB landscape (Pan et al. 2011; Cooper et al. 2016).

Within chromosomes, regions exhibit different degrees of DSB reduction

To examine whether the reduction in DSBs detected by Spo11-oligo complex labeling is uniform across the genome, or whether particular chromosomal regions exhibit variation, the fold change in Spo11-oligo counts was plotted over the span of each of the 16 chromosomes (**Fig. 3.5A**). The total number of reads in the mutant maps were first scaled to 25% (*red1*), 13% (*hop1*), and 53% (*mek1*) of the wild type reads based on the results from Spo11-oligo complex labeling experiments. Three patterns emerge: (1) the reduction in DSBs was not uniform along chromosomes; instead there were sub-chromosomal domains with more DSB reduction than others. This was observed in all three mutants, but was more prominent in *red1* and *hop1*, where greater amplitude of peaks and valleys were observed (**Fig. 3.5A**), and the distribution of fold change was more spread out (**Fig. 3.5B**). (2) The fold reduction in DSBs along short

chromosomes (especially I and VI) was greater than the genome-average fold reduction in *red1* and *hop1*, but not *mek1* (discussed further below). (3) Domain structure of the differential fold-reduction was highly correlated between *red1* and *hop1* (Pearson's $r = 0.938$), but only weakly correlated when *red1* or *hop1* was compared with *mek1* (Pearson's $r = 0.400$ – 0.447) (**Fig. 3.5C**). Locus-to-locus variation in DSBs and recombination frequency has been noted in *red1* and *hop1* mutants (Hollingsworth and Byers 1989; Rockmill and Roeder 1990; Mao-Draayer et al. 1996). Additionally, the highly correlated pattern of domain behavior in *red1* and *hop1* mutants is consistent with the close interaction between Red1 and Hop1 based on genetic, biochemical, cytological, and molecular biology data (Hollingsworth and Ponte 1997; Smith and Roeder 1997; de los Santos and Hollingsworth 1999; Woltering et al. 2000; Borner et al. 2008; Panizza et al. 2011). Notably, patterns of domain behavior in *mek1* are clearly different from *red1* and *hop1*.

DSB suppression near centromeres, telomeres, and rDNA are maintained

As introduced in **Chapter 1**, DSB frequency is reduced within ~5–10 kb from centromeres, and up to ~20 kb from telomeres (two- to three-fold below the genome average) (Blitzblau et al. 2007; Buhler et al. 2007; Pan et al. 2011). DSBs are also suppressed within the rDNA—which consists of ~140 copies of a 9.1 kb repeat—and in the regions flanking the rDNA array (Petes and Botstein 1977; Gottlieb and Esposito 1989; Mieczkowski et al. 2007; Vader et al. 2011). To examine whether these regions remain suppressed for DSBs in the absence of Red1, Hop1, or Mek1, the fold change in Spo11-oligo counts within hotspots was calculated, and hotspots were grouped by chromosomal context (**Fig. 3.6A**). Compared to wild type, Spo11-oligo counts in subtelomeric hotspots were reduced slightly more than the average change in *red1*, *hop1*, and *mek1*, whereas Spo11-oligo counts in pericentric hotspots appeared to be

more reduced than the average reduction in *mek1* but not the other mutants (**Fig. 3.6A**). The moderate reduction in Spo11-oligo counts within subtelomeric regions compared to wild type was also seen when plotting Spo11-oligo density averaged across the 32 chromosome arms as a function of distance from telomeres (**Fig. 3.6B**). Spo11-oligo density near centromeres was more suppressed in *mek1*, up to ~10 kb away from centromeres (**Fig. 3.6C**).

Spo11 oligos in the rDNA-proximal regions were more suppressed than the average reduction in *mek1*, and this suppression was unique to that region of chromosome XII (**Fig. 3.6A, D**). This suggests that Mek1 plays a role in promoting DSBs in the proximity of the rDNA array. Mek1 localizes to the nucleolus, along with Red1, but not Hop1 (Smith and Roeder 1997; Bailis and Roeder 1998), yet it is not clear how it could be promoting DSBs in this region.

Taken together, DSBs continue to be suppressed near centromeres, telomeres, and the rDNA in the absence of Red1, Hop1, and Mek1. Unexpectedly, DSBs in rDNA-proximal regions are also more severely reduced in the absence of Mek1.

DSBs on short chromosomes are most affected in the absence of Red1 and Hop1

To assess whether all chromosomes exhibit the same degree of fold reduction as genome average, I calculated the fold change in scaled Spo11-oligo density for each chromosome. In both *red1* and *hop1*, all chromosomes showed reduced Spo11-oligo density compared to wild type, but remarkably, the reduction was more pronounced in short chromosomes, particularly chromosomes I and VI (**Fig. 3.7A**). This result suggests that the shortest chromosomes behave differently from longer chromosomes in the absence of Red1 or Hop1. The different behavior for short and long chromosomes was not detected in the *mek1* mutant (**Fig. 3.7A**).

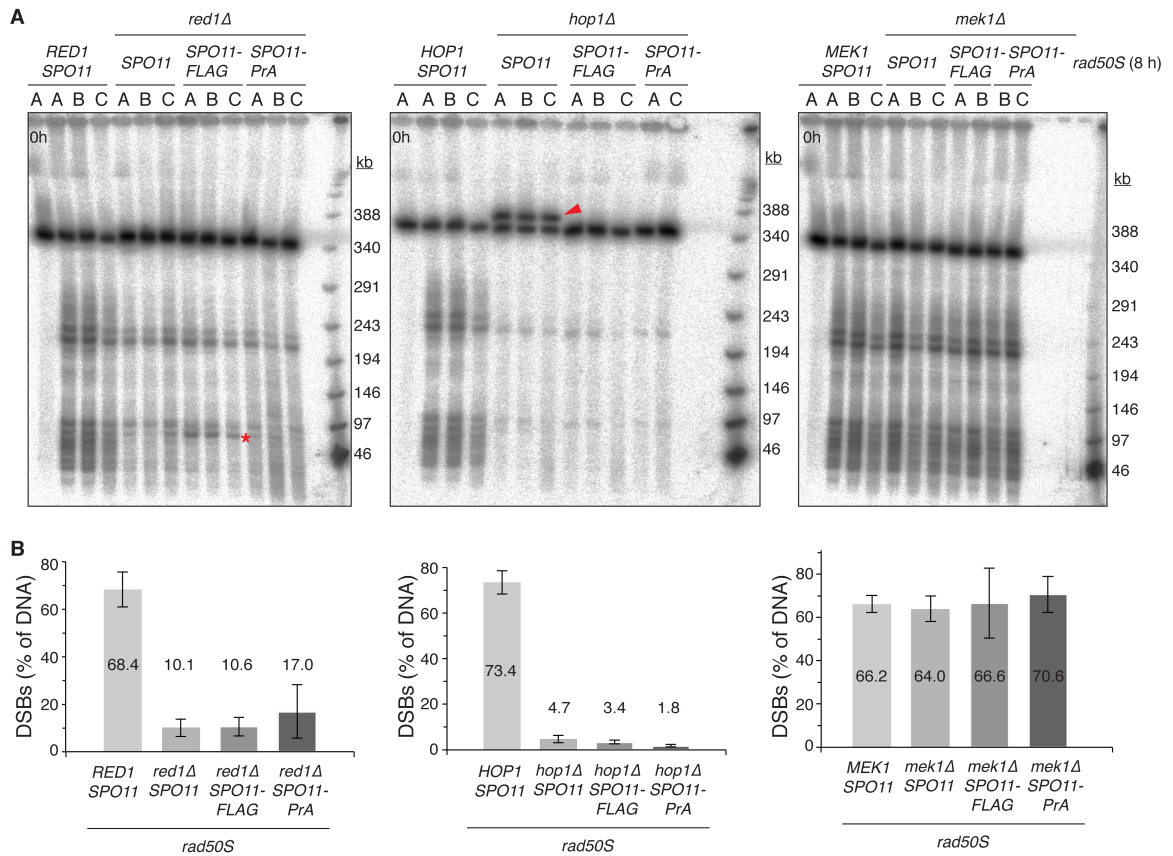


Figure 3.1. Spo11 tagged with Flag or PrA has little or no defect in DSB levels in *red1*, *hop1*, or *mek1* mutant backgrounds. (A) Southern blot analyses to detect meiotic DSBs on chromosome III by using the *CHA1* probe. All strains are in the *rad50S* background, and DNA samples were from sporulation cultures harvested at the 8 h time point, unless indicated. Red asterisk indicates a DSB hotspot between 46–97 kb that is more prominent in the *red1 SPO11-Flag rad50S* strain. Red arrowhead indicates a chromosome III length polymorphism in the *hop1 SPO11 rad50S* strain. (B) Quantification of DSBs detected in panel A. Values denote the mean and standard deviation from 3 or 2 (*hop1 SPO11-PrA*, *mek1 SPO11-FLAG*, *mek1 SPO11-PrA*) biological replicates.

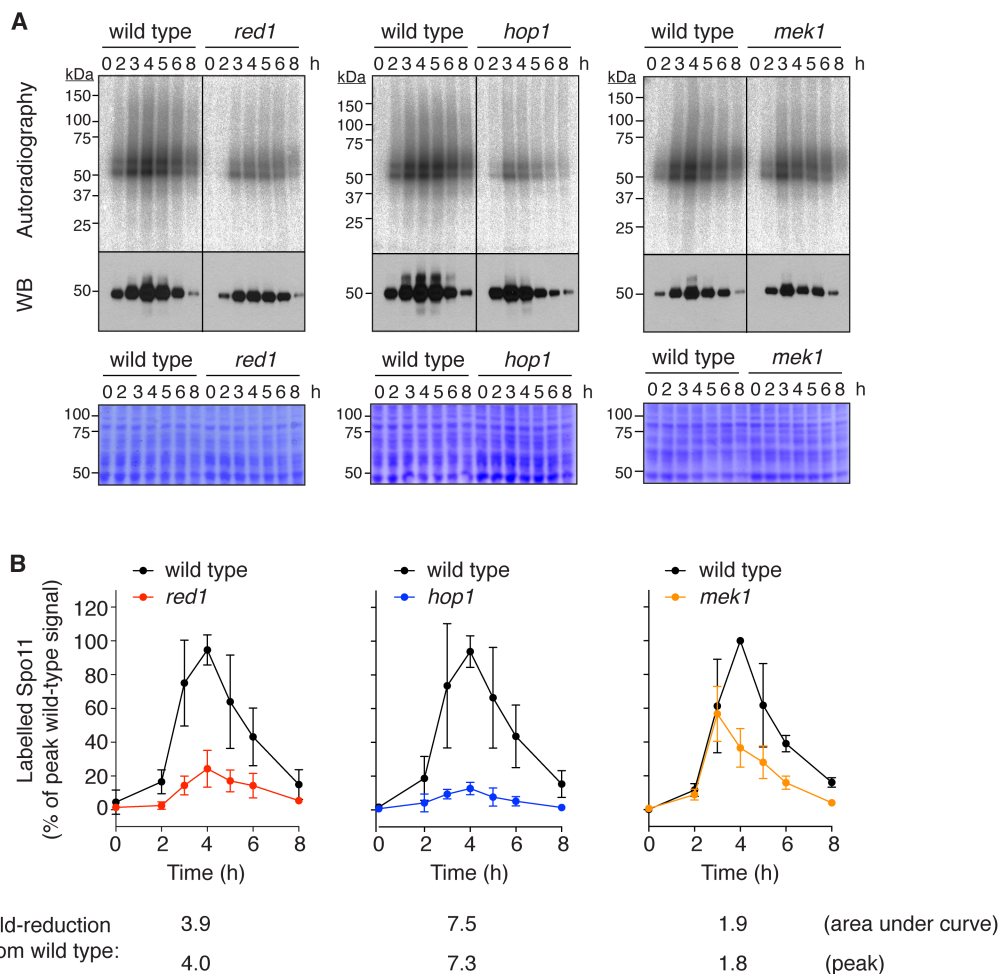


Figure 3.2. Fewer DSBs form in *red1*, *hop1*, and *mek1* mutants. (A) Representative Spo11-oligo complex time courses in *red1*, *hop1*, or *mek1* mutants in *SPO11-Flag* background. Radiolabeled Spo11-oligo complexes were detected by autoradiography (top), and total Spo11 protein was detected by anti-Flag western blot (WB, middle). Extract samples were also run separately and stained with Coomassie as control for input to the immunoprecipitation (bottom). (B) Quantification of Spo11-oligo complex time courses (mean \pm s.d. for 4 experiments, except *red1*, where n=5 experiments). Mutants are plotted in comparison with wild-type data collected in parallel.

Table 3.1. Mapping statistics for *red1*, *hop1*, *mek1* Spo11 oligo sequences

Dataset	Strain number	No. of reads (total reads)	No. mapped	No. mapped uniquely to genome
red1-A	SKY4337	1,566,026	1,382,633	1,314,478 (95.1%)
red1-B	SKY4337	985,332	758,904	743,571 (98.0%)
hop1-A	SKY4363	2,416,642	2,089,770	2,041,651 (97.7%)
hop1-B	SKY4363	5,748,207	5,045,895	4,964,591 (98.4%)
mek1-A	SKY4347	1,983,809	1,689,505	1,663,929 (98.5%)
mek1-B	SKY4347	19,391,195	16,716,069	16,366,408 (97.9%)

All strains are *S. cerevisiae* SK1 background, mapped to type strain S288C (sacCer2 assembly).

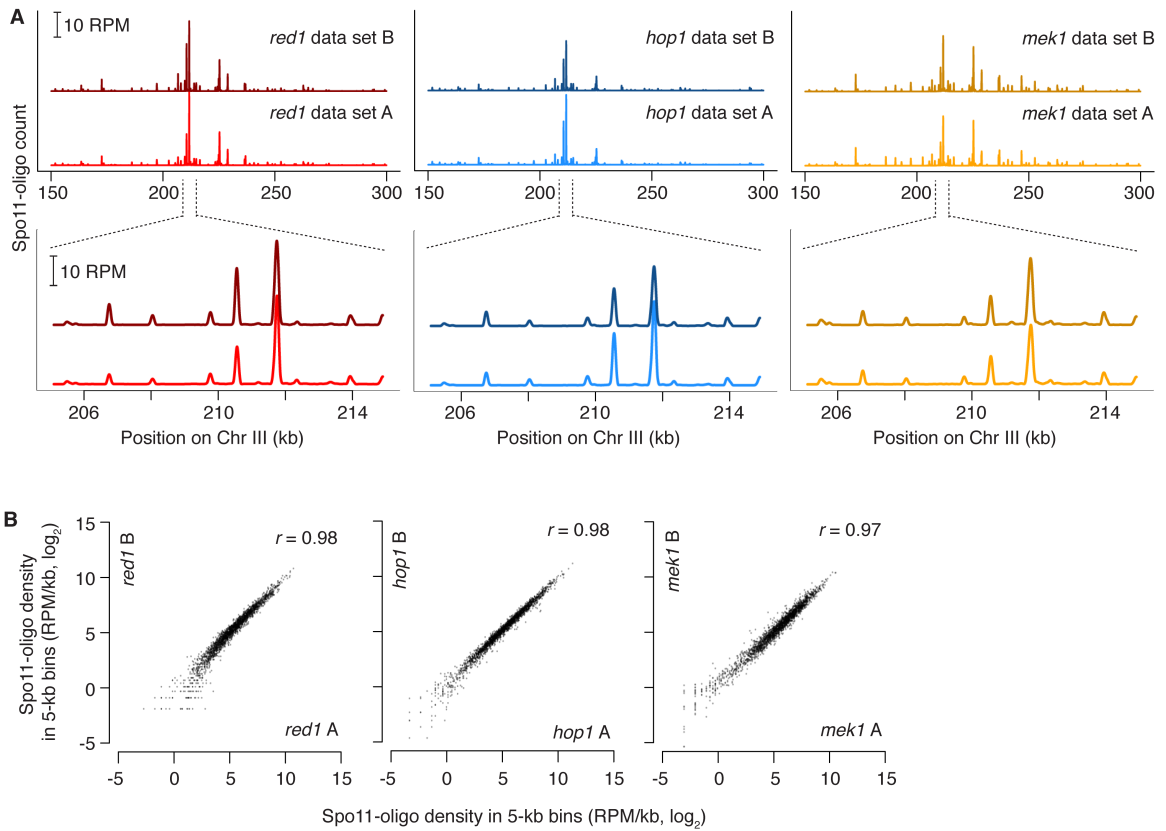


Figure 3.3. Reproducibility of biological replicate Spo11-oligo maps in *red1*, *hop1*, and *mek1* mutants. (A) Spo11 oligos map to the same locations in independent data sets. Spo11-oligo maps were smoothed with a 201-bp Hann window. (B) Uniquely mapped Spo11 oligos were summed in non-overlapping 5-kb bins. Pairwise correlation coefficients are shown (Pearson's r).

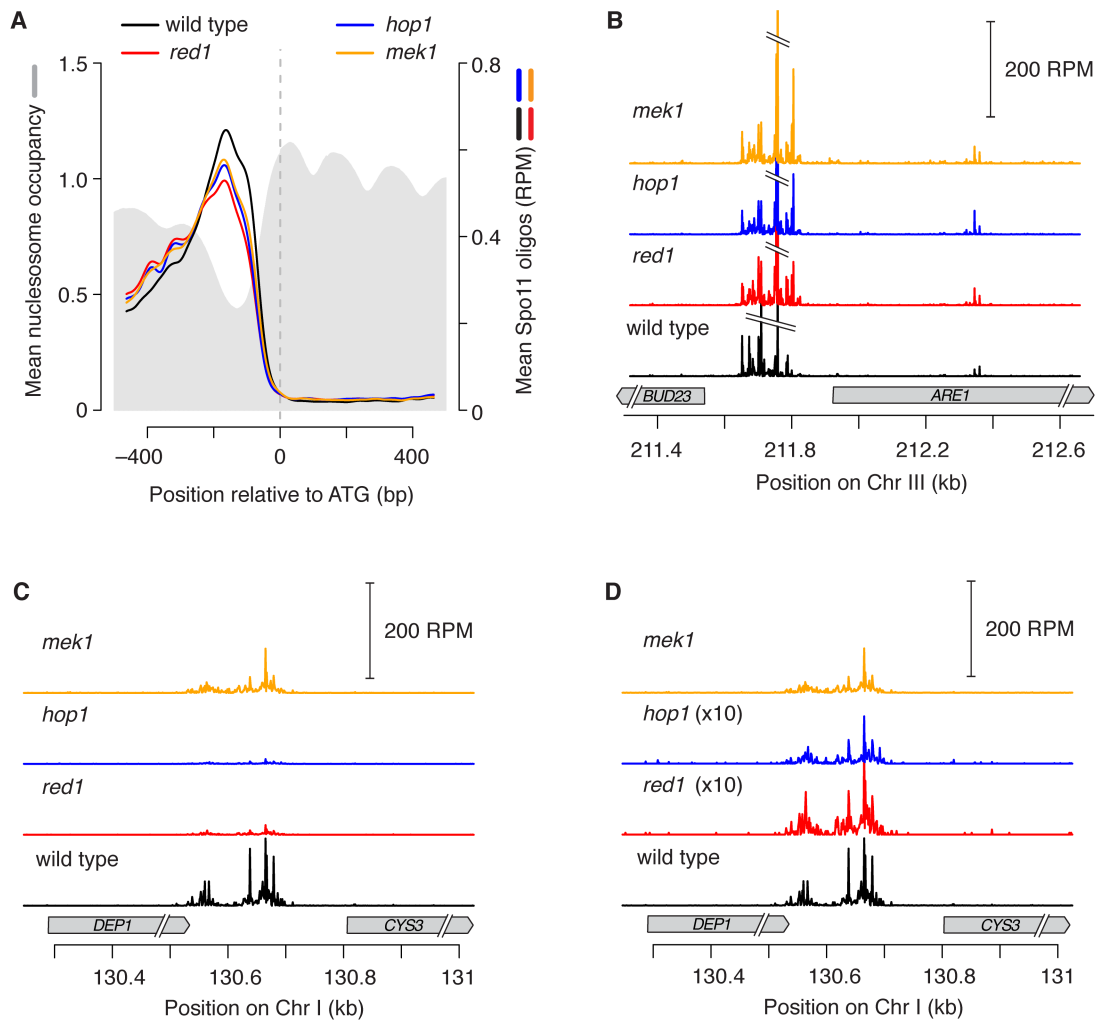


Figure 3.4. Fine-scale DSB patterns are minimally affected in the absence of Red1, Hop1, or Mek1. (A) DSBs still preferentially occur in promoter NDRs in *red1*, *hop1*, and *mek1*. Average Spo11-oligo densities and wild type nucleosome profiles around start codons (n=5766). (B–D) The DSB pattern within hotspots is largely unaltered in *red1*, *hop1*, or *mek1*, even if DSB frequency is lower. Examples at two hotspots are shown: (B) *ARE1*, (C and D) *CYS3*. DSBs are barely detectable at *CYS3* in *red1* and *hop1* (C), but the locations of the breaks that are made are the same as in wild type and *mek1*, as seen when multiplying the reads by 10 (D). Wild type Spo11-oligo maps are from (Zhu and Keeney 2015).

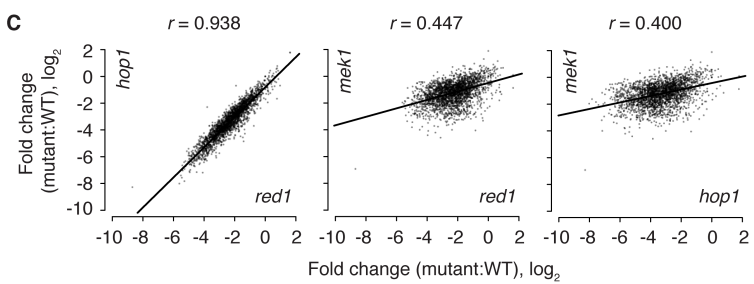
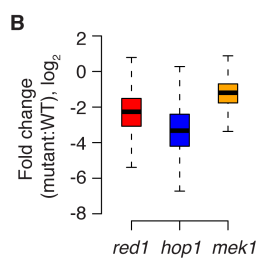
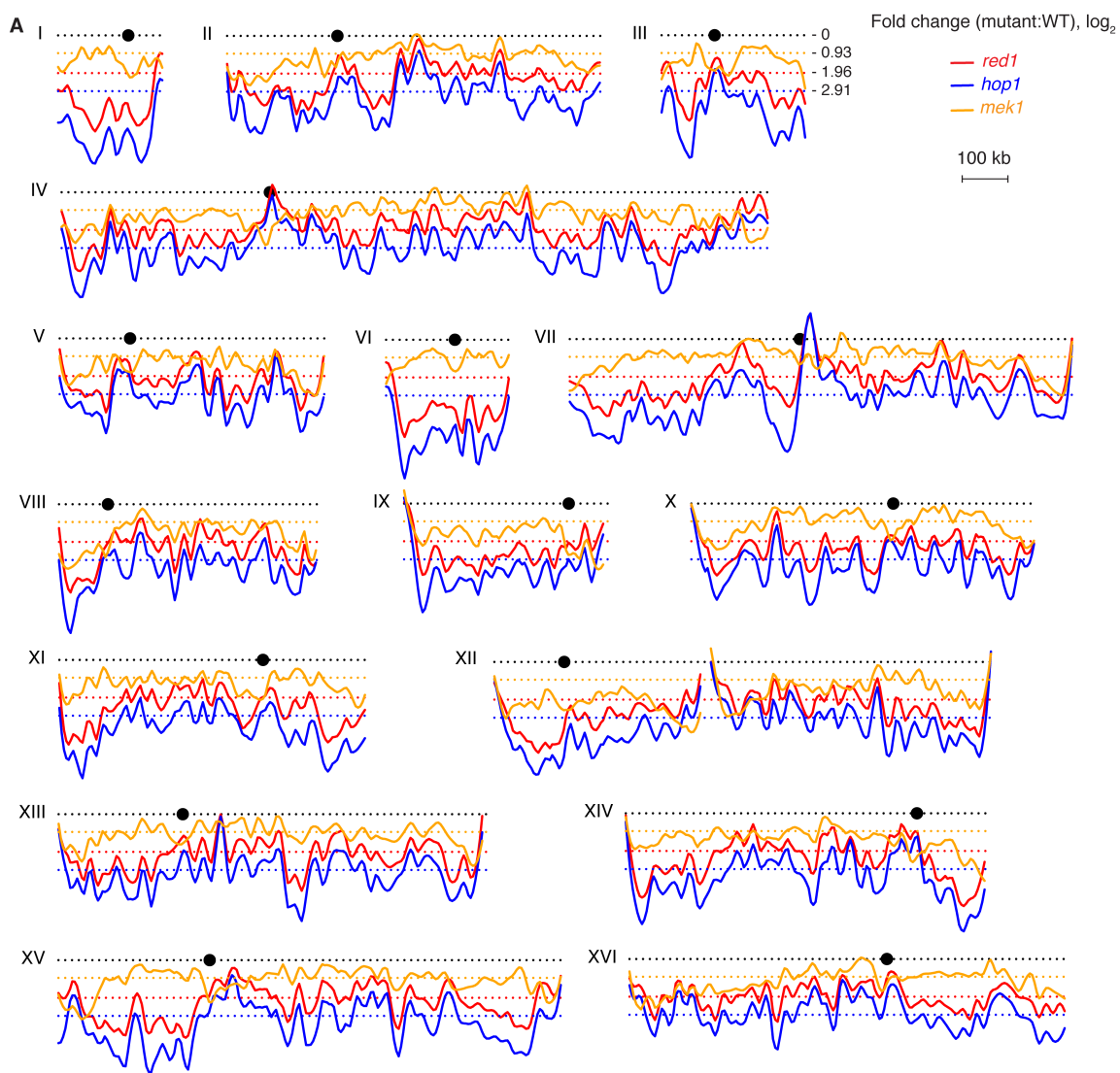


Figure 3.5. Regional variation along chromosomes in response to *red1*, *hop1*, or *mek1* mutation. (A) The genome was divided into non-overlapping 5-kb bins, and fold change (mutant over wild type) in Spo11-oligo counts was plotted for each bin in \log_2 scale along the length of each chromosome; lines represent loess smoothing of the individual data points (which are not shown, for clarity). Horizontal dotted lines indicate no change from wild type (black), or genome-average fold change in *red1* (red), *hop1* (blue), or *mek1* (orange). Centromere positions are indicated with filled circles. (B) Distribution of fold change in Spo11-oligo counts in 5-kb bins in *red1*, *hop1*, or *mek1* relative to wild type. Box plots are as in Fig. 2.4D. (C) Comparisons of fold change in Spo11-oligo counts within 5-kb bins between mutants. Pairwise correlation coefficients are shown (Pearson's *r*). Maps were scaled by 3.9-fold (*red1*), 7.5-fold (*hop1*), and 1.9-fold (*mek1*) based on Fig. 3.2B.

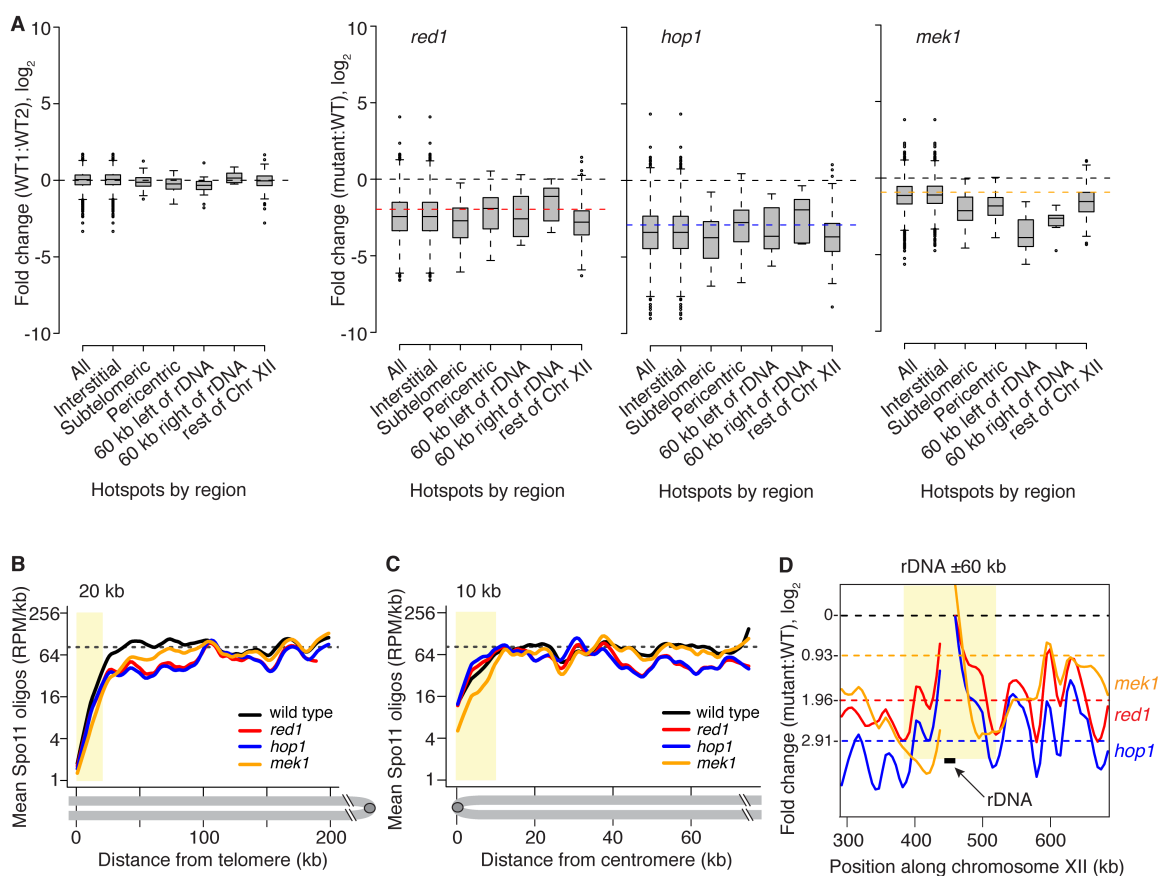


Figure 3.6. DSB suppression in sub-chromosomal regions is maintained in *red1*, *hop1*, and *mek1* mutants. (A) Change in scaled Spo11-oligo counts in hotspots grouped by chromosomal context. Hotspot list is from (Pan et al. 2011). Black dashed line indicates no change from wild type. Colored dashed lines indicate average change from wild type (red, *red1*; blue, *hop1*; orange, *mek1*). Subtelomeric hotspots include hotspots within 20 kb from telomere ends; pericentric hotspots include hotspots within 10 kb of a centromere. The rDNA coordinates used were 451,577–467,570 on chromosome XII; 60 kb were added to the left or right of these coordinates as indicated. (B) DSBs are still suppressed near telomeres and (C) near centromeres relative to the regions flanking them. Spo11-oligo densities in 500 bp segments were averaged across all 32 chromosome arms and smoothed (lowess). Dashed black line indicates genome average in wild type; yellow shading shows the DSB suppression zones in wild type. Note that the mutant Spo11-oligo maps were not scaled to reflect overall reduction in breaks in B and C. (D) Fold change in Spo11-oligo counts within 5-kb bins around the rDNA-proximal region on chromosome XII in *red1*, *hop1*, or *mek1* compared to wild type. The data points (not shown) were smoothed with loess smoothing. Horizontal dashed lines indicate genome-average change from wild type (red, *red1*; blue, *hop1*; orange, *mek1*). The yellow box indicates the rDNA region plus 60 kb to the left and right. Note that the black rectangle representing the location of the rDNA is only a 2-repeat placeholder for the full rDNA array.

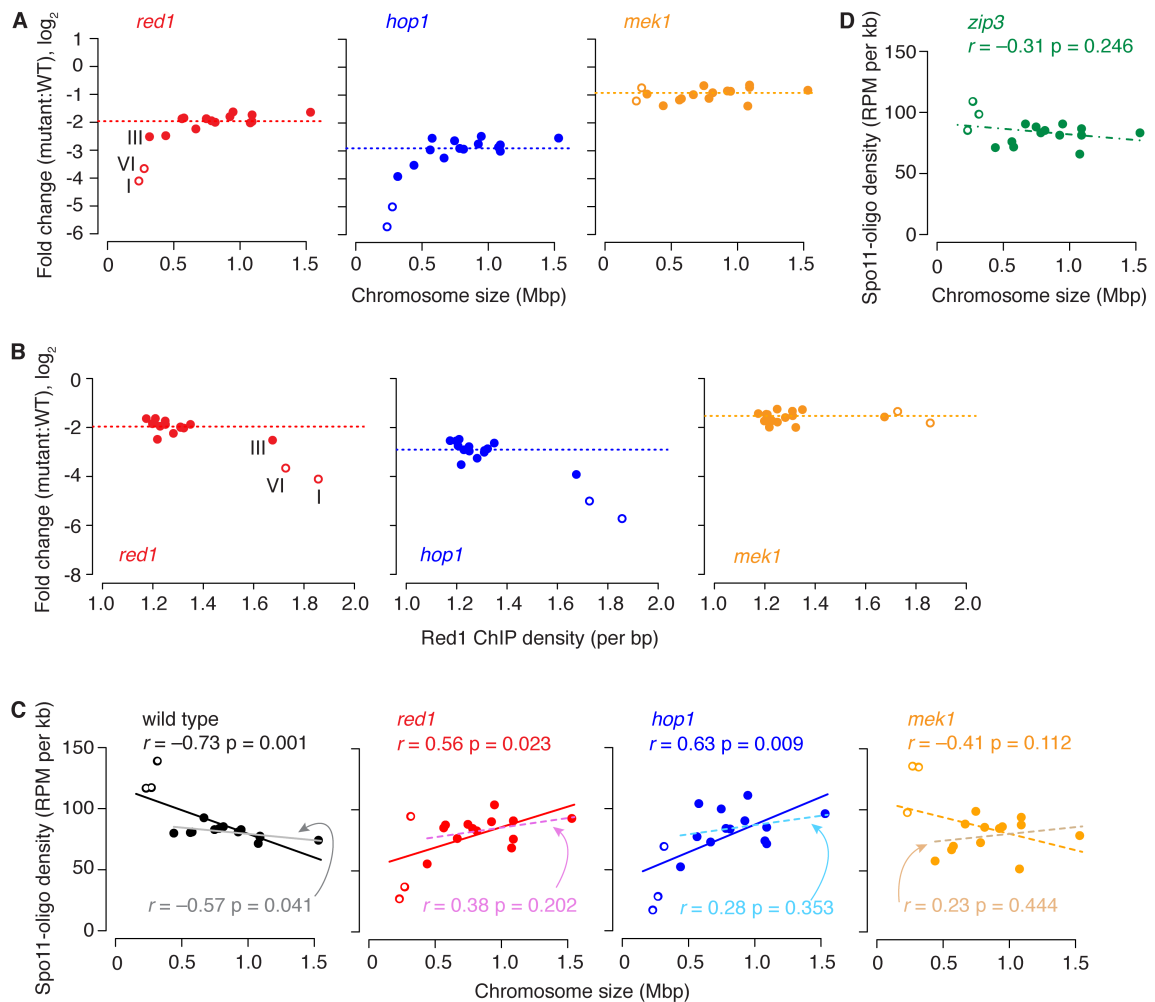


Figure 3.7. Short chromosomes behave differently in terms of DSB density in *red1* and *hop1*, but not in *mek1*. (A) Fold change (mutant over wild type) in Spo11-oligo density for each chromosome. Mutant maps were scaled as in Fig. 3.5. (B) Chromosomes I and VI (open circles), which exhibit the highest Red1 protein enrichment in wild type, also exhibit the most fold reduction in scaled Spo11-oligo density in *red1* and *hop1*. Red1 ChIP-seq dataset from (Sun et al. 2015). Dotted lines in panels A and B denote genome average fold change in Spo11-oligo density; open circles represent chromosomes I and VI. (C) Relationship between chromosome size and Spo11-oligo density. Each point represents one chromosome. The r value above the points indicates Pearson's correlation for all chromosomes, and r value below the points (in lighter color) indicates Pearson's correlation when excluding chromosomes I, III, and VI. Dashed lines, not statistically significant ($p > 0.05$). (D) Same analysis as in panel C, but for *zip3* dataset from (Thacker et al. 2014).

Short chromosomes are enriched for Red1 protein, and this bias towards short chromosomes is independent of Rec8 but dependent on Hop1 (Panizza et al. 2011; Sun et al. 2015). In the absence of Hop1, Red1 protein density is nearly the same on all chromosomes, suggesting that Hop1 either suppresses Red1 enrichment on medium and long chromosomes, or stimulates Red1 enrichment on short chromosomes (Sun et al. 2015). Thus, short chromosomes, which have the highest Red1 ChIP density in wild type, suffer greater than average DSB reduction in *red1* and *hop1*, (**Fig. 3.7B**).

Notably, chromosomes I, III, and VI are the three shortest chromosomes in *S. cerevisiae*, but chromosome III in *red1* and *hop1* appears to behave differently from the other short chromosomes in terms of DSB density. Chromosomes I and VI are most depleted for DSBs in *red1* and *hop1*, whereas chromosome III exhibits an intermediate phenotype (**Fig. 3.7A**). On the other hand, chromosome III behaves like chromosomes I and VI in terms of Red1 protein enrichment (**Fig. 3.7B**). One possibility is that there is a threshold behavior in terms of chromosome size and DSB defect in *red1* and *hop1*. Alternatively, chromosome III is special and behaves differently from other short chromosomes because it contains a ~100 kb zone suppressed for DSBs (between *CEN* and *MAT* loci), with flanking arm regions highly enriched for Red1 and DSBs (Baudat and Nicolas 1997; Blat et al. 2002).

As noted in **Chapters 1 and 2**, shorter chromosomes exhibit higher DSB density (Pan et al. 2011). The negative correlation between chromosome length and DSB density has been proposed to arise through homolog engagement feedback inhibition of DSBs, whereby Spo11 activity is inhibited upon engagement of homologous chromosomes (Thacker et al. 2014). According to the model, shorter chromosomes take longer to engage their homolog, possibly due to fewer overall DSBs translating to fewer opportunities for strand invasion and homology search, and therefore have a longer window of opportunity to accumulate DSBs. A manifestation of homolog engagement

feedback inhibition is that shorter chromosomes exhibit more DSBs per base pair of chromosome length compared to longer chromosomes.

In the *red1* and *hop1* mutants, the relationship between chromosome length and DSB density shifts to a positive correlation (**Fig. 3.7C**). Excluding the three shortest chromosomes from the analysis results in no significant correlation between DSB density and chromosome length in *red1* and *hop1*, whereas the negative correlation is retained in wild type (**Fig. 3.7C**). Thus, the shortest chromosomes drive the positive correlation seen in *red1* and *hop1* (a result of the pronounced depletion in DSBs discussed above), but are not responsible for the loss of negative correlation. Medium and long chromosomes no longer accumulate DSBs in a length-dependent manner, suggesting impaired homolog engagement feedback inhibition.

In the *mek1* mutant, the negative correlation between DSB density and chromosome length is lost or negligible (**Fig. 3.7C**). Excluding the three shortest chromosomes from the analysis results in no significant correlation, suggesting that the short chromosomes are responsible for any residual negative correlation (**Fig. 3.7C**). Thus, as in *red1* and *hop1*, homolog engagement feedback inhibition appears to be impaired in *mek1*. However, short chromosomes are still capable of accumulating higher DSB density in *mek1* even though the size-dependent effect on DSB density is disrupted, presumably a result of Red1 and Hop1 promoting extra DSBs on short chromosomes. Consistent with this working model, short chromosomes also appear modestly enriched for DSBs in the *zip3* mutant defective for homolog engagement (**Fig. 3.7D**) (Thacker et al. 2014).

From these analyses, we can discern two independent layers that contribute to higher DSB density in short chromosomes: (1) a Red1/Hop1-dependent effect that promotes DSBs specifically on the two shortest chromosomes, and (2) the chromosome-size effect from homolog engagement feedback inhibition, of which Red1, Hop1, and

Mek1 also play a role, most likely by promoting IH recombination. These independent effects on DSB formation in short chromosomes agree with previous proposals formulated by Sun, Klein, Hochwagen and colleagues predicting the elimination of preferential DSB formation on short chromosomes in the *hop1* mutant (Sun et al. 2015).

DSB reduction within subchromosomal domains in *red1* and *hop1* is weakly correlated with enrichment of Red1

The two shortest chromosomes, which are most enriched for Red1 protein in wild type, also exhibit the most severe DSB reduction in the absence of Red1 or Hop1. The correlation between the extent of DSB reduction in the mutant and Red1 enrichment in wild type might be specific for chromosomes I and VI. However, it is possible that the severity of DSB reduction correlates with wild type Red1 enrichment at the scale of chromosomal domains. In order to test this hypothesis, I investigated whether zones of severe DSB depletion seen along chromosomes in *red1* and *hop1* (**Fig. 3.5A**) reflect zones that were most enriched for Red1 in the wild type. For this analysis, Spo11-oligo counts were calculated for non-overlapping 20-kb bins along the genome. In *red1* and *hop1*, bins with highest Red1 ChIP density also appeared to have the greatest fold reduction in Spo11-oligo counts, although the correlation was weak (**Fig. 3.8A**). When considering the coefficient of determination (R^2), Red1 ChIP signal in wild type explains only 6.6% of the variation in DSB change seen in *red1*, and 6.9% of the variation seen in *hop1* (**Fig. 3.8A**). The quintile with greatest fold reduction in DSBs in *red1* and *hop1* showed a weak tendency to be more enriched for Red1 in wild type (**Fig. 3.8B**). This trend does not seem to be driven entirely by short chromosomes (**Fig. 3.8A, C**), suggesting that zones within medium and large chromosomes highly enriched for Red1 in wild type also tend to be most depleted for DSBs in *red1* and *hop1*. Nor is it driven by

pericentromeric or subtelomeric regions, as the weak correlations were also detected when including only interstitial regions in the analysis (**Fig. 3.8D**).

In contrast, no correlation was detected between Red1 enrichment in wild type and DSB reduction in *mek1*; bins with highest Red1 ChIP density exhibited fold reduction in DSBs similar to the genome-average reduction (**Fig. 3.8A**). Likewise, the quintile with greatest fold reduction in DSBs in *mek1* was not more enriched for Red1 in wild type (**Fig. 3.8B-D**).

In yeast, DSB distribution is correlated with ChIP enrichment of chromosome structure proteins (e.g., Red1, Hop1) and DSB proteins (Rec114, Mer2, Mei4, Rec102). The correlations are weak over short scales (<10 kb) but become stronger with increasing size scales, then saturate at ~20–30 kb (Blat et al. 2002; Pan et al. 2011; Panizza et al. 2011) (**Fig. 3.9A**), suggesting that domains (tens of kb) highly enriched for these proteins also tend to be domains with high DSB frequency. In the absence of Red1 or Hop1, patterns of correlation between Spo11 oligos in the mutant and ChIP enrichment of chromosome structure proteins in wild type over different size scales were altered (**Fig. 3.9A**). The difference is more striking at scales >10 kb, where little or no correlation is detected between Spo11 oligos in *red1* and *hop1* and distribution of chromosome structure proteins in wild type. An exception is Rec8: DSBs made in *red1* and *hop1* mutants displayed similar correlations with wild type Rec8 enrichment as DSBs made in wild type.

The magnitude of change in DSBs in *red1* and *hop1* showed a weak negative correlation with enrichment of proteins associated with chromosome axes in wild type (**Fig. 3.9B**). This result suggests that domains enriched for chromosome structure and DSB proteins in wild type are slightly more dependent on Red1 and Hop1 for DSB formation, so these domains show greater decrease in DSBs in the *red1* and *hop1* mutants. This weak negative correlation is consistent with the 20-kb scale analysis with

Red1 protein enrichment described above (**Figs. 3.8**), and demonstrates that the weak negative correlation is detected at other size scales.

The weak correlation between Red1 enrichment in wild type and DSB reduction in *red1* and *hop1* mutants is consistent with a previous study that compared low-resolution DSB analysis in *red1* with Red1 ChIP on chromosome III in wild type (Blat et al. 2002). Chromosomes I and VI most likely represent a special scenario in which hyperaccumulation of Red1 in wild type promotes higher DSB levels, so they are more depleted for DSBs in the absence of Red1 or Hop1 (**Fig. 3.7B**). The next chromosome to be most enriched for Red1 (chromosome X) does not appear to exhibit a greater fold-reduction in DSBs compared to the rest of the chromosomes in either *red1* or *hop1* mutants (**Fig. 3.7B**), supporting the conclusion that there is little correlation between Red1 enrichment and DSB reduction in the mutants.

DSB heat in wild type is positively correlated with Red1 and Hop1 protein enrichment, and Red1/Hop1-rich domains tend to be slightly more depleted for DSBs in *red1* and *hop1* mutants. This predicts that the hotter domains would be more depleted for DSBs in *red1* and *hop1* mutants. To test this prediction, I compared hotspot fold change in *red1* or *hop1* with hotspot heat in the wild type. Change in both *red1* and *hop1* showed a weak, almost negligible, negative correlation with DSB activity in wild type (**Fig. 3.9C**). Hotspot heat in wild type explains only 3.3% of variation in fold change in hotspot heat in *red1*, and 6.7% of variation in fold change in *hop1*. Negative correlations between DSB fold change in *red1* and *hop1* and DSB activity in wild type are weak over smaller scales (i.e., hotspot scale), but become stronger over larger domain sizes (**Fig. 3.9D**). Thus, there is a very weak tendency for hotter hotspots (sub-kb scale) to be more depleted for breaks, but over domains tens of kilobases wide, regions with higher DSB activity do exhibit greater decrease in DSBs in *red1* and *hop1*. These results are consistent with a previous observation that the magnitude of recombination defect

observed in *red1* mutants varied systematically with the wild type recombination frequency, that is, hotter loci exhibited greater reduction in the absence of Red1 (Schwacha and Kleckner 1997).

The *mek1* phenotype is different from that of *red1* and *hop1*: patterns of correlation between Spo11 oligos in the mutant and ChIP enrichment of chromosome structure proteins in wild type over different size scales were similar to wild type (**Fig. 3.9A**). Therefore, domains highly enriched for axis and DSB proteins in wild type are still domains with high break frequency in the absence of Mek1. In addition, the magnitude of DSB fold change in *mek1* shows a weak positive correlation with enrichment of several of the proteins at the chromosome axis (e.g., Hop1, Rec114, Mer2, and Mei4), with highest correlation for binning windows >20 kb (**Fig. 3.9B**). The distributions of Rec102, Rec104, Red1, and Rec8 were uncorrelated or weakly anti-correlated with DSB fold change in *mek1* (**Fig. 3.9B**). When examining Spo11 oligo fold change in *mek1* with DSB activity in wild type, no correlation was detected at the hotspot scale (**Fig. 3.9C**), and correlations remained consistently weak over larger domain sizes (**Fig. 3.9D**). Thus, unlike Red1 or Hop1, domains enriched for chromosome structure proteins and DSB proteins are not dependent on Mek1 for DSB activity.

Discussion

The role of Red1 and Hop1 in DSB formation

The available data suggest that Red1 and Hop1 have both intrinsic and extrinsic roles in shaping the DSB landscape: intrinsic roles in promoting DSB formation on all chromosomes, with an extra boost for DSBs on the two shortest chromosomes (I and VI), and an extrinsic role via homolog engagement feedback inhibition (**Fig. 3.10A**). Both Red1 and Hop1 recruit the DSB machinery to axial sites and in the absence of either

protein, Mer2 and Rec114 are no longer enriched at axial sites, as detected by ChIP (Panizza et al. 2011). Therefore, in a *red1* or *hop1* mutant, DSB protein recruitment and binding may be less efficient and/or stable, so the DSB machinery produces only 10–25% of wild type DSBs. A potential role for Hop1 in stabilizing the interaction between DSB proteins and axial sites is supported by reports of interactions between Hop1 and DSB proteins, and the inherent HORMA domain structure of Hop1 as potentially binding multiple partner proteins (de Massy 2013; Rosenberg and Corbett 2015). A genetic interaction between *HOP1* and *REC104* has been reported in which overexpression of *REC104* rescued the spore viability defect of a *hop1* non-null allele (Hollingsworth and Johnson 1993; Friedman et al. 1994). Furthermore, Hop1 interacts with Rec114 by yeast two-hybrid (S. Globus and S. Keeney, unpublished).

DSB patterns within hotspots in *red1* and *hop1* are very similar as in wild type, despite the absence of axis core components. Perhaps Rec8 at axis sites (and residual Hop1 that can associate with chromatin independently of Red1) can partially compensate in the absence of Red1, and both Rec8 and Red1 are able to partially compensate in the absence of Hop1. Nevertheless, it is paradoxical that in the absence of Hop1, only ~10% of DSBs are made, even though Rec8 and Red1 are present and axial elements form (as detected by electron microscopy) (Hollingsworth and Byers 1989; Loidl et al. 1994; Sun et al. 2015). On the other hand, cells are more proficient at making breaks (25% of wild type DSBs) in the absence of Red1, in which Rec8 is present but Hop1 is apparently not chromatin-associated (Sun et al. 2015), and axial elements (as detected by electron microscopy) fail to form (Rockmill and Roeder 1990). A possible model to explain the difference in severity of DSB phenotype is as follows: Red1 inhibits DSBs and promotes chromatin enrichment of Hop1, and Hop1 promotes DSBs and inhibits Red1's inhibition on DSBs (**Fig. 3.10B**). DSB numbers are more depleted in the absence of Hop1 than in the absence of Red1 because the inhibitory

effect of Red1 on DSB formation is not counteracted in the absence of Hop1. An alternative possibility is that the Hop1 ChIP data in *red1* is misleading, and on a single-cell basis, there is enough Hop1 chromatin association to support DSB formation in the absence of Red1.

The extrinsic role of Mek1 in regulating DSB numbers

The importance of Red1 and Hop1 in DSB formation has been undisputed in the meiosis field, but it has not been clear whether Mek1 affects DSB formation and repair, or only DSB repair. Reports on DSB phenotype in *mek1* have been conflicting, and interpretations are confounded by the possibility that most (or all) of the reduced steady-state DSB levels reflect processing of DSBs by IS recombination (Wan et al. 2004; Niu et al. 2005). Some studies have concluded that *mek1* itself does not confer a DSB formation defect (Wan et al. 2004; Callender and Hollingsworth 2010). In contrast to Southern blot DSB assays, quantification of Spo11-oligo complexes measures break formation without confounding effects of break repair. However, since the turnover of Spo11-oligo complexes is not well understood, it remains plausible that their turnover is intimately linked with repair of DSB ends, and the reduced steady-state levels of Spo11-oligo complexes in *mek1* reflects faster repair by IS recombination.

An alternative and more likely possibility is that the effect of *mek1* on DSB numbers is indirect via restraints on cell cycle progression (**Fig. 3.10A**). Unlike the Spo11-oligo complex time course profiles in *red1* and *hop1*, which resemble the wild-type profile (except for the reduction in number), the shape of the profile in *mek1* is altered, with Spo11-oligo complex levels increasing normally at first (up until 3 h), then decreasing prematurely (**Fig. 3.2B**). Earlier turnover of Spo11-oligo complexes may be linked to premature Ndt80 activation, since turnover of Spo11-oligo complexes appears to be dependent on activation of the Ndt80 transcription factor that governs exit from

pachytene stage (Thacker et al. 2014). In addition, activation of the meiotic recombination checkpoint (of which Red1, Hop1, and Mek1 are involved in) in the presence of DSBs blocks Ndt80 activation; this ensures that cells do not progress to metaphase until DSBs are repaired (Tung et al. 2000; Okaz et al. 2012; Carballo et al. 2013). Premature Ndt80 activation and earlier turnover of Spo11-oligo complexes in *mek1* would reconcile seemingly conflicting results: earlier peak and overall reduction in Spo11-oligo complexes (**Fig. 3.2B**), despite wild-type levels of DSBs detected by *rad50S* Southern blot (**Fig. 3.1**), and prior conclusions that Mek1 is not needed for DSB formation (Wan et al. 2004; Callender and Hollingsworth 2010). Therefore, absence of Mek1 probably does not confer a defect on DSB formation but instead affects DSB numbers through regulation of meiotic progression (“extrinsic”). An implication of this interpretation is that the area under the curve measurement of the Spo11-oligo complex time course is not the best proxy for scaling the *mek1* Spo11-oligo map, since the assumption that Spo11-oligo complex lifespan is unchanged is violated. However, since the fold reduction in Spo11-oligo complexes detected in *mek1* is very similar whether measuring area under the curve (1.9) or peak (1.8), the overall conclusions presented in this chapter are probably the same if using the peak value as scaling factor for the Spo11-oligo maps.

If premature Ndt80 activation in the *mek1* mutant is occurring through a recombination checkpoint defect, then *red1* and *hop1* mutants would also be expected to exhibit premature Ndt80 activation, since Red1 and Hop1 are also implicated in the recombination checkpoint. However, earlier turnover of Spo11-oligo complexes is not detected in *red1* and *hop1*. A possible explanation is that Mek1 is present and can still partially inhibit Ndt80 activation in *red1* and *hop1* mutants. Alternatively, this role of Mek1 is independent of Red1 and Hop1.

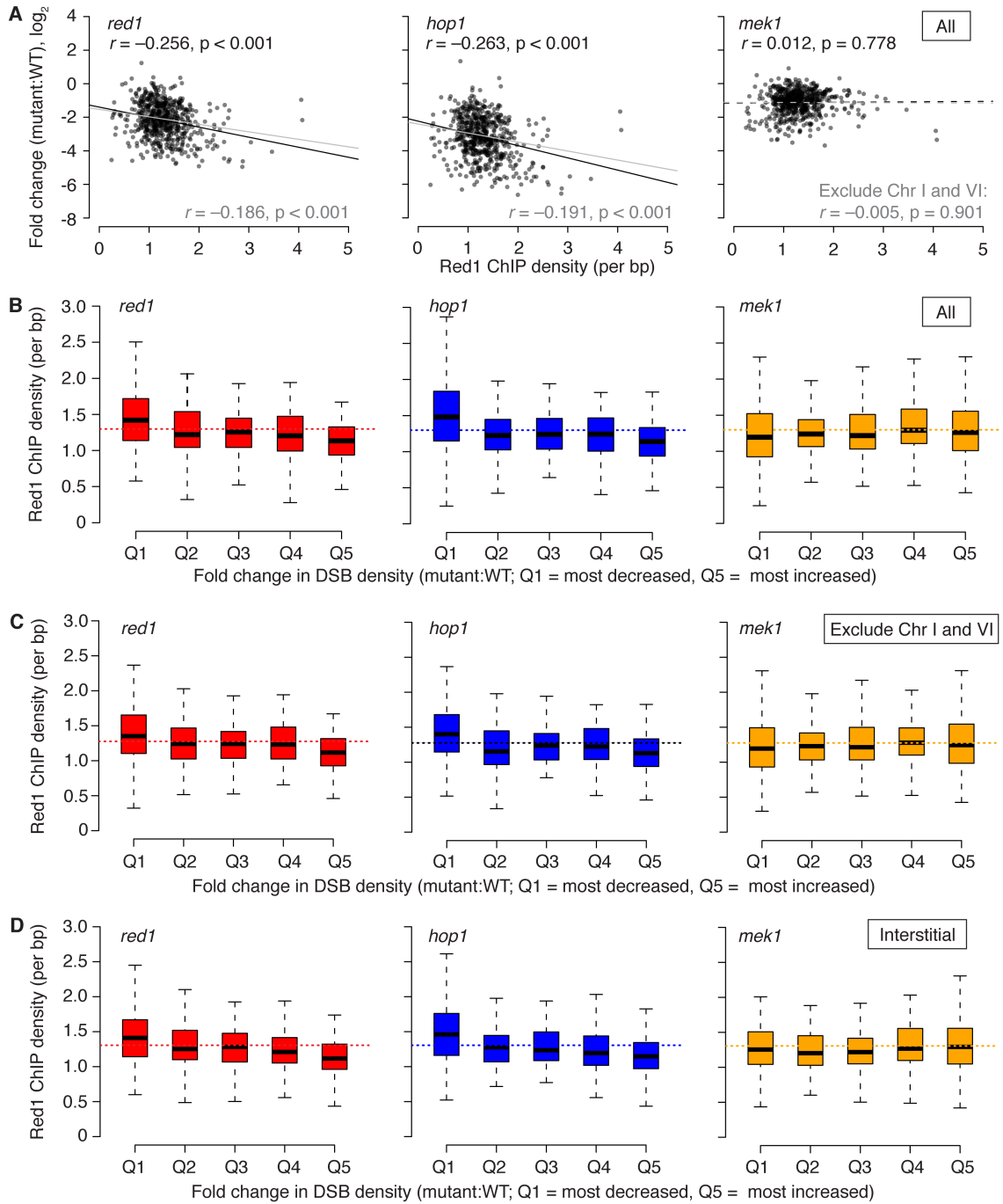


Figure 3.8. Genomic regions that exhibit the greatest fold decrease in DSBs in *red1* and *hop1* mutants exhibit a weak tendency to have been most enriched for Red1 in the wild type. (A) Fold change (mutant over wild type) in scaled Spo11 oligos within 20-kb bins genome wide plotted against Red1 ChIP density (dataset from (Sun et al. 2015)). Black r , Pearson's correlation; dashed regression line denotes nonsignificant ($p>0.05$). Gray, excluding chromosomes I and VI. (B) Genome-wide 20-kb bins showing the most reduction in Spo11 oligos in *red1* and *hop1*, but not in *mek1*, were the most enriched for Red1 protein in the wild type. 20-kb bins were sorted and split into quintiles based on degree of \log_2 fold change in Spo11-oligos from wild type, with Q1 indicating the bins with most decrease, and Q5 indicating the bins with most increase in DSBs in the mutants. This weak tendency is still observed when excluding bins on the two shortest chromosomes (C), and when excluding pericentric (10 kb from centromeres) and subtelomeric (20 kb from chromosome ends) regions (D). Dotted lines, genome average.

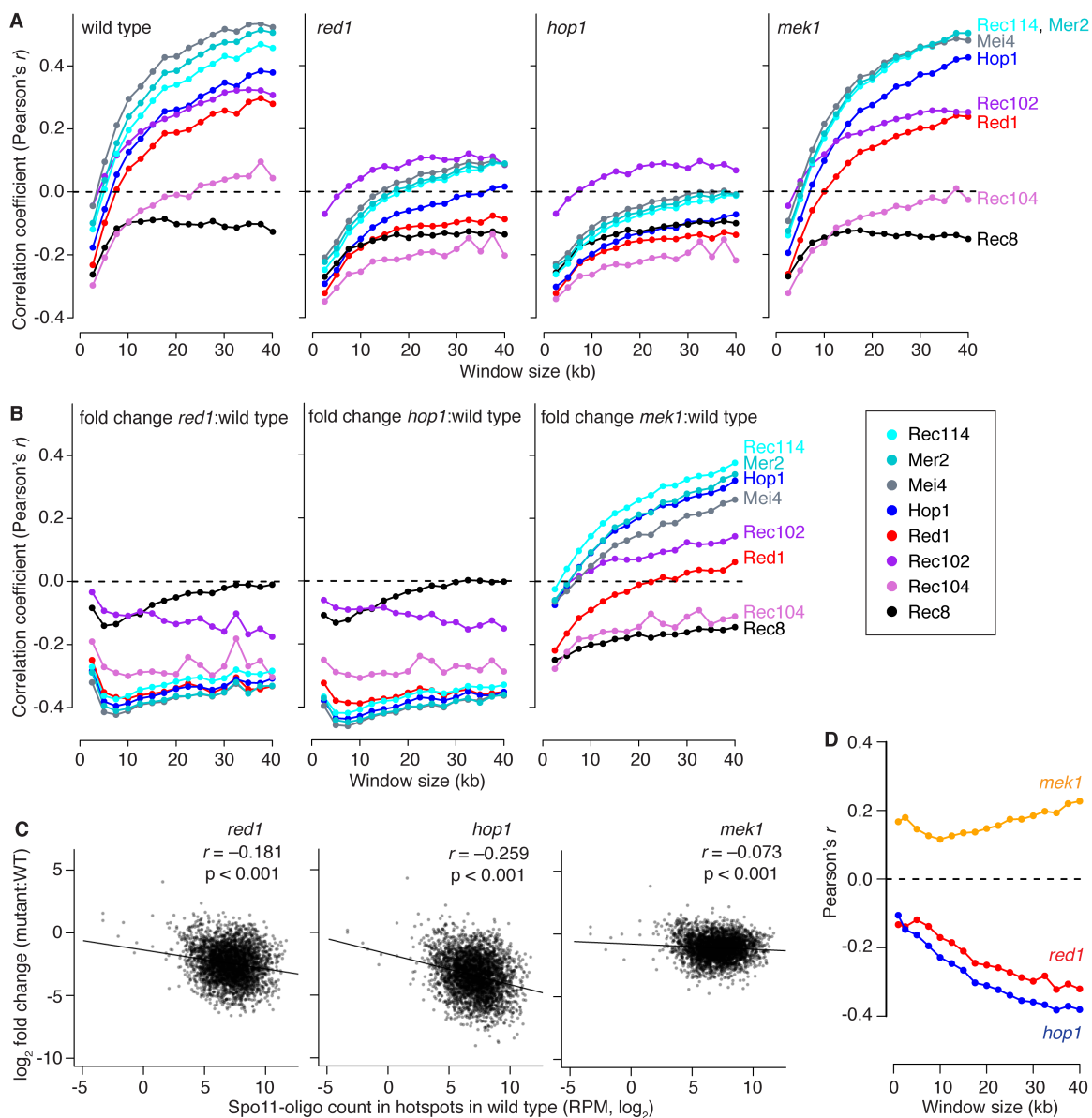


Figure 3.9. Domains of correlated behavior are altered in *red1* and *hop1*, but not in *mek1*. (A) Correlation between Spo11 oligos in *red1*, *hop1*, or *mek1* and binding of indicated proteins in wild type, binned in non-overlapping windows of varying size. (B) Correlation between \log_2 fold change in mutant (*red1*, *hop1*, or *mek1*) over wild type and binding of indicated proteins in wild type, at varying window sizes. CHIP-chip data in panels A and B are from (Panizza et al. 2011). (C) Weak anticorrelation for *red1* and *hop1* are detected when examining hotspots, but no correlation is detected in *mek1*. Only interstitial hotspots ($n=3468$) from (Pan et al. 2011) were analyzed; wild type Spo11-oligo counts are from (Zhu and Keeney 2015). Spo11-oligo counts were scaled as in Fig. 3.5. r , Pearson's correlation. (D) Correlation (Pearson's r) between \log_2 fold change mutant over wild type Spo11-oligo density and DSB activity in wild type at varying window sizes.

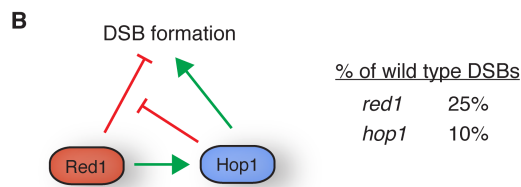
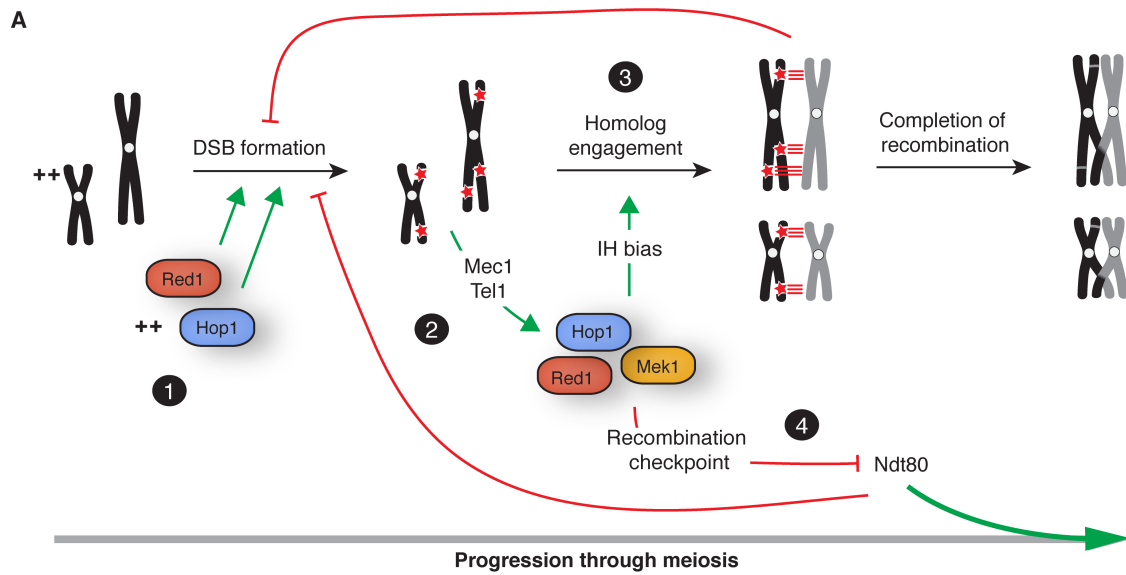


Figure 3.10. Model for the effects of Red1, Hop1, and Mek1 on DSB numbers. (A) Meiotic prophase I progression. (1) Red1 and Hop1 promote DSB formation (red stars) on all chromosomes, and they also promote extra DSBs on the two shortest chromosomes (indicated by ++). (2) DSB formation activates the damage-responsive kinases Tel1/Mec1, which restrain Spo11 activity via a negative feedback loop (not shown), and in a separate circuit, results in Hop1 phosphorylation and Mek1 activation, which promotes interhomolog recombination (IH bias). (3) Engagement of homologous chromosomes gives rise to alterations to the chromosome structure that inhibit further DSB formation. All three proteins (Red1, Hop1, Mek1) appear to be involved in homolog engagement feedback inhibition. (4) Red1, Hop1, and Mek1 are involved in the recombination checkpoint, which inhibits Ndt80 to ensure that cells do not progress through meiosis until DSBs are repaired. Ndt80 activation results in exit from the pachytene stage, which ends the DSB-permissive period. It is not clear whether the role of Mek1 in preventing premature Ndt80 activation is separate, or involves Red1 and Hop1. Upon completion of recombination, some DSBs are repaired as COs, and others as NCOs. For simplicity, not all known feedback circuits are shown. (B) Alternative model for how Red1 and Hop1 might be promoting DSB formation. In this model, Red1 promotes DSBs through Hop1, and Red1 on its own has an inhibitory effect on break formation. This model attempts to explain the more severe DSB defect detected in *hop1* compared to *red1*.

Why are some loci more depleted for DSBs in *red1* or *hop1*?

Previous investigations have noticed locus-to-locus variation in *red1* and *hop1* DSB and/or recombination defects (Rockmill and Roeder 1990; Mao-Draayer et al. 1996), and this effect is also detected in the genome-wide DSB maps. The locus-specific severity of the DSB defect in *red1* has been concluded to be independent of Red1 protein enrichment in the wild type (Blat et al. 2002), yet at other times proposed to be dependent on Red1 enrichment (Kim et al. 2010), and has been noted to correspond with recombination frequency in the wild type (Schwacha and Kleckner 1997). My analyses indicate that sites more enriched for Red1 protein and DSB activity in wild type tend to exhibit the most DSB depletion in *red1* and *hop1* mutants, but the correlations are weak. Chromosomes I and VI (on a whole-chromosome level) behave differently in this regard, since they are highly enriched for Red1 protein in wild type and are severely depleted for DSBs in *red1* and *hop1* mutants. It is still not clear what drives the variation in DSB defect. Perhaps sites with less fold reduction in DSBs in the mutants represent sites that can recruit and/or stabilize DSB proteins independently of Red1/Hop1.

Other aspects to consider when interpreting these results are the limitations of ChIP data. Red1 and Hop1 bind chromatin genome-wide (except possibly the rDNA, in the case of Hop1 (Smith and Roeder 1997; Borner et al. 2008)), which means that enriched domains are not the only places where the proteins associate, and cutoffs for defining enrichment are somewhat arbitrary. Furthermore, both ChIP and Spo11-oligo maps are population average measurements. In the scenario in which a domain with high Red1 protein enrichment in wild type is strongly correlated with DSB depletion in a *red1* or *hop1* mutant on a single-cell basis, the effects of eliminating Red1 or Hop1 will be mitigated when examining the average from a population of cells (e.g., if the precise boundaries of the domains and the precise locations of DSB formation vary from cell to cell). Along the same lines, it is difficult to define what a domain is in a ChIP-seq profile

due to the spatial resolution, combined with it being a population average measurement. For example, spatial resolution is constrained by cross-linking and shearing efficiency: an immunoprecipitated 500 bp chromatin fragment in a ChIP-seq experiment provides information that the protein was bound to that fragment, but not where along that fragment.

An extra layer of complexity is added when considering the implications of homolog engagement feedback inhibition on ChIP measurements. A possible mechanism for shutting down break formation is via displacement of Hop1, Red1, and DSB proteins from chromatin, based on studies in yeast and mouse (Wojtasz et al. 2009; Daniel et al. 2011; Carballo et al. 2013; Keeney et al. 2014; Thacker et al. 2014; Subramanian et al. 2016). If domains enriched for Red1/Hop1 experience more DSBs on average, they also probably experience homolog engagement feedback inhibition more effectively on average, and are therefore subject to homolog engagement-mediated Red1/Hop1 depletion more strongly. Therefore, the degree of Red1 and Hop1 intrinsic enrichment might be underestimated in the wild type.

Dual layer of control promotes DSBs on short chromosomes

In theory, short chromosomes are at higher risk of missegregation during the first meiotic division, since there are fewer opportunities for breaks to form on a per base pair basis if DSBs were randomly distributed. However, DSB distribution is nonrandom (Baudat and Nicolas 1997; Gerton et al. 2000; Borde et al. 2004; Blitzblau et al. 2007; Buhler et al. 2007; Pan et al. 2011), and in fact, short chromosomes acquire higher DSB density than longer chromosomes (Pan et al. 2011), translating to higher recombination density (Kaback et al. 1989; Kaback et al. 1992; Mortimer et al. 1992; Chen et al. 2008a; Mancera et al. 2008). Size-dependent DSB density was proposed to arise from homolog engagement feedback inhibition (Thacker et al. 2014). Here, I uncover another layer that

contributes to higher DSB density in short chromosomes, in which Red1 and Hop1 exert preferential DSB formation on the two shortest chromosomes. Unlike homolog engagement feedback inhibition, this layer is not chromosome-size dependent *per se*, but appears to be specific to chromosomes I and VI. In the *zip3* mutant where homolog engagement feedback inhibition is disrupted, short chromosomes on average still exhibit higher DSB density than the rest of the chromosomes (**Fig. 3.7D**) (Thacker et al. 2014), consistent with Red1 and Hop1 still exerting an effect on break formation on chromosomes I and VI.

The effect of Red1 and Hop1 on DSBs in chromosomes I and VI is more prominent, but it is not clear whether this effect extends to chromosome III. The chromosome III phenotype resembles that of medium chromosomes in terms of DSB density, but resembles short chromosomes in terms of Red1 ChIP enrichment. One possibility is that there is a threshold behavior in terms of chromosome size and DSB defect in *red1* and *hop1*. Alternatively, chromosome III could represent a separate category, since it is an atypical chromosome. As discussed in **Chapter 2**, chromosome III carries the mating type locus in budding yeast, and behaves differently in other regards, most likely due to constraint by the *CEN-MAT* linkage. Since the ~100 kb region between the *CEN* and *MAT* loci is suppressed for DSBs, recombination is largely restricted to the flanking arm regions (Baudat and Nicolas 1997; Blat et al. 2002). In addition, these flanking arm regions are highly enriched for Red1 (Baudat and Nicolas 1997; Blat et al. 2002). Perhaps the arm regions of chromosome III (excluding the *CEN-MAT* DSB-suppressed zone) behave like chromosomes I and VI in terms of Red1/Hop1 dependence for DSB formation.

How could greater enrichment of Red1 and Hop1 on shorter chromosomes be promoting more DSBs? The available data suggest that higher density of Red1 and Hop1 on chromosomes I and VI is able to recruit more DSB proteins (e.g., Mer2,

Rec114, Mei4). Mer2 and Rec114 are more enriched on the three shortest chromosomes (Panizza et al. 2011; H. Murakami and S. Keeney, unpublished), and this biased enrichment is dependent on Red1 and Hop1 (H. Murakami and S. Keeney, unpublished). In addition, the higher density on short chromosomes is not dependent on *SPO11*, and therefore is not tied to homolog engagement feedback mechanism (Panizza et al. 2011; Sun et al. 2015). Many questions remain: What is the basis for Red1 enrichment on short chromosomes? One model is that Hop1 suppresses Red1 on larger chromosomes, and/or stimulates Red1 binding on short chromosomes. How does Hop1 generate chromosome-size bias in protein enrichment? An alternative model is that Red1 enrichment on short chromosomes is an intrinsic property of chromosomes I, III, and VI, independently of their size.

Axial element proteins and homolog engagement feedback inhibition of DSBs

Red1, Hop1, and Mek1 are required for normal levels of IH recombination, and are fully or partially required for complete SC assembly (Hollingsworth and Byers 1989; Rockmill and Roeder 1990; Rockmill and Roeder 1991; Leem and Ogawa 1992). By extension, these three proteins would thus be predicted to be at least partially required for efficient homolog engagement and thus for the concomitant feedback inhibition of DSBs. The *red1*, *hop1*, and *mek1* mutants exhibit loss of the size-dependent effect on DSB density, suggesting that homolog engagement feedback inhibition of DSBs is attenuated. The *mek1* mutant phenotype most resembles the *zip3* mutant in this regard, but the phenotype in *red1* and *hop1* is obscured by the much stronger dependence of short chromosomes on Red1/Hop1 for DSB formation. The loss of the size-dependent effect on break density in *red1* and *hop1* is revealed only upon excluding the short chromosomes from the analysis. This example illustrates the complexity of mutant

phenotypes because of intersecting networks of DSB control pathways and their homeostatic behavior.

Sites of preferred DSB formation are robust to changes in meiotic chromosome organization

The Spo11-oligo maps demonstrate that despite having an effect on DSB levels, absence of Red1, Hop1, or Mek1 do not grossly alter many features of the DSB distribution. Specifically, Spo11 still preferentially cleaves DNA within promoter NDRs, the DSB pattern within hotspots is maintained, and DSB suppression is still detected in subtelomeric, pericentric, and rDNA-proximal regions. Spo11 preferential cleavage persists despite breaks not being made in the context of axial elements in the *red1* mutant, and with loop-axis structures most likely strongly altered in the *hop1* mutant as well (even if some aspect of axial elements form, as detected by electron microscopy (Hollingsworth and Byers 1989)). My findings are consistent with the retention of fine-scale hotspot location in the *rec8* mutant, despite altered Red1 distributions (Sun et al. 2015; M. van Overbeek, M. Sasaki, and S. Keeney, unpublished), and with axial element proteins exerting an effect on the DSB distribution over larger distances (Blat et al. 2002; Panizza et al. 2011). The maintenance of DSB patterns within hotspots nevertheless suggests that loop-axis organization is largely dispensable for DSB site selection (discussed in **Chapter 4**).

Overall, the results presented in this chapter are consistent with the model of the DSB landscape being shaped by a hierarchical combination of factors (Pan et al. 2011; Thacker et al. 2014). Eliminating one factor does not drastically change the DSB distribution because each factor contributes only partially to the likelihood that a base pair will be cleaved by Spo11, and in addition, the mechanism of DSB formation is inherently homeostatic and robust. For example, in the *pch2* and *sir2* mutants,

suppression of DSBs in the rDNA-proximal region is lost, and other large (10–100 kb) subchromosomal domains show altered DSB activity (Mieczkowski et al. 2007; Vader et al. 2011; Zhu 2015). However, the spatial distribution of hotspots in other parts of the genome appear to be maintained, indicating that other layers of the hierarchy, such as Spo11 preference for cleaving DNA at NDRs are likely retained (Mieczkowski et al. 2007; Vader et al. 2011; Zhu 2015). Likewise, in the *mcm21* mutant pericentric DSBs are no longer suppressed, but other aspects of the landscape are essentially identical to wild type (Vincenten et al. 2015). Absence of the H3K4 methyltransferase Set1 results in reduced DSBs at many hotspots, but alternative DSB-promoting mechanisms give rise to increased DSB frequency within hotspots that were weak in wild type (Borde et al. 2009; Zhu 2015). Thus, the locations of preferred DSB formation are quite robust to perturbations, including perturbations to the higher-order chromatin structure. That fewer breaks are made in the Red1, Hop1, and Mek1 at essentially the same locations as in wild type most likely reflects these proteins' roles impinging upon various networks that ensure DSB homeostasis (as well as the intrinsic roles in DSB formation in the case of Red1 and Hop1) (Cooper et al. 2014; Keeney et al. 2014).

CHAPTER 4: CONCLUDING DISCUSSION

Main conclusions

The investigations described in the preceding chapters provide insight into the mechanisms that shape and regulate the meiotic DSB landscape. In **Chapter 2**, I compared the meiotic DSB landscape in *Saccharomyces* species up to 15 My diverged to examine the evolutionary dynamics of recombination hotspots. My analyses led to the conclusion that DSB hotspots and the DSB landscape are conserved in widely diverged *Saccharomyces* species. Importantly, my results support the model that hotspots can be conserved over evolutionary time scales if DSBs are targeted to functional genomic elements, indicating that selective constraints can counteract the tendency of biased gene conversion to eliminate hotspots. In light of comparative studies of meiotic recombination landscapes in other taxa, I proposed that the evolutionary dynamics of the recombination landscape—whether hotspots diverge rapidly or are conserved—depend on the underlying mechanism of DSB formation. In **Chapter 3**, I examined DSB maps in the absence of chromosome structure proteins Red1 and Hop1, and the associated kinase Mek1, to elucidate their roles in shaping the DSB landscape. Red1 and Hop1 promote DSB formation genome-wide and also influence DSB numbers via feedback networks. Unexpectedly, Red1 and Hop1 promote more DSBs on the two shortest chromosomes in *S. cerevisiae*. On the other hand, Mek1 most likely has little or no intrinsic role in DSB formation, but affects DSB numbers through regulatory pathways.

Potential implications and perspectives

Mechanism of meiotic recombination initiation

Lessons from species comparative studies of the DSB landscape. Many of the features that are known to shape the DSB landscape in *S. cerevisiae* (e.g., histone modification, loop-axis organization, recombination checkpoints, feedback circuits) have not been formally examined in the context of meiotic recombination in other *Saccharomyces* species. However, conservation of the DSB landscape in species 15 My diverged (**Chapter 2**) implies that the architects of the landscape are also conserved and contribute similarly as in *S. cerevisiae*. For example, the Spo11-oligo density analysis in translocated chromosomes with different chromosome lengths (chromosome VI in *S. mikatae* and the spontaneous translocation in *S. cerevisiae* YPS128) allow us to infer that homolog engagement feedback circuit is conserved. DSB suppression near centromeres implies that kinetochore function in preventing Spo11 activity in that region is conserved. Likewise, CHIP experiments of chromosome structure proteins and DSB proteins associated with axial sites (e.g., Rec8, Red1, Hop1, Rec114) can be performed in *S. paradoxus*, *S. mikatae*, and *S. kudriavzevii* to infer the loop-axis organization in these species, but the Spo11-oligo map analysis at 20-kb size scale already suggests that the position of loops and axes along chromosomes is conserved. Nevertheless, in the instances where hotspots are not conserved, such experiments in *Saccharomyces* species to map features that contribute to the DSB landscape would be useful to understand the cause of hotspot divergence (discussed below).

The DSB landscape is governed by intersecting networks of DSB control pathways. The DSB maps in *red1*, *hop1*, and *mek1* mutants in **Chapter 3** provide an example of how the multiple intersecting control pathways that regulate and shape the DSB landscape make it difficult to predict the effect of a mutation on DSB numbers. Absence of Red1 and Hop1 affect the intrinsic potential of the DSB substrate and/or

DSB machinery to make breaks, and also attenuate the downstream homolog engagement feedback circuit due to their role in recombination partner choice. The role of Mek1 in recombination partner choice and the recombination checkpoint also means that in its absence, homolog engagement and control of cell cycle progression are impaired.

Are loop-axis structures and TLACs dispensable for shaping the DSB landscape? As mentioned in **Chapter 1**, loop-axis organization is one of the factors that influence the DSB landscape. DSBs form preferentially within loop regions instead of protein-rich axes, but many proteins required for DSB formation and recombination localize to the axes (Blat et al. 2002; Glynn et al. 2004; Kugou et al. 2009; Pan et al. 2011; Panizza et al. 2011; Ito et al. 2014). The TLAC model—loop tethering to the axis—has been proposed to explain these conflicting observations (Blat et al. 2002; Kleckner 2006). A possible mechanism for how loop tethering might occur is through Spp1, which physically interacts with Mer2 at the axis, and H3K4me3 marks near gene promoters on chromatin loops (Acquaviva et al. 2012; Sommermeyer et al. 2013), thereby influencing the location of DSBs.

The Spo11-oligo maps in **Chapter 3** show that DSB patterns within hotspots in *red1* and *hop1* mutants are similar to wild type despite the absence of core chromosome structure proteins that promote the organization of loop-axis structures. This suggests that loop-axis organization is largely dispensable for DSB site selection and for DSB patterns at scales <10 kb. If loop-axis structures are indeed disrupted in *red1* and *hop1* mutants, the fact that DSB patterns within hotspots persist would argue against the TLAC model having a large influence on DSB site selection and shaping the DSB landscape. In support of this view, H3K4 trimethylation levels have modest predictive power to explain variation in DSB frequency (Tischfield and Keeney 2012). Alternatively, loop-axis structures might not actually be disrupted in *red1* and *hop1* mutants, and other

chromosome axis components (e.g., Rec8, condensin) might either function redundantly or compensate in the absence of Red1/Hop1.

The shape of the yeast DSB landscape may be under selection

Is there selective pressure to maintain patterns of recombination? In

Chapter 2, the conservation of both DSB distribution and frequency led to the speculation that selective pressures may operate more directly on the DSB landscape. Selective pressure to maintain accurate meiotic chromosome segregation may influence and constrain the distribution of recombination events. For example, mechanisms are in place to prevent chromosome missegregation from crossovers occurring too close or too far from the centromere. Crossovers too close to the centromere might disrupt local sister chromatid cohesion and result in precocious separation of sister chromatids, chromosome missegregation, and spore inviability (Rockmill et al. 2006). Pericentric crossovers are minimized by kinetochore-mediated local suppression of DSBs and crossover recombination (Vincenten et al. 2015). At the other end of the spectrum, the spindle checkpoint helps rescue chromosome segregation when crossovers are far (>100 kb) from the centromere by enabling re-orientation on the spindle pole (in meiosis I homologs need to attach to opposite spindle poles [bi-orientation] instead of to the same spindle pole [mono-orientation] for proper segregation; the spindle checkpoint helps correct instances where homologs mono-orient) (Lacefield and Murray 2007).

Precise patterns of the recombination landscape may be under selection because of the benefits conferred from disrupting or maintaining linkage groups. For example, it has been argued that the tight linkage between the mating type locus and the centromere has been selected for in yeast evolution (Knop 2006). Mating of non-sister spores within the same ascus (intratetrad mating) is common in *Saccharomyces*, estimated to be 94% of all matings in the wild (only 5% of matings are estimated to occur

between spores from different asci) (Tsai et al. 2008). The *CEN-MAT* linkage has been proposed to allow yeast to maintain a high degree of heterozygosity in centromere-linked genes in the face of frequent intratetrad mating (inbreeding) (Taxis et al. 2005; Knop 2006). The model is that spores with recessive lethal mutations between the *CEN* and *MAT* loci can mate with a non-sister spore within the ascus (without undergoing haploid mitotic divisions) and mask the recessive lethal mutations. Thus, heterozygosity is maintained and a larger fraction of cells can survive (Taxis et al. 2005; Knop 2006). In support of this model, Taxis, Knop and colleagues found enrichment of essential genes in regions near the centromere (Taxis et al. 2005). Thus, intratetrad mating would provide a way to maintain heterozygosity at centromere-linked essential genes.

In addition, the *CEN-MAT* linkage has been proposed to ensure the formation of dyad spores with opposite mating types during nutrient limitation (**Fig. 4.1**) (Taxis et al. 2005; Lacefield and Ingolia 2006). Upon carbon source limitation during sporulation (e.g., low levels of acetate in the medium), yeast cells make fewer spores, usually dyads instead of tetrads (Davidow et al. 1980; Okamoto and Iino 1981). It turns out that yeast cells preferentially package chromosomes derived from homologs (non-sisters) into two spores, as a result of spore formation bias at the newer spindle pole bodies that were duplicated during meiosis II (Taxis et al. 2005). The low frequency of recombination between the *CEN* and *MAT* loci allows most non-sister dyads to be of opposite mating types, which ensures that the spores will be able to undergo intratetrad mating and return to diploidy upon germination (Taxis et al. 2005).

Along the same lines, modeling studies suggest that the nonrandom meiotic recombination distribution, in particular crossovers, is related to clustering of essential genes in the yeast genome (Keller and Knop 2009). Clustering of essential genes (thus, linkage of essential genes) in yeast has been proposed to allow purging of deleterious mutations in essential genes while minimizing the number of individuals lost after mating

and homozygotization (Keller and Knop 2009). In the computer simulations, *CEN-MAT* linkage and essential gene clustering provided cumulative fitness benefit, and were able to predict the nonrandom distribution of crossovers (Keller and Knop 2009). However, it is difficult to precisely define the mechanism(s) that gave rise to the *S. cerevisiae* genome architecture (e.g., gene clustering) over its evolutionary history, especially since there is no record for the actual events that led to the current genome arrangement. For example, patterns of essential gene clustering may be driven in combination with other mechanisms, such as selective advantage for co-expression of genes (Hurst et al. 2002; Hurst et al. 2004).

Selection for DSB proficiency in short chromosomes. In **Chapter 3**, analyses of Spo11-oligo maps in *red1* and *hop1* mutants revealed that Red1 and Hop1 provide an intrinsic boost of DSBs in the two shortest chromosomes. Thus, more DSBs are promoted in short chromosomes through a dual layer of control: intrinsically by Red1/Hop1 enrichment and greater dependence on these proteins for DSB formation, and extrinsically by homolog engagement feedback inhibition (Thacker et al. 2014). A potential implication of the added intrinsic role of Red1 and Hop1 in promoting more DSBs on chromosomes I and VI is that these short chromosomes may be less dependent than medium chromosomes on homolog engagement feedback inhibition to acquire enough DSBs for generating crossovers. That is, by the time feedback inhibition kicks in, short chromosomes have acquired a relatively high DSB density due to the Red1/Hop1 enrichment.

The intrinsic boost of DSBs in chromosomes I and VI implies that there is selection for DSB proficiency in short chromosomes, most likely to prevent missegregation. If so, this observation supports the idea that the specific shape of the yeast DSB landscape confers fitness benefits, which was proposed in **Chapter 2**.

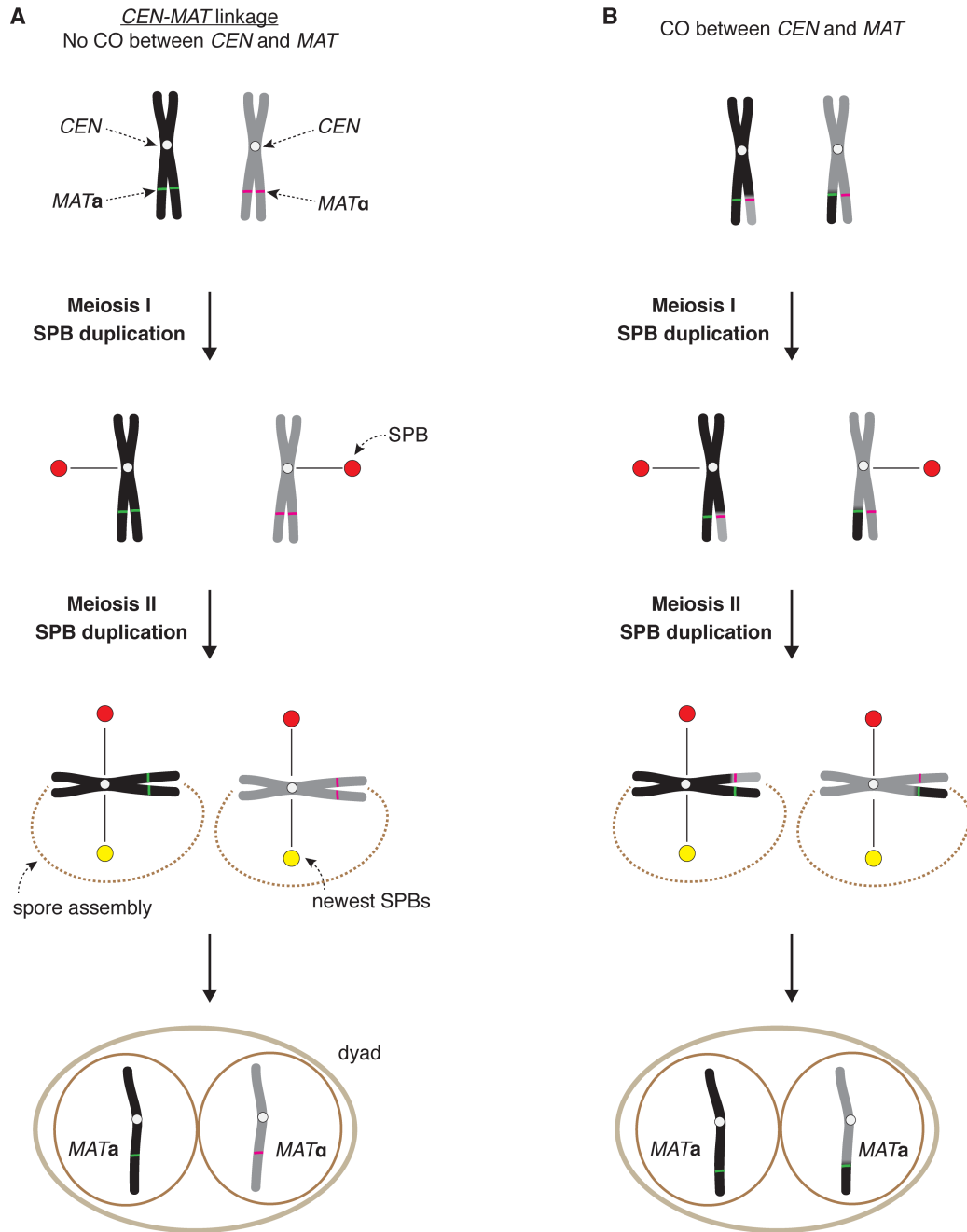


Figure 4.1. *CEN-MAT* linkage increases the formation of spores with opposite mating types under limited nutrient availability. (A) Scenario with *CEN-MAT* linkage. No crossovers (CO) between these loci. Under poor sporulation conditions, dyads form with high frequency. When forming dyads, the two newer spindle pole bodies (SPB) shown in yellow are more often chosen for spore assembly; thus, genomes derived from a different meiosis II spindle (non-sisters) are packaged into spores. The spores in the dyad are of opposite mating types and can undergo intratetrad mating to restore the diploid. For simplicity, only chromosome III is shown. (B) If recombination were to occur between the *CEN* and *MAT* loci, the resulting spores in the dyad would be of the same mating type and would be unable to mate.

Implications of recombination evolutionary dynamics on genome organization

Species in different taxa demonstrate different hotspot evolutionary dynamics based primarily on the presence or absence of a PRDM9-like system, but also on whether Spo11 cleavage is targeted to functional genomic elements. This observation led to the proposed model that DSB landscape conservation or divergence depends on the underlying mode of hotspot designation (**Chapter 2**). What effect does a rapidly-evolving recombination landscape have on genome architecture and on the organism? Potential implications include, but are not limited to, more variation in allele combinations, more variation in haplotypes within a population, more phenotypic diversity, more variation for selection to act upon, and/or increased likelihood for a host to eliminate transposable elements from its genome. The question remains as to whether such rapid change in the recombination landscape is advantageous (as in organisms with PRDM9).

In a system where hotspot locations can change abruptly, recombination at novel hotspots could break apart advantageous allele combinations and threaten genomic integrity if it occurs at certain places of the genome. For example, DSBs in repetitive element could lead to non-allelic homologous recombination and potentially give rise to chromosome rearrangements (e.g., duplications, deletions, inversions, translocations) (Sasaki et al. 2010; Kim et al. 2016). If so, do organisms with a PRDM9 system to target hotspots have different quality control mechanisms to check gamete viability? It is possible to envision that having a PRDM9-like system could be detrimental to unicellular organisms, since novel recombination hotspots can lead to unfavorable genome structure alterations and inviability, whereas in multicellular organisms defective meiotic products can be eliminated and the germ cells can go through other rounds of meiosis without conferring lethality to the organism. However, these scenarios present a question about what happens on the flip side, that is, what effects stable recombination

landscapes have on genome architecture. For example, the haplotypes might be more static, or the stability of the recombination landscape might promote conservation of genome organization.

A combination of molecular approaches for studying the mechanisms that shape the recombination landscape (e.g., fine-scale DSB and recombination maps) and detailed analysis of genome organization across a broad range of species, not limited to laboratory model organisms, will yield insight into the implications of meiotic recombination on genome evolution. These approaches can be further combined with an understanding of interspecies social dynamics (e.g., host-pathogen) in the organism's natural habitat. For example, meiotic recombination rates and evolutionary dynamics might be different between pathogenic and non-pathogenic organisms in a hypothetical scenario where rapid hotspot evolution is advantageous for generating novel combinations of alleles to overcome newly evolved host-resistance mechanisms. However, from a practical standpoint it is difficult to dissect causal relationships and establish whether a particular process confers a selective advantage, since many forces are likely at play over the evolutionary history of an organism. Thus, many of the potential implications discussed here are highly speculative and are difficult to test, but are nonetheless interesting ideas to consider.

Meiotic recombination and genome base composition. High rates of meiotic recombination are hypothesized to affect genome base composition by increasing GC content, mediated by GC-biased gene conversion (Duret and Galtier 2009). GC-biased gene conversion is the biased transmission of GC alleles due to biased mismatch repair at sites of recombination, where AT/GC heteroduplex sites tend to be repaired as GC. This results in preferential transmission of GC-alleles over AT-alleles near recombination hotspots. Evidence for GC-biased mismatch repair has been reported in meiotic products in yeasts (Mancera et al. 2008; Lesecque et al. 2013) and humans (Odenthal-

Hesse et al. 2014; Arbeithuber et al. 2015; Williams et al. 2015). A potential implication is that the strength of the correlation between recombination and GC content should be weaker in species where the DSB landscape evolves rapidly, and stronger in species with stable DSB landscapes (Mugal et al. 2015). Signatures of GC-biased gene conversion would not be expected to accumulate as much if hotspots are rapidly changing. Consistent with this prediction, meiotic recombination in organisms with stable recombination landscapes, such as dogs and birds, exhibits localized signatures of GC-biased gene conversion (higher than expected equilibrium levels of GC content) (Auton et al. 2013; Singhal et al. 2015). However, whether signatures of GC-biased gene conversion in dogs and birds are stronger than those detected in humans and chimpanzee (Auton et al. 2012) remains to be seen, and requires a detailed systematic comparison across species.

Future directions

DSB landscape conservation in yeast

Most DSB hotspot locations and hotspot heat are very well conserved between *Saccharomyces*. However, it is not known why particular hotspots are less conserved than others. A systematic analysis of hotspots that are not conserved in the different *Saccharomyces* species would be useful to examine features that result in poor conservation. Potential culprits for poor hotspot conservation in a species include diverged nucleosome structure resulting in loss of NDR, reduced H3K4me3, altered temporal or spatial pattern of transcription factor binding, altered loop-axis organization at that locus, or differences in recombination checkpoint activation and regulatory circuits.

Another potential question is whether hotspots that are least conserved exhibit greater sequence divergence. If these sequence differences are enough to alter features that influence Spo11 cleavage probability (e.g., nucleosome positioning, transcription factor binding, higher-order chromatin organization), then DSB distribution and frequency within the hotspot might be less conserved. However, the opposite prediction could also hold true. Hotspots that are most conserved might exhibit greater sequence divergence because frequent gene conversion events can result in mutation (i.e., if meiotic recombination is mutagenic (Nishant et al. 2010; Arbeithuber et al. 2015)). Higher rates of recombination appear to be associated with higher levels of DNA sequence variation in *Drosophila*, but it is not clear whether this is driven by the mutagenic effect of recombination (Begun and Aquadro 1992; Charlesworth and Campos 2014). In yeast, one study detected no correlation between recombination rates and sequence divergence (Noor 2008), but the study relied on recombination data for *S. cerevisiae* only, despite comparing sequence divergence between *S. cerevisiae* and *S. paradoxus*.

According to the model proposed for DSB hotspot conservation in yeast, hotspots escape biased gene conversion-mediated erosion if they are located in genomic regions that are under selective constraint. A prediction from this model is that hotspots in promoters of essential genes should be more conserved than those in nonessential genes. One way to address this question is to compare the degree of conservation of hotspots that overlap promoters of essential genes with the degree of conservation of hotspots that overlap promoters of nonessential genes. A limitation of this analysis is that the genes that are essential for yeast in their natural habitat (and over their evolutionary history) may not be the same genes that we define as essential or nonessential in the lab environment.

Role of chromosome structure proteins in shaping the DSB landscape

Should Mek1 be grouped with Red1/Hop1? Historically, there has been a tendency for Red1, Hop1, and Mek1 to be indiscriminately categorized into one group, based on physical interactions and shared function in promoting IH recombination. However, my analyses of the Spo11-oligo maps demonstrate that many phenotypes of the DSB landscape that are shared between *red1* and *hop1* are not shared with *mek1*. For example, patterns of domain behavior in *mek1* are clearly different from *red1* and *hop1*. In addition, absence of Mek1 seems to result in shorter Spo11-oligo complex lifespan, and this phenotype is not detected in *red1* or *hop1*. An outstanding question is, how similar is *mek1* to *red1* and *hop1* in terms of the DSB landscape? The DSB maps can be compared with those of other mutants (e.g., *zip3*, *rec8*, *set1*, etc) to determine whether it is justified to group *red1*, *hop1*, and *mek1* together, or whether *mek1* alters the DSB landscape more similarly to other mutants.

The link between Mek1 and Ndt80. The Spo11-oligo complex time course in *mek1* suggests that Spo11-oligo complexes undergo turnover earlier than in wild type, leading to the proposal that Mek1 inhibits premature activation of Ndt80. In addition, Mek1 appears to have little or no intrinsic role in DSB formation. Examination of Spo11-oligo complexes in the *mek1 ndt80* double mutant would test this model. If premature activation of Ndt80 is the cause of the earlier peak of Spo11-oligo complexes in *mek1*, and if Mek1 is indeed not required for DSB formation, then Spo11-oligo complexes in the double mutant are expected to reach maximum level at 4 h (like wild type), and exhibit no peak fold reduction from wild type. In fact, peak Spo11-oligo complex levels at 4 h in *mek1 ndt80* are expected to be higher than wild type if homolog engagement is perturbed in the absence of Mek1.

Is chromosome III as dependent on Red1/Hop1 for DSBs as I and VI? From the current analysis, it is not clear whether Red1 and Hop1 promote extra DSBs on

chromosome III, as they do for chromosomes I and VI. Chromosomes I and VI are 230 kb and 270 kb, respectively. Chromosome III is 317 kb, and the next shortest chromosome is chromosome IX (440 kb). Like I and VI, chromosome III is also highly enriched for Red1 protein (Blat et al. 2002; Panizza et al. 2011; Sun et al. 2015), but the DSB phenotype in *red1* and *hop1* is intermediate between that of the two shortest chromosomes and medium chromosomes. One possibility is that the Red1-enriched arms of chromosome III are disproportionately affected in terms of DSBs in the absence of Red1/Hop1, but the central DSB-suppressed zone is masking the effect. A way to test this would be to examine DSB density only within the arms, excluding the *CEN-MAT* locus.

Are chromosomes I and VI special, or just short? Another pending question is whether Red1 enrichment on chromosomes I and VI (and their higher dependence on Red1/Hop1 for DSBs) is an intrinsic property of those chromosomes, or whether it is chromosome-length dependent. Engineering a translocation chromosome where chromosome I or VI is stitched onto parts of a longer chromosome would help answer this question. If Red1 enrichment is intrinsic to chromosomes I and VI, then the segment originating from chromosome I and/or VI should retain high Red1 protein enrichment, whereas the remainder of the engineered chromosome should not be as enriched. Alternatively, if the effect is chromosome-length dependent, then the segment originating from chromosomes I/VI should behave like a long chromosome. Red1 protein enrichment can also be examined in *S. mikatae*, to see whether chromosome VI retains features of the shorter ancestral chromosome VI, or whether the boost for DSBs on ancestral chromosome VI was lost after *S. mikatae* chromosome VI became a medium chromosome.

CHAPTER 5: MATERIALS AND METHODS

Yeast strains and culture methods

Studies on the evolutionary dynamics of the recombination landscape (**Chapter 2**) were done in the following *Saccharomyces* species strains: *S. cerevisiae* SK1, YPS128 and UWOPS03-461.4, *S. paradoxus* YPS138, *S. mikatae* IFO1815, *S. kudriavzevii* ZP591 (**Table 5.1**). *SPO11* in each species was C-terminally tagged with three Flag epitope repeats by targeted integration of a *6His-3FLAG-loxP-kanMX-loxP* construct amplified from an *S. cerevisiae* SK1 *SPO11-Flag* strain provided by Kunihiro Ohta, Univ. Tokyo (Kugou et al. 2009)). Yeasts were transformed using standard lithium acetate methods, with modifications to heat shock incubation times and temperatures for each species, as specified in (Scannell et al. 2011) for *S. mikatae* and *S. kudriavzevii*, and as specified by Jeremy Roop (Rachel Brem laboratory, UC Berkeley, personal communication) for *S. paradoxus*. Briefly, heat shocks were done for 8 min at 37°C for *S. paradoxus*, 5 min at 37°C for *S. mikatae*, and 30 min at 34°C for *S. kudriavzevii*. Since all strains were homothallic diploids, homozygous tagged strains were generated by transformation, followed by sporulation, tetrad dissection, and screening self-diploidized spore clones for resistance to G418. Correct tagging was verified by PCR and Southern blot.

Studies on the role of chromosome structure proteins on the recombination initiation landscape (**Chapter 3**) were done with the strains of the SK1 background listed in **Table 5.2**. The *red1* and *mek1* deletions were made in the *spo11-HA3-His6::KanMX* strain background by Julian Lange (Keeney lab, MSKCC). *RED1* and *MEK1* coding sequences were replaced with the hygromycin B drug resistance cassette (*hphMX4*) amplified from plasmid pMJ696 (identical to pAG32 in (Goldstein and McCusker 1999)). Yeasts were transformed using standard lithium acetate methods. The *hop1* deletion

was generated in the same manner, but in the *SPO11-6His-3FLAG-loxP-kanMX-loxP* strain background. Gene disruption was verified by PCR and Southern blotting. Null alleles were moved into strains with the *SPO11-Flag* allele described above, and/or the *SPO11-PrA* allele (Thacker et al. 2014), by crossing and tetrad dissection.

Synchronous meiotic cultures of *S. cerevisiae* SK1 were prepared as described in (Neale and Keeney 2009), with cells from a saturated overnight YPD (1% Bacto yeast extract, 2% Bacto peptone, 2% dextrose) culture used to inoculate a 14 h pre-sporulation culture in YPA (1% yeast extract, 2% peptone, 1% potassium acetate) and sporulation in 2% potassium acetate, 0.2 × supplements (2 µg/mL adenine, 2 µg/mL histidine, 6 µg/mL leucine, 2 µg/mL tryptophan, 2 µg/mL uracil). For wild-derived *S. cerevisiae*, *S. paradoxus* and *S. kudriavzevii*, 14 h pre-sporulation in YPA was followed by sporulation in 1% potassium acetate, 0.2 × supplements. For *S. mikatae*, the above conditions result in premature meiotic entry, so sporulation conditions were based instead on methods of (Murakami and Keeney 2014). Briefly, a 7 h starter culture in SPS (0.5% yeast extract, 1% peptone, 0.67% yeast nitrogen base without amino acids, 1% potassium acetate, 0.05 M potassium biphthalate, pH 5.5) was used to inoculate a 16 h pre-sporulation culture in SPS, and sporulation was done in 1% potassium acetate, 0.001% polypropylene glycol supplemented with 0.32% amino acid complementation medium (1.5% lysine, 2% histidine, 2% arginine, 1% leucine, 0.2% uracil, 1% tryptophan). All SK1 culturing steps were performed at 30°C. All other strains and species were cultivated at room temperature (growth on solid media) or 23°C (all growth in liquid media). For all strains and species, cells were transferred to sporulation media to a cell density (OD₆₀₀) of 6.0.

For Spo11-oligo mapping, ≥ 600 mL sporulation culture volume was harvested 4 h (*S. cerevisiae* YPS128, *S. paradoxus*, *S. mikatae*), 6 h (*S. cerevisiae* UWOPS03-461.4), or 9 h (*S. kudriavzevii*) after transfer to sporulation media, corresponding with the

approximate time of peak levels of Spo11-oligo complexes (**Fig. 2.2**). Because of the severe DSB defect in *red1* and *hop1* (**Figs. 3.1, 3.2**), Spo11 oligos from multiple (4–5) cultures were pooled to generate each Spo11-oligo map. For each mutant, various pre-sporulation and sporulation cultures of independent colonies were set up, with 600 mL of sporulation culture harvested at 4 h after transfer to sporulation media. The *mek1* maps were generated from a single meiotic culture, since the DSB defect is not as severe.

To assess culture synchrony, meiotic division profiles were obtained by collecting aliquots at various times from synchronous meiotic cultures, fixing in 50% (v/v) ethanol, and staining with 0.05 µg/mL 4', 6-diamidino-2-phenylindole (DAPI). Mono-, bi- and tetranucleate cells were scored by fluorescence microscopy.

Detection of meiotic DSBs by Southern blotting

Genomic DNA was isolated at 0 or 8 h in meiosis from two to three independent cultures for each genotype. DNA was prepared in low-melting agarose plugs as described (Borde et al. 2000; Murakami et al. 2009) to avoid shearing of high molecular weight fragments. DNA embedded in agarose plugs was separated by pulsed-field gel electrophoresis, then probed by Southern blot with part of the *CHA1* open reading frame (SGD coordinates 15838 to 16857) to detect DSBs on chromosome III, as described in (Murakami et al. 2009). Hybridization signal was detected by phosphorimager, and DSB frequency was calculated as the percent of hybridizing signal in each lane. Observed DSB frequencies were Poisson corrected (as described in (Murakami and Keeney 2014), then signals from 0 h lanes were subtracted from all lanes.

End-labeling of Spo11-oligo complexes

To detect Spo11-oligo complexes, previously described methods were used for denaturing cell extract preparation, anti-Flag immunoprecipitation (IP), end-labeling with

terminal deoxynucleotidyl transferase, and SDS-PAGE (Neale and Keeney 2009; Thacker et al. 2014). Radiolabeled complexes were detected by phosphorimager. Briefly, Spo11-oligo complexes were immunoprecipitated from whole-cell extracts by using mouse monoclonal anti-Flag M2 antibody (Sigma). Precipitated Spo11-oligo complexes were end-labeled with [α - 32 P]dCTP in a terminal deoxynucleotidyl transferase reaction. Spo11-oligo complexes were eluted, resolved by SDS-PAGE, then transferred onto PVDF membrane and visualized by phosphorimager. The polyacrylamide gel after transfer was also exposed alongside the membrane to detect signal of Spo11-oligo complexes that were not transferred to the membrane, and were left behind in the gel. During quantification, signal detected from the membrane was added to the signal detected in the gel after transfer to obtain total Spo11-oligo complex levels. To detect total Spo11 protein, blots were probed with mouse monoclonal anti-Flag M2 conjugated to horseradish peroxidase (Sigma) and detected by chemiluminescence. Protein quantity was estimated by separating whole-cell extract in SDS-PAGE and staining with Coomassie Brilliant Blue.

To estimate the fold-reduction in Spo11-oligo complexes in the *red1*, *hop1*, and *mek1* mutants, signal from the autoradiograph was quantified over the entire lane with the ImageGauge software, and subtracted of background (signal from 0 h lane, which should contain no DSBs). Spo11-oligo complex quantifications from biological replicate experiments were averaged, and peak values or area under the curve measurements were calculated for the wild type and mutant (GraphPad Prism).

Spo11-oligo purification

Spo11-oligo mapping has been previously described (Pan et al. 2011; Thacker et al. 2014; Vincenten et al. 2015; Zhu and Keeney 2015). For SK1, I used a previously published Spo11-oligo map (two biological replicates) prepared from a strain in which

Spo11 was tagged with five copies of a fragment of protein A (Thacker et al. 2014). New maps were generated for this study in the other strains/species carrying *SPO11-Flag*. Processing of cell lysates for Spo11-oligo purification and sequencing library preparation were essentially as described (Zhu and Keeney 2015), except that Spo11-Flag IP was carried out with protein G Dynabeads (Life Technologies) instead of protein G agarose beads. In the first round of IP, 400 μ L protein G Dynabeads pre-bound with 80 μ L of 1 mg/mL mouse anti-Flag M2 antibody (Sigma) was used per 25 mL whole-cell extract in 50 mL IP volume. Pre-binding of antibody to beads was carried out with pre-washed protein G Dynabeads (washed twice with 1 \times IP buffer (1% Triton X-100, 15 mM Tris-HCl, pH 8.0, 150 mM NaCl, 1 mM EDTA)) and anti-Flag antibody in 1 mL 1 \times IP buffer for 10 min at 37°C, with end-over-end rotation. Beads were subsequently washed twice with 1 \times IP buffer prior to use in the IP. For the second round of IP, 125 μ L protein G Dynabeads pre-bound with 25 μ L of 1 mg/mL anti-Flag antibody was used in an 800 μ L IP volume.

Some modifications to the protocol were made to purify enough Spo11 oligos from *red1* and *hop1* strains for mapping (to give an example of the yield, in one experiment from a single meiotic culture I obtained 122 fmol of Spo11 oligos from *red1*, 141 fmol from *hop1*, and 1497 fmol for *mek1*). For *red1* dataset A, Spo11 oligos were pooled from five cultures (C1, C2, D2, E, F) harvested 4 h after transfer to sporulation media, and pooling was done after eluting from the first immunoprecipitation and at the last step of oligo purification (after proteinase K treatment and ethanol precipitation of the oligos); for *red1* dataset B, Spo11 oligos were pooled from four cultures (A1, A2, B1, B2) after eluting from the first immunoprecipitation, and during resuspension of the oligos after proteinase K treatment and ethanol precipitation. For *hop1* dataset A, Spo11 oligos were pooled from five cultures (A1, A2, B1, B2, D) after eluting from the first immunoprecipitation step; for *hop1* dataset B, Spo11 oligos from five cultures (G1, G2, H1, H2, K1) were pooled after eluting from the first immunoprecipitation step, and at the

last step of oligo purification, after proteinase K treatment and ethanol precipitation of the oligos. For *mek1*, each dataset is of Spo11 oligos purified from one 600 mL sporulation culture harvest at 4 h after transfer to sporulation media.

Protein G dynabeads were used for immunoprecipitation. For the second round of immunoprecipitation of Spo11-oligo complexes pooled from five cultures, the total IP volume was increased to 4 mL, and 500 μ L of Dynabeads Protein G slurry were pre-bound to 100 μ L 1 mg/mL anti-Flag antibody (as opposed to 125 μ L of Dynabeads Protein G slurry pre-bound to 25 μ L 1 mg/mL anti-Flag antibody, and a 2nd IP volume of 800 μ L).

Sequencing (Illumina HiSeq 2500, 2 x 75 bp paired-end reads) was performed in the MSKCC Integrated Genomics Operation, and mapping of the sequencing reads was performed by N. Socci at the MSKCC Bioinformatics Core.

Mapping of sequenced Spo11 oligos

Clipping of library adapters and mapping of reads was performed by the Bioinformatics Core Facility (MSKCC) using a custom pipeline as described (Pan et al. 2011; Thacker et al. 2014; Zhu and Keeney 2015). *S. cerevisiae* SK1, YPS128, and UWOPS03-461.4 Spo11-oligo reads were mapped to the sacCer2 genome assembly of type strain S288C from SGD (*Saccharomyces* Genome Database), *S. paradoxus* reads were mapped to *S. paradoxus* YPS138 genome assembly from SGRP (*Saccharomyces* Genome Resequencing Project) or CBS432 type strain genome assembly from (Scannell et al. 2011), and *S. mikatae* and *S. kudriavzevii* were mapped to their strain genome assemblies from (Scannell et al. 2011). The genome assemblies of *S. mikatae* and *S. kudriavzevii* contain unplaced contigs; mapping included these contigs, but downstream analyses were done on chromosomes 1–16 only. For all analyses of *S. paradoxus*, we used maps based on the genome assembly for the same strain

background from which Spo11 oligos were purified (YPS138), except for the analysis of large-scale correlations with GC content in **Fig. 2.10**, in which Spo11-oligo reads mapped to the type strain CBS432 were compared with GC content in the CBS432 genome sequence due to the latter being a more complete sequence assembly. Sequence read totals and mapping statistics are described in **Table 2.1** (yeast species) and **Table 3.1** (*red1*, *hop1*, *mek1*). Statistical analyses were performed using R (RStudio version 0.98.1091, R version 3.0.1).

Raw and processed sequence reads for the *Saccharomyces* species maps have been deposited in the Gene Expression Omnibus (GEO) database (<http://www.ncbi.nlm.nih.gov/geo>) as accession number GSE71887. Raw and processed sequence reads for *S. cerevisiae* SK1 *mcm21* Spo11-oligo maps have been deposited as accession number GSE72683. These accessions also contain the curated maps (unique mapping reads only, normalized to reads per million mapped) in wiggle format to allow direct visualization in appropriate genome browsers, e.g., the UCSC browser (<https://genome.ucsc.edu>) using genome version sacCer2 for *S. cerevisiae* maps, or the Integrative Genomics Viewer (IGV) genome browser (Broad Institute) and loading the appropriate genome assembly files. Sequencing data for *red1*, *hop1*, *mek1* will be deposited at GEO prior to publication of these studies.

DSB hotspots in *Saccharomyces* species maps were identified using the method from (Pan et al. 2011), with minor modifications. Hotspots were defined as clusters of Spo11 oligos meeting cutoffs for size and Spo11-oligo density similar to the previous definitions. Briefly, candidate hotspots were first identified as regions where the Spo11-oligo map smoothed with a 201-bp Hann window was >0.193 RPM per bp (which is ≥ 2.2 -fold over the genome average Spo11-oligo density in the four species; more specifically: 2.3-fold in *S. cerevisiae* and *S. paradoxus*, 2.2-fold in *S. mikatae* and *S. kudriavzevii*). Within these candidate regions, hotspot boundaries were defined as the

leftmost and rightmost coordinates to which reads were mapped. Hotspots separated by less than 200 bp were merged, then hotspot lists were filtered to remove calls less than 25 bp wide and/or containing fewer than 10 RPM total.

Defining matched promoter-containing intergenic regions

Lists of IGRs were compiled for *S. cerevisiae* S288C (sacCer2 assembly), *S. paradoxus* YPS138 (SGRP), *S. mikatae* IFO1815 (Scannell et al. 2011), and *S. kudriavzevii* ZP591 (Scannell et al. 2011) based on the list of genes in their respective genome annotations. Genes annotated as “dubious ORFs” in *S. cerevisiae* were excluded in all species prior to compiling IGRs. After further excluding overlapping genes/transcription units, total numbers of IGRs and the breakdown into divergent-, tandem-, and convergent-oriented flanking transcription units compiled were: *S. cerevisiae*, 5715 (1493 divergent, 2746 tandem, 1476 convergent); *S. paradoxus*, 5337 (1404 divergent, 2539 tandem, 1394 convergent); *S. mikatae*, 5637 (1458 divergent, 2726 tandem, 1453 convergent); *S. kudriavzevii*, 5549 (1436 divergent, 2678 tandem, 1435 convergent).

IGRs were assigned names by concatenating the annotated names of the flanking genes. A list (n=7138) of the names of all IGRs present in the four species was then compiled with unique IGR names as separate entries (that is, IGR names found in multiple species were entered only once). If the assigned IGR name was the same in all four species, the IGR was provisionally designated as matched. IGRs not matched this way were then manually curated. Oftentimes, apparently species-specific IGRs simply reflected mis-annotation of one flanking gene with the name of a paralog or of another member of a multi-gene family, so these were changed to match the gene name order in *S. cerevisiae* and scored as matched. Annotations of IGRs close to the chromosome ends that were different from *S. cerevisiae* were left as is, since subtelomeric region

sequences pose a challenge for whole-genome assembly due to duplication blocks and repeats (Louis 1995), and tend to be less conserved between yeast species (Brown et al. 2010). IGR names missing in a species due to indels or gaps in the genome sequence were also left as is.

After this curation, the list contained 6656 different IGR names among the four species. The following criteria were then used to define matched promoter-containing IGRs: the IGR name is present in all four species, is on the same chromosome (except if the IGR is on a segment that had undergone reciprocal translocation in *S. mikatae*), has the same flanking transcript orientation, and contains a promoter(s) (i.e., divergent or tandem orientation) in all four species. After applying the above criteria and excluding IGRs with no sequence coverage, the list was narrowed down to 3426 matched promoter-containing IGRs (Table S4 in (Lam and Keeney 2015), available at <https://www.sciencemag.org/content/350/6263/932/suppl/DC1>).

To calculate the fractional overlap of hotspots between species within the defined regions of synteny encompassing the 3426 promoter IGRs, the ~4000 hotspots from each species were queried for overlap with the coordinates of the IGRs. Approximately 70% of total hotspots in each species overlapped the 3426 promoter IGRs based on this criterion (71.7% in *S. cerevisiae* SK1, 72.0% YPS128, 71.4% UWOPS03-461.4, 74.2% *S. paradoxus*, 73.2% *S. mikatae*, 70.2% *S. kudriavzevii*). The remaining ~30% of hotspots in each species that are excluded from subsequent analyses either overlap promoter IGRs that are not in common amongst the four species based on our stringent criteria for inter-species IGR matching (e.g., 19% of *S. cerevisiae* promoter IGRs), or do not overlap IGRs.

Percent sequence divergence was calculated for the 3426 matched promoter IGRs by performing global (Needleman-Wunsch) pairwise sequence alignments (pairwiseAlignment function from Biostrings package) for each IGR sequence in all six

pairwise inter-species comparisons, taking the median percent sequence identity across the 3426 IGR sequence alignments, and subtracting from 100%. Genome assembly and annotations for *S. cerevisiae* in the inter-species comparisons were from strain S288C (SGD sacCer2).

For intra-species (SK1, YPS128, UWOPS03-461.4) sequence divergence calculations, genome assemblies and annotations for each *S. cerevisiae* strain were from SGRP. Because of incomplete genome assemblies and annotations, fewer matched promoter IGRs could be aligned in the pairwise intra-species comparisons. For example, IGR sequences with stretches of “N”s (representing unknown sequence) longer than 25% of the IGR length, instances where the IGR coordinates extend beyond the length of the chromosome-length scaffold, or instances where the IGR name did not match any of the IGRs in the strain’s genome annotation were excluded from the pairwise alignment analysis. Total numbers of IGRs aligned are 3368 in SK1 vs. UWOPS03-461.4 and SK1 vs. YPS128 (out of 3426, or 98.3% of matched promoter IGRs), and 3385 in UWOPS03-461.4 vs. YPS128 (98.8%).

Analysis of large-scale interstitial regions

To compare syntenic interstitial genomic regions between species, a common coordinate system was generated for pairwise comparisons with *S. cerevisiae* by using syntenic genes as points of reference when dividing the genome into bins. First, stretches of synteny within interstitial regions (excluding 20 kb from ends of chromosomes, and 10 kb from each side of the centromere) were defined by going through the list of genes in the *S. cerevisiae* S288C genome annotation, and querying whether there was a match with the same gene order in the species being compared (i.e., the gene was consecutive to the previous gene that had a match). If there was no match for a gene in the appropriate position in the second species, the stretch of synteny

ended, and a new one was begun. Although the gene lists were curated for mis-annotations with paralog/multi-gene family names to maximize synteny with *S. cerevisiae* (see above), many of the remaining breaks in synteny probably reflect unresolved annotation discrepancies. Other synteny breaks likely reflect species or strain-specific presence of transposable elements or copy number variants for multicopy gene families.

Bins of 20 kb were subsequently defined in *S. cerevisiae* within each stretch of synteny, starting with the left-most base pair coordinate in the stretch of synteny, and calculating the midpoint (start + 10 kb) and end coordinates of the bin. To determine the equivalent bin coordinates in the comparand species, we measured the distance from the midpoint to the start of the next gene in *S. cerevisiae*. The start coordinate of the orthologous gene in the comparand species was then used as a fiduciary mark, and the bin midpoint was defined as lying the same distance from this mark as was measured in *S. cerevisiae*. Bin boundaries were then set 10 kb to the left and right of this midpoint, and Spo11 oligos were summed within the bins. Total numbers of 20-kb bins defined genome-wide in each species' comparison with *S. cerevisiae* are: *S. paradoxus*, 491; *S. mikatae*, 448; *S. kudriavzevii*, 459. Spo11-oligo counts were then summed up within the start and end coordinates of each 20-kb bin in each species. Bin coordinates and Spo11-oligo counts are listed in Table S5 from (Lam and Keeney 2015) (<https://www.sciencemag.org/content/350/6263/932/suppl/DC1>).

Coordinates of *S. mikatae* translocations

The two reciprocal translocations in *S. mikatae* IFO1815 were originally mapped by pulsed-field gel electrophoresis (Fischer et al. 2000), and later confirmed with whole-genome sequencing (Kellis et al. 2003; Scannell et al. 2011). Based on the gene order in the *Saccharomyces sensu stricto* Resources genome browser

(www.saccharomycessensustricto.org) (Scannell et al. 2011), the translocation breakpoints can be further narrowed down to chr VI *YFR006W*-*YFR009W*, chr VII *YGR023W*-*YGR027C* and *YGR188C*-*YGR189W*, and chr XVI *YPL116W*-*YPL103C*. Thus, the left-most ~165 kb region of *S. mikatae* chr VI, which encompasses the left arm and centromere, is syntenic with the left arm and centromere of *S. cerevisiae* chr VI up to *YFR006W*, then transitions to a ~303 kb segment syntenic with *S. cerevisiae* chr VII from *YGR027C* to *YGR187C*, and switches to a ~308 kb segment syntenic with *S. cerevisiae* chr XVI from *YPL116W* to *YPL273W*. The left-most ~531 kb of *S. mikatae* chr VII is syntenic with *S. cerevisiae*, up to *YGR023W*, then transitions to a ~110 kb segment syntenic with the right arm of *S. cerevisiae* chr VI (starting with *YFR009W*). The left arm of *S. mikatae* chr XVI is syntenic with a ~193 kb segment in *S. cerevisiae* chr VII, from *YGR288W* to *YGR189W*, but the remainder of the left arm (starting from *YPL103C*), centromere, and right arm are syntenic with the *S. cerevisiae* chr XVI.

To calculate Spo11-oligo density within syntenic segments on different chromosome-length contexts in *S. cerevisiae* and *S. mikatae*, the following coordinates were used: *S. cerevisiae* 6L, chr VI 1–160,000 bp; *S. mikatae* 6L, chr VI 1–165,160 bp (sequence to the left of *YFR006W*/Smik_6.88); *S. cerevisiae* 6R, chr VI 162,000–270,161 bp; *S. mikatae* 7R, chr VII 524,000–628,517 bp (sequence to the right of *YFR009W*/Smik_7.313). Coordinates for control segments are as follow: *S. cerevisiae* 4L, chr IV 22,823–190,586 bp; *S. mikatae* 4L, chr IV 887–167,444 bp (*YKL124W*/Smik_11.115 to *YDL148C*/Smik_4.87); *S. cerevisiae* 11L, chr XI 210,093–371,390 bp; *S. mikatae* 11L, chr XI 196,553–357,829 bp (*YKL124W*/Smik_11.115 to *YKL035W*/Smik_11.212).

Table 5.1. Yeast strains (*Saccharomyces* species)

Strain number	Species	Genotype
SKY2521	<i>S. kudriavzevii</i> IFO1802	<i>MATa/α</i>
SKY2522	<i>S. mikatae</i> IFO1815	<i>MATa/α</i>
SKY2523	<i>S. paradoxus</i> YPS138	<i>MATa/α</i>
SKY4411	<i>S. paradoxus</i> YPS138	<i>MATa/α; spo11-6His-3FLAG-loxP-kanMX-loxP^{rr}</i>
SKY4416 ^a	<i>S. kudriavzevii</i> ZP591	<i>MATa/α</i>
SKY4479 ^b	<i>S. cerevisiae</i> YPS128	<i>MATa/α</i>
SKY4481 ^b	<i>S. cerevisiae</i> UWOPS03-461.4	<i>MATa/α</i>
SKY4488	<i>S. kudriavzevii</i> ZP591	<i>MATa/α; spo11-6His-3FLAG-loxP-kanMX-loxP^{rr}</i>
SKY4490	<i>S. mikatae</i> IFO1815	<i>MATa/α; spo11-6His-3FLAG-loxP-kanMX-loxP^{rr}</i>
SKY4632	<i>S. cerevisiae</i> YPS128	<i>MATa/α; spo11-6His-3FLAG-loxP-kanMX-loxP^{rr}; T(III;XIII)</i>
SKY4633	<i>S. cerevisiae</i> YPS128	<i>MATa/α; spo11-6His-3FLAG-loxP-kanMX-loxP^{rr}</i>
SKY4664	<i>S. cerevisiae</i> UWOPS03-461.4	<i>MATa/α; spo11-6His-3FLAG-loxP-kanMX-loxP^{rr}</i>
SKY4812	<i>S. cerevisiae</i> YPS128	<i>MATa/α; dmc1Δ::HphMX^{rr}</i>
SKY4820	<i>S. cerevisiae</i> YPS128	<i>MATa/α; spo11-6His-3FLAG-loxP-kanMX-loxP^{rr}; dmc1Δ::HphMX^{rr}; T(III;XIII)</i>
SKY4821	<i>S. cerevisiae</i> UWOPS03-461.4	<i>MATa/α; spo11-6His-3FLAG-loxP-kanMX-loxP^{rr}; dmc1Δ::HphMX^{rr}</i>
SKY4822	<i>S. cerevisiae</i> UWOPS03-461.4	<i>MATa/α; dmc1Δ::HphMX^{rr}</i>
SKY4823	<i>S. paradoxus</i> YPS138	<i>MATa/α; spo11-6His-3FLAG-loxP-kanMX-loxP^{rr}; dmc1Δ::HphMX^{rr}</i>
SKY4824	<i>S. paradoxus</i> YPS138	<i>MATa/α; dmc1Δ::HphMX^{rr}</i>
SKY4827	<i>S. mikatae</i> IFO1815	<i>MATa/α; spo11-6His-3FLAG-loxP-kanMX-loxP^{rr}; dmc1Δ::HphMX^{rr}</i>
SKY4828	<i>S. kudriavzevii</i> ZP591	<i>MATa/α; spo11-6His-3FLAG-loxP-kanMX-loxP^{rr}; dmc1Δ::HphMX^{rr}</i>
SKY4830	<i>S. kudriavzevii</i> ZP591	<i>MATa/α; dmc1Δ::HphMX^{rr}</i>
SKY4835	<i>S. mikatae</i> IFO1815	<i>MATa/α; dmc1Δ::HphMX^{rr}</i>
SKY4978	<i>S. cerevisiae</i> YPS128	<i>MATa/α; spo11-6His-3FLAG-loxP-kanMX-loxP^{rr}; dmc1Δ::HphMX^{rr}</i>

^a FM1158 from Chris Todd Hittinger

^b From Ed Louis

Table 5.2. Yeast strains (*red1*, *hop1*, *mek1*)

Strain number		Genotype
SKY4365x SKY4366	<i>rad50S</i>	<i>MATa/MATα</i> , <i>ho::LYS2</i> ^{"/} , <i>lys2</i> ^{"/} , <i>ura3</i> ^{"/} , <i>leu2</i> ^{"/} , <i>his3::hisG</i> ^{"/} , <i>rad50-K181::URA3</i> ^{"/}
SKY4337	<i>red1Δ SPO11-FLAG</i>	<i>MATa/MATα</i> , <i>ho::LYS2</i> ^{"/} , <i>lys2</i> ^{"/} , <i>ura3</i> ^{"/} , <i>leu2</i> ^{"/} , <i>arg4-bgl</i> ^{"/} , <i>nuc1Δ::LEU2</i> ^{"/} , <i>SPO11-6His-3FLAG-loxP-kanMX-loxP</i> ^{"/} , <i>red1Δ::HphMX</i> ^{"/}
SKY4347	<i>mek1Δ SPO11-FLAG</i>	<i>MATa/MATα</i> , <i>ho::LYS2</i> ^{"/} , <i>lys2</i> ^{"/} , <i>ura3</i> ^{"/} , <i>leu2</i> ^{"/} , <i>arg4-bgl</i> ^{"/} , <i>nuc1Δ::LEU2</i> ^{"/} , <i>SPO11-6His-3FLAG-loxP-kanMX-loxP</i> ^{"/} , <i>mek1Δ::HphMX</i> ^{"/}
SKY4363	<i>hop1Δ SPO11-FLAG</i>	<i>MATa/MATα</i> , <i>ho::LYS2</i> ^{"/} , <i>lys2</i> ^{"/} , <i>ura3</i> ^{"/} , <i>leu2Δ</i> ^{"/} , <i>arg4-bgl</i> ^{"/} , <i>nuc1Δ::LEU2</i> ^{"/} , <i>SPO11-6His-3FLAG-loxP-kanMX-loxP</i> ^{"/} , <i>hop1Δ::HphMX</i> ^{"/}
SKY4371	<i>red1Δ rad50S</i>	<i>MATa/MATα</i> , <i>ho::LYS2</i> ^{"/} , <i>lys2</i> ^{"/} , <i>ura3</i> ^{"/} , <i>leu2</i> ^{"/} , <i>red1Δ::HphMX</i> ^{"/} , <i>rad50-K181::URA3</i> ^{"/}
SKY4374	<i>mek1Δ rad50S</i>	<i>MATa/MATα</i> , <i>ho::LYS2</i> ^{"/} , <i>lys2</i> ^{"/} , <i>ura3</i> ^{"/} , <i>leu2</i> ^{"/} , <i>mek1Δ::HphMX</i> ^{"/} , <i>rad50-K181::URA3</i> ^{"/}
SKY4378	<i>mek1Δ rad50S SPO11-FLAG</i>	<i>MATa/MATα</i> , <i>ho::LYS2</i> ^{"/} , <i>lys2</i> ^{"/} , <i>ura3</i> ^{"/} , <i>leu2</i> ^{"/} , <i>arg4-bgl</i> ^{"/} , <i>nuc1Δ::LEU2</i> ^{"/} , <i>SPO11-6His-3FLAG-loxP-kanMX-loxP</i> ^{"/} , <i>mek1Δ::HphMX</i> ^{"/} , <i>rad50-K181::URA3</i> ^{"/}
SKY4381	<i>hop1Δ rad50S SPO11-FLAG</i>	<i>MATa/MATα</i> , <i>ho::LYS2</i> ^{"/} , <i>lys2</i> ^{"/} , <i>ura3</i> ^{"/} , <i>leu2</i> ^{"/} , <i>arg4-bgl</i> ^{"/} , <i>nuc1Δ::LEU2</i> ^{"/} , <i>SPO11-6His-3FLAG-loxP-kanMX-loxP</i> ^{"/} , <i>hop1Δ::HphMX</i> ^{"/} , <i>rad50-K181::URA3</i> ^{"/}
SKY4383	<i>hop1Δ rad50S</i>	<i>MATa/MATα</i> , <i>ho::LYS2</i> ^{"/} , <i>lys2</i> ^{"/} , <i>ura3</i> ^{"/} , <i>leu2</i> ^{"/} , <i>arg4-bgl</i> ^{"/} , <i>nuc1Δ::LEU2</i> ^{"/} , <i>hop1Δ::HphMX</i> ^{"/} , <i>rad50-K181::URA3</i> ^{"/}
SKY4394	<i>red1Δ rad50S SPO11-FLAG</i>	<i>MATa/MATα</i> , <i>ho::LYS2</i> ^{"/} , <i>lys2</i> ^{"/} , <i>ura3</i> ^{"/} , <i>leu2</i> ^{"/} , <i>arg4-bgl</i> ^{"/} , <i>nuc1Δ::LEU2</i> ^{"/} , <i>SPO11-6His-3FLAG-loxP-kanMX-loxP</i> ^{"/} , <i>red1Δ::HphMX</i> ^{"/} , <i>rad50-K181::URA3</i> ^{"/}
SKY4399	<i>red1Δ rad50S SPO11-PrA</i>	<i>MATa/MATα</i> , <i>ho::LYS2</i> ^{"/} , <i>lys2</i> ^{"/} , <i>ura3</i> ^{"/} , <i>leu2::hisG</i> ^{"/} , <i>his3::hisG</i> ^{"/} , <i>SPO11-PrA::HIS5</i> ^{"/} , <i>red1Δ::HphMX</i> ^{"/} , <i>rad50-K181::URA3</i> ^{"/}
SKY4403	<i>mek1Δ rad50S SPO11-PrA</i>	<i>MATa/MATα</i> , <i>ho::LYS2</i> ^{"/} , <i>lys2</i> ^{"/} , <i>ura3</i> ^{"/} , <i>leu2::hisG</i> ^{"/} , <i>his3::hisG</i> ^{"/} , <i>SPO11-PrA::HIS5</i> ^{"/} , <i>mek1Δ::HphMX</i> ^{"/} , <i>rad50-K181::URA3</i> ^{"/}
SKY4408	<i>hop1Δ rad50S SPO11-PrA</i>	<i>MATa/MATα</i> , <i>ho::LYS2</i> ^{"/} , <i>lys2</i> ^{"/} , <i>ura3</i> ^{"/} , <i>leu2</i> ^{"/} , <i>his3::hisG</i> ^{"/} , <i>SPO11-PrA::HIS5</i> ^{"/} , <i>hop1Δ::HphMX</i> ^{"/} , <i>rad50-K181::URA3</i> ^{"/}

Nucleosome occupancy (MNase-seq)

Nucleosome mapping in the *Saccharomyces* species was performed as described for SK1 meiotic nucleosome maps in (Pan et al. 2011). Synchronous meiotic cultures were set up for each species and/or strain background as described above, except volumes were scaled-down to 200 mL for pre-sporulation, and approximately 110 mL for sporulation, at $OD_{600} = 1.9$. 100 mL samples were harvested at 4 h (*S. paradoxus*, *S. mikatae*, and *S. cerevisiae* YPS128), 6 h (*S. cerevisiae* UWOPS03-461.4), or 9 h (*S. kudriavzevii*) after transfer to sporulation media, and cross-linked with 1% formaldehyde for 15 min with rocking. Chromatin extraction, MNase digestion, DNA purification, and sequencing library construction were performed as described (Pan et al. 2011). Amounts of MNase used to generate mononucleosome-sized DNA were 5 U and 10 U (*S. mikatae*); 10 U (*S. cerevisiae* UWOPS03-461.4); 20 U (*S. kudriavzevii*); 20 U and 40 U (*S. cerevisiae* YPS128, *S. paradoxus*). Library preparation and Illumina sequencing (2 x 50 bp paired-end reads) were performed by the MSKCC Integrated Genomics Operation. Mapping of sequencing reads was performed by N. Socci at the MSKCC Bioinformatics Core.

S. cerevisiae YPS128 and UWOPS03-461.4. Illumina reads were mapped to the sacCer2 genome assembly, *S. paradoxus* reads were mapped to *S. paradoxus* YPS138 genome assembly from SGRP or CBS432 type strain genome assembly from (Scannell et al. 2011), and *S. mikatae* and *S. kudriavzevii* were mapped to their strain genome assemblies from (Scannell et al. 2011). The reads were first clipped to remove any Illumina adapter sequences present and reads shorter than 35 bp were discarded (both ends of paired end reads were discarded). The clipped reads were then mapped to the proper target genome using BWA MEM (default options). The output SAM files were coordinate sorted and read groups added and merged into single sample BAM files using the PICARD toolkit. The output BAM files were then post-processed with a series

of custom scripts to filter for uniquely mapping and properly paired reads. Proper pairing was defined as reads where the chromosome of each pair is the same, insert size was less than 250 bp, and strands were in opposite/inward orientation ($==> <==$). This was done using bedtools to convert the BAM files to Paired BED files (bedpe) and then filtering. The filtered read pairs were used to compute genome-wide coverage using the bedtools genomecov program.

Raw and processed reads have been deposited in the GEO database under accession number GSE71929. This accession also contains text files containing the calculated raw occupancy score at each base position in the genome.

Analysis of human hotspots

For the human data from (Pratto et al. 2014), hotspot strength comparison was performed with a subset of 37,345 hotspots present in at least one of the three individuals (AA_1 , AA_2 , AB_1). Hotspots with strength of 0 were excluded, since these might be arising from technical reasons instead of representing actual variation in hotspot strength. This exclusion means that the extent of complete hotspot loss in individuals will be underestimated. The DNA recognition preference of the *PRDM9* B allele is not detectably different from the DNA recognition preference of the *PRDM9* A allele, and therefore hotspots found in these three individuals are considered as defined by the same *PRDM9* allele (Baudat et al. 2010; Pratto et al. 2014).

Estimating species divergence in terms of sexual generations

Since yeasts more commonly undergo asexual reproduction and undergo sexual reproduction less frequently (~1 sexual cycle every 1000 mitotic divisions, estimates by (Tsai et al. 2008) based on *S. paradoxus* population studies), perhaps a more equitable comparison of evolutionary divergence between species that undergo obligate sexual

reproduction (e.g., human, chimp, mouse) and species that undergo facultative sexual reproduction (e.g., yeasts), is to compare divergence in terms of sexual generations by dividing millions of years of evolution by sexual cycle length, especially when considering changes that are incorporated during sexual cycles. The following are the values used in our estimation.

Human vs. chimp comparison:

5 My divergence

Sexual cycle length 20 years (human), 10 years (chimp)

$5,000,000 \text{ years} / 20 \text{ years} = 250,000 \text{ generations (human)}$ since divergence with last common ancestor shared with chimps

$5,000,000 \text{ years} / 10 \text{ years} = 500,000 \text{ generations (chimp)}$ since divergence with last common ancestor shared with humans

Human vs. mouse comparison:

75 My divergence

Sexual cycle length 20 years (human), 2 months (0.17 years) (mouse)

$75,000,000 \text{ years} / 20 \text{ years} = 3,750,000 \text{ generations (human)}$ since divergence with last common ancestor shared with mice

$75,000,000 \text{ years} / 0.17 \text{ years} = 44,000,000 \text{ generations (mouse)}$ since divergence with last common ancestor shared with humans

S. cerevisiae vs. *S. kudriavzevii* comparison:

15 My divergence

1 sexual cycle every 1000 mitotic divisions

Estimated length of mitotic divisions in wild habitat: 6 h (Mitotic divisions in the lab environment are approximately every 90 minutes, under controlled, optimal temperature and nutrient availability. In the natural environment, we envision fluctuation in

temperature and climate, and nutrient availability to result in longer division times, or even periods of non-dividing state (Liti 2015).)

Sexual cycle length:

1000 mitotic divisions x 6 h = 6000 h (250 days, or 0.68 years)

1 sexual cycle every 0.68 years

15,000,000 years/0.68 years = 22,000,000 sexual generations divergence between *S. cerevisiae* and *S. kudriavzevii*

Inbreeding predominates over outcrossing in wild populations of yeast, either via mating of spores from the same tetrad (automixis), or autodiploidization (mating type switching followed by mating of cells from the same haploid spore clone), with frequencies estimated at 0.94 and 0.05, respectively (Tsai et al. 2008). The estimated frequency of outcrossing is 0.01 (Johnson et al. 2004; Tsai et al. 2008). Automixis yields a complex genomic mix of heterozygosity and homozygosity dependent on centromere linkage, mating type locus linkage to its centromere, and degree of heterozygosity in the parental cell that underwent meiosis. Autodiploidization yields an essentially entirely homozygous diploid (except at the mating type locus). Because the effects of biased gene conversion are only relevant at heterozygous loci, a conservative calculation of sexual divergence in *S. cerevisiae* and *S. kudriavzevii* would be to consider only the frequency of outcrossing in our calculations:

0.001 (sexual cycles per mitotic division) x 0.01 (outcrosses per sexual cycle) = 1

outcrossed sexual cycle every 100,000 mitotic divisions

100,000 mitotic divisions x 6 h = 600,000 h (25,000 days, or 1 outcrossed meiosis every 68.5 years)

15,000,000 years/68.5 years = 220,000 sexual generations divergence between *S. cerevisiae* and *S. kudriavzevii*

If we instead use the estimate for *S. cerevisiae* of 1 outcrossing event every 50,000 mitotic divisions (Ruderfer et al. 2006), the number of sexual generations since the last common ancestor of *S. cerevisiae* and *S. kudriavzevii* is 440,000. These numbers are the same order of magnitude as the divergence between humans and chimps (250,000 human generations, 500,000 chimp generations). Therefore, yeast species in this study have undergone ample cycles of meiosis in a heterozygous state to detect erosion of hotspot alleles if meiotic drive from biased gene conversion is not opposed by other selective constraints.

APPENDIX: INVESTIGATING THE ROLE OF REC104 PHOSPHORYLATION

Summary

In budding yeast, at least nine other proteins besides Spo11 are required for DSB formation, including Rec104, but their precise roles are not clear. Rec104 forms a functional unit with Rec102 and interacts closely with Spo11. Rec104 is phosphorylated during meiosis independent of DSBs. I set out to investigate the biological significance of Rec104 phosphorylation in an attempt to dissect its contribution to meiotic recombination. I uncovered meiotic phenotypes for two sets of *rec104* mutant alleles. One set of *rec104* alleles has alanine substitutions in serines/threonines within RxxS/T motifs, which match consensus motifs for several yeast kinases. The other set has alanine substitutions in serines/threonines within putative target sites for Cdc7 phosphorylation. The available data support the hypothesis that Rec104 phosphorylation is important for its role in DSB formation.

Introduction

DSB proteins in *S. cerevisiae*

Meiotic recombination is initiated by the formation of DNA DSBs (160 DSBs/yeast cell (Pan et al. 2011)) made by Spo11 (Bergerat et al. 1997; Keeney et al. 1997) (**Fig. 1.2**). In budding yeast, at least nine other proteins are required for DSB formation (Rec102, Rec104, Rec114, Mei4, Mer2, Mre11, Rad50, Xrs2, and Ski8). Null mutants in any of these genes fail to form DSBs, fail to undergo recombination, and exhibit severely reduced spore viability, presumably due to chromosome missegregation (Keeney 2001; Keeney 2007). The DSB proteins assemble into three distinct subcomplexes: Spo11-Ski8-Rec102-Rec104 (Salem et al. 1999; Kee and Keeney 2002;

Jiao et al. 2003; Kee et al. 2004; Maleki et al. 2007), Mer2-Rec114-Mei4 (Arora et al. 2004; Li et al. 2006; Maleki et al. 2007; Sasanuma et al. 2008), and Mre11-Rad50-Xrs2 (Borde 2007) (**Fig. 1.3A**). However, it is not well understood how these proteins contribute to DSB formation. Possible functions include recruitment of Spo11 to specific sites in the genome, activating Spo11 function, and/or coordinating DSB formation with higher-order chromosome structure (Keeney 2007). Recent investigations indicate a prominent role of some DSB proteins in promoting Spo11-mediated DSB formation in the context of TLACs through interactions between Mer2, Spp1, and H3K4me3 (Acquaviva et al. 2012; Sommermeyer et al. 2013), as well as coordinating DSB formation with replication timing (Murakami and Keeney 2014) (Discussed in **Chapter 1**).

Characteristics of Rec104

REC104 was identified in a selection for mutants defective in the early steps of meiotic recombination (Malone et al. 1991). Diploid *rec104* strains show no meiotic recombination, reduced sporulation, and spore inviability (Malone et al. 1991; Galbraith and Malone 1992). Rec104 forms a functional complex with Rec102—they are mutually dependent on each other (also partially dependent on Spo11 and Ski8) for nuclear localization and chromatin association (Salem et al. 1999; Jiao et al. 2003; Arora et al. 2004; Kee et al. 2004; Maleki et al. 2007). Rec104, Rec102, and Spo11 bind to chromatin as a preformed complex (Prieler et al. 2005). Rec104 is required for Spo11 chromatin binding (Sasanuma et al. 2007) and association with DSB hotspots (Jiao et al. 2003; Maleki et al. 2007). Besides interacting with Rec102, Rec104 also shows two-hybrid interaction with Rec114, Spo11, Ski8, and Mei4 (**Fig. 1.3**). Rec104 interactions with the latter three likely depend on a meiosis-specific post-translational modification or accessory protein (Arora et al. 2004; Maleki et al. 2007).

Rec104 is phosphorylated in a DSB-independent manner during meiosis (Kee et al. 2004). Normal Rec104 phosphorylation is dependent on Rec102, since unphosphorylated Rec104 remains abundant in the *rec102* strain, whereas phosphorylation levels are not detectably altered in the absence of other DSB proteins. Nevertheless, the phosphorylation site(s), the responsible kinase(s), and whether phosphorylation is required for Rec104 function are still unknown.

Possible regulatory function of Rec104 phosphorylation in meiotic recombination

Formation of meiotic DSBs must be tightly controlled and coordinated with processing and repair to maintain genome integrity, yet the mechanism for the spatial and temporal regulation is not completely understood. Rec104 phosphorylation could play a role in regulating DSB formation since it is dynamically phosphorylated during meiosis, phosphorylation depends on the presence of at least one other DSB protein, and phosphorylation coincides with the timing of break formation in meiotic cultures, raising the possibility that it is a pre-requisite for DSB formation. These observations hint at a role for Rec104 phosphorylation in meiosis, although the possibility that phosphorylation regulates aspects of Rec104 independent of its role in recombination cannot be excluded.

Mer2 and Rec114 are other DSB proteins that undergo phosphorylation (Henderson et al. 2006; Li et al. 2006; Sasanuma et al. 2008; Wan et al. 2008). Phosphorylation of Mer2 by cell cycle regulatory factors Cdc7 and CDK-S is required for DSB formation (Henderson et al. 2006; Sasanuma et al. 2008; Wan et al. 2008). This Mer2 phosphorylation regulates Mer2 interaction with other DSB proteins, thereby promoting their recruitment to chromatin (Henderson et al. 2006; Sasanuma et al. 2008; Wan et al. 2008; Murakami and Keeney 2014). Regulation of Mer2 exemplifies how phosphorylation of DSB proteins may contribute to the regulation of DSB formation.

Data suggest that CDK-S and Cdc7 have other targets that are essential for DSB formation (Wan et al. 2008), but it is not yet known how these kinases influence DSB formation independent of Mer2. Rec104 is a possible substrate for CDK-S or Cdc7 because it is phosphorylated, it is necessary for DSB formation, and its primary sequence contains consensus target sites for both kinases (S-P for CDK-S (Montagnoli et al. 2006); S/T-D/E for Cdc7 (Cho et al. 2006)) (**Fig. A.1**). Rec104 also contains four RxxS/T motifs, which are common consensus target sites of calmodulin-dependent kinases (CAMK) and AGC (PKA, PKC, PKG) kinase families (e.g., Akt, RSK) (Pearson and Kemp 1991; Jacinto and Lorberg 2008; Yoshizaki and Okuda 2014). In fact, 19% of the Rec104 amino acid sequence consists of potential Ser or Thr phosphoacceptor sites (35 out of 182 residues).

The goal of this project was to characterize the role of Rec104 phosphorylation and gain further insights into the regulatory mechanism of meiotic DSB formation. I generated two sets of *rec104* mutants to try to identify phosphorylation-defective alleles; one set has mutated RxxS/T sites (S69, S101, S150, S172, denoted as *rec104* [R] alleles), and the other has mutated Cdc7 consensus target sites S/T-D/E (T24, S111, S141, S160, denoted as *rec104* [C] alleles). Initial studies were done with myc-tagged Rec104, but subsequent analysis demonstrated synergistic defects between the epitope tag and the point mutations. The phosphorylation status of the mutant protein and the meiotic phenotypes (spore viability, DSB formation, and protein cellular localization) are described below.

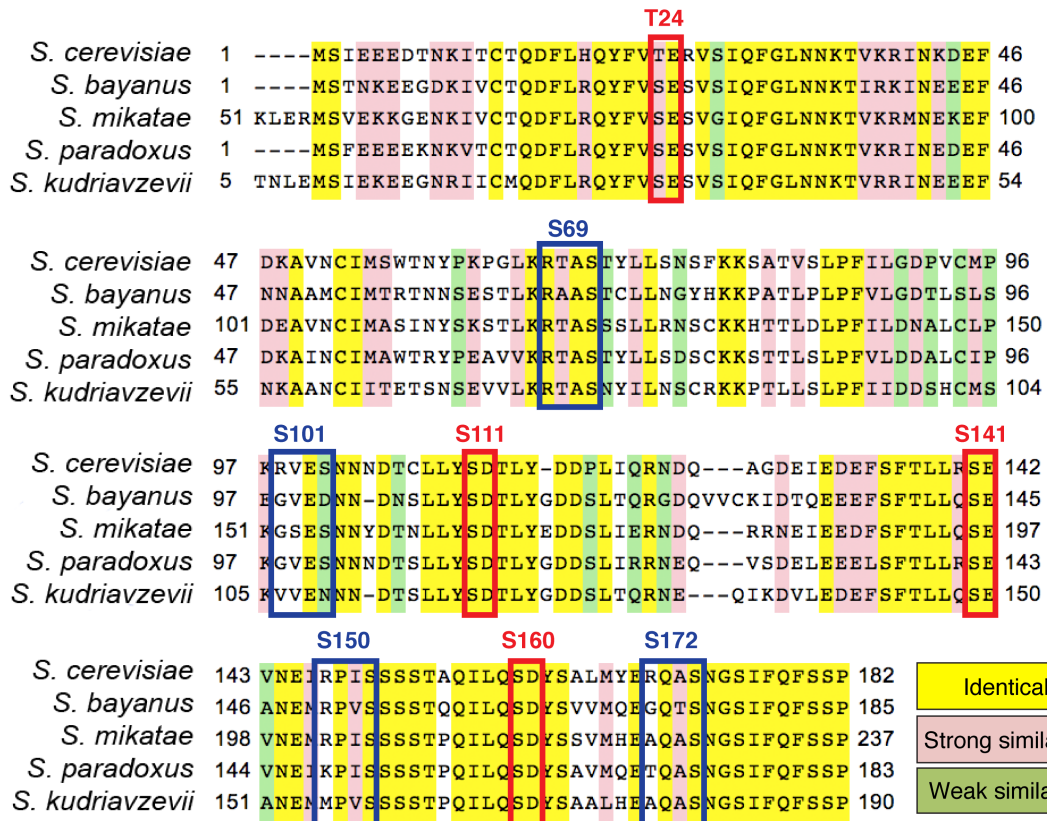


Figure A.1. Rec104 amino acid sequence alignment in *Saccharomyces* species. Source: Yeast Genome Database. Color shading indicates sequence identity: yellow, identical; pink, strong similarity; green, weak similarity. Motifs for [R] alleles are indicated in blue, and motifs for [C] alleles are indicated in red.

Results

The *rec104-4A[R]* allele causes defects in phosphorylation, subcellular localization, and DSB formation

The *rec104-4A[R]* allele was generated by alanine substitution of 4 serines within RxxS/T motifs (**Fig. A.2A**). The myc-tagged version exhibits ~10% spore viability (**Fig. A.2B**). I performed western blot analysis to examine the phosphorylation status of the protein. Rec104 is expressed only during meiosis; in a typical meiotic time-course, steady-state Rec104 protein levels begin to be detected after ~1 h in sporulation media, peak at ~4 h, and gradually taper off (Kee et al. 2004). With standard SDS-PAGE, Rec104 can be detected as a doublet at early meiotic time-points (e.g., 2 h), but the slower-migrating species representing phosphorylated Rec104 predominates thereafter (Kee et al. 2004) (**Fig. A.2C**). On the other hand, myc-Rec104 resolved with phosphate-affinity Phos-tag SDS-PAGE (Kinoshita et al. 2006) followed by anti-myc western blot exhibited a distinct and reproducible mobility shift pattern, with multiple slower-migrating bands presumably representing different phosphorylated species of Rec104 (**Fig. A.2C**, Phos-tag). Most myc-*rec104-4A[R]* protein migrated at the positions expected for unphosphorylated protein on both Phos-tag and conventional SDS-PAGE (**Fig. A.2C**). Moreover, unlike wild type, the mutant protein underwent little or no mobility shift upon phosphatase treatment (**Fig. A.2D**). Together, these results suggest that the protein is already mostly unphosphorylated. A mutant with only two out of the four sites mutated (*myc-rec104-S150A, S172A*) exhibited an intermediate phenotype, with 34% spore viability and partial phosphorylation (data not shown).

Rec104 localizes to the nucleus, but is dispersed throughout the cell in *rec102Δ*, and localization is also impaired in *spo11Δ* and *ski8Δ* mutants (Kee et al. 2004). The myc-*rec104-4A[R]* protein showed mixed nuclear/cytoplasmic localization (**Fig. A.2E**), reminiscent of Rec104 localization in *spo11Δ* and *ski8Δ*.

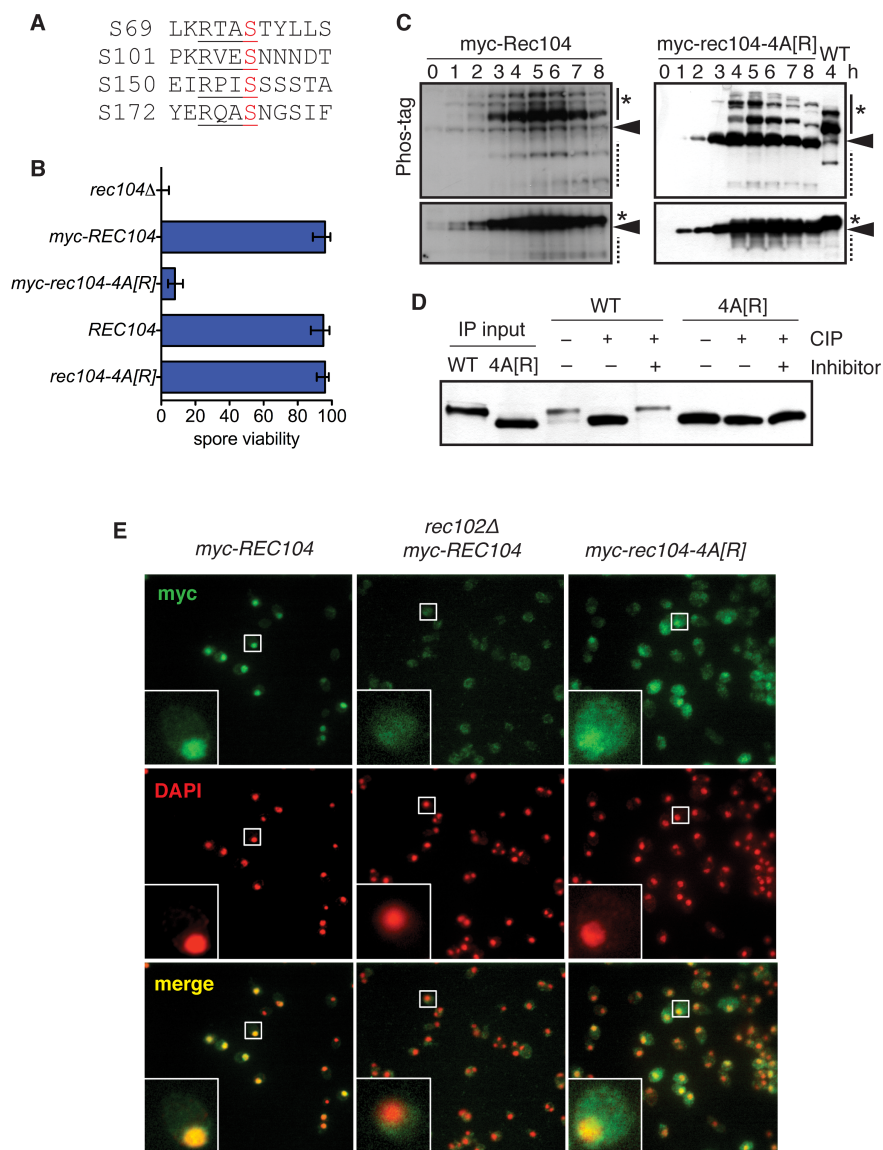


Figure A.2. Spore viability, phosphorylation, and nuclear localization phenotypes of the *rec104* RxxS/T mutant alleles. (A) Residues flanking the four target serines (red) within RxxS/T motifs (underlined) in Rec104. These four serines are mutated to alanines in the *rec104-4A[R]* allele. (B) Spore viability of myc-tagged or untagged versions of the *rec104-4A[R]* alleles ($n \geq 19$ tetrads). Error bars represent 95% CI of a proportion. (C) Western blot of myc-Rec104 or myc-*rec104-4A[R]* meiotic time-course using Phos-tag SDS-PAGE (top) or normal SDS-PAGE (bottom). Arrowhead, unphosphorylated Rec104; asterisk, phosphorylated Rec104; dotted line, protein degradation product. (D) Immunoprecipitated myc-Rec104 (WT) or myc-*rec104-4A[R]* (4A[R]) were treated with calf intestinal phosphatase (CIP) with or without phosphatase inhibitors. (E) Whole-cell immunostaining of the indicated strains to assess nuclear localization. Cells were fixed at the 4 h time point in meiosis.

To investigate whether the *myc-rec104-4A*[R] mutant is capable of generating meiotic DSBs, I detected DSBs on chromosome III by Southern blot. The *myc-rec104-4A*[R] allele caused severely reduced steady-state DSB levels (~10-fold reduction from peak wild-type level) (**Fig. A.3A**), consistent with the protein localization and the severe spore viability defects.

Analyses with the untagged *rec104-4A*[R] allele indicated that most of the DSB and spore viability defects are due to the combination with the myc epitope tag. Without the tag, peak steady-state DSB levels were reduced ~2-fold (instead of ~10-fold) (**Fig. A.3A**), and spore viability was indistinguishable from wild type (**Fig. A.2B**). The 2-fold reduction in steady-state DSB levels was also detected on chromosome IX, indicating that this phenotype is not specific to chromosome III (**Fig. A.3B**). The untagged phosphomimetic mutant *rec104-4D*[R] exhibited wild type steady-state DSB levels (data not shown). All mutants exhibited similar kinetics of meiotic division as wild type (**Fig. A.3C**).

In the *sae2* mutant, Spo11 is not released from the DSB ends, resulting in a block to DSB repair (Keeney and Kleckner 1995; McKee and Kleckner 1997; Prinz et al. 1997), thereby allowing quantification of absolute levels of DSBs formed. DSBs were reduced 3.5-fold in the *rec104-4A*[R] mutant when measured in the *sae2* mutant background (**Fig. A.3D**). Note that DSBs were not measured in an untagged *REC104 sae2* strain, but the levels detected in *myc-REC104 sae2* are similar to those reported in the literature, e.g., (Murakami et al. 2003).

The *myc-rec104-3A*[C] allele causes delayed DSB formation

The *rec104*-[C] allele was generated by alanine substitution of serines/threonines within consensus target sites for Cdc7 (**Fig. A.4A**). *Myc-rec104-4A*[C] exhibited $\leq 10\%$ spore viability, whereas mutating only three of the four sites (T24A, S111A, S160A)

resulted in normal spore viability (**Fig. A.4B**). Myc-rec104-3A[C] and 4A[C] proteins were still mostly phosphorylated, although the apparently unphosphorylated species appeared to become more prominent at later time-points (>6 h) in the 3A[C] mutant (**Fig. A.4C**). Furthermore, both mutant proteins were capable of localizing properly to the nucleus (**Fig. A.4D**, compare with myc-Rec104 in **Fig. A.2E**). Consistent with the spore viability defect, steady-state DSB levels were reduced >10-fold in the *myc-rec104-4A[C]* mutant when measured on chromosomes III and IX (**Fig. A.5A, B**). DSB levels were also severely reduced in a *sae2* background (8-fold on chromosome III; 40-fold on chromosome IX) (**Fig. A.5D**).

Steady-state DSB levels in the *myc-rec104-3A[C]* mutant were only moderately reduced (~1.5-fold) (**Fig. A.5A, B**), with a similar reduction in DSB levels (2-fold) on chromosome III in the *sae2* background (**Fig. A.5D**). This modest reduction in DSBs is consistent with normal spore viability (Martini et al. 2006). Interestingly, a reproducible 1 h delay in peak steady-state DSB levels was detected in this mutant, which is more discernable when expressing DSB frequency as percent of maximum signal in the time-course (**Fig. A.5A, B**). Despite the delay in DSB formation, meiotic divisions in *myc-rec104-3A[C]* occurred with normal kinetics (**Fig. A.5C**). To rule out the possibility that the DSB delay is due to culture-to-culture variability, Orc6 phosphorylation was used as a marker for replication timing (Weinreich et al. 1999) within the same culture. Orc6 is a subunit of the Origin Recognition Complex (ORC) required to initiate replication, and is phosphorylated at the G1-S transition (Liang and Stillman 1997). Orc6 phosphorylation was detected after 2 h in sporulation media in both wild type and *myc-rec104-3A[C]* mutant cultures (**Fig. A.5E**), demonstrating that the delay in appearance of DSBs in the mutant is not due to delayed replication timing in that culture.

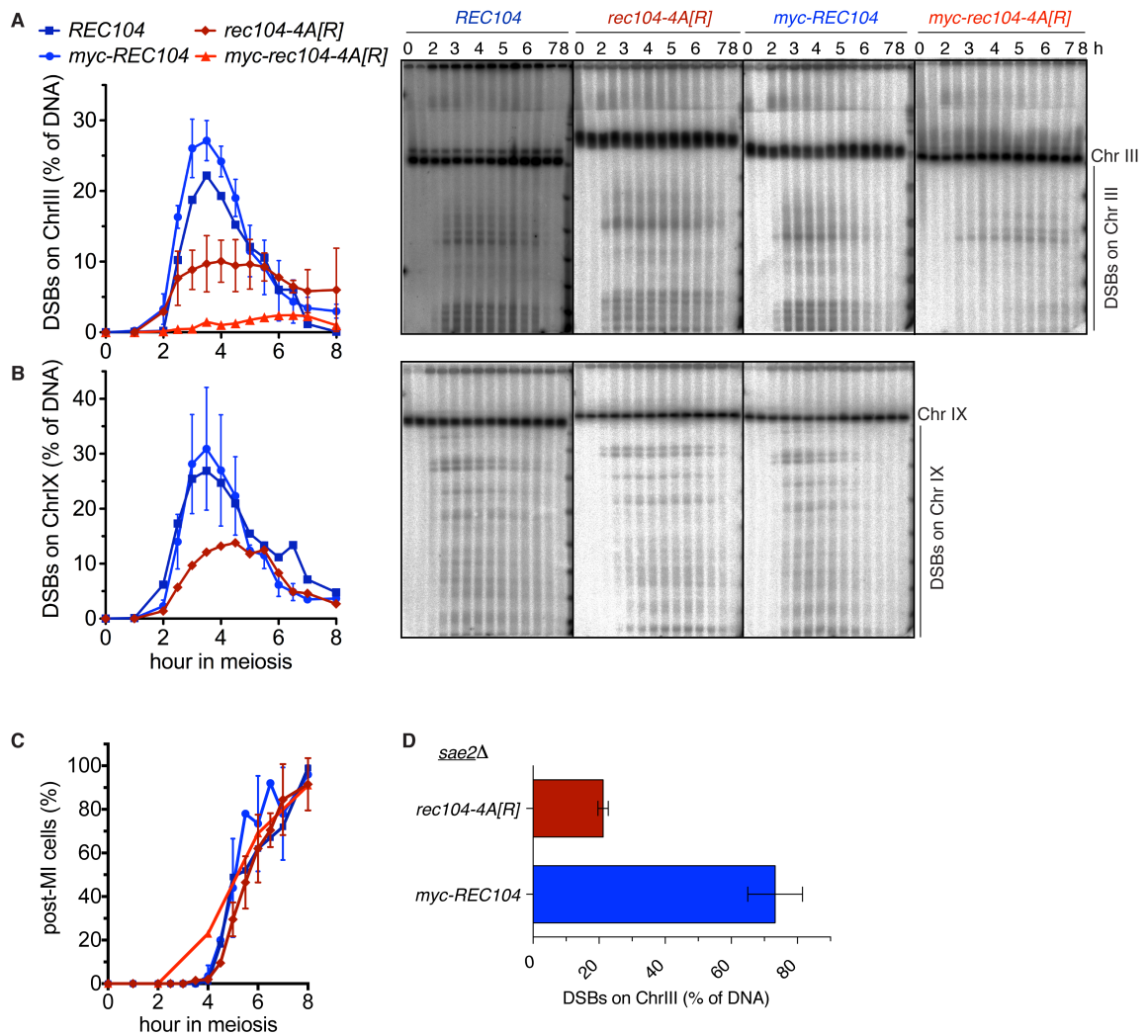


Figure A.3. The *rec104-4A[R]* alleles exhibit reduced levels of DSBs. (A, B) Meiotic time course of DSB signal from chromosome III (A) or chromosome IX (B) in the myc-tagged or untagged *rec104-4A[R]* mutant. Representative Southern blots used to detect DSBs are shown on the right, and quantifications are shown on the left. For *myc-REC104*, and *rec104-4A[R]* DSBs on chromosome III, values are the mean \pm s.d. from two independent experiments. (C) Fraction of cells that have completed meiosis I at the indicated time points taken from the same meiotic cultures as in (A) and (B), scored as cells with ≥ 2 DAPI-stained nuclei. (D) Comparison of DSBs on chromosome III in the *sae2Δ* mutant (8 h time point). Values are the mean \pm s.d. from three independent cultures.

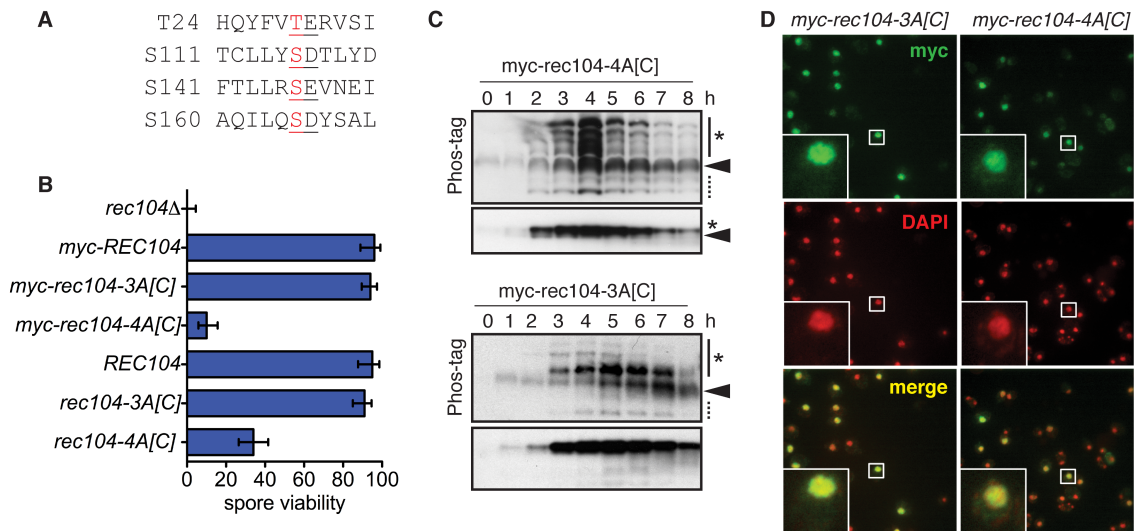


Figure A.4. Spore viability, phosphorylation, and subcellular localization phenotypes of the *rec104* Cdc7 consensus site mutation alleles. (A) Residues flanking the four target serines (red) within S/T-D/E motifs (underlined) in Rec104. These four serines were mutated to alanines in the *rec104-4A[C]* allele, and T24, S111, S160 were mutated to alanines in the *rec104-3A[C]* allele. (B) Spore viability of myc-tagged or untagged *rec104*-[C] alleles ($n \geq 19$ tetrads). Error bars represent 95% CI of a proportion. (C) Western blot of meiotic time courses of the indicated mutants. Markings are as described in Fig. A.2C. (D) Whole-cell immunostaining to assess nuclear localization. Cells were fixed at the 4 h time point in meiosis.

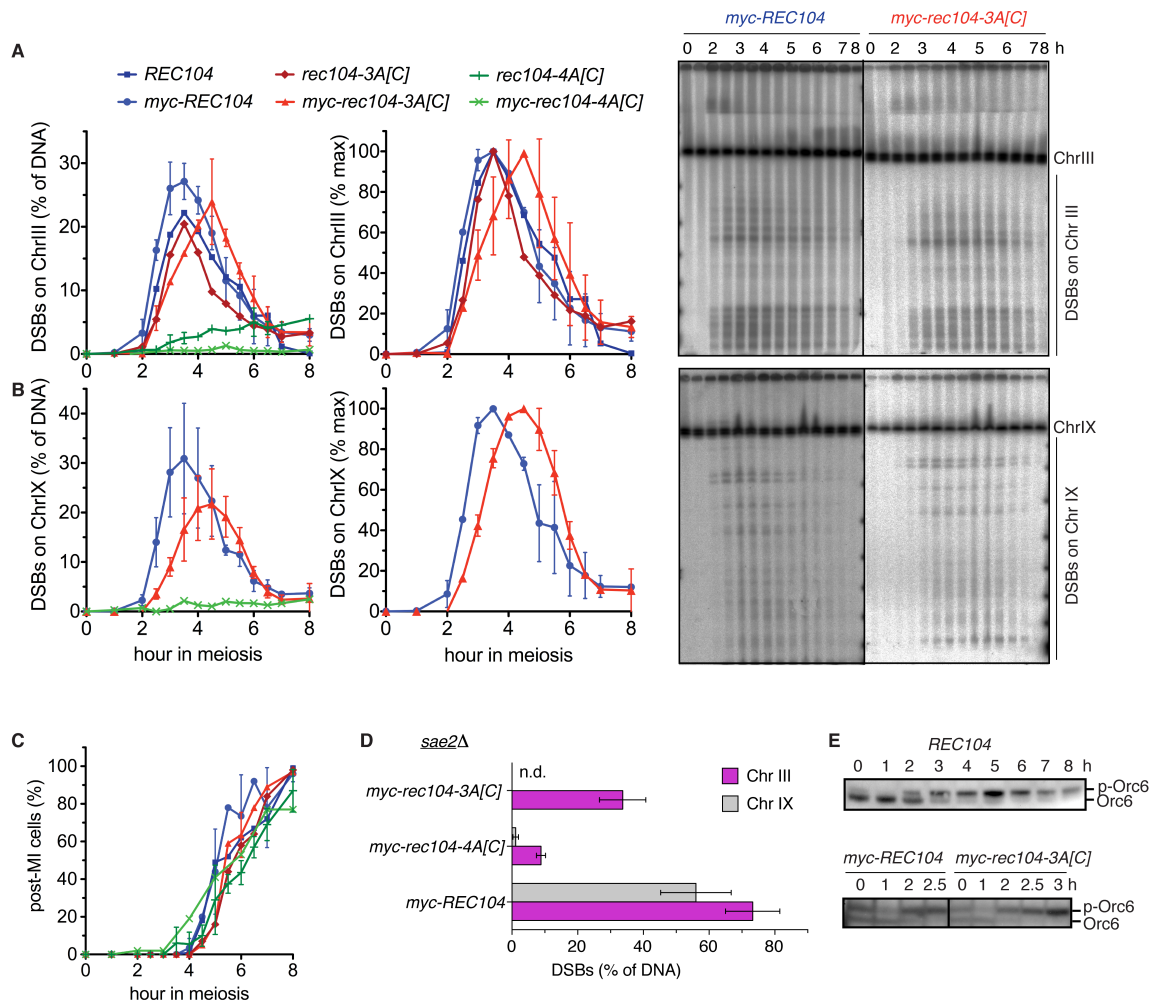


Figure A.5. The *myc-rec104-3A[C]* allele causes a delay in DSB formation. (A, B) Meiotic time course measuring DSB signal on chromosome III (A) or chromosome IX (B) in *myc*-tagged or untagged *rec104*-[C] mutants. DSBs are expressed as percent of total lane signal on the left graph, and as percent of maximum signal on the right graph to emphasize the timing difference in peak DSB levels. Representative Southern blots used to detect DSBs are also shown for *myc-REC104* and *myc-rec104-3A[C]*. Graphed values are the mean \pm s.d. from two independent experiments, except for *REC104*, *myc-rec104-4A[C]*, and *rec104-3A[C]*. (C) Fraction of cells that have completed meiosis I at the indicated time points taken from the same meiotic cultures as in (A) and (B), scored as cells with ≥ 2 DAPI-stained nuclei. (D) Comparison of DSBs on chromosomes III and IX in the *sae2Δ* mutant (8 h time point). Values are the mean \pm s.d. from three independent cultures. (E) Western blots of meiotic time courses for the indicated strains, probed with anti-Orc6 antibody. P-Orc6 indicates phosphorylated Orc6.

Examination of untagged versions of the *rec104*-[C] alleles demonstrated that a portion of the phenotypes could be ascribed to the combination of the point mutations with the myc epitope tag. Untagged *rec104-3A*[C] did not exhibit delayed DSB formation, but did retain an ~1.5-fold reduction in peak DSB levels (**Fig. A.5A**). Untagged *rec104-4A*[C] still exhibited spore viability and DSB defects (~30% spore viability, and ~5-fold reduction in DSBs), albeit less severe than with the myc-tagged version (**Fig. A.4B, A.5A**). The DSBs also appeared to persist to later time points in *rec104-4A*[C].

Conclusions

Thus far, data from the *rec104-4A*[R] allele suggest that Rec104 phosphorylation is important for normal DSB levels. However, it remains to be seen whether the phosphorylation and localization defects in the *rec104-4A* [R] mutant are tag-independent. If they are, one possible scenario is that Rec104 phosphorylation at the RxxS/T sites promotes interaction with Spo11 and/or Ski8, and subsequently, nuclear localization and/or retention. To test this model, and to help uncover the cause of compromised break formation, the chromatin association of *rec104-4A*[R] can be examined, as well as its interaction with other DSB proteins. The behaviors of other DSB proteins (e.g. Rec102, Spo11) known to depend on *REC104* can also be examined in the *rec104-4A*[R] mutant. Potential candidate kinases for phosphorylating these sites would be CAMK and AGC family kinases, which prefer RxxS/T motifs (Pearson and Kemp 1991; Jacinto and Lorberg 2008; Yoshizaki and Okuda 2014). Top candidates include Snf1, Gin4, Hsl1, Kcc4, Kin4, Rck2, Sky1, Tos3, Tpk2, and Yck1, based on data from a high-throughput peptide library screen to determine kinase consensus phosphorylation site motifs (Mok et al. 2009), although other criteria (e.g., kinase activity during early meiotic time-points) would help further narrow down the list.

Although it is still unknown whether Cdc7 phosphorylates Rec104, and it is unclear whether the *rec104*-[C] alleles are indeed phosphorylation-defective mutants, the *myc-rec104-3A*[C] allele is a novel mutant that exhibits delayed DSB formation. As such, it can be exploited as a tool to investigate how cells integrate DSB timing with the timing of other events in meiosis. The *myc-rec104-4A*[C] allele causes severe DSB and spore viability defects, but the mutant protein localizes to the nucleus normally, suggesting that interactions with Rec102, Spo11, and Ski8 are likely maintained. A similar analysis as that proposed for the *rec104*-[R] allele can be applied to investigate the underlying cause of the defects in this mutant.

Materials and Methods

Strains and culture methods

Yeast strains in the SK1 background are listed in **Table A.1**. Mutant *rec104* alleles were generated by PCR mutagenesis using primers containing the base pair alterations, and *REC104* cloned into the pRS306 plasmid (marked with *URA3*) as template (Sikorski and Hieter 1989). Two-step gene replacement as described in (Rothstein 1991) was used to generate yeast strains with the mutant *rec104* alleles at the endogenous locus. First, plasmids containing the desired mutation were linearized with *BspI* and integrated at the *REC104* locus in the *rec104* null yeast strain. This was followed by 5-fluoroorotic acid (5-FOA) counterselection, which leads to popout of the integrating vector sequences (including the *URA3* marker), but leaves behind the *rec104* mutant allele. The *rec104* point mutations were verified by sequencing; yeast strains with plasmid integration or popout were verified by PCR and Southern blot genotyping.

Synchronized meiotic cultures were prepared as described previously (Alani et al. 1990; Padmore et al. 1991), and similar to that described in **Chapter 5**. Briefly, yeast

cells from overnight YPD cultures were inoculated in liquid YPA (1% yeast extract, 2% Bacto peptone, 1% potassium acetate) at a cell density (OD_{600}) of 0.2, and cultured for 13.5 h at 30°C. Cells were harvested, washed and then resuspended in 2% potassium acetate, in the same volume as the YPA inoculation.

To determine meiosis I nuclear division profiles, aliquots from synchronized meiotic cultures were collected at various time-points and fixed with 50% (v/v) ethanol. 0.05 μ g/mL 4', 6-diamidino-2-phenylindole (DAPI) was added to the fixed cells prior to transferring them to glass slides. Mononucleate, binucleate, and tetranucleate cells were scored by fluorescence microscopy of at least 100 cells per time-point.

For spore viability tests, cells were sporulated in liquid sporulation culture (2% potassium acetate) for 2 days at 30°C, and tetrads were dissected on YPD plates (1% yeast extract, 2% Bacto peptone, 2% glucose, 2% agar) after incubation with 1 μ L of 10 mg/mL zymolyase 20T (US Biological) for 20 min at 30°C to digest the ascus. Spores were allowed to germinate and grow at 30°C for 2 days.

Phos-tag SDS-PAGE and western analysis

Whole-cell extracts were prepared by lysing cells in 20% TCA with glass beads in a bead-beater, collecting the cell extract, centrifuging, and resuspending the pellets in Laemmli buffer. Phos-tag gels were prepared by adding 75 μ M Phos-tag and 150 μ M $MnCl_2$ to a 10% SDS-polyacrylamide gel before casting. Electrophoresis with Phos-tag gels was carried out at 100 V for 3 h. Non-Phos-tag gels were 7.5% SDS-polyacrylamide gels, and electrophoresis was carried out at 150 V for 1.25 h. After SDS-PAGE, Phos-tag gels were equilibrated for 10 min in semi-dry transfer buffer (48 mM Tris, 39 mM glycine, 0.0375% SDS, 20% methanol), with 1 mM EDTA. Protein transfer onto PVDF membrane was done by semi-dry transfer for 15 min at 25 V. Blots were probed with mouse anti-myc (9E10) antibody (1:7000), and then with anti-mouse IgG conjugated to

horseradish peroxidase (HRP) (1:10000). Chemiluminescent detection with ECL+ (Amersham) was performed according to manufacturer's instructions.

For anti-Orc6 western blots, mouse anti-Orc6 (SB49, Weinreich et al 1999) was used at 1:2000 dilution, and anti-mouse IgG conjugated to HRP at 1:8000 dilution. Mouse anti-Orc6 antibody was generously provided by Bruce Stillman (Cold Spring Harbor Laboratory).

Phosphatase treatment

Phosphatase treatment of immunoprecipitated material was performed as described in (Kee et al. 2004). Briefly, $\sim 4 \times 10^8$ cells were harvested at 4 h in meiosis from synchronized meiotic cultures, and lysed by agitation with glass beads in 20% TCA. Precipitated material was dissolved in Laemmli buffer, then diluted 10-fold with 0.01% SDS, 1.1% Triton X-100, 1.2 mM EDTA, 16.7 mM Tris-HCl, pH 8.1, 167 mM NaCl, plus protease inhibitors. Myc-Rec104 was immunoprecipitated with anti-myc antibody (9E10) for 2 h at 4°C with end-over-end rotation, followed by incubation with protein G agarose beads (Roche) for 1 h at 4°C with end-over-end rotation. The immunoprecipitate was then equilibrated in phosphatase buffer (New England BioLabs) and divided into three aliquots: (1) untreated, (2) treated with 50 units lambda phosphatase, (3) treated with 50 units lambda phosphatase plus phosphatase inhibitors (50 mM EDTA, 50 mM NaF, 10 mM Na_3VO_4). Samples were then boiled in SDS buffer and analyzed by western blotting.

Indirect Immunofluorescence

Whole-cell immunostaining was conducted as described in (Kee et al. 2004), with some modifications. Whole cells from a 5 mL aliquot harvested at the 4 h time point from synchronous meiotic cultures ($\text{OD}_{600} = \sim 1$) were fixed with 4% formaldehyde for 90 min. Fixed cells were washed three times with 0.1 M KPHO_4 , pH 6.5, then once with 0.1 M

K₂HPO₄, pH 6.5, 1.2 M sorbitol. Cell walls in one half of the cell pellet were partially digested by 20 min incubation at 30°C in 60 µg/mL zymolyase 100T in 0.1 M K₂HPO₄ pH 6.5, 1.2 M sorbitol, 0.14 M β-mercaptoethanol. Spheroplasts were harvested, gently washed twice with 0.1 M K₂HPO₄, pH 6.5, 1.2 M sorbitol and stored on ice until ready to apply to microscope slides. Cells were applied onto multi-well slides coated with 1 mg/mL poly-lysine, then fixed and permeabilized with methanol and acetone. Indirect immunofluorescent staining was carried out by blocking with 1X TBS, 1% bovine serum albumin (BSA) for 20 min, followed by primary antibody staining with mouse anti-myc (9E10) (1:500) dilution for 2 h in a humid chamber, four washes with 1X TBS, 1% BSA, then secondary antibody staining with goat anti-mouse IgG coupled to Alexa 488 (1:200) dilution for 1 h. Slides were washed twice with 1X TBS, 1% BSA, stained with 100 ng/mL DAPI for 10 min, washed once with 1X TBS, then mounted with cover slips in antifade Vectashield H-1000. Images were captured on an Axio Observer.Z1 (Zeiss) microscope and processed using Slidebook software (Intelligent Imaging Innovations).

Southern blots for DSB detection

Genomic DNA was isolated at the indicated time points from synchronous meiotic cultures, and prepared in low melting agarose plugs as described (Borde et al. 2000; Murakami et al. 2009) to avoid shearing of high molecular weight fragments. DNA embedded in agarose plugs was separated by pulsed-field gel electrophoresis, then probed by Southern blot with part of the *CHA1* open reading frame (SGD coordinates 15838 to 16857) to detect DSBs on chromosome III, or *POT1* (SGD coordinates 40223 to 40728) to detect DSBs on chromosome IX. Hybridization signal was detected by phosphorimager, and DSB frequency was calculated as the percent of hybridizing signal each lane. Observed DSB frequencies were Poisson corrected as described in

(Murakami and Keeney 2014), then signals from 0 h lanes were subtracted from all lanes.

Table A.1. Yeast strains (*rec104* mutant alleles)

Strain number		Genotype
SKY165	<i>REC104</i>	<i>MATa/MATα, ho::LYS2⁺ lys2⁻ ura3⁻ leu2::hisG⁺</i>
SKY304	<i>rec104</i>	<i>MATa/MATα, ho::LYS2⁺ lys2⁻ ura3⁻ leu2::hisG⁺, rec104Δ⁺</i>
SKY791	<i>myc-REC104</i>	<i>MATa/MATα, ho::LYS2⁺, ura3⁻, leu2::hisG⁺, myc-REC104</i> (Kee et al. 2004)
SKY4125	<i>myc-REC104 sae2</i>	<i>MATa/MATα, ho::LYS2⁺ lys2⁻ ura3⁻ leu2::hisG⁺ myc-REC104⁺, sae2::LEU2⁺</i>
ILY131	<i>myc-rec104-4A[R]</i>	<i>MATa/MATα, ho::LYS2⁺ lys2⁻ ura3⁻ leu2::hisG⁺, myc-rec104-S69A, S101A, S150A, S172A⁺</i> (Note: SKY301 transformed with <i>URA3</i> integration plasmid at <i>REC104</i> locus, then allele-replaced with 5-FOA)
ILY136	<i>myc-rec104-4A[R] sae2</i>	<i>MATa/MATα, ho::LYS2⁺, lys2⁻, ura3⁻, leu2::hisG⁺, sae2::LEU2⁺, myc-rec104-S69A, S101A, S150A, S172A⁺</i>
ILY166.1	<i>myc-rec104-2A[R]</i>	<i>MATa/MATα, ho::LYS2⁺ lys2⁻ ura3⁻ leu2::hisG⁺, rec104Δ⁺, myc-rec104-S150A, S172A::URA3::rec104⁺</i> (plasmid-integrated at <i>REC104</i> promoter)
ILY159	<i>rec104-4A[R]</i>	<i>MATa/MATα, ho::LYS2⁺ lys2⁻ ura3⁻ leu2::hisG⁺, rec104-S69A, S101A, S150A, S172A⁺</i>
ILY196	<i>rec104-4A[R] sae2</i>	<i>MATa/MATα, ho::LYS2⁺, lys2⁻, ura3⁻, leu2::hisG⁺, sae2::LEU2⁺, rec104-S69A, S101A, S150A, S172A⁺</i>
ILY162	<i>rec104-4D[R]</i>	<i>MATa/MATα, ho::LYS2⁺ lys2⁻ ura3⁻ leu2::hisG⁺, rec104-S69D, S101D, S150D, S172D⁺</i> (Note: slow growth, irregularly shaped spore clones)
ILY107	<i>myc-rec104-3A[C]</i>	<i>MATa/MATα, ho::LYS2⁺ lys2⁻ ura3⁻ leu2::hisG⁺, myc-rec104-T24A, S111A, S160A⁺</i>
ILY138	<i>myc-rec104-3A[C] sae2</i>	<i>MATa/MATα, ho::LYS2⁺, lys2⁻, ura3⁻, leu2::hisG⁺, sae2::LEU2⁺, myc-rec104-T24A, S111A, S160A, sae2</i>
ILY74	<i>myc-rec104-4A[C]</i>	<i>MATa/MATα, ho::LYS2⁺ lys2⁻ ura3⁻ leu2::hisG⁺, myc-rec104-T24A, S111A, S141A, S160A⁺</i>
SKY4130	<i>myc-rec104-4A[C] sae2</i>	<i>MATa/MATα, ho::LYS2⁺ lys2⁻ ura3⁻ leu2::hisG⁺, myc-rec104-T24A, S111A, S141A, S160A, sae2::LEU2⁺</i>
ILY204	<i>rec104-3A[C]</i>	<i>MATa/MATα, ho::LYS2⁺ lys2⁻ ura3⁻ leu2::hisG⁺, rec104Δ⁺, rec104-T24A, S111A, S160A⁺</i>
ILY110	<i>rec104-4A[C]</i>	<i>MATa/MATα, ho::LYS2⁺ lys2⁻ ura3⁻ leu2::hisG⁺, rec104Δ⁺, rec104-T24A, S111A, S141A, S160A⁺</i>
ILY143	<i>rec104-4A[C] sae2</i>	<i>MATa/MATα, ho::LYS2⁺ lys2⁻ ura3⁻ leu2::hisG⁺, rec104Δ⁺, rec104-T24A, S111A, S141A, S160A⁺, sae2::LEU2⁺</i>

REFERENCES

- Acquaviva L, Székvölgyi L, Dichtl B, Dichtl BS, de La Roche Saint-André C, Nicolas A, Géli V. 2012. The COMPASS subunit Spp1 links histone methylation to initiation of meiotic recombination. *Science* **339**: 215-218.
- Agashe B, Prasad CK, Siddiqi I. 2002. Identification and analysis of DYAD: A gene required for meiotic chromosome organisation and female meiotic progression in *Arabidopsis*. *Development* **129**: 3935-3943.
- Alani E, Padmore R, Kleckner N. 1990. Analysis of wild-type and *rad50* mutants of yeast suggests an intimate relationship between meiotic chromosome synapsis and recombination. *Cell* **61**: 419-436.
- Allers T, Lichten M. 2001. Differential timing and control of noncrossover and crossover recombination during meiosis. *Cell* **106**: 47-57.
- Alpi A, Pasierbek P, Gartner A, Loidl J. 2003. Genetic and cytological characterization of the recombination protein RAD-51 in *Caenorhabditis elegans*. *Chromosoma* **112**: 6-16.
- Anderson LK, Offenberg HH, Verkuijlen WMHC, Heyting C. 1997. RecA-like proteins are components of early meiotic nodules in lily. *Proc Natl Acad Sci U S A* **94**: 6868-6873.
- Anuradha S, Muniyappa K. 2004. *Saccharomyces cerevisiae* Hop1 zinc finger motif is the minimal region required for its function in vitro. *J Biol Chem* **279**: 28961-28969.
- Aravind L, Koonin EV. 1998. The HORMA domain: a common structural denominator in mitotic checkpoints, chromosome synapsis and DNA repair. *Trends in biochemical sciences* **23**: 284-286.
- Arbeithuber B, Betancourt AJ, Ebner T, Tiemann-Boege I. 2015. Crossovers are associated with mutation and biased gene conversion at recombination hotspots. *Proc Natl Acad Sci U S A* **112**: 2109-2114.
- Argunhan B, Farmer S, Leung WK, Terentyev Y, Humphries N, Tsubouchi T, Toyozumi H, Tsubouchi H. 2013. Direct and indirect control of the initiation of meiotic recombination by DNA damage checkpoint mechanisms in budding yeast. *PLoS One* **8**: e65875.
- Armstrong SJ, Caryl AP, Jones GH, Franklin FC. 2002. Asy1, a protein required for meiotic chromosome synapsis, localizes to axis-associated chromatin in *Arabidopsis* and *Brassica*. *J Cell Sci* **115**: 3645-3655.
- Arnheim N, Calabrese P, Tiemann-Boege I. 2007. Mammalian meiotic recombination hot spots. *Annu Rev Genet* **41**: 369-399.

- Arora C, Kee K, Maleki S, Keeney S. 2004. Antiviral protein Ski8 is a direct partner of Spo11 in meiotic DNA break formation, independent of its cytoplasmic role in RNA metabolism. *Mol Cell* **13**: 549-559.
- Ashley T, Plug AW, Xu J, Solari AJ, Reddy G, Golub EI, Ward DC. 1995. Dynamic changes in Rad51 distribution on chromatin during meiosis in male and female vertebrates. *Chromosoma* **104**: 19-28.
- Auton A, Fledel-Alon A, Pfeifer S, Venn O, Segurel L, Street T, Leffler EM, Bowden R, Aneas I, Broxholme J et al. 2012. A fine-scale chimpanzee genetic map from population sequencing. *Science* **336**: 193-198.
- Auton A, Rui Li Y, Kidd J, Oliveira K, Nadel J, Holloway JK, Hayward JJ, Cohen PE, Grealis JM, Wang J et al. 2013. Genetic recombination is targeted towards gene promoter regions in dogs. *PLoS Genet* **9**: e1003984.
- Axelsson E, Webster MT, Ratnakumar A, Ponting CP, Lindblad-Toh K. 2012. Death of PRDM9 coincides with stabilization of the recombination landscape in the dog genome. *Genome Res* **22**: 51-63.
- Bailis JM, Roeder GS. 1998. Synaptonemal complex morphogenesis and sister-chromatid cohesion require Mek1-dependent phosphorylation of a meiotic chromosomal protein. *Genes Dev* **12**: 3551-3563.
- Bailis JM, Roeder GS. 2000. Pachytene exit controlled by reversal of Mek1-dependent phosphorylation. *Cell* **101**: 211-221.
- Baker CL, Kajita S, Walker M, Saxl RL, Raghupathy N, Choi K, Petkov PM, Paigen K. 2015. PRDM9 drives evolutionary erosion of hotspots in *Mus musculus* through haplotype-specific initiation of meiotic recombination. *PLoS Genet* **11**: e1004916.
- Barlow AL, Benson FE, West SC, Hultén MA. 1997. Distribution of the Rad51 recombinase in human and mouse spermatocytes. *EMBO J* **16**: 5207-5215.
- Baudat F, Buard J, Grey C, Fledel-Alon A, Ober C, Przeworski M, Coop G, de Massy B. 2010. PRDM9 is a major determinant of meiotic recombination hotspots in humans and mice. *Science* **327**: 836-840.
- Baudat F, Imai Y, de Massy B. 2013. Meiotic recombination in mammals: localization and regulation. *Nat Rev Genet* **14**: 794-806.
- Baudat F, Manova K, Yuen JP, Jasin M, Keeney S. 2000. Chromosome synapsis defects and sexually dimorphic meiotic progression in mice lacking Spo11. *Mol Cell* **6**: 989-998.
- Baudat F, Nicolas A. 1997. Clustering of meiotic double-strand breaks on yeast chromosome III. *Proc Natl Acad Sci U S A* **94**: 5213-5218.
- Begun DJ, Aquadro CF. 1992. Levels of naturally occurring DNA polymorphism correlate with recombination rates in *D. melanogaster*. *Nature* **356**: 519-520.

- Benjamin KR, Zhang C, Shokat KM, Herskowitz I. 2003. Control of landmark events in meiosis by the CDK Cdc28 and the meiosis-specific kinase Ime2. *Genes Dev* **17**: 1524-1539.
- Berchowitz LE, Hanlon SE, Lieb JD, Copenhaver GP. 2009. A positive but complex association between meiotic double-strand break hotspots and open chromatin in *Saccharomyces cerevisiae*. *Genome Res* **19**: 2245-2257.
- Berg IL, Neumann R, Lam KW, Sarbajna S, Odenthal-Hesse L, May CA, Jeffreys AJ. 2010. PRDM9 variation strongly influences recombination hot-spot activity and meiotic instability in humans. *Nat Genet* **42**: 859-863.
- Berg IL, Neumann R, Sarbajna S, Odenthal-Hesse L, Butler NJ, Jeffreys AJ. 2011. Variants of the protein PRDM9 differentially regulate a set of human meiotic recombination hotspots highly active in African populations. *Proc Natl Acad Sci U S A* **108**: 12378-12383.
- Bergerat A, de Massy B, Gadelle D, Varoutas PC, Nicolas A, Forterre P. 1997. An atypical topoisomerase II from *Archaea* with implications for meiotic recombination. *Nature* **386**: 414-417.
- Berglund J, Quilez J, Arndt PF, Webster MT. 2015. Germline methylation patterns determine the distribution of recombination events in the dog genome. *Genome Biol Evol* **7**: 522-530.
- Bhalla N, Dernburg AF. 2008. Prelude to a division. *Annu Rev Cell Dev Biol* **24**: 397-424.
- Bishop DK, Nikolski Y, Oshiro J, Chon J, Shinohara M, Chen X. 1999. High copy number suppression of the meiotic arrest caused by a *dmc1* mutation: *REC114* imposes an early recombination block and *RAD54* promotes a *DMC1*-independent DSB repair pathway. *Genes Cells* **4**: 425-444.
- Bishop DK, Park D, Xu L, Kleckner N. 1992. *DMC1*: A meiosis-specific yeast homolog of *E. coli recA* required for recombination, synaptonemal complex formation, and cell cycle progression. *Cell* **69**: 439-456.
- Blat Y, Protacio RU, Hunter N, Kleckner N. 2002. Physical and functional interactions among basic chromosome organizational features govern early steps of meiotic chiasma formation. *Cell* **111**: 791-802.
- Bleuyard JY, Gallego ME, White CI. 2004. Meiotic defects in the *Arabidopsis rad50* mutant point to conservation of the MRX complex function in early stages of meiotic recombination. *Chromosoma* **113**: 197-203.
- Blitzblau HG, Bell GW, Rodriguez J, Bell SP, Hochwagen A. 2007. Mapping of meiotic single-stranded DNA reveals double-strand-break hotspots near centromeres and telomeres. *Curr Biol* **17**: 2003-2012.
- Blitzblau HG, Chan CS, Hochwagen A, Bell SP. 2012. Separation of DNA replication from the assembly of break-competent meiotic chromosomes. *PLoS Genet* **8**: e1002643.

- Blitzblau HG, Hochwagen A. 2013. ATR/Mec1 prevents lethal meiotic recombination initiation on partially replicated chromosomes in budding yeast. *eLife* **2**: e00844.
- Boateng KA, Yang X, Dong F, Owen HA, Makaroff CA. 2008. SWI1 is required for meiotic chromosome remodeling events. *Mol Plant* **1**: 620-633.
- Bonfils S, Rozalen AE, Smith GR, Moreno S, Martin-Castellanos C. 2011. Functional interactions of Rec24, the fission yeast ortholog of mouse Mei4, with the meiotic recombination-initiation complex. *J Cell Sci* **124**: 1328-1338.
- Borde V. 2007. The multiple roles of the Mre11 complex for meiotic recombination. *Chromosome Res* **15**: 551-563.
- Borde V, Goldman ASH, Lichten M. 2000. Direct coupling between meiotic DNA replication and recombination initiation. *Science* **290**: 806-809.
- Borde V, Lin W, Novikov E, Petrini JH, Lichten M, Nicolas A. 2004. Association of Mre11p with double-strand break sites during yeast meiosis. *Mol Cell* **13**: 389-401.
- Borde V, Robine N, Lin W, Bonfils S, Géli V, Nicolas A. 2009. Histone H3 lysine 4 trimethylation marks meiotic recombination initiation sites. *EMBO J* **28**: 99-111.
- Borde V, Wu T-C, Lichten M. 1999. Use of a recombination reporter insert to define meiotic recombination domains on chromosome III of *Saccharomyces cerevisiae*. *Mol Cell Biol* **19**: 4832-4842.
- Borner GV, Barot A, Kleckner N. 2008. Yeast Pch2 promotes domainal axis organization, timely recombination progression, and arrest of defective recombinosomes during meiosis. *Proc Natl Acad Sci U S A* **105**: 3327-3332.
- Boulton A, Myers RS, Redfield RJ. 1997. The hotspot conversion paradox and the evolution of meiotic recombination. *Proc Natl Acad Sci U S A* **94**: 8058-8063.
- Brick K, Smagulova F, Khil P, Camerini-Otero RD, Petukhova GV. 2012. Genetic recombination is directed away from functional genomic elements in mice. *Nature* **485**: 642-645.
- Broverman SA, Meneely PM. 1994. Meiotic mutants that cause a polar decrease in recombination on the X chromosome in *Caenorhabditis elegans*. *Genetics* **136**: 119-127.
- Brown CA, Murray AW, Verstrepen KJ. 2010. Rapid expansion and functional divergence of subtelomeric gene families in yeasts. *Curr Biol* **20**: 895-903.
- Buard J, Barthès P, Grey C, de Massy B. 2009. Distinct histone modifications define initiation and repair of meiotic recombination in the mouse. *EMBO J* **28**: 2616-2624.

- Buhler C, Borde V, Lichten M. 2007. Mapping meiotic single-strand DNA reveals a new landscape of DNA double-strand breaks in *Saccharomyces cerevisiae*. *PLoS Biol* **5**: e324.
- Burgess SM. 2002. Homologous chromosome associations and nuclear order in meiotic and mitotically dividing cells of budding yeast. *Advances in genetics* **46**: 49-90.
- Busygina V, Sehorn MG, Shi IY, Tsubouchi H, Roeder GS, Sung P. 2008. Hed1 regulates Rad51-mediated recombination via a novel mechanism. *Genes Dev* **22**: 786-795.
- Calabrese P. 2007. A population genetics model with recombination hotspots that are heterogeneous across the population. *Proc Natl Acad Sci U S A* **104**: 4748-4752.
- Callender TL, Hollingsworth NM. 2010. Mek1 suppression of meiotic double-strand break repair is specific to sister chromatids, chromosome autonomous and independent of Rec8 cohesin complexes. *Genetics* **185**: 771-782.
- Cao L, Alani E, Kleckner N. 1990. A pathway for generation and processing of double-strand breaks during meiotic recombination in *S. cerevisiae*. *Cell* **61**: 1089-1101.
- Carballo JA, Johnson AL, Sedgwick SG, Cha RS. 2008. Phosphorylation of the axial element protein Hop1 by Mec1/Tel1 ensures meiotic interhomolog recombination. *Cell* **132**: 758-770.
- Carballo JA, Panizza S, Serrentino M-E, Johnson AL, Geymonat M, Borde V, Klein F, Cha RS. 2013. Budding yeast ATM/ATR control meiotic double-strand break (DSB) levels by down-regulating Rec114, an essential component of the DSB-machinery. *PLoS Genet* **9**: e1003545.
- Carlton PM, Farruggio AP, Dernburg AF. 2006. A link between meiotic prophase progression and crossover control. *PLoS Genet* **2**: e12.
- Caryl AP, Armstrong SJ, Jones GH, Franklin FC. 2000. A homologue of the yeast *HOP1* gene is inactivated in the *Arabidopsis* meiotic mutant *asy1*. *Chromosoma* **109**: 62-71.
- Cervantes MD, Farah JA, Smith GR. 2000. Meiotic DNA breaks associated with recombination in *S. pombe*. *Mol Cell* **5**: 883-888.
- Chan AH, Jenkins PA, Song YS. 2012. Genome-wide fine-scale recombination rate variation in *Drosophila melanogaster*. *PLoS Genet* **8**: e1003090.
- Charlesworth B, Campos JL. 2014. The relations between recombination rate and patterns of molecular variation and evolution in *Drosophila*. *Annu Rev Genet* **48**: 383-403.
- Chen C, Jomaa A, Ortega J, Alani EE. 2014. Pch2 is a hexameric ring ATPase that remodels the chromosome axis protein Hop1. *Proc Natl Acad Sci U S A* **111**: E44-53.

- Chen SY, Tsubouchi T, Rockmill B, Sandler JS, Richards DR, Vader G, Hochwagen A, Roeder GS, Fung JC. 2008a. Global analysis of the meiotic crossover landscape. *Dev Cell* **15**: 401-415.
- Chen YT, Venditti CA, Theiler G, Stevenson BJ, Iseli C, Gure AO, Jongeneel CV, Old LJ, Simpson AJ. 2005. Identification of CT46/HORMAD1, an immunogenic cancer/testis antigen encoding a putative meiosis-related protein. *Cancer immunity* **5**: 9.
- Chen Z, Yang H, Pavletich NP. 2008b. Mechanism of homologous recombination from the RecA-ssDNA/dsDNA structures. *Nature* **453**: 489-484.
- Cherry SM, Adelman CA, Theunissen JW, Hassold TJ, Hunt PA, Petrini JH. 2007. The Mre11 complex influences DNA repair, synapsis, and crossing over in murine meiosis. *Curr Biol* **17**: 373-378.
- Chin GM, Villeneuve AM. 2001. *C. elegans* mre-11 is required for meiotic recombination and DNA repair but is dispensable for the meiotic G2 DNA damage checkpoint. *Genes Dev* **15**: 522-534.
- Cho WH, Lee YJ, Kong SI, Hurwitz J, Lee JK. 2006. CDC7 kinase phosphorylates serine residues adjacent to acidic amino acids in the minichromosome maintenance 2 protein. *Proc Natl Acad Sci U S A* **103**: 11521-11526.
- Choi K, Henderson IR. 2015. Meiotic recombination hotspots - a comparative view. *Plant J* **83**: 52-61.
- Choi K, Zhao X, Kelly KA, Venn O, Higgins JD, Yelina NE, Hardcastle TJ, Ziolkowski PA, Copenhaver GP, Franklin FC et al. 2013. *Arabidopsis* meiotic crossover hot spots overlap with H2A.Z nucleosomes at gene promoters. *Nat Genet* **45**: 1327-1336.
- Chu S, Herskowitz I. 1998. Gametogenesis in yeast is regulated by a transcriptional cascade dependent on Ndt80. *Mol Cell* **1**: 685-696.
- Chuang CN, Cheng YH, Wang TF. 2012. Mek1 stabilizes Hop1-Thr318 phosphorylation to promote interhomolog recombination and checkpoint responses during yeast meiosis. *Nucleic Acids Res* **40**: 11416-11427.
- Chung G, Rose AM, Petalcorin MI, Martin JS, Kessler Z, Sanchez-Pulido L, Ponting CP, Yanowitz JL, Boulton SJ. 2015. REC-1 and HIM-5 distribute meiotic crossovers and function redundantly in meiotic double-strand break formation in *Caenorhabditis elegans*. *Genes Dev* **29**: 1969-1979.
- Colaiácovo MP, MacQueen AJ, Martinez-Perez E, McDonald K, Adamo A, La Volpe A, Villeneuve AM. 2003. Synaptonemal complex assembly in *C. elegans* is dispensable for loading strand-exchange proteins but critical for proper completion of recombination. *Dev Cell* **5**: 463-474.

- Cole F, Baudat F, Grey C, Keeney S, de Massy B, Jasin M. 2014. Mouse tetrad analysis provides insights into recombination mechanisms and hotspot evolutionary dynamics. *Nat Genet* **46**: 1072-1080.
- Cole F, Keeney S, Jasin M. 2010. Evolutionary conservation of meiotic DSB proteins: More than just Spo11. *Genes Dev* **24**: 1201-1207.
- Consortium TIH. 2005. A haplotype map of the human genome. *Nature* **437**: 1299-1320.
- Coop G, Myers SR. 2007. Live hot, die young: transmission distortion in recombination hotspots. *PLoS Genet* **3**: e35.
- Coop G, Przeworski M. 2007. An evolutionary view of human recombination. *Nat Rev Genet* **8**: 23-34.
- Coop G, Wen X, Ober C, Pritchard JK, Przeworski M. 2008. High-resolution mapping of crossovers reveals extensive variation in fine-scale recombination patterns among humans. *Science* **319**: 1395-1398.
- Cooper TJ, Garcia V, Neale MJ. 2016. Meiotic DSB patterning: A multifaceted process. *Cell Cycle* **15**: 13-21.
- Cooper TJ, Wardell K, Garcia V, Neale MJ. 2014. Homeostatic regulation of meiotic DSB formation by ATM/ATR. *Exp Cell Res* **329**: 124-131.
- Corbett KD, Benedetti P, Berger JM. 2007. Holoenzyme assembly and ATP-mediated conformational dynamics of topoisomerase VI. *Nat Struct Mol Biol* **14**: 611-619.
- Couteau F, Nabeshima K, Villeneuve A, Zetka M. 2004. A component of *C. elegans* meiotic chromosome axes at the interface of homolog alignment, synapsis, nuclear reorganization, and recombination. *Curr Biol* **14**: 585-592.
- Couteau F, Zetka M. 2005. HTP-1 coordinates synaptonemal complex assembly with homolog alignment during meiosis in *C. elegans*. *Genes Dev* **19**: 2744-2756.
- Cromie G, Smith GR. 2007a. Meiotic Recombination in *Schizosaccharomyces pombe*: A Paradigm for Genetic and Molecular Analysis. in *Recombination and Meiosis* (eds. R Egel, DH Lankenau), pp. 195-230. Springer-Verlag, Berlin Heidelberg.
- Cromie GA, Hyppa RW, Cam HP, Farah JA, Grewal SI, Smith GR. 2007. A discrete class of intergenic DNA dictates meiotic DNA break hotspots in fission yeast. *PLoS Genet* **3**: e141.
- Cromie GA, Rubio CA, Hyppa RW, Smith GR. 2005. A natural meiotic DNA break site in *Schizosaccharomyces pombe* is a hotspot of gene conversion, highly associated with crossing over. *Genetics* **169**: 595-605.
- Cromie GA, Smith GR. 2007b. Branching out: meiotic recombination and its regulation. *Trends Cell Biol* **17**: 448-455.

- Daniel K, Lange J, Hached K, Fu J, Anastassiadis K, Roig I, Cooke HJ, Stewart AF, Wassmann K, Jasin M et al. 2011. Meiotic homologue alignment and its quality surveillance are controlled by mouse HORMAD1. *Nat Cell Biol* **13**: 599-610.
- Davidow LS, Goetsch L, Byers B. 1980. Preferential occurrence of nonsister spores in two-spored asci of *Saccharomyces cerevisiae*: evidence for regulation of spore-wall formation by the spindle pole body. *Genetics* **94**: 581-595.
- Davies B, Hatton E, Altemose N, Hussin JG, Pratto F, Zhang G, Hinch AG, Moralli D, Biggs D, Diaz R et al. 2016. Re-engineering the zinc fingers of PRDM9 reverses hybrid sterility in mice. *Nature* **530**: 171-176.
- Davis L, Rozalen AE, Moreno S, Smith GR, Martin-Castellanos C. 2008. Rec25 and Rec27, novel linear-element components, link cohesin to meiotic DNA breakage and recombination. *Curr Biol* **18**: 849-854.
- de Castro E, Soriano I, Marin L, Serrano R, Quintales L, Antequera F. 2012. Nucleosomal organization of replication origins and meiotic recombination hotspots in fission yeast. *EMBO J* **31**: 124-137.
- de los Santos T, Hollingsworth NM. 1999. Red1p, a MEK1-dependent phosphoprotein that physically interacts with Hop1p during meiosis in yeast. *J Biol Chem* **274**: 1783-1790.
- de Massy B. 2013. Initiation of meiotic recombination: how and where? Conservation and specificities among eukaryotes. *Annu Rev Genet* **47**: 563-599.
- de Massy B, Rocco, V., and Nicolas, A. 1995. The nucleotide mapping of DNA double-strand breaks at the CYS3 initiation site of meiotic recombination in *Saccharomyces cerevisiae*. *EMBO J* **14**: 4589-4598.
- De Muyt A, Pereira L, Vezon D, Chelysheva L, Gendrot G, Chambon A, Laine-Choinard S, Pelletier G, Mercier R, Nogue F et al. 2009. A high throughput genetic screen identifies new early meiotic recombination functions in *Arabidopsis thaliana*. *PLoS Genet* **5**: e1000654.
- De Muyt A, Vezon D, Gendrot G, Gallois JL, Stevens R, Grelon M. 2007. AtPRD1 is required for meiotic double strand break formation in *Arabidopsis thaliana*. *EMBO J* **26**: 4126-4137.
- Dehé P-M, Géli V. 2006. The multiple faces of Set1. *Biochem Cell Biol* **84**: 536-548.
- Dehé PM, Dichtl B, Schaff D, Roguev A, Pamblanco M, Lebrun R, Rodriguez-Gil A, Mkandawire M, Landsberg K, Shevchenko A et al. 2006. Protein interactions within the Set1 complex and their roles in the regulation of histone 3 lysine 4 methylation. *J Biol Chem* **281**: 35404-35412.
- Dernburg AF, McDonald K, Moulder G, Barstead R, Dresser M, Villeneuve AM. 1998. Meiotic recombination in *C. elegans* initiates by a conserved mechanism and is dispensable for homologous chromosome synapsis. *Cell* **94**: 387-398.

- Di Giacomo M, Barchi M, Baudat F, Edelman W, Keeney S, Jasin M. 2005. Distinct DNA-damage-dependent and -independent responses drive the loss of oocytes in recombination-defective mouse mutants. *Proc Natl Acad Sci U S A* **102**: 737-742.
- Diaz RL, Alcid AD, Berger JM, Keeney S. 2002. Identification of residues in yeast Spo11p critical for meiotic DNA double-strand break formation. *Mol Cell Biol* **22**: 1106-1115.
- Dobson MJ, Pearlman RE, Karaiskakis A, Spyropoulos B, Moens PB. 1994. Synaptonemal complex proteins: occurrence, epitope mapping and chromosome disjunction. *J Cell Sci* **107**: 2749-2760.
- Dujon B. 2006. Yeasts illustrate the molecular mechanisms of eukaryotic genome evolution. *Trends Genet* **22**: 375-387.
- Duret L, Galtier N. 2009. Biased gene conversion and the evolution of mammalian genomic landscapes. *Ann Rev Genomics Hum Genet* **10**: 285-311.
- Durocher D, Jackson SP. 2002. The FHA domain. *FEBS letters* **513**: 58-66.
- Edlinger B, Schlögelhofer. 2011. Have a break: Determinants of meiotic DNA double strand break (DSB) formation and processing in plants. *J Exp Bot* **62**: 1545-1563.
- Eichinger CS, Jentsch S. 2010. Synaptonemal complex formation and meiotic checkpoint signaling are linked to the lateral element protein Red1. *Proc Natl Acad Sci U S A* **107**: 11370-11375.
- Eickbush TH, Eickbush DG. 2007. Finely orchestrated movements: evolution of the ribosomal RNA genes. *Genetics* **175**: 477-485.
- Ellermeier C, Smith GR. 2005. Cohesins are required for meiotic DNA breakage and recombination in *Schizosaccharomyces pombe*. *Proc Natl Acad Sci U S A* **102**: 10952-10957.
- Evans DH, Li YF, Fox ME, Smith GR. 1997. A WD repeat protein, Rec14, essential for meiotic recombination in *Schizosaccharomyces pombe*. *Genetics* **146**: 1253-1264.
- Fan QQ, Petes TD. 1996. Relationship between nuclease-hypersensitive sites and meiotic recombination hot spot activity at the *HIS4* locus of *Saccharomyces cerevisiae*. *Mol Cell Biol* **16**: 2037-2043.
- Fan QQ, Xu F, White MA, Petes TD. 1997. Competition between adjacent meiotic recombination hotspots in the yeast *Saccharomyces cerevisiae*. *Genetics* **145**: 661-670.
- Ferdous M, Higgins JD, Osman K, Lambing C, Roitinger E, Mechtler K, Armstrong SJ, Perry R, Pradillo M, Cunado N et al. 2012. Inter-homolog crossing-over and synapsis in *Arabidopsis* meiosis are dependent on the chromosome axis protein AtASY3. *PLoS Genet* **8**: e1002507.

- Finn K, Lowndes NF, Grenon M. 2012. Eukaryotic DNA damage checkpoint activation in response to double-strand breaks. *Cell Mol Life Sci* **69**: 1447-1473.
- Fischer G, James SA, Roberts IN, Oliver SG, Louis EJ. 2000. Chromosomal evolution in *Saccharomyces*. *Nature* **405**: 451-454.
- Fowler KR, Gutierrez-Velasco S, Martin-Castellanos C, Smith GR. 2013. Protein determinants of meiotic DNA break hot spots. *Mol Cell* **49**: 983-996.
- Fowler KR, Sasaki M, Milman N, Keeney S, Smith GR. 2014. Evolutionarily diverse determinants of meiotic DNA break and recombination landscapes across the genome. *Genome Res* **24**: 1650-1664.
- Frazer KA Ballinger DG Cox DR Hinds DA Stuve LL Gibbs RA Belmont JW Boudreau A Hardenbol P Leal SM et al. 2007. A second generation human haplotype map of over 3.1 million SNPs. *Nature* **449**: 851-861.
- Friberg U, Rice WR. 2008. Cut thy neighbor: cyclic birth and death of recombination hotspots via genetic conflict. *Genetics* **179**: 2229-2238.
- Friedman DB, Hollingsworth NM, Byers B. 1994. Insertional mutations in the yeast *HOP1* gene: evidence for multimeric assembly in meiosis. *Genetics* **136**: 449-464.
- Fukuda T, Daniel K, Wojtasz L, Toth A, Hoog C. 2010. A novel mammalian HORMA domain-containing protein, *HORMAD1*, preferentially associates with unsynapsed meiotic chromosomes. *Exp Cell Res* **316**: 158-171.
- Fukuda T, Kugou K, Sasanuma H, Shibata T, Ohta K. 2008. Targeted induction of meiotic double-strand breaks reveals chromosomal domain-dependent regulation of Spo11 and interactions among potential sites of meiotic recombination. *Nucleic Acids Res* **36**: 984-997.
- Galbraith AM, Malone RE. 1992. Characterization of *REC104*, a gene required for early meiotic recombination in the yeast *Saccharomyces cerevisiae*. *Dev Genet* **13**: 392-402.
- Garcia V, Gray S, Allison RM, Cooper TJ, Neale MJ. 2015. Tel1(ATM)-mediated interference suppresses clustered meiotic double-strand-break formation. *Nature* **520**: 114-118.
- Garcia V, Phelps SEL, Gray S, Neale MJ. 2011. Bidirectional resection of DNA double-strand breaks by Mre11 and Exo1. *Nature* **479**: 241-244.
- Gerton JL, DeRisi J, Shroff R, Lichten M, Brown PO, Petes TD. 2000. Global mapping of meiotic recombination hotspots and coldspots in the yeast *Saccharomyces cerevisiae*. *Proc Natl Acad Sci U S A* **97**: 11383-11390.
- Glynn EF, Megee PC, Yu H-G, Mistrot C, Unal E, Koshland DE, DeRisi J, Gerton JL. 2004. Genome-wide mapping of the cohesin complex in the yeast *Saccharomyces cerevisiae*. *PLoS Biol* **2**: e259.

- Goldfarb T, Lichten M. 2010. Frequent and efficient use of the sister chromatid for DNA double-strand break repair during budding yeast meiosis. *PLoS Biol* **8**: e1000520.
- Goldstein AL, McCusker JH. 1999. Three new dominant drug resistance cassettes for gene disruption in *Saccharomyces cerevisiae*. *Yeast* **15**: 1541-1553.
- Goodstadt L, Ponting CP. 2011. Is the control of recombination conserved among diverse eukaryotes? *Heredity* **106**: 710-711.
- Goodyer W, Kaitna S, Couteau F, Ward JD, Boulton SJ, Zetka M. 2008. HTP-3 links DSB formation with homolog pairing and crossing over during *C. elegans* meiosis. *Dev Cell* **14**: 263-274.
- Gottlieb S, Esposito RE. 1989. A new role for a yeast transcriptional silencer gene, SIR2, in regulation of recombination in ribosomal DNA. *Cell* **56**: 771-776.
- Govin J, Dorsey J, Gaucher J, Rousseaux S, Khochbin S, Berger SL. 2010. Systematic screen reveals new functional dynamics of histones H3 and H4 during gametogenesis. *Genes Dev* **24**: 1772-1786.
- Graille M, Cladiere L, Durand D, Lecointe F, Gadelle D, Quevillon-Cheruel S, Vachette P, Forterre P, van Tilbeurgh H. 2008. Crystal structure of an intact type II DNA topoisomerase: insights into DNA transfer mechanisms. *Structure* **16**: 360-370.
- Gray S, Allison RM, Garcia V, Goldman AS, Neale MJ. 2013. Positive regulation of meiotic DNA double-strand break formation by activation of the DNA damage checkpoint kinase Mec1(ATR). *Open Biol* **3**: 130019.
- Gregan J, Rabitsch PK, Sakem B, Csutak O, Latypov V, Lehmann E, Kohli J, Nasmyth K. 2005. Novel genes required for meiotic chromosome segregation are identified by a high-throughput knockout screen in fission yeast. *Curr Biol* **15**: 1663-1669.
- Grey C, Barthes P, Chauveau-Le Fric G, Langa F, Baudat F, de Massy B. 2011. Mouse PRDM9 DNA-binding specificity determines sites of histone H3 lysine 4 trimethylation for initiation of meiotic recombination. *PLoS Biol* **9**: e1001176.
- Gutz H. 1971. Site specific induction of gene conversion in *Schizosaccharomyces pombe*. *Genetics* **69**: 317-337.
- Hamant O, Ma H, Cande WZ. 2006. Genetics of meiotic prophase I in plants. *Annu Rev Plant Biol* **57**: 267-302.
- Handel MA, Schimenti JC. 2010. Genetics of mammalian meiosis: Regulation, dynamics and impact on fertility. *Nat Rev Genet* **11**: 124-136.
- Hassold T, Hunt P. 2001. To err (meiotically) is human: the genesis of human aneuploidy. *Nat Rev Genet* **2**: 280-291.
- Hawley RS, Irick H, Zitron AE, Haddox DA, Lohe A, New C, Whitley MD, Arbel T, Jang J, McKim K et al. 1992. There are two mechanisms of achiasmate segregation in

- Drosophila* females, one of which requires heterochromatic homology. *Dev Genet* **13**: 440-467.
- Hayashi K, Yoshida K, Matsui Y. 2005. A histone H3 methyltransferase controls epigenetic events required for meiotic prophase. *Nature* **438**: 374-378.
- Hayashi M, Chin GM, Villeneuve AM. 2007. *C. elegans* germ cells switch between distinct modes of double-strand break repair during meiotic prophase progression. *PLoS Genet* **3**: e191.
- Hayashi M, Mlynarczyk-Evans S, Villeneuve AM. 2010. The synaptonemal complex shapes the crossover landscape through cooperative assembly, crossover promotion and crossover inhibition during *Caenorhabditis elegans* meiosis. *Genetics* **186**: 45-58.
- Heil CS, Noor MA. 2012. Zinc finger binding motifs do not explain recombination rate variation within or between species of *Drosophila*. *PLoS One* **7**: e45055.
- Henderson KA, Kee K, Maleki S, Santini PA, Keeney S. 2006. Cyclin-Dependent Kinase directly regulates initiation of meiotic recombination. *Cell* **125**: 1321-1332.
- Henzel JV, Nabeshima K, Schvarzstein M, Turner BE, Villeneuve AM, Hillers KJ. 2011. An asymmetric chromosome pair undergoes synaptic adjustment and crossover redistribution during *Caenorhabditis elegans* meiosis: implications for sex chromosome evolution. *Genetics* **187**: 685-699.
- Hinch AG, Tandon A, Patterson N, Song Y, Rohland N, Palmer CD, Chen GK, Wang K, Buxbaum SG, Akyzbekova EL et al. 2011. The landscape of recombination in African Americans. *Nature* **476**: 170-175.
- Hirota K, Steiner WW, Shibata T, Ohta K. 2007. Multiple modes of chromatin configuration at natural meiotic recombination hot spots in fission yeast. *Eukaryot Cell* **6**: 2072-2080.
- Ho HC, Burgess SM. 2011. Pch2 acts through Xrs2 and Tel1/ATM to modulate interhomolog bias and checkpoint function during meiosis. *PLoS Genet* **7**: e1002351.
- Hochwagen A, Marais GA. 2010. Meiosis: a PRDM9 guide to the hotspots of recombination. *Curr Biol* **20**: R271-274.
- Hochwagen A, Tham W-H, Brar GA, Amon A. 2005. The FK506 binding protein Fpr3 counteracts protein phosphatase 1 to maintain meiotic recombination checkpoint activity. *Cell* **122**: 861-873.
- Hollingsworth NM, Byers B. 1989. *HOP1*: a yeast meiotic pairing gene. *Genetics* **121**: 445-462.
- Hollingsworth NM, Johnson AD. 1993. A conditional allele of the *Saccharomyces cerevisiae* *HOP1* gene is suppressed by overexpression of two other meiosis-specific genes: *RED1* and *REC104*. *Genetics* **133**: 785-797.

- Hollingsworth NM, Ponte L. 1997. Genetic interactions between *HOP1*, *RED1* and *MEK1* suggest that *MEK1* regulates assembly of axial element components during meiosis in the yeast *Saccharomyces cerevisiae*. *Genetics* **147**: 33-42.
- Humphryes N, Hochwagen A. 2014. A non-sister act: recombination template choice during meiosis. *Exp Cell Res* **329**: 53-60.
- Hunter N. 2007. Meiotic Recombination. in *Molecular Genetics of Recombination* (eds. A Aguilera, R Rothstein), pp. 381-442. Springer-Verlag, Heidelberg.
- Hunter N, Kleckner N. 2001. The single-end invasion: An asymmetric intermediate at the double-strand break to double-holliday junction transition of meiotic recombination. *Cell* **106**: 59-70.
- Hurst LD, Pal C, Lercher MJ. 2004. The evolutionary dynamics of eukaryotic gene order. *Nat Rev Genet* **5**: 299-310.
- Hurst LD, Williams EJ, Pal C. 2002. Natural selection promotes the conservation of linkage of co-expressed genes. *Trends Genet* **18**: 604-606.
- Hyppa RW, Smith GR. 2010. Crossover invariance determined by partner choice for meiotic DNA break repair. *Cell* **142**: 243-255.
- International HapMap C Frazer KA Ballinger DG Cox DR Hinds DA Stuve LL Gibbs RA Belmont JW Boudreau A Hardenbol P et al. 2007. A second generation human haplotype map of over 3.1 million SNPs. *Nature* **449**: 851-861.
- Ito M, Kugou K, Fawcett JA, Mura S, Ikeda S, Innan H, Ohta K. 2014. Meiotic recombination cold spots in chromosomal cohesion sites. *Genes Cells* **19**: 359-373.
- Jacinto E, Lorberg A. 2008. TOR regulation of AGC kinases in yeast and mammals. *The Biochem J* **410**: 19-37.
- Jang JK, Sherizen DE, Bhagat R, Manheim EA, McKim KS. 2003. Relationship of DNA double-strand breaks to synapsis in *Drosophila*. *J Cell Sci* **116**: 3069-3077.
- Jeffreys AJ, Kauppi L, Neumann R. 2001. Intensely punctate meiotic recombination in the class II region of the major histocompatibility complex. *Nat Genet* **29**: 217-222.
- Jeffreys AJ, Neumann R. 2002. Reciprocal crossover asymmetry and meiotic drive in a human recombination hot spot. *Nat Genet* **31**: 267-271.
- Jeffreys AJ, Neumann R. 2009. The rise and fall of a human recombination hot spot. *Nat Genet* **41**: 625-629.
- Jiao K, Salem L, Malone R. 2003. Support for a meiotic recombination initiation complex: Interactions among Rec102p, Rec104p, and Spo11p. *Mol Cell Biol* **23**: 5928-5938.

- Johnson LJ, Koufopanou V, Goddard MR, Hetherington R, Schafer SM, Burt A. 2004. Population genetics of the wild yeast *Saccharomyces paradoxus*. *Genetics* **166**: 43-52.
- Jolivet S, Vezon D, Froger N, Mercier R. 2006. Non conservation of the meiotic function of the Ski8/Rec103 homolog in *Arabidopsis*. *Genes Cells* **11**: 615-622.
- Joshi N, Barot A, Jamison C, Borner GV. 2009. Pch2 links chromosome axis remodeling at future crossover sites and crossover distribution during yeast meiosis. *PLoS Genet* **5**: e1000557.
- Joyce EF, Pedersen M, Tiong S, White-Brown SK, Paul A, Campbell SD, McKim KS. 2011. *Drosophila* ATM and ATR have distinct activities in the regulation of meiotic DNA damage and repair. *J Cell Biol* **195**: 359-367.
- Kaback DB, Guacci V, Barber D, Mahon JW. 1992. Chromosome size-dependent control of meiotic recombination. *Science* **256**: 228-232.
- Kaback DB, Steensma HY, de Jonge P. 1989. Enhanced meiotic recombination on the smallest chromosome of *Saccharomyces cerevisiae*. *Proc Natl Acad Sci U S A* **86**: 3694-3698.
- Kan F, Davidson MK, Wahls WP. 2010. Meiotic recombination protein Rec12: Functional conservation, crossover homeostasis and early crossover/non-crossover decision. *Nucleic Acids Res* **39**: 1460-1472.
- Kauppi L, Barchi M, Baudat F, Romanienko PJ, Keeney S, Jasin M. 2011. Distinct properties of the XY pseudoautosomal region crucial for male meiosis. *Science* **331**: 916-920.
- Kauppi L, Barchi M, Lange J, Baudat F, Jasin M, Keeney S. 2013. Numerical constraints and feedback control of double-strand breaks in mouse meiosis. *Genes Dev* **27**: 873-886.
- Kauppi L, Jeffreys AJ, Keeney S. 2004. Where the crossovers are: recombination distributions in mammals. *Nat Rev Genet* **5**: 413-424.
- Kaur T, Rockman MV. 2014. Crossover heterogeneity in the absence of hotspots in *Caenorhabditis elegans*. *Genetics* **196**: 137-148.
- Kee K, Keeney S. 2002. Functional interactions between *SPO11* and *REC102* during initiation of meiotic recombination in *Saccharomyces cerevisiae*. *Genetics* **160**: 111-122.
- Kee K, Protacio RU, Arora C, Keeney S. 2004. Spatial organization and dynamics of the association of Rec102 and Rec104 with meiotic chromosomes. *EMBO J* **23**: 1815-1824.
- Keeney S. 2001. Mechanisms and control of meiotic recombination initiation. *Curr Top Dev Biol* **52**: 1-53.

- Keeney S. 2007. Spo11 and the formation of DNA double-strand breaks in meiosis. in *Recombination and Meiosis* (eds. R Egel, DH Lankenau), pp. 81-123. Springer-Verlag, Berlin Heidelberg.
- Keeney S, Giroux CN, Kleckner N. 1997. Meiosis-specific DNA double-strand breaks are catalyzed by Spo11, a member of a widely conserved protein family. *Cell* **88**: 375-384.
- Keeney S, Kleckner N. 1995. Covalent protein-DNA complexes at the 5' strand termini of meiosis-specific double-strand breaks in yeast. *Proc Natl Acad Sci U S A* **92**: 11274-11278.
- Keeney S, Lange J, Mohibullah N. 2014. Self-organization of meiotic recombination initiation: general principles and molecular pathways. *Annu Rev Genet* **48**: 187-214.
- Keller PJ, Knop M. 2009. Evolution of mutational robustness in the yeast genome: a link to essential genes and meiotic recombination hotspots. *PLoS Genet* **5**: e1000533.
- Kellis M, Patterson N, Endrizzi M, Birren B, Lander ES. 2003. Sequencing and comparison of yeast species to identify genes and regulatory elements. *Nature* **423**: 241-254.
- Khil PP, Smagulova F, Brick KM, Camerini-Otero RD, Petukhova GV. 2012. Sensitive mapping of recombination hotspots using sequencing-based detection of ssDNA. *Genome Res* **22**: 957-965.
- Kim KP, Weiner BM, Zhang L, Jordan A, Dekker J, Kleckner N. 2010. Sister cohesion and structural axis components mediate homolog bias of meiotic recombination. *Cell* **143**: 924-937.
- Kim S, Peterson SE, Jasin M, Keeney S. 2016. Mechanisms of germ line genome instability. *Semin Cell Dev Biol* S1084-9521(16)30059-3.
- Kim Y, Rosenberg SC, Kugel CL, Kostow N, Rog O, Davydov V, Su TY, Dernburg AF, Corbett KD. 2014. The chromosome axis controls meiotic events through a hierarchical assembly of HORMA domain proteins. *Dev Cell* **31**: 487-502.
- Kinoshita E, Kinoshita-Kikuta E, Takiyama K, Koike T. 2006. Phosphate-binding tag, a new tool to visualize phosphorylated proteins. *Mol Cell Proteomics* **5**: 749-757.
- Kironmai KM, Muniyappa K, Friedman DB, Hollingsworth NM, Byers B. 1998. DNA-binding activities of Hop1 protein, a synaptonemal complex component from *Saccharomyces cerevisiae*. *Mol Cell Biol* **18**: 1424-1435.
- Kleckner N. 1996. Meiosis: How could it work? *Proc Natl Acad Sci U S A* **93**: 8167-8174.
- Kleckner N. 2006. Chiasma formation: Chromatin/axis interplay and the role(s) of the synaptonemal complex. *Chromosoma* **115**: 175-194.

- Klein F, Mahr P, Galova M, Buonomo SB, Michaelis C, Nairz K, Nasmyth K. 1999. A central role for cohesins in sister chromatid cohesion, formation of axial elements, and recombination during yeast meiosis. *Cell* **98**: 91-103.
- Kniewel R. 2012. Histone H3 phosphorylation and chromatin organization in yeast meiosis. Cornell University, New York.
- Knop M. 2006. Evolution of the hemiascomycete yeasts: on life styles and the importance of inbreeding. *BioEssays* **28**: 696-708.
- Kon N, Krawchuk MD, Warren BG, Smith GR, Wahls WP. 1997. Transcription factor Mts1/Mts2 (Atf1/Pcr1, Gad7/Pcr1) activates the M26 meiotic recombination hotspot in *Schizosaccharomyces pombe*. *Proc Natl Acad Sci U S A* **94**: 13765-13770.
- Kong A, Thorleifsson G, Gudbjartsson DF, Masson G, Sigurdsson A, Jonasdottir A, Walters GB, Jonasdottir A, Gylfason A, Kristinsson KT et al. 2010. Fine-scale recombination rate differences between sexes, populations and individuals. *Nature* **467**: 1099-1103.
- Kugou K, Fukuda T, Yamada S, Ito M, Sasanuma H, Mori S, Katou Y, Itoh T, Matsumoto K, Shibata T et al. 2009. Rec8 guides canonical Spo11 distribution along yeast meiotic chromosomes. *Mol Biol Cell* **20**: 3064-3076.
- Kumar R, Bourbon HM, de Massy B. 2010. Functional conservation of Mei4 for meiotic DNA double-strand break formation from yeasts to mice. *Genes Dev* **24**: 1266-1280.
- Kumar R, de Massy B. 2010. Initiation of meiotic recombination in mammals. *Genes* **1**: 521-549.
- Kumar R, Ghyselinc N, Ishiguro K, Watanabe Y, Kouznetsova A, Hoog C, Strong E, Schimenti J, Daniel K, Toth A et al. 2015. MEI4 - a central player in the regulation of meiotic DNA double-strand break formation in the mouse. *J Cell Sci* **128**: 1800-1811.
- Lacefield S, Ingolia N. 2006. Signal transduction: external signals influence spore-number control. *Curr Biol* **16**: R125-127.
- Lacefield S, Murray AW. 2007. The spindle checkpoint rescues the meiotic segregation of chromosomes whose crossovers are far from the centromere. *Nat Genet* **39**: 1273-1277.
- Lai YJ, Lin FM, Chuang MJ, Shen HJ, Wang TF. 2011. Genetic requirements and meiotic function of phosphorylation of the yeast axial element protein Red1. *Mol Cell Biol* **31**: 912-923.
- Lake CM, Nielsen RJ, Guo F, Unruh JR, Slaughter BD, Hawley RS. 2015. Vilya, a component of the recombination nodule, is required for meiotic double-strand break formation in *Drosophila*. *eLife* **4**: e08287.

- Lake CM, Nielsen RJ, Hawley RS. 2011. The *Drosophila* zinc finger protein trade embargo is required for double strand break formation in meiosis. *PLoS Genet* **7**: e1002005.
- Lam I, Keeney S. 2014. Mechanism and regulation of meiotic recombination initiation. *Cold Spring Harb Perspect Biol* **7**: a016634.
- Lam I, Keeney S. 2015. Nonparadoxical evolutionary stability of the recombination initiation landscape in yeast. *Science* **350**: 932-937.
- Lammers JH, Offenbergh HH, van Aalderen M, Vink AC, Dietrich AJ, Heyting C. 1994. The gene encoding a major component of the lateral elements of synaptonemal complexes of the rat is related to X-linked lymphocyte-regulated genes. *Mol Cell Biol* **14**: 1137-1146.
- Lange J, Pan J, Cole F, Thelen MP, Jasin M, Keeney S. 2011. ATM controls meiotic double-strand-break formation. *Nature* **479**: 237-240.
- Latypov V, Rothenberg M, Lorenz A, Octobre G, Csutak O, Lehmann E, Loidl J, Kohli J. 2010. Roles of Hop1 and Mek1 in meiotic chromosome pairing and recombination partner choice in *Schizosaccharomyces pombe*. *Mol Cell Biol* **30**: 1570-1581.
- Leem SH, Ogawa H. 1992. The *MRE4* gene encodes a novel protein kinase homologue required for meiotic recombination in *Saccharomyces cerevisiae*. *Nucleic Acids Res* **20**: 449-457.
- Lesecque Y, Glemin S, Lartillot N, Mouchiroud D, Duret L. 2014. The Red Queen model of recombination hotspots evolution in the light of archaic and modern human genomes. *PLoS Genet* **10**: e1004790.
- Lesecque Y, Mouchiroud D, Duret L. 2013. GC-biased gene conversion in yeast is specifically associated with crossovers: molecular mechanisms and evolutionary significance. *Mol Biol Evol* **30**: 1409-1419.
- Li J, Hooker GW, Roeder GS. 2006. *Saccharomyces cerevisiae* Mer2, Mei4 and Rec114 form a complex required for meiotic double-strand break formation. *Genetics* **173**: 1969-1981.
- Liang C, Stillman B. 1997. Persistent initiation of DNA replication and chromatin-bound MCM proteins during the cell cycle in *cdc6* mutants. *Genes Dev* **11**: 3375-3386.
- Libby BJ, De La Fuente R, O'Brien MJ, Wigglesworth K, Cobb J, Inselman A, Eaker S, Handel MA, Eppig JJ, Schimenti JC. 2002. The mouse meiotic mutation *mei1* disrupts chromosome synapsis with sexually dimorphic consequences for meiotic progression. *Dev Biol* **242**: 174-187.
- Libby BJ, Reinholdt LG, Schimenti JC. 2003. Positional cloning and characterization of *Mei1*, a vertebrate-specific gene required for normal meiotic chromosome synapsis in mice. *Proc Natl Acad Sci U S A* **100**: 15706-15711.

- Lichten M. 2008. Meiotic chromatin: The substrate for recombination initiation. in *Recombination and Meiosis* (eds. R Egel, DH Lankenau), pp. 165-193. Springer-Verlag, Heidelberg.
- Lichten M, de Massy B. 2011. The impressionistic landscape of meiotic recombination. *Cell* **147**: 267-270.
- Lichten M, Goldman ASH. 1995. Meiotic recombination hotspots. *Annu Rev Genetics* **29**: 423-444.
- Lin FM, Lai YJ, Shen HJ, Cheng YH, Wang TF. 2010. Yeast axial-element protein, Red1, binds SUMO chains to promote meiotic interhomologue recombination and chromosome synapsis. *EMBO J* **29**: 586-596.
- Liti G. 2015. The fascinating and secret wild life of the budding yeast *S. cerevisiae*. *eLife* **4**.
- Liti G, Carter DM, Moses AM, Warringer J, Parts L, James SA, Davey RP, Roberts IN, Burt A, Koufopanou V et al. 2009. Population genomics of domestic and wild yeasts. *Nature* **458**: 337-341.
- Liti G, Nguyen Ba AN, Blythe M, Muller CA, Bergstrom A, Cubillos FA, Dafhnis-Calas F, Khoshraftar S, Malla S, Mehta N et al. 2013. High quality de novo sequencing and assembly of the *Saccharomyces arboricolus* genome. *BMC genomics* **14**: 69.
- Liu H, Jang JK, Kato N, McKim KS. 2002. Mei-P22 encodes a chromosome-associated protein required for the initiation of meiotic recombination in *Drosophila melanogaster*. *Genetics* **162**: 245-258.
- Liu J, Wu TC, Lichten M. 1995. The location and structure of double-strand DNA breaks induced during yeast meiosis: evidence for a covalently linked DNA-protein intermediate. *EMBO J* **14**: 4599-4608.
- Loidl J. 2006. *S. pombe* linear elements: The modest cousins of synaptonemal complexes. *Chromosoma* **115**: 260-271.
- Loidl J, Klein F, Scherthan H. 1994. Homologous pairing is reduced but not abolished in asynaptic mutants of yeast. *J Cell Biol* **125**: 1191-1200.
- Longhese MP, Bonetti D, Guerini I, Manfrini N, Clerici M. 2009. DNA double-strand breaks in meiosis: checking their formation, processing and repair. *DNA repair* **8**: 1127-1138.
- Lorenz A, Estreicher A, Kohli J, Loidl J. 2006. Meiotic recombination proteins localize to linear elements in *Schizosaccharomyces pombe*. *Chromosoma* **115**: 330-340.
- Lorenz A, Wells JL, Pryce DW, Novatchkova M, Eisenhaber F, McFarlane RJ, Loidl J. 2004. *S. pombe* meiotic linear elements contain proteins related to synaptonemal complex components. *J Cell Sc* **117**: 3343-3351.

- Louis EJ. 1995. The chromosome ends of *Saccharomyces cerevisiae*. *Yeast* **11**: 1553-1573.
- Lu S, Zong C, Fan W, Yang M, Li J, Chapman AR, Zhu P, Hu X, Xu L, Yan L et al. 2012. Probing meiotic recombination and aneuploidy of single sperm cells by whole-genome sequencing. *Science* **338**: 1627-1630.
- Luo G, Yao MS, Bender CF, Mills M, Bladl AR, Bradley A, Petrini JH. 1999. Disruption of mRad50 causes embryonic stem cell lethality, abnormal embryonic development, and sensitivity to ionizing radiation. *Proc Natl Acad Sci U S A* **96**: 7376-7381.
- Lydall D, Nikolsky Y, Bishop DK, Weinert T. 1996. A meiotic recombination checkpoint controlled by mitotic checkpoint genes. *Nature* **383**: 840-843.
- Mahadevaiah SK, Turner JM, Baudat F, Rogakou EP, de Boer P, Blanco-Rodriguez J, Jasin M, Keeney S, Bonner WM, Burgoyne PS. 2001. Recombinational DNA double-strand breaks in mice precede synapsis. *Nat Genet* **27**: 271-276.
- Maleki S, Neale MJ, Arora C, Henderson KA, Keeney S. 2007. Interactions between Mei4, Rec114, and other proteins required for meiotic DNA double-strand break formation in *Saccharomyces cerevisiae*. *Chromosoma* **116**: 471-486.
- Malone RE, Bullard S, Hermiston M, Rieger R, Cool M, Galbraith A. 1991. Isolation of mutants defective in early steps of meiotic recombination in the yeast *Saccharomyces cerevisiae*. *Genetics* **128**: 79-88.
- Malone RE, Pittman DL, Nau JJ. 1997. Examination of the intron in the meiosis-specific recombination gene *REC114* in *Saccharomyces*. *Mol Gen Genet* **255**: 410-419.
- Mancera E, Bourgon R, Brozzi A, Huber W, Steinmetz LM. 2008. High-resolution mapping of meiotic crossovers and non-crossovers in yeast. *Nature* **454**: 479-485.
- Manzano-Winkler B, McGaugh SE, Noor MA. 2013. How hot are *Drosophila* hotspots? examining recombination rate variation and associations with nucleotide diversity, divergence, and maternal age in *Drosophila pseudoobscura*. *PLoS One* **8**: e71582.
- Mao-Draayer Y, Galbraith AM, Pittman DL, Cool M, Malone RE. 1996. Analysis of meiotic recombination pathways in yeast *Saccharomyces cerevisiae*. *Genetics* **144**: 71-86.
- Marie-Nelly H, Marbouty M, Cournac A, Flot JF, Liti G, Parodi DP, Syan S, Guillen N, Margeot A, Zimmer C et al. 2014. High-quality genome (re)assembly using chromosomal contact data. *Nat Commun* **5**: 5695.
- Martin-Castellanos C, Blanco M, Rozalen AE, Perez-Hidalgo L, Garcia AI, Conde F, Mata J, Ellermeier C, Davis L, San-Segundo P et al. 2005. A large-scale screen in *S. pombe* identifies seven novel genes required for critical meiotic events. *Curr Biol* **15**: 2056-2062.

- Martin-Castellanos C, Fowler KR, Smith GR. 2013. Making chromosomes hot for breakage. *Cell Cycle* **12**: 1327-1328.
- Martinez-Perez E, Villeneuve AM. 2005. HTP-1-dependent constraints coordinate homolog pairing and synapsis and promote chiasma formation during *C. elegans* meiosis. *Genes Dev* **19**: 2727-2743.
- Martini E, Diaz RL, Hunter N, Keeney S. 2006. Crossover homeostasis in yeast meiosis. *Cell* **126**: 285-295.
- Masai H, Arai K. 2002. Cdc7 kinase complex: a key regulator in the initiation of DNA replication. *J Cell Physiol* **190**: 287-296.
- McKee AH, Kleckner N. 1997. Mutations in *Saccharomyces cerevisiae* that block meiotic prophase chromosome metabolism and confer cell cycle arrest at pachytene identify two new meiosis-specific genes *SAE1* and *SAE3*. *Genetics* **146**: 817-834.
- McKim KS, Green-Marroquin BL, Sekelsky JJ, Chin G, Steinberg C, Khodosh R, Hawley RS. 1998. Meiotic synapsis in the absence of recombination. *Science* **279**: 876-878.
- McMahill MS, Sham CW, Bishop DK. 2007. Synthesis-dependent strand annealing in meiosis. *PLoS Biol* **5**: e299.
- McVean GA, Myers SR, Hunt S, Deloukas P, Bentley DR, Donnelly P. 2004. The fine-scale structure of recombination rate variation in the human genome. *Science* **304**: 581-584.
- Mehrotra S, McKim KS. 2006. Temporal analysis of meiotic DNA double-strand break formation and repair in *Drosophila* females. *PLoS Genet* **2**: e200.
- Meneely PM, McGovern OL, Heinis FI, Yanowitz JL. 2012. Crossover distribution and frequency are regulated by *him-5* in *Caenorhabditis elegans*. *Genetics* **190**: 1251-1266.
- Mercier R, Armstrong SJ, Horlow C, Jackson NP, Makaroff CA, Vezon D, Pelletier G, Jones GH, Franklin FC. 2003. The meiotic protein SWI1 is required for axial element formation and recombination initiation in *Arabidopsis*. *Development* **130**: 3309-3318.
- Mercier R, Mezard C, Jenczewski E, Macaisne N, Grelon M. 2015. The molecular biology of meiosis in plants. *Annu Rev Plant Biol* **66**: 297-327.
- Mercier R, Vezon D, Bullier E, Motamayor JC, Sellier A, Lefevre F, Pelletier G, Horlow C. 2001. SWITCH1 (SWI1): a novel protein required for the establishment of sister chromatid cohesion and for bivalent formation at meiosis. *Genes Dev* **15**: 1859-1871.
- Mieczkowski PA, Dominska M, Buck MJ, Gerton JL, Lieb JD, Petes TD. 2006. Global analysis of the relationship between the binding of the Bas1p transcription factor

and meiosis-specific double-strand DNA breaks in *Saccharomyces cerevisiae*. *Mol Cell Biol* **26**: 1014-1027.

- Mieczkowski PA, Dominska M, Buck MJ, Lieb JD, Petes TD. 2007. Loss of a histone deacetylase dramatically alters the genomic distribution of Spo11p-catalyzed DNA breaks in *Saccharomyces cerevisiae*. *Proc Natl Acad Sci U S A* **104**: 3955-3960.
- Milman N, Higushi E, Smith GR. 2009. Meiotic DNA double-strand break repair requires two nucleases, MRN and Ctp1, to produce a single size class of Rec12 (Spo11)-oligonucleotide complexes. *Mol Cell Biol* **29**: 5998-6005.
- Miyoshi T, Ito M, Kugou K, Yamada S, Furuichi M, Oda A, Yamada T, Hirota K, Masai H, Ohta K. 2012. A central coupler for recombination initiation linking chromosome architecture to S phase checkpoint. *Mol Cell* **47**: 722-733.
- Miyoshi T, Ito M, Ohta K. 2013. Spatiotemporal regulation of meiotic recombination by Liaisonin. *BioArchitecture* **3**: 1-5.
- Moens PB, Pearlman RE, Heng HHQ, Traut W. 1998. Chromosome cores and chromatin at meiotic prophase. *Curr Top Dev Biol* **37**: 241-262.
- Mok J, Im H, Snyder M. 2009. Global identification of protein kinase substrates by protein microarray analysis. *Nat Protoc* **4**: 1820-1827.
- Molnar M, Parisi S, Kakihara Y, Nojima H, Yamamoto A, Hiraoka Y, Bozsi A, Sipiczki M, Kohli J. 2001. Characterization of *rec7*, an early meiotic recombination gene in *Schizosaccharomyces pombe*. *Genetics* **157**: 519-532.
- Montagnoli A, Valsasina B, Brotherton D, Troiani S, Rainoldi S, Tenca P, Molinari A, Santocanale C. 2006. Identification of Mcm2 phosphorylation sites by S-phase-regulating kinases. *J Biol Chem* **281**: 10281-10290.
- Morgan TH. 1912. Complete linkage in the second chromosome of the male of *Drosophila*. *Science* **36**: 719-720.
- Mortimer RK, Contopoulou CR, King JS. 1992. Genetic and physical maps of *Saccharomyces cerevisiae*, Edition 11. *Yeast* **8**: 817-902.
- Mugal CF, Weber CC, Ellegren H. 2015. GC-biased gene conversion links the recombination landscape and demography to genomic base composition: GC-biased gene conversion drives genomic base composition across a wide range of species. *BioEssays* **37**: 1317-1326.
- Muniyappa K, Kshirsagar R, Ghodke I. 2014. The HORMA domain: an evolutionarily conserved domain discovered in chromatin-associated proteins, has unanticipated diverse functions. *Gene* **545**: 194-197.
- Muñoz-Fuentes V, Di Rienzo A, Vila C. 2011. Prdm9, a major determinant of meiotic recombination hotspots, is not functional in dogs and their wild relatives, wolves and coyotes. *PLoS One* **6**: e25498.

- Murakami H, Borde V, Nicolas A, Keeney S. 2009. Gel electrophoresis assays for analyzing DNA double-strand breaks in *Saccharomyces cerevisiae* at various spatial resolutions. *Methods Mol Biol* **557**: 117-142.
- Murakami H, Borde V, Shibata T, Lichten M, Ohta K. 2003. Correlation between premeiotic DNA replication and chromatin transition at yeast recombination initiation sites. *Nucleic Acids Res* **31**: 4085-4090.
- Murakami H, Keeney S. 2008. Regulating the formation of DNA double-strand breaks in meiosis. *Genes Dev* **22**: 286-292.
- Murakami H, Keeney S. 2014. Temporospatial coordination of meiotic DNA replication and recombination via DDK recruitment to replisomes. *Cell* **158**: 861-873.
- Murakami H, Nicolas A. 2009. Locally, meiotic double-strand breaks targeted by Gal4BD-Spo11 occur at discrete sites with a sequence preference. *Mol Cell Biol* **29**: 3500-3516.
- Murton BL, Chin WL, Ponting CP, Itzhaki LS. 2010. Characterising the binding specificities of the subunits associated with the KMT2/Set1 histone lysine methyltransferase. *J Mol Biol* **398**: 481-488.
- Myers S, Bottolo L, Freeman C, McVean G, Donnelly P. 2005. A fine-scale map of recombination rates and hotspots across the human genome. *Science* **310**: 321-324.
- Myers S, Bowden R, Tumian A, Bontrop RE, Freeman C, MacFie TS, McVean G, Donnelly P. 2010. Drive against hotspot motifs in primates implicates the *PRDM9* gene in meiotic recombination. *Science* **327**: 876-879.
- Myers S, Freeman C, Auton A, Donnelly P, McVean G. 2008. A common sequence motif associated with recombination hot spots and genome instability in humans. *Nat Genet* **40**: 1124-1129.
- Nabeshima K, Villeneuve AM, Hillers KJ. 2004. Chromosome-wide regulation of meiotic crossover formation in *Caenorhabditis elegans* requires properly assembled chromosome axes. *Genetics* **168**: 1275-1292.
- Nambiar M, Smith GR. 2016. Repression of harmful meiotic recombination in centromeric regions. *Semin Cell Dev Biol* S1084-9521(16)30039-8.
- Narasimhan VM, Hunt KA, Mason D, Baker CL, Karczewski KJ, Barnes MR, Barnett AH, Bates C, Bellary S, Bockett NA et al. 2016. Health and population effects of rare gene knockouts in adult humans with related parents. *Science*: aac8624.
- Neale MJ, Keeney S. 2009. End-labeling and analysis of Spo11-oligonucleotide complexes in *Saccharomyces cerevisiae*. *Methods Mol Biol* **557**: 183-195.
- Neale MJ, Pan J, Keeney S. 2005. Endonucleolytic processing of covalent protein-linked DNA double-strand breaks. *Nature* **436**: 1053-1057.

- Nichols MD, DeAngelis K, Keck JL, Berger JM. 1999. Structure and function of an archaeal topoisomerase VI subunit with homology to the meiotic recombination factor Spo11. *EMBO J* **18**: 6177-6188.
- Nicolas A, Treco D, Schultes NP, Szostak JW. 1989. An initiation site for meiotic gene conversion in the yeast *Saccharomyces cerevisiae*. *Nature* **338**: 35-39.
- Nishant KT, Chen C, Shinohara M, Shinohara A, Alani E. 2010. Genetic analysis of baker's yeast Msh4-Msh5 reveals a threshold crossover level for meiotic viability. *PLoS Genet* **6**.
- Niu H, Li X, Job E, Park C, Moazed D, Gygi SP, Hollingsworth NM. 2007. Mek1 kinase is regulated to suppress double-strand break repair between sister chromatids during budding yeast meiosis. *Mol Cell Biol* **27**: 5456-5467.
- Niu H, Wan L, Baumgartner B, Schaefer D, Loidl J, Hollingsworth NM. 2005. Partner choice during meiosis is regulated by Hop1-promoted dimerization of Mek1. *Mol Biol Cell* **16**: 5804-5818.
- Niu H, Wan L, Busygina V, Kwon Y, Allen JA, Li X, Kunz RC, Kubota K, Wang B, Sung P et al. 2009. Regulation of meiotic recombination via Mek1-mediated Rad54 phosphorylation. *Mol Cell* **36**: 393-404.
- Nonomura K, Nakano M, Fukuda T, Eiguchi M, Miyao A, Hirochika H, Kurata N. 2004. The novel gene HOMOLOGOUS PAIRING ABERRATION IN RICE MEIOSIS1 of rice encodes a putative coiled-coil protein required for homologous chromosome pairing in meiosis. *Plant Cell* **16**: 1008-1020.
- Noor MA. 2008. Mutagenesis from meiotic recombination is not a primary driver of sequence divergence between *Saccharomyces species*. *Mol Biol Evol* **25**: 2439-2444.
- Odenthal-Hesse L, Berg IL, Veselis A, Jeffreys AJ, May CA. 2014. Transmission distortion affecting human noncrossover but not crossover recombination: a hidden source of meiotic drive. *PLoS Genet* **10**: e1004106.
- Offenberg HH, Schalk JA, Meuwissen RL, van Aalderen M, Kester HA, Dietrich AJ, Heyting C. 1998. SCP2: a major protein component of the axial elements of synaptonemal complexes of the rat. *Nucleic Acids Res* **26**: 2572-2579.
- Ohta K, Shibata T, Nicolas A. 1994. Changes in chromatin structure at recombination initiation sites during yeast meiosis. *EMBO J* **13**: 5754-5763.
- Okamoto S, Iino T. 1981. Selective abortion of two nonsister nuclei in a developing ascus of the *hfd-1* mutant in *Saccharomyces cerevisiae*. *Genetics* **99**: 197-209.
- Okaz E, Arguello-Miranda O, Bogdanova A, Vinod PK, Lipp JJ, Markova Z, Zagoriy I, Novak B, Zachariae W. 2012. Meiotic prophase requires proteolysis of M phase regulators mediated by the meiosis-specific APC/C^{Am1}. *Cell* **151**: 603-618.

- Oliver PL, Goodstadt L, Bayes JJ, Birtle Z, Roach KC, Phadnis N, Beatson SA, Lunter G, Malik HS, Ponting CP. 2009. Accelerated evolution of the Prdm9 speciation gene across diverse metazoan taxa. *PLoS Genet* **5**: e1000753.
- Padmore R, Cao L, Kleckner N. 1991. Temporal comparison of recombination and synaptonemal complex formation during meiosis in *S. cerevisiae*. *Cell* **66**: 1239-1256.
- Page SL, Hawley RS. 2003. Chromosome choreography: The meiotic ballet. *Science* **301**: 785-789.
- Page SL, Hawley RS. 2004. The genetics and molecular biology of the synaptonemal complex. *Annu Rev Cell Dev Biol* **20**: 525-558.
- Page SL, Nielsen RJ, Teeter K, Lake CM, Ong S, Wright KR, Dean KL, Agne D, Gilliland WD, Hawley RS. 2007. A germline clone screen for meiotic mutants in *Drosophila melanogaster*. *Fly* **1**: 172-181.
- Pan J, Sasaki M, Kniewel R, Murakami H, Blitzblau HG, Tischfield SE, Zhu X, Neale MJ, Jasin M, Socci ND et al. 2011. A hierarchical combination of factors shapes the genome-wide topography of yeast meiotic recombination initiation. *Cell* **144**: 719-731.
- Panizza S, Mendoza MA, Berlinger M, Huang L, Nicolas A, Shirahige K, Klein F. 2011. Spo11-accessory proteins link double-strand break sites to the chromosome axis in early meiotic recombination. *Cell* **146**: 372-383.
- Parvanov ED, Petkov PM, Paigen K. 2010. Prdm9 controls activation of mammalian recombination hotspots. *Science* **327**: 835.
- Pawlowski WP, Golubovskaya IN, Timofejeva L, Meeley RB, Sheridan WF, Cande WZ. 2004. Coordination of meiotic recombination, pairing, and synapsis by PHS1. *Science* **303**: 89-92.
- Pearson RB, Kemp BE. 1991. Protein kinase phosphorylation site sequences and consensus specificity motifs: tabulations. *Methods Enzymol* **200**: 62-81.
- Peciña A, Smith KN, Mezard C, Murakami H, Ohta K, Nicolas A. 2002. Targeted stimulation of meiotic recombination. *Cell* **111**: 173-184.
- Peters AD. 2008. A combination of cis and trans control can solve the hotspot conversion paradox. *Genetics* **178**: 1579-1593.
- Petes TD. 2001. Meiotic recombination hot spots and cold spots. *Nat Rev Genet* **2**: 360-369.
- Petes TD, Botstein D. 1977. Simple Mendelian inheritance of the reiterated ribosomal DNA of yeast. *Proc Natl Acad Sci U S A* **74**: 5091-5095.
- Pineda-Krch M, Redfield RJ. 2005. Persistence and loss of meiotic recombination hotspots. *Genetics* **169**: 2319-2333.

- Pokholok DK, Harbison CT, Levine S, Cole M, Hannett NM, Lee TI, Bell GW, Walker K, Rolfe PA, Herbolsheimer E et al. 2005. Genome-wide map of nucleosome acetylation and methylation in yeast. *Cell* **122**: 517-527.
- Ponting CP. 2011. What are the genomic drivers of the rapid evolution of PRDM9? *Trends Genet* **27**: 165-171.
- Pratto F, Brick K, Khil P, Smagulova F, Petukhova GV, Camerini-Otero RD. 2014. DNA recombination. Recombination initiation maps of individual human genomes. *Science* **346**: 1256442.
- Prieler S, Penkner A, Borde V, Klein F. 2005. The control of Spo11's interaction with meiotic recombination hotspots. *Genes Dev* **19**: 255-269.
- Prinz S, Amon A, Klein F. 1997. Isolation of *COM1*, a new gene required to complete meiotic double-strand break-induced recombination in *Saccharomyces cerevisiae*. *Genetics* **146**: 781-795.
- Przewloka MR, Glover DM. 2009. The kinetochore and the centromere: a working long distance relationship. *Annu Rev Genet* **43**: 439-465.
- Ptak SE, Hinds DA, Koehler K, Nickel B, Patil N, Ballinger DG, Przeworski M, Frazer KA, Paabo S. 2005. Fine-scale recombination patterns differ between chimpanzees and humans. *Nat Genet* **37**: 429-434.
- Puizina J, Siroky J, Mokros P, Schweizer D, Riha K. 2004. Mre11 deficiency in *Arabidopsis* is associated with chromosomal instability in somatic cells and Spo11-dependent genome fragmentation during meiosis. *Plant Cell* **16**: 1968-1978.
- Reddy KC, Villeneuve AM. 2004. *C. elegans* HIM-17 links chromatin modification and competence for initiation of meiotic recombination. *Cell* **118**: 439-452.
- Reinholdt LG, Schimenti JC. 2005. Mei1 is epistatic to Dmc1 during mouse meiosis. *Chromosoma* **114**: 127-134.
- Replansky T, Koufopanou V, Greig D, Bell G. 2008. *Saccharomyces sensu stricto* as a model system for evolution and ecology. *Trends Ecol Evol* **23**: 494-501.
- Richard G-F, Kerrest A, Lafontaine I, Dujon B. 2005. Comparative genomics of hemiascomycete yeasts: Genes involved in DNA replication, repair, and recombination. *Mol Biol Evol* **22**: 1011-1023.
- Robert T, Nore A, Brun C, Maffre C, Crimi B, Bourbon HM, de Massy B. 2016. The TopoVIB-Like protein family is required for meiotic DNA double-strand break formation. *Science* **351**: 943-949.
- Rocco V, Nicolas A. 1996. Sensing of DNA non-homology lowers the initiation of meiotic recombination in yeast. *Genes Cells* **1**: 645-661.

- Rockmill B, Lefrancois P, Voelkel-Meiman K, Oke A, Roeder GS, Fung JC. 2013. High throughput sequencing reveals alterations in the recombination signatures with diminishing Spo11 activity. *PLoS Genet* **9**: e1003932.
- Rockmill B, Roeder GS. 1988. *RED1*: A yeast gene required for the segregation of chromosomes during the reductional division of meiosis. *Proc Natl Acad Sci U S A* **85**: 6057-6061.
- Rockmill B, Roeder GS. 1990. Meiosis in asynaptic yeast. *Genetics* **126**: 563-574.
- Rockmill B, Roeder GS. 1991. A meiosis-specific protein kinase homolog required for chromosome synapsis and recombination. *Genes Dev* **5**: 2392-2404.
- Rockmill B, Voelkel-Meiman K, Roeder GS. 2006. Centromere-proximal crossovers are associated with precocious separation of sister chromatids during meiosis in *Saccharomyces cerevisiae*. *Genetics* **174**: 1745-1754.
- Roeder GS. 1995. Sex and the single cell: meiosis in yeast. *Proc Natl Acad Sci U S A* **92**: 10450-10456.
- Roeder GS, Bailis JM. 2000. The pachytene checkpoint. *Trends Genet* **16**: 395-403.
- Romanienko PJ, Camerini-Otero RD. 2000. The mouse Spo11 gene is required for meiotic chromosome synapsis. *Mol Cell* **6**: 975-987.
- Rosenberg SC, Corbett KD. 2015. The multifaceted roles of the HORMA domain in cellular signaling. *J Cell Biol* **211**: 745-755.
- Rosu S, Zawadzki KA, Stamper EL, Libuda DE, Reese AL, Dernburg AF, Villeneuve AM. 2013. The *C. elegans* DSB-2 protein reveals a regulatory network that controls competence for meiotic DSB formation and promotes crossover assurance. *PLoS Genet* **9**: e1003674.
- Rothstein R. 1991. Targeting, disruption, replacement, and allele rescue: Integrative DNA transformation in yeast. *Methods Enzymol* **194**: 281-301.
- Ruderfer DM, Pratt SC, Seidel HS, Kruglyak L. 2006. Population genomic analysis of outcrossing and recombination in yeast. *Nat Genet* **38**: 1077-1081.
- Salem L, Walter N, Malone R. 1999. Suppressor analysis of the *Saccharomyces cerevisiae* gene *REC104* reveals a genetic interaction with *REC102*. *Genetics* **151**: 1261-1272.
- San Filippo J, Sung P, Klein H. 2008. Mechanism of eukaryotic homologous recombination. *Ann Rev Biochem* **77**: 229-257.
- San-Segundo PA, Roeder GS. 1999. Pch2 links chromatin silencing to meiotic checkpoint control. *Cell* **97**: 313-324.

- Sanchez-Moran E, Santos JL, Jones GH, Franklin FC. 2007. ASY1 mediates AtDMC1-dependent interhomolog recombination during meiosis in *Arabidopsis*. *Genes Dev* **21**: 2220-2233.
- Sasaki M, Lange J, Keeney S. 2010. Genome destabilization by homologous recombination in the germ line. *Nature* **11**: 182-195.
- Sasanuma H, Hirota K, Fukuda T, Kakusho N, Kugou K, Kawasaki Y, Shibata T, Masai H, Ohta K. 2008. Cdc7-dependent phosphorylation of Mer2 facilitates initiation of yeast meiotic recombination. *Genes Dev* **22**: 398-410.
- Sasanuma H, Murakami H, Fukuda T, Shibata T, Nicolas A, Ohta K. 2007. Meiotic association between Spo11 regulated by Rec102, Rec104 and Rec114. *Nucleic Acids Res* **35**: 1119-1133.
- Scannell DR, Zill OA, Rokas A, Payen C, Dunham MJ, Eisen MB, Rine J, Johnston M, Hittinger CT. 2011. The awesome power of yeast evolutionary genetics: new genome sequences and strain resources for the *Saccharomyces sensu stricto* genus. *G3* **1**: 11-25.
- Schild D, Byers B. 1978. Meiotic effects of DNA-defective cell division cycle mutations of *Saccharomyces cerevisiae*. *Chromosoma* **70**: 109-130.
- Schwacha A, Kleckner N. 1994. Identification of joint molecules that form frequently between homologs but rarely between sister chromatids during yeast meiosis. *Cell* **76**: 51-63.
- Schwacha A, Kleckner N. 1997. Interhomolog bias during meiotic recombination: meiotic functions promote a highly differentiated interhomolog-only pathway. *Cell* **90**: 1123-1135.
- Sclafani RA. 2000. Cdc7p-Dbf4p becomes famous in the cell cycle. *J Cell Sci* **113**: 2111-2117.
- Serrentino M-E, Borde V. 2012. The spatial regulation of meiotic recombination hotspots: Are all DSB hotspots crossover hotspots? *Exp Cell Res* **318**: 1347-1352.
- Shi X, Kachirskaia I, Walter KL, Kuo JH, Lake A, Davrazou F, Chan SM, Martin DG, Fingerman IM, Briggs SD et al. 2007. Proteome-wide analysis in *Saccharomyces cerevisiae* identifies several PHD fingers as novel direct and selective binding modules of histone H3 methylated at either lysine 4 or lysine 36. *J Biol Chem* **282**: 2450-2455.
- Shin YH, Choi Y, Erdin SU, Yatsenko SA, Kloc M, Yang F, Wang PJ, Meistrich ML, Rajkovic A. 2010. Hormad1 mutation disrupts synaptonemal complex formation, recombination, and chromosome segregation in mammalian meiosis. *PLoS Genet* **6**: e1001190.
- Shingu Y, Mikawa T, Onuma M, Hirayama T, Shibata T. 2010. A DNA-binding surface of SPO11-1, an *Arabidopsis* SPO11 orthologue required for normal meiosis. *FEBS J* **277**: 2360-2374.

- Shuster EO, Byers B. 1989. Pachytene arrest and other meiotic effects of the start mutations in *Saccharomyces cerevisiae*. *Genetics* **123**: 29-43.
- Sikorski RS, Hieter P. 1989. A system of shuttle vectors and yeast host strains designed for efficient manipulation of DNA in *Saccharomyces cerevisiae*. *Genetics* **122**: 19-27.
- Singh ND, Aquadro CF, Clark AG. 2009. Estimation of fine-scale recombination intensity variation in the *white-echinus* interval of *D. melanogaster*. *J Mol Evol* **69**: 42-53.
- Singhal S, Leffler EM, Sannareddy K, Turner I, Venn O, Hooper DM, Strand AI, Li Q, Raney B, Balakrishnan CN et al. 2015. Stable recombination hotspots in birds. *Science* **350**: 928-932.
- Smagulova F, Brick K, Pu Y, Camerini-Otero RD, Petukhova GV. 2016. The evolutionary turnover of recombination hot spots contributes to speciation in mice. *Genes Dev* **30**: 266-280.
- Smagulova F, Gregoret IV, Brick K, Khil P, Camerini-Otero RD, Petukhova GV. 2011. Genome-wide analysis reveals novel molecular features of mouse recombination hotspots. *Nature* **472**: 375-378.
- Smith AV, Roeder GS. 1997. The yeast Red1 protein localizes to the cores of meiotic chromosomes. *J Cell Biol* **136**: 957-967.
- Smith KN, Penkner A, Ohta K, Klein F, Nicolas A. 2001. B-type cyclins *CLB5* and *CLB6* control the initiation of recombination and synaptonemal complex formation in yeast meiosis. *Curr Biol* **11**: 88-97.
- Smukowski CS, Noor MA. 2011. Recombination rate variation in closely related species. *Heredity* **107**: 496-508.
- Smukowski Heil CS, Ellison C, Dubin M, Noor MA. 2015. Recombining without hotspots: a comprehensive evolutionary portrait of recombination in two closely related species of *Drosophila*. *Genome Biol Evol* **7**: 2829-2842.
- Sollier J, Lin W, Soustelle C, Suhre K, Nicolas A, Géli V, de La Roche Saint-André C. 2004. Set1 is required for meiotic S-phase onset, double-strand break formation and middle gene expression. *EMBO J* **23**: 1957-1967.
- Sommermeier V, Béneut C, Chaplais E, Serrentino M-E, Borde V. 2013. Spp1, a member of the Set1 complex, promotes meiotic DSB formation in promoters by tethering histone H3K4 methylation sites to chromosome axes. *Mol Cell* **49**: 43-54.
- Sourirajan A, Lichten M. 2008. Polo-like kinase Cdc5 drives exit from pachytene during budding yeast meiosis. *Genes Dev* **22**: 2627-2632.
- Stamper EL, Rodenbusch SE, Rosu S, Ahringer J, Villeneuve AM, Dernburg AF. 2013. Identification of DSB-1, a protein required for initiation of meiotic recombination in

- C. elegans*, illuminates a checkpoint that promotes crossover assurance. *PLoS Genet* **9**: e1003679.
- Stanzione M, Baumann M, Papanikos F, Dereli I, Lange J, Ramlal A, Trankner D, Shibuya H, de Massy B, Watanabe Y et al. submitted. Meiotic DNA break formation requires the unsynapsed chromosome axis-binding protein IHO1 (CCDC36) in mice.
- Steiner S, Kohli J, Ludin K. 2010. Functional interactions among members of the meiotic initiation complex in fission yeast. *Curr Genet* **56**: 237-249.
- Stevison LS, Woerner AE, Kidd JM, Kelley JL, Veeramah KR, McManus KF, Great Ape Genome P, Bustamante CD, Hammer MF, Wall JD. 2015. The time scale of recombination rate evolution in Great Apes. *Mol Biol Evol* **33**: 928-945.
- Stracker TH, Theunissen JW, Morales M, Petrini JH. 2004. The Mre11 complex and the metabolism of chromosome breaks: the importance of communicating and holding things together. *DNA repair* **3**: 845-854.
- Subramanian VV, Hochwagen A. 2014. The meiotic checkpoint network: step-by-step through meiotic prophase. *Cold Spring Harb Perspect Biol* **6**: a016675.
- Subramanian VV, MacQueen AJ, Vader G, Shinohara M, Sanchez A, Borde V, Shinohara A, Hochwagen A. 2016. Chromosome Synapsis Alleviates Mek1-Dependent Suppression of Meiotic DNA Repair. *PLoS Biol* **14**: e1002369.
- Sun H, Treco D, Schultes NP, Szostak JW. 1989. Double-strand breaks at an initiation site for meiotic gene conversion. *Nature* **338**: 87-90.
- Sun H, Treco D, Szostak JW. 1991. Extensive 3'-overhanging, single-stranded DNA associated with the meiosis-specific double-strand breaks at the *ARG4* recombination initiation site. *Cell* **64**: 1155-1161.
- Sun X, Huang L, Markowitz TE, Blitzblau HG, Chen D, Klein F, Hochwagen A. 2015. Transcription dynamically patterns the meiotic chromosome-axis interface. *eLife* **4**: e07424.
- Székvolgyi L, Nicolas A. 2010. From meiosis to postmeiotic events: Homologous recombination is obligatory but flexible. *FEBS J* **277**: 571-589.
- Szostak JW, Orr-Weaver TL, Rothstein RJ, Stahl FW. 1983. The double-strand-break repair model for recombination. *Cell* **33**: 25-35.
- Tarsounas M, Morita T, Pearlman RE, Moens PB. 1999. RAD51 and DMC1 form mixed complexes associated with mouse meiotic chromosome cores and synaptonemal complexes. *J Cell Biol* **147**: 207-219.
- Taxis C, Keller P, Kavagiou Z, Jensen LJ, Colombelli J, Bork P, Stelzer EH, Knop M. 2005. Spore number control and breeding in *Saccharomyces cerevisiae*: a key role for a self-organizing system. *J Cell Biol* **171**: 627-640.

- Terentyev Y, Johnson R, Neale MJ, Khisroon M, Bishop-Bailey A, Goldman AS. 2010. Evidence that *MEK1* positively promotes interhomologue double-strand break repair. *Nucleic Acids Res* **38**: 4349-4360.
- Thacker D, Mohibullah N, Zhu X, Keeney S. 2014. Homologue engagement controls meiotic DNA break number and distribution. *Nature* **510**: 241-246.
- Thomas JH, Emerson RO, Shendure J. 2009. Extraordinary molecular evolution in the *PRDM9* fertility gene. *PLoS One* **4**: e8505.
- Tirosh I, Sigal N, Barkai N. 2010. Divergence of nucleosome positioning between two closely related yeast species: genetic basis and functional consequences. *Mol Syst Biol* **6**: 365.
- Tischfield SE, Keeney S. 2012. Scale matters: The spatial correlation of yeast meiotic DNA breaks with histone H3 trimethylation is driven largely by independent colocalization at promoters. *Cell Cycle* **11**: 1496-1503.
- Tsai IJ, Bensasson D, Burt A, Koufopanou V. 2008. Population genomics of the wild yeast *Saccharomyces paradoxus*: Quantifying the life cycle. *Proc Natl Acad Sci U S A* **105**: 4957-4962.
- Tsai IJ, Burt A, Koufopanou V. 2010. Conservation of recombination hotspots in yeast. *Proc Natl Acad Sci U S A* **107**: 7847-7852.
- Tsankov AM, Thompson DA, Socha A, Regev A, Rando OJ. 2010. The role of nucleosome positioning in the evolution of gene regulation. *PLoS Biol* **8**: e1000414.
- Tsui K, Dubuis S, Gebbia M, Morse RH, Barkai N, Tirosh I, Nislow C. 2011. Evolution of nucleosome occupancy: conservation of global properties and divergence of gene-specific patterns. *Mol Cell Biol* **31**: 4348-4355.
- Tung KS, Hong EJ, Roeder GS. 2000. The pachytene checkpoint prevents accumulation and phosphorylation of the meiosis-specific transcription factor Ndt80. *Proc Natl Acad Sci U S A* **97**: 12187-12192.
- Ubeda F, Wilkins JF. 2011. The Red Queen theory of recombination hotspots. *J Evol Biol* **24**: 541-553.
- Vader G, Blitzblau HG, Tame MA, Falk JE, Curtin L, Hochwagen A. 2011. Protection of repetitive DNA borders from self-induced meiotic instability. *Nature* **477**: 115-119.
- Vincenten N, Kuhl LM, Lam I, Oke A, Kerr AR, Hochwagen A, Fung J, Keeney S, Vader G, Marston AL. 2015. The kinetochore prevents centromere-proximal crossover recombination during meiosis. *eLife* **4**: e10850.
- Vrielynck N, Chambon A, Vezon D, Pereira L, Chelysheva L, De Muyt A, Mezard C, Mayer C, Grelon M. 2016. A DNA topoisomerase VI-like complex initiates meiotic recombination. *Science* **351**: 939-943.

- Wahls WP, Smith GR. 1994. A heteromeric protein that binds to a meiotic homologous recombination hot spot: correlation of binding and hot spot activity. *Genes Dev* **8**: 1693-1702.
- Wan L, de los Santos T, Zhang C, Shokat K, Hollingsworth NM. 2004. Mek1 kinase activity functions downstream of *RED1* in the regulation of meiotic double strand break repair in budding yeast. *Mol Biol Cell* **15**: 11-23.
- Wan L, Niu H, Futcher B, Zhang C, Shokat KM, Boulton SJ, Hollingsworth NM. 2008. Cdc28-Clb5 (CDK-S) and Cdc7-Dbf4 (DDK) collaborate to initiate meiotic recombination in yeast. *Genes Dev* **22**: 386-397.
- Weinreich M, Liang C, Stillman B. 1999. The Cdc6p nucleotide-binding motif is required for loading mcm proteins onto chromatin. *Proc Natl Acad Sci U S A* **96**: 441-446.
- White MA, Dominska M, Petes TD. 1993. Transcription factors are required for the meiotic recombination hotspot at the *HIS4* locus in *Saccharomyces cerevisiae*. *Proc Natl Acad Sci U S A* **90**: 6621-6625.
- Williams AL, Genovese G, Dyer T, Altemose N, Truax K, Jun G, Patterson N, Myers SR, Curran JE, Duggirala R et al. 2015. Non-crossover gene conversions show strong GC bias and unexpected clustering in humans. *eLife* **4**: e04637.
- Winckler W, Myers SR, Richter DJ, Onofrio RC, McDonald GJ, Bontrop RE, McVean GA, Gabriel SB, Reich D, Donnelly P et al. 2005. Comparison of fine-scale recombination rates in humans and chimpanzees. *Science* **308**: 107-111.
- Wojtasz L, Daniel K, Roig I, Bolcun-Filas E, Xu H, Boonsanay V, Eckmann CR, Cooke HJ, Jasin M, Keeney S et al. 2009. Mouse *HORMAD1* and *HORMAD2*, two conserved meiotic chromosomal proteins, are depleted from synapsed chromosome axes with the help of *TRIP13* AAA-ATPase. *PLoS Genet* **5**: e1000702.
- Woltering D, Baumgartner B, Bagchi S, Larkin B, Loidl J, De los Santos T, Hollingsworth NM. 2000. Meiotic segregation, synapsis, and recombination checkpoint functions require physical interaction between the chromosomal proteins Red1p and Hop1p. *Mol Cell Biol* **20**: 6646-6658.
- Wu T-C, Lichten M. 1994. Meiosis-induced double-strand break sites determined by yeast chromatin structure *Science* **263**: 515-518.
- Wu TC, Lichten M. 1995. Factors that affect the location and frequency of meiosis-induced double-strand breaks in *Saccharomyces cerevisiae*. *Genetics* **140**: 55-66.
- Xiao Y, Weaver DT. 1997. Conditional gene targeted deletion by Cre recombinase demonstrates the requirement for the double-strand break repair Mre11 protein in murine embryonic stem cells. *Nucleic Acids Res* **25**: 2985-2991.

- Xu L, Ajimura M, Padmore R, Klein C, Kleckner N. 1995. *NDT80*, a meiosis-specific gene required for exit from pachytene in *Saccharomyces cerevisiae*. *Mol Cell Biol* **15**: 6572-6581.
- Xu L, Kleckner N. 1995. Sequence non-specific double-strand breaks and interhomolog interactions prior to double-strand break formation at a meiotic recombination hot spot in yeast. *EMBO J* **14**: 5115-5128.
- Xu L, Weiner BM, Kleckner N. 1997. Meiotic cells monitor the status of the interhomolog recombination complex. *Genes Dev* **11**: 106-118.
- Yamada S, Ohta K, Yamada T. 2013. Acetylated histone H3K9 is associated with meiotic recombination hotspots, and plays a role in recombination redundantly with other factors including the H3K4 methylase Set1 in fission yeast. *Nucleic Acids Res* **41**: 3504-3517.
- Yoshizaki H, Okuda S. 2014. Elucidation of the evolutionary expansion of phosphorylation signaling networks using comparative phosphomotif analysis. *BMC genomics* **15**: 546.
- Young JA, Hyppa RW, Smith GR. 2004. Conserved and nonconserved proteins for meiotic DNA breakage and repair in yeasts. *Genetics* **167**: 593-605.
- Young JA, Schreckhise RW, Steiner WW, Smith GR. 2002. Meiotic recombination remote from prominent DNA break sites in *S. pombe*. *Mol Cell* **9**: 253-263.
- Yu HG, Koshland DE. 2003. Meiotic condensin is required for proper chromosome compaction, SC assembly, and resolution of recombination-dependent chromosome linkages. *J Cell Biol* **163**: 937-947.
- Zakharyevich K, Ma Y, Tang S, Hwang PY-H, Boiteux S, Hunter N. 2010. Temporally and biochemically distinct activities of Exo1 during meiosis: Double-strand break resection and resolution of double Holliday junctions. *Mol Cell* **40**: 1001-1015.
- Zanders SE, Eickbush MT, Yu JS, Kang JW, Fowler KR, Smith GR, Malik HS. 2014. Genome rearrangements and pervasive meiotic drive cause hybrid infertility in fission yeast. *eLife* **3**: e02630.
- Zetka MC, Kawasaki I, Strome S, Muller F. 1999. Synapsis and chiasma formation in *Caenorhabditis elegans* require HIM-3, a meiotic chromosome core component that functions in chromosome segregation. *Genes Dev* **13**: 2258-2270.
- Zhang C, Song Y, Cheng ZH, Wang YX, Zhu J, Ma H, Xu L, Yang ZN. 2012. The *Arabidopsis thaliana* DSB formation (*AtDFO*) gene is required for meiotic double-strand break formation. *Plant J* **72**: 271-281.
- Zhang L, Kim KP, Kleckner NE, Storlazzi A. 2011. Meiotic double-strand breaks occur once per pair of (sister) chromatids and, via Mec1/ATR and Tel1/ATM, once per quartet of chromatids. *Proc Natl Acad Sci U S A* **108**: 20036-20041.

- Zhang L, Ma H. 2012. Complex evolutionary history and diverse domain organization of SET proteins suggest divergent regulatory interactions. *New Phytol* **195**: 248-263.
- Zhu J, Petersen S, Tessarollo L, Nussenzweig A. 2001. Targeted disruption of the Nijmegen breakage syndrome gene *NBS1* leads to early embryonic lethality in mice. *Curr Biol* **11**: 105-109.
- Zhu X. 2015. A high-resolution view of meiotic recombination initiation in *Saccharomyces cerevisiae*. Weill Cornell Graduate School of Medical Sciences, New York.
- Zhu X, Keeney S. 2015. High-resolution global analysis of the influences of Bas1 and Ino4 transcription factors on meiotic DNA break distributions in *Saccharomyces cerevisiae*. *Genetics* **201**: 525-542.
- Zickler D, Kleckner N. 1999. Meiotic chromosomes: Integrating structure and function. *Annu Rev Genet* **33**: 603-754.
- Zickler D, Kleckner N. 2015. Recombination, Pairing, and Synapsis of Homologs during Meiosis. *Cold Spring Harb Perspect Biol* **7**: a016626.